Fall 2019

Frontiers in Fast Voltammetry: Novel Analytes and Applications

Jordan Holmes

FRONTIERS IN FAST VOLTAMMETRY: NOVEL ANALYTES AND APPLICATIONS

by

Jordan Holmes

Bachelor of Science
Florida State University, 2015

Submitted in Partial Fulfillment of the Requirements

For the Degree of Doctor of Philosophy in

Chemistry

College of Arts and Sciences

University of South Carolina

2019

Accepted by:

Parastoo Hashemi, Major Professor

Timothy Shaw, Committee Member

Hans-Conrad Zur Loye, Committee Member

Jamie Lead, Committee Member

Cheryl L. Addy, Vice Provost and Dean of the Graduate School

DEDICATION

To Ronald, Stephen, and Bryan Holmes

ACKNOWLEDGEMENTS

I would like to acknowledge my incredible research advisor, Dr. Parastoo Hashemi for support always. Dr. Hashemi lead by example, inspiring me to become a confident scientist and teaching me to perform science with integrity. You have shown me what it means to be an excellent mentor and for that I will be forever grateful. I would also like to thank the members of my committee, Dr. Timothy Shaw, Dr. Hans-Conrad Zur Loye, and Dr. Jamie Lead, for challenging me, helping me think critically, and making me a better, more well-rounded scientist. To Dr. Pavithra Pathirathna and Dr. Thushani Siriwardhane, thank you for training me in the laboratory, editing my writing, and teaching me about metal electrochemistry. To the past and present members of the Hashemi Lab, Dr. Yuanyuan Yang, Dr. Srimal Samaranayake, Dr. Aya Adballa, Dr. Alyssa West, Shane Berger, Melinda Hersey, Rhiannon Robke, Anna Marie Buchanan, Colby Witt, Dr. Yangguang Ou, Brenna Parke, and Melissa Hexter: Thank you for helping me perform experiments, brainstorm ideas, interpret unexpected experimental results, and edit my writing, but above all, thank you for your friendship. I will always cherish the memories made and friendships forged during our time in the Hashemi Lab.

To the friends that I have made since moving to Columbia, South Carolina: I cannot thank you all enough for making me feel welcome when I first began graduate school. I am so grateful for the sense of belonging and community offered to me by my friends Kristen Pace, Alicia Dahl, Roma Amin, Courtney Dinardo, Elizabeth Ruiz and Lauren Formoso, ladies that have become my family away from home. To my friends

back home, Taylor Aspery, Sarah Zhu, Anna Roman, Hannah Lyons, Shelby Grice, Lauren Flowers, Chase Schuldt, Chella Stearns, and Sarah Foster: Thank you for always keeping in touch in the midst of exciting and hectic life changes. It is your unwavering friendship that has kept me motivated without fear of missing out. I would specifically like to thank Kristen Pace for being the best roommate, friend, and confidant I could ever ask for. You have been like a second sister to me and I will always cherish the memories we made together both at Florida State University and the University of South Carolina. To my late friend Philip Schlenoff, for encouraging me to pursue a career in research and driving my passion towards studying mental illness.

To my boyfriend, Nathan Berenbrok, it is difficult to express how appreciative I am to have you in my life, for never letting me give up, for always pushing me to be better, and for all of your support throughout the last few months of my thesis work. When life got chaotic with an unexpected move, job hunt, and a puppy, you were there for me every step of the way.

Finally, I am so grateful for the love and support from my parents, Stephen and Amy Holmes, from my siblings, Bryan and Madison Holmes, my grandparents, Ronald and Evelyn Holmes, and Irvin and Ann Kupper, and our fur babies, Sprinkles, Ribby, Wilfred, Rupert, Maisy, and Otto. Thank you for leading the way, making everything I have accomplished possible, inspiring me to pursue and achieve my dreams in both science and higher education.

ABSTRACT

Electrochemical sensors are beneficial towards the development and advancement of monitoring devices. As this type of technology progresses, so does our ability to create state-of-the-art sensing strategies to probe environmental and biological systems at the source. In the environment, it is essential to monitor particularly harmful contaminants like trace metals in order to better mitigate risk. Additionally, biological molecules are often times challenging to measure because matrices are complex and difficult to probe; Recent advancements in chemical *ex vivo* and *in vivo* sensing platforms have offered insight into physiological processes. The brain in particular requires a sophisticated, implantable sensor as biomarkers from the periphery do not reflect brain concentrations. The overarching goal of this dissertation is to develop electrochemical sensing strategies to measure molecules that are chemically elusive in the environment and in the brain using a powerful electrochemical technique called fast-scan cyclic voltammetry (FSCV). FSCV offers selective and sensitive measurements in real-time on an electrode small enough to probe systems without perturbation or eliciting an immune response. While traditionally employed to measure dopamine neurotransmission *in vivo*, here we expand the scope of FSCV to explore novel analytes and model systems, including those beyond the brain. First, we discuss the significance of on-site, *in situ* and real-time analysis for trace metal monitoring in dynamic environmental systems. We introduce our approach using ionophore-grafted carbon fiber microelectrodes (CFM) to selectively detect Cu(II) metal ions and characterize the Cu(II)-ionophore grafted CFM interface.

Second, we explore the functionality of human induced pluripotent stem cells derived into serotonin neurons (5-HTNs) in a multifaceted voltammetric and biophysical study, finding that 5-HTNs possess *in vivo* chemical characteristics. We then investigate the electroactivity of glutamate, a neurotransmitter that is difficult to measure electrochemically, finding that glutamate electropolymerizes forming poly-glutamic acid (PGA) at high potentials and fast scan rates. We characterize the PGA coating and our results suggests that glutamate polymerizes in brain tissue, improving the sensitivity of sensors during *in vivo* analysis. Finally, we present a sensing strategy for direct, enzyme-free glutamate detection while avoiding polymerization and characterize the analytical performance of the glutamate voltammetric signature. Together, our data showcases the power of FSCV for rapid trace metal monitoring, serotonin detection in 5-HTNs, electropolymerization, and sensing of new and challenging analytes.

PREFACE

This dissertation is closely based on the following refereed publications:

Chapter 2: Holmes, J.; Pathirathna, P.; Hashemi, P.: "Novel frontiers in voltammetric trace metal analysis: Towards real time, on-site, in situ measurements." *Trac-Trend Anal Chem* **2019,** *111*, 206-219.

Chapter 3: Holmes, J.; Ou, Y.; Hashemi, P.: "Ionophore-grafted carbon fiber microelectrodes as a trace metal speciation sensor." – *In preparation* – Environmental Science and Technology.

Chapter 4: Holmes, J.; Lau, T.; Saylor, R.A.; Hersey, M.; Keen, D.; Fernández-Novel, N.; Hampel, L.; Nijhout, H. F.; Reed, M. C.; Best, J.; Koch, P.; Hashemi, P.: "Human stem cell-derived serotonin neurons with *in vivo* biophysical and neurochemical characteristics" – *In preparation* – Proceedings of the National Academy of Sciences of the United States of America.

Chapter 5: Holmes, J.; Batey, L.; Hashemi, P.: "Radical-initiated electropolymerization of poly-glutamic acid on carbon: Implications for biological analysis" – *Under review* – Journal of the American Chemical Society.

Chapter 6: Holmes, J.; Buchanan, A. M.; Witt, C. E.; Redden, B.; Wiskur, S.; Hashemi, P.: "Enzyme-free glutamate sensing using fast voltammetry on carbon fiber microelectrodes" – *In preparation* – Analytical Chemistry

TABLE OF CONTENTS

Dedication iii

Acknowledgements iv

Abstract vi

Preface viii

List of Tables xiii

List of Figures xiv

List of Symbols xvi

List of Abbreviations xvii

Chapter 1: Introduction 1

1.1 Environmental Sensors 2

1.2 Biological Sensors 3

1.3 Electrochemical Sensing Techniques 4

1.4 Frontiers and Innovation 12

1.5 Scope of Dissertation 14

1.6 References 16

Chapter 2: Novel frontiers in voltammetric trace metal analysis: Towards real time, on-site, *in situ* measurements 29

2.1 Abstract 30

2.2 Introduction 30

2.3 Criteria for on-site, *in situ* analysis – the 6 S's 32

2.4 Voltammetric Techniques 33

2.5 Electrochemical probe design and material 39

2.6 Portable voltammetric instrumentation 52

2.7 Towards on-site, *in situ* trace metal analysis.....54

2.8 Conclusion 58

2.9 References 59

Chapter 3: Ionophore-grafted carbon fiber microelectrodes as a trace metal speciation sensor. 90

3.1 Abstract 91

3.2 Introduction 92

3.3 Materials and Methods 94

3.4 Results and Discussion.....97

3.5 Conclusion and Future Directions.....105

3.6 References 106

Chapter 4: Human Stem Cell-Derived Serotonin Neurons with *In Vivo* Biophysical and Neurochemical Characteristics 110

4.1 Significance.....111

4.2 Abstract 111

4.3 Introduction 112

4.4 Results.....114

4.5 Discussion 124

4.6 Methods.....134

4.7 References 143

Chapter 5: Radical-initiated Electropolymerization of Poly-Glutamic Acid on Carbon: Implications for Biological Analysis 156

5.1 Abstract 157

5.2 Introduction 158

5.3 Results and Discussion 160

5.4 Conclusion 176

5.5 References 177

Chapter 6: Enzyme-free Glutamate Sensing using Fast Voltammetry on Carbon Fiber Microelectrodes 191

6.1 Abstract 192

6.2 Introduction 193

6.3 Results and Discussion 195

6.4 Conclusion 204

6.5 Materials and Methods 205

6.6 References 207

Chapter 7: Conclusions and Future Prospects 213

Appendix A: Human Stem Cell-Derived Serotonin Neurons with *In Vivo* Biophysical and Neurochemical Characteristics Supplemental Information 216

A.1 Stimulation Paradigm 217

A.2 Cell Medium Optimization 218

A.3 Modelling External Tryptophan 219

A.4 References 220

Appendix B: Radical-Initiated Electropolymerization of Poly-Glutamic Acid on Carbon: Implications for Biological Analysis Supplemental Information 221

B.1 Experimental Section 222

B.2 References 226

Appendix C: Permission to Reprint: Chapter 2 228

LIST OF TABLES

Table 2.1. Electrochemical Detection Methods for On-Site Sensing. 55

Table A.1 Stimulation Paradigm.....217

LIST OF FIGURES

Figure 1.1. Microscopy images of the CFM surface. 6

Figure 1.2. FSCV scheme 8

Figure 2.1. Scheme of the main voltammetric techniques and modulations used for metal analysis.....34

Figure 2.2. Real-time complexation analysis with FSCV.....37

Figure 2.3. The FSCAV response and formation constants for 16 different Cu(II) – ligand complexes fit to an exponential curve. 39

Figure 2.4. Scheme of a Boron Doped Diamond Paste Electrode (BDDPE) on an electrochemical paper based analytical device 41

Figure 2.5. Representative assembly of a three-electrode system, microfluidic channels, and customized detection circuits fabricated onto a microchip 42

Figure 2.6. Selectivity of ionophore-grafted CFM in the presence of mixed metals.....48

Figure 2.7. Diagram of a total analysis system designed for on-site sensing: incorporating microfluidic tubing, a peristaltic pump, a rotary disc voltammetric sensor, portable potentiostat, data acquisition board, electronic controller, and USB and power inputs 53

Figure 3.1. Ionic strength characterization 99

Figure 3.2. Adsorption profile of Cu(II) on ionophore-grafted CFMs 101

Figure 3.3. Waveform optimization in media containing interferences 102

Figure 3.4. Interference fouling and recovery 104

Figure 4.1. Generation of hiPSC-derived serotonin neurons.....114

Figure 4.2. Visualization of synaptic and extrasynaptic 5-HT release 118

Figure 4.3. Transporter mediated serotonin uptake 121

Figure 4.4 ESCIT-mediated SERT internalization. 123

Figure 5.1. PGA electropolymerization on CFMs 164

Figure 5.2. PGA coating on CFMs 168

Figure 5.3. PGA film morphology 170

Scheme 1. PGA electropolymerization mechanism.....173

Figure 5.4. Sensitivity and kinetic response of modified CFMs.....175

Figure 6.1. Glutamate detection with FSCV.....196

Figure 6.2 Properties of glutamate-CFM interaction. 197

Figure 6.3 Glutamate waveform selectivity.....200

Figure 6.4 Voltammetric characterization of glutamate-ionophore binding. 202

Figure 6.5 *In vivo* glutamate detection.....203

Figure A.1 FSCV electrolytic buffer optimization 219

Figure A.2 External tryptophan affects vesicular and extracellular serotonin.....220

LIST OF SYMBOLS

Γ	Surface concentration
F	Faradays constant
eht	Extracellular serotonin
bht	Autoreceptors bound to eht
G*	Activation of G-protein
T*	Activation of regulatory T-protein
b0	Total concentration of autoreceptors
g0	Total concentration of G-proteins
t0	Total concentration of T-proteins
fire(t)	firing rate of neuron
vht	vesicular concentration of 5-HT

LIST OF ABBREVIATIONS

5-HIAA ..... 5-Hydroxyindoleacetic acid

5-HT 5-Hydroxytryptamine/Serotonin

5-HTN ..... Serotonin Neurons

AFM ..... Atomic Force Microscopy

ASP ..... (4-(4-(dimethylamino)-styryl)-N-methylpyridinium)

ASV ..... Anodic Stripping Voltammetry

BDDPE ..... Boron Doped Diamond Printed Electrode

biiiTub ..... Betaiii-Tubulin

BiFE ..... Bismuth Film Electrode

BSN ..... Bassoon

BNS-STED ..... Bassoon positive neurites

CFM ..... Carbon Fiber Microelectrode

CNS ..... Central Nervous System

CNT ..... Carbon Nanotube

CPE ..... Carbon Paste Electrode

CSPE ..... Carbon Stencil Printed Electrode

CV ..... Cyclic Voltammogram

DA ..... Dopamine

DAT ..... Dopamine Transporter

DMG ..... Dimethylglyoxime

DNR ..... Dorsal Raphe Nucleus

DPASV ..... Differential Pulse Anodic Stripping Voltammetry

EDX .....Energy Dispersive X-Ray Spectroscopy

EG .....Expanded Graphite

ESCIT ..... Escitalopram

FFN ..... False Fluorescent Neurotransmitter

FIA ..... Flow Injection Analysis

FM.....Fluorescent marker

FSCAV..... Fast-scan Controlled Adsorption Voltammetry

FSCV.....Fast-scan Cyclic Voltammetry

GCE.....Glassy Carbon Electrode

hiPSC .....Human Induced Pluripotent Stem Cells

IPA ..... Isopropyl Alcohol

IIP.....Ion Imprinted Polymer

LOD .....Limit of Detection

LOC.....Lab-on-a-chip

LPE ..... Lithographically Printed Electrode

Mag-IIP-NPs.....Magnetic Ion Imprinted Polymer Nanoparticles

MEA.....Microelectrode Array

MPCE.....Magneto Carbon Paste Electrode

MWCNT ..... Multiwalled Carbon Nanotubes

NA..... Nafion

NET.....Norepinephrine Transporter

NP ..... Nanoparticles

NSC..... Neuronal Stem Cells

OCT..... Organic Cation Transporter

PANI PDTDA ..... Polyaniline-Poly(2,2'-Dithiodianiline)

PCL-STED ..... Piccolo-Positive Structure

PGA ..... Poly-glutamic Acid

POC ..... Point-of-Care

ROI ..... Regions of Interest

SEM ..... Scanning Electron Microscopy

SERT ..... Serotonin Transporter

SNR ..... Substantia Nigra Reticulata

SPAN ..... Sulfonated Polyaniline

SPCE ..... Screen Printed Carbon Electrode

SPGE ..... Screen Printed Gold Electrode

SPE ..... Screen Printed Electrode

SSRI ..... Serotonin Selective Reuptake Inhibitor

SWASV ..... Square Wave Anodic Stripping Voltammetry

SV ..... Stripping Voltammetry

TH ..... Tyrosine Hydroxylase

TPH2 ..... Tryptophan Hydroxylase-2

TRP ..... Tryptophan

μPAD ..... Microfluidic Paper-Based Analytical Device

VGME ..... Vibrating Gold Microwire Electrode

VIP ..... Voltammetric *In Situ* Profiling

VMAT2 ..... Vesicular Monoamine Transporter-2

CHAPTER 1

INTRODUCTION

Sensing devices have been commonplace for decades in automobiles, hospitals, and homes, however, as technology becomes more sophisticated, we find ourselves in a better position to create more sophisticated sensing strategies. Sensors are particularly useful for environmental and human health monitoring, where the luxury of sample collection and secondary analysis is not always afforded in terms of time and practicality. Innovative sensing devices that operate on-site and on-line are highly beneficial. Examples of these sensors include smart watches capable of monitoring exercise and vital signs,[1] a wearable ring sensor for detecting nerve gases and explosives,[2] and chemical sensor arrays that help identify entrapped humans from metabolic traces emitted from skin and breath.[3] In addition to protecting human safety, the development of novel, fast, portable sensors serves as a means to investigate various environmental and biological processes that have been difficult to assess in the past due to the delicate nature of these systems. The overarching research goal of this dissertation is to develop new sensing platforms in application to biological and environmental phenomena. First, we identify the importance of environmental and biological sensing, followed by a discussion of sensing techniques, and finally introduce sensing platforms at the frontier of innovation.

1.1 Environmental Sensors

Environmental pollutants, such as heavy metals, are pervasive, bioaccumulate and find their way to humans *via* several different exposure routes.[4-6] Pollutants can originate from both natural and anthropogenic sources, examples of which include dynamic weather events, agricultural runoff, aging infrastructure, and industrial effluents.[7,8] In these scenarios, early detection of hazardous chemicals is essential for more effective and efficient mitigation. As mentioned above, metal ions are particularly pervasive and damaging to human health.[9]

1.1.1 Metals

Metals such as Pb, Cr, Cd, As, Hg, and Cu exist at trace concentrations and are considered particularly damaging to human health.[9,10] Minor variations in environmental parameters, such as pH and temperature, can cause metals to change speciation by readily fluctuating between ligand-bound and "free" or hexa-aqua complexed states. Generally, the 'free' form of these metals is more significant since it is the free metal that is more likely to engage in chemical processes.

While spectroscopy offers excellent sensitivity and selectivity for total metal analysis, spectrometers are bulky, and portability is limited. Moreover, speciation analysis is complicated to perform spectroscopically. Electrochemical techniques are attractive for trace metal analysis because they report free metal concentrations and have more opportunity for portability. **Chapter 2** of this dissertation is a review article defining criteria important for trace metal analysis and highlighting electrochemical methods applied on-site and *in situ* within the last 10 years.[11]

1.2 Biological Sensors

Biological systems are chemically complex and dynamic, facets which make the assessment of physiology and function challenging. Materials for probing biological systems must be biocompatible because the body has a sophisticated immune response tasked at rejecting foreign entities. To overcome these challenges, there have been many recent advancements in chemical and biological sensing platforms both *ex vivo* and *in vivo*. Many *ex vivo* measurements can be made from non-invasive, wearable sensors such as smartwatches[12] or temporary tattoos[13] that measure chemicals like glucose and lactate in external bodily fluids (i.e. tears or perspiration).[14-16] *In vivo* chemical sensors have become smaller, easier to implant, and cause minimal tissue damage; They are often utilized to study complex organs like the gut or lymph nodes.[17-19] The introduction of biocompatible carbon probes and versatility of carbon materials, like diamond,[20] nanotubes,[21] and fiber,[22,23] are largely responsible for making these innovative sensing strategies possible. As a result, sensing accomplished at or near the site of patient care is gaining popularity and many point-of-care (POC) devices have been integrated into the clinic.[24-26]

1.2.1 Neurotransmission

Of bodily systems, the brain remains particularly challenging to study because biomarkers from the periphery do not reflect brain concentrations. Molecules in the brain are subject to a chemical trafficking system called the blood brain barrier that controls diffusion between the blood and the brain. The brain houses the central nervous system (CNS), the primary function of which is to send and receive signals that coordinate activity and sensation. Chemical signals between neurons are transmitted rapidly *via*

neurotransmitters with discrete functions that are still not well defined. Traditionally during transmission, neurotransmitters are released from the presynaptic neuron and interact with receptors on the postsynaptic terminal, propagating the signal. In some cases, neurotransmitters can also interact with autoreceptors, located throughout the membrane on the presynaptic neuron, that regulate release and signal the neurons to cease firing. Neurotransmission is tightly regulated through a variety of mechanisms. The fate of most neurotransmitters involves being quickly uptaken by transporters on the presynaptic terminal, though some can also be uptaken by glial transporters or metabolized by enzymes. Additionally, transporters have been described as "promiscuous."[27] For example, serotonin can be uptaken by dopamine transporters (DATs), norepinephrine transporters (NETs),[28,29] or organic cation transporters (OCTs),[30-33] among others. Multiple transporters result in multiple reuptake mechanisms that have been modelled by our group.[34,35]

In the case of glutamate and GABA, the major excitatory and inhibitory transmitters, signaling events are contained for the most part in the synaptic clefts between neurons. Alternatively, less tightly regulated transmitters such as dopamine, serotonin, and histamine tend to release more often from varicosities without a post synaptic counterpart, spilling out into the extracellular space in a process called "volume transmission."[36,37]

1.3 Electrochemical Sensing Techniques

Making measurements in delicate systems like natural waters or live tissue requires tools and techniques tailored to fit the needs of the application. Oftentimes the removal of samples from the source irreversibly alters the nature (speciation) of the

sample. Electrochemistry is an attractive measurement method for analysis at the source because electrodes are generally portable, can be fashioned into many configurations (even down to the nano-scale),[38] and are easily implanted or integrated for *in situ* or *in vivo* capacities. Furthermore, there are many electrochemical techniques and electrode materials that offer unique benefits for different measurement scenarios.

1.3.1 Electrode Materials and Configurations

Electrodes can be fashioned out of many different materials, with metals being most common (*i.e.* gold or platinum), however, to be utilized in biological systems, the electrode material must be biocompatible. Carbon has since emerged as the ultimate electrode material, providing excellent electrochemical properties, such as 1) self-renewal due to overoxidation 2) a adsorptive surface 3) a broad potential window, 4) simple functionalization, 5) biocompatibility, 6) sustainability and 7) cost effectiveness.[39-42] Importantly, carbon can be fashioned into microelectrodes that offer valuable benefits over macroelectrodes. Micron dimensions mean that there is a smaller IR drop across the electrode (because of increased analyte mass transport to the electrode surface due to hemispherical diffusion). Additionally, a smaller electrode footprint means minimal disturbance to tissue.[43,44] Specifically, cylindrical carbon fiber microelectrodes (CFMs) have shown routine utility for the most intricate of biological measurements, including in the brain.[22,23] Combining the benefits of both microelectrodes and carbon materials, CFMs can be fabricated *via* several methods, either encapsulated in glass or an epoxy resin, providing a robust configuration. Hallmark surface striations magnifies surface area for enhanced sensitivity as seen in **Figure 1.1**. Additionally, CFMs exhibit excellent

stability and reproducibly over time, evidenced by long shelf lives and continuous *in vivo* monitoring in some cases for several weeks.[45]

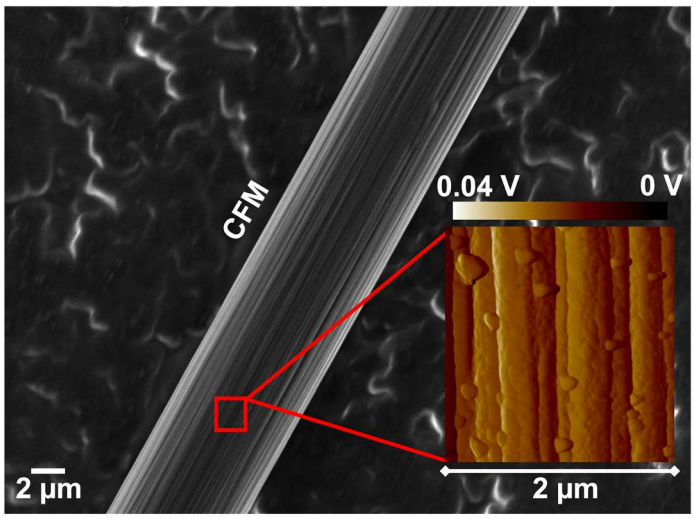

Figure 1.1. Microscopy images of the CFM surface. Scanning electron microscopy (SEM) was used to image a CFM. Inset: Atomic force microscopy shows striated surface features.

1.3.2 Techniques

Electrochemical techniques must satisfy a series of basic criteria to serve as a sufficient detection platform, originally coined by Lama *et al.* as the **4 S's**: **sensitivity, selectivity, speed, and size**.[46] It is essential to be able to measure and identify analytes at trace concentrations (<1 ppm). In systems where concentrations are dynamic, as in neurotransmission, high temporal resolution is critical for observing release and reuptake events. Finally, electrode dimensions in the low microns offer enhanced electrochemical properties and are able to navigate living tissue with minimal damage and inflammation.[47]

There are several electrochemical techniques for environmental or *in vivo* measurements that have revealed important information. One technique that is able to check all four boxes is fast-scan cyclic voltammetry (FSCV).

1.3.2.1 Fast-Scan Cyclic Voltammetry

Fast voltammetry was first developed in 1984 by Stamford *et al.*[48] Unlike conventional cyclic voltammetry, FSCV applies an electrochemical waveform every 100 ms, sweeping through a potential range at fast scan rates of up to 1000 V/s or faster. Fast scan rates previously limited this technique because of a large, capacitive (or non-faradaic) background that masked the faradaic current. The integration of background subtraction[49] has allowed for quantification of faradaic peaks and for a suite of analytes and applications to be investigated. With a given waveform, molecules will oxidize or reduce at discrete potentials, offering specificity. FSCV data is typically portrayed by a 2D representation of a 3D plot (time, potential, and current) called a color plot where current is assigned a false color. **Figure 1.2** provides an example of representative FSCV data including a color plot, cyclic voltammogram (CV), and current vs. time trace of serotonin collected *in vivo*. When a serotonin specific waveform is applied, serotonin molecules undergo a 2-electron redox process and a color plot is generated. On the color plot, serotonin oxidation is responsible for the green event around 0.7 V, and reduction for the blue event around 0 V. The vertical line on the color plot is used to regenerate the CV plotting current vs. potential (yellow star), where distinct redox peaks serve as a qualitative fingerprint to identify specific analytes. The horizontal line on the color plot is extracted to regenerate the current vs. time trace (red star), enabling quantitative analysis.

Calibrations are performed to convert current into concentration and allow for concentration changes to be measured during neurotransmission events.

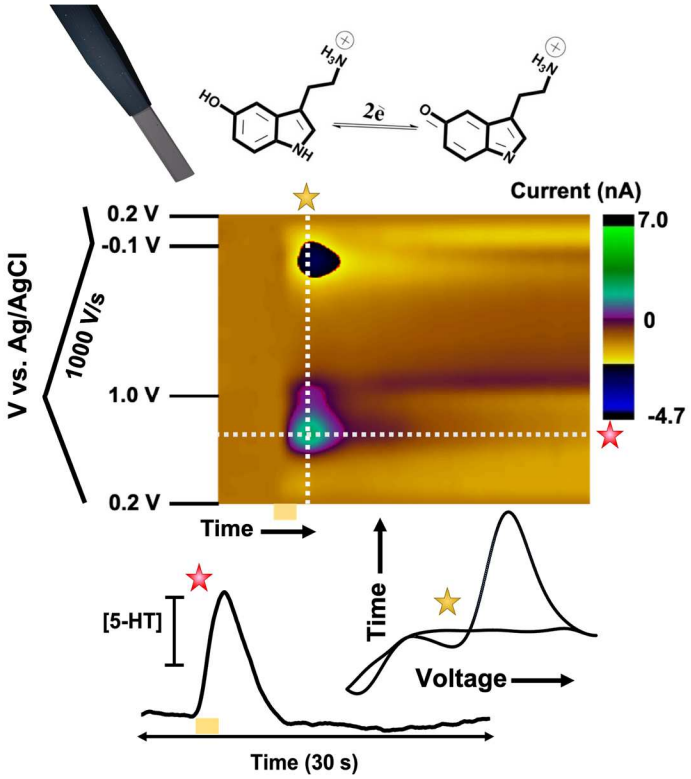

Figure 1.2. FSCV scheme. A CFM applies a serotonin specific waveform and measures the oxidation and reduction of serotonin molecules, depicting information in a color plot. The representative CV and concentration time traces are denoted with yellow and red stars, respectively.

1.3.2.2 Fast-scan controlled adsorption voltammetry (FSCAV)

Fast scan rates require background subtraction to account for a large background charging current that is the result of high scan rates, thus a response must be evoked (electrically, pharmacologically or behaviorally) and the basal and steady state level cannot be known. A new method emerged, coined FSCAV, in 2013 for ambient dopamine analysis comprised of three measurement steps: 1) minimized adsorption, 2) controlled adsorption period of 10 s to preconcentration the analyte to the carbon surface

and 3) measurement.[50] Since then, this technique has been applied *in vivo* to measure tonic dopamine and serotonin.[51,52] The drawback of FSCAV is that the temporal resolution is reduced to 30 s however this method still represents an improvement over other methods for basal analysis that have minutes or 10s of minutes temporal resolutiont.[53,54] These two fast voltammetric techniques, FSCV and FSCAV, can be coupled at a single sensor.

1.3.3 Analytes/ applications

The high temporal resolution of FSCV is particularly useful for observing release and reuptake events during neurotransmission. With this method, the dopamine system in anesthetized and freely moving animals, in different brain regions, and in disease models has been extensively characterized.[55-58] New waveforms and methods have branched from this work, allowing for other important analytes to be quantified *in vivo*, such as serotonin,[59] histamine,[60] and others.[17,61-64] Specifically, serotonin was a rather elusive molecule for many years, and detection *in vivo* was challenging because serotonin oxidation generates a suite of oxidation products that foul the electrode surface. The development of a serotonin specific waveform[58] coupled with a method to electroplate Nafion™ (NA) allowed for serotonin to be detected in the substantia nigra region in the rodent brain for the first time in 2009.[59] Since then, serotonin FSCV has been utilized to equate neurochemistry between gender,[65] study the effects of serotonin selective reuptake inhibitors (SSRIs),[65,66] and map transporter populations in many different brain regions.[35,67]

In addition to neurotransmission, FSCV has also exhibited utility for trace metal monitoring in real water samples. Pathirathna *et al.* first introduced a waveform in 2012,

generating a signature Cu(II) signal,[68] and extensively characterized the thermodynamic properties of Cu(II) on CFMs and Cu(II) speciation in several publications between 2014 and 2016.[69-72] Following this, Yang *et al.* and Siriwardhane *et al.* took similar approaches to measure Pb(II), Ca(II), Al(II), and other metals with FSCV.[73,74] Yang *et al.* showcased the power of FSCV for trace metal monitoring by measuring Pb(II) in storm water samples, a promising step towards more environmental applications.[74]

1.3.4 Electrode modification strategies

Voltammetry offers some selectivity over other techniques, because different analytes oxidize and reduce at discrete potentials. However, voltammetry is not sufficient to resolve multiple transmitters when redox peaks of similar height overlap for two analytes present in a solution. In these cases, there are several ways to improve selectivity by modifying electrochemical surfaces.

1.3.4.1 Conductive Polymers

Conductive polymers are extremely useful for electrochemical analysis because they contain small, charged pores that facilitate electrostatic migration of molecules to the electrode. Perhaps the most widely employed polymer for biological analysis is NA, a cation exchange polymer made up of bulky sulfonated and fluorinated functional groups. NA coatings are simple to prepare, and highly effective for repelling interferences present in the extracellular matrix of the brain, such as ascorbic acid and 5-hydroxyindoleacetic acid (5-HIAA), the major serotonin metabolite.[59] Amino acids offer unique properties as conductive coatings because they can be electropolymerized *in situ*. When a potential is offered, amino functional groups oxidize forming a radical. This radical initiates a bond with the carbon surface and polymer growth is propagated by continuing the potential

application.[75-78] There are many amino acids that form polymers, however one of particular interest is poly-glutamic acid (PGA). Glutamate is ubiquitous across brain regions and zwitterionic at physiological pH as a monomer, however the polymer possesses an overall negative charge. **Chapter 5** of this dissertation provides evidence that glutamate polymerizes *in vivo* during FSCV analysis and offers sensitivity improvements for dopamine detection.

1.3.4.2 Ionophores

Another approach to improving selectivity over interferences is the incorporation of an ionophore, or a molecule that specifically binds an ion to form a complex. Ionophores are particularly useful for metals and have been used for decades as chelating agents and more recently, as fluorescent tags for spectroscopic analysis.[79,80] In electrochemistry, ionophores are typically utilized in ion-selective electrodes, suspended in a polymeric matrix. A Nernstian signal arises when the ions partition into this polymer layer, driven by a concentration dependent thermodynamic equilibrium. Because equilibrium through thick polymer layers can be a slow process, the temporal resolution of these probes is often slow. Yang *et al*. recently pioneered a polymer-free surface modification that couples ionophore-grafted CFMs with FSCV.[81] This synthetic protocol consists of 3 steps: 1) reductive coupling of a diazonium salt onto the CFM, 2) silylation of remaining active sites, and 3) attachment of a Cu(II)-specific ionophore *via* click chemistry. **Chapter 3** of this dissertation continues on this work by optimizing the modification method and further characterizing the analytical performance of ionophore-grafted CFMs.

1.4 Frontiers and innovation –

The overarching goal of this dissertation is to further the scope of FSCV in terms of application and analytes.

1.4.1 Translational sensing

Our lab first pioneered serotonin sensing *in vivo* with FSCV, laying the groundwork for investigating serotonin neurochemistry.[59] We now seek to take the next step in translating serotonin measurements to explore human neurochemistry. There are prior reports of voltammetry performed in humans on Parkinson's Disease patients undergoing surgery deep brain stimulation,[82] however these experiments are limited and there are many challenges associated with them including little control over electrode placement, background noise, and difficulties verifying chemical species during the experiment. Additionally, control data cannot be obtained because human experiments can only be performed on patients that are already undergoing surgical procedures for major neurological illnesses. At this time, it is not feasible to probe the human brain in a meaningful way with electrochemical sensors, and biomarkers from serum do not reflect the brain. This presents an intriguing analytical challenge to identify a means to study human neurochemistry with a suitable model.

1.4.1.1 Induced pluripotent stem cells

In efforts to locate a model from outside of the brain that reflect neurochemistry, human inducible pluripotent stem cells (hiPSCs) are an interesting approach. hiPSCs are created by harvesting and treating skin samples with a suite of chemical reprogramming factors.[83] An *in vitro* differentiation protocol can be followed to derive serotonin neurons

from hiPSCs, based on a modified protocol comprised of four stages by Lu and colleagues.[84] Successful differentiation is evidenced by the presence of important transcription factors indicating a serotonergic fate throughout different stages of differentiation. In the final stage of differentiation, hiPSCs demonstrate serotonin phenotype markers, including tryptophan hydroxylase-2 (the protein responsible for serotonin synthesis) and SERTs (serotonin transporters), and stained positive for serotonin. Cultures like these are excellent *in vitro* models because they contain more complete neural networks, testing positive for GABAergic, glutamatergic or motoneuron phenotypes within the culture. hiPSCs are attractive for diagnostics, since samples can be collected from the periphery, are readily available, controllable, and patient specific. **Chapter 4** of this dissertation details fast serotonin measurements in hiPSCs as a functional model to study serotonin neurochemistry *ex vivo*.

1.4.2 New analytes

FSCV *in vivo* has been limited to a small number of analytes, including dopamine and serotonin, however recently, there have been great strides to expand this technique to other critical analytes, such as adenosine, hydrogen peroxide, and histamine.[60,61,64] Another neurotransmitter analyte of particular interest is glutamate, the primary excitatory neurotransmitter in the brain. Glutamate is particularly difficult to measure electrochemically because it is not electroactive in the potential window of traditional electrode materials. Enzymes are heavily relied on for glutamate sensing; glutamate oxidase produces hydrogen peroxide, an electroactive molecule, as a product of glutamate oxidation.[85] Enzyme biosensors carry analytical challenges such as low immobilization efficiency, shelf life, and large probe size.[86,87] Additionally, glutamate

does possess some electrochemical properties because, as mentioned previously, glutamate electropolymerizes forming PGA when a potential is offered.[88,89] Furthermore, there are physiological challenges associated with glutamate detection: glutamate transmission is highly regulated and is generally limited to the synaptic cleft. CFMs implanted into brain tissue are typically small enough to prevent damage, but too large to penetrate the synapse, sampling from the extracellular matrix. Glutamate signaling is less regulated extracellularly in the Purkinje layer of the cerebellum where it is thought that glutamate is volume transmitted.[90-92] **Chapter 6** of this dissertation explores a voltammetric approach towards direct glutamate detection

1.5 Scope of dissertation

This dissertation presents the development and applications of fast voltammetric techniques at CFMs for real-time, sensitive and selective analysis of Cu(II), serotonin and glutamate.

Chapter 2 presents a published literature review of the development and application of electrochemical approaches towards rapid, field portable devices. In this work, 6 criteria are defined for a suitable device capable on-site and in situ analysis of trace metals. Highlighted in this article are electroanalytical sensing component advancements such as in green electrode materials, surface modifications, and ultra-fast novel techniques.

Chapter 3 presents the fabrication of ionophore-grafted CFMs for selective Cu(II) detection with fast-voltammetry. In this chapter, the fabrication process of creating ionophore-grafted CFMs is optimized, providing a stable and selective detection platform

for Cu(II) in the presence of mixed divalent metal ions. This work characterizes the analytical response of ionophore grafted CFMs in the context of ionic strength, adsorption efficiency, and reusability of electrodes.

Chapter 4 presents derived serotonin neurons from hiPSCs as a novel and translational model for studying brain serotonin. In this chapter, we apply a suite of methods to investigate the biophysical and neurochemical characteristics of 5-HTNs. We verify chemical functionality *via* electrically evoked serotonin release and reuptake from cells with FSCV and show that dose dependent alterations in reuptake following administration of a serotonin selective reuptake inhibitor (SSRI). A relationship between *in vivo* serotonin responses in the rodent brain and *in vitro* responses in hiPSCs is constructed, in an effort to translate FSCV results and draw conclusions about the chemical mechanisms behind depression in the human brain.

Chapter 5 presents a multifaceted approach towards characterizing PGA coated CFMs deposited with fast voltammetry. Voltammetric, microscopic, and spectroscopic analyses are performed to optimize waveforms used for deposition and determine the mechanism of polymerization. We found that PGA coatings can be visualized on CFMs, and the non-uniform morphology of PGA suggests a nucleation and growth-like mechanism of deposition. Additionally, we compare PGA-CFMs to CFMs that have been exposed to brain tissue, finding similarities in analytical performance and provide evidence to support that improvements to *in vivo*-CFMs are a result of *in situ* electropolymerization of ambient glutamate in the extracellular space of the brain.

Chapter 6 presents a sensing paradigm for glutamate detection. These findings are novel because until recently, it has been generally accepted that glutamate is not electroactive. For the first time here, we optimize a waveform for voltammetric glutamate measurements while evading electropolymerization with FSCV. The voltammetric signal is characterized with respect to sensitivity and electron transfer mechanism. Additionally, we found that many neurochemically relevant molecules do not interfere with the glutamate signal. Finally, we collected preliminary *in vivo* data measuring glutamate release in the Purkinje layer in the cerebellum.

Chapter 7 summarizes the work and proposes future directions.

1.6 References

(1) Reeder, B.; David, A. Health at hand: A systematic review of smart watch uses for health and wellness. *J Biomed Inform* **2016,** *63*, 269.

(2) Sempionatto, J. R.; Mishra, R. K.; Martin, A.; Tang, G. D.; Nakagawa, T.; Lu, X. L.; Campbell, A. S.; Lyu, K. M. J.; Wang, J. Wearable Ring-Based Sensing Platform for Detecting Chemical Threats. *Acs Sensors* **2017,** *2* (10), 1531.

(3) Guntner, A. T.; Pineau, N. J.; Mochalski, P.; Wiesenhofer, H.; Agapiou, A.; Mayhew, C. A.; Pratsinis, S. E. Sniffing Entrapped Humans with Sensor Arrays. *Analytical Chemistry* **2018,** *90* (8), 4940.

(4) Mahboob, S.; Al-Ghanim, K. A.; Al-Misned, F.; Shahid, T.; Sultana, S.; Sultan, T.; Hussain, B.; Ahmed, Z. Impact of Water Pollution on Trophic Transfer of Fatty Acids in Fish, Microalgae, and Zoobenthos in the Food Web of a Freshwater Ecosystem. *Biomolecules* **2019,** *9* (6).

(5) Vijver, M. G.; Van Gestel, C. A. M.; Lanno, R. P.; Van Straalen, N. M.; Peijnenburg, W. J. G. M. Internal metal sequestration and its ecotoxicological relevance: A review. *Environ Sci Technol* **2004,** *38* (18), 4705.

(6) Penicaud, V.; Lacoue-Labarthe, T.; Bustamante, P. Metal bioaccumulation and detoxification processes in cephalopods: A review. *Environ Res* **2017,** *155*, 123.

(7) Butler, L. J.; Scammell, M. K.; Benson, E. B. The Flint, Michigan, Water Crisis: A Case Study in Regulatory Failure and Environmental Injustice. *Environ Justice* **2016,** *9* (4), 93.

(8) Weston, D. P.; Asbell, A. M.; Lesmeister, S. A.; Teh, S. J.; Lydy, M. J. Urban and agricultural pesticide inputs to a critical habitat for the threatened delta smelt (Hypomesus transpacificus). *Environ Toxicol Chem* **2014,** *33* (4), 920.

(9) Ali, H.; Khan, E. Trophic transfer, bioaccumulation, and biomagnification of non-essential hazardous heavy metals and metalloids in food chains/webs-Concepts and implications for wildlife and human health. *Hum Ecol Risk Assess* **2019,** *25* (6), 1353.

(10) Chakraborti, D.; Rahman, M. M.; Mukherjee, A.; Alauddin, M.; Hassan, M.; Dutta, R. N.; Pati, S.; Mukherjee, S. C.; Roy, S.; Quamruzzman, Q.et al. Groundwater arsenic contamination in Bangladesh-21 Years of research. *J Trace Elem Med Biol* **2015,** *31*, 237.

(11) Holmes, J.; Pathirathna, P.; Hashemi, P. Novel frontiers in voltammetric trace metal analysis: Towards real time, on-site, in situ measurements. *Trac-Trend Anal Chem* **2019,** *111*, 206.

(12) Wang, C.; Hu, K.; Li, W. J.; Wang, H. Y.; Li, H.; Zou, Y.; Zhao, C. C.; Li, Z.; Yu, M.; Tan, P. C.et al. Wearable Wire-Shaped Symmetric Supercapacitors Based on Activated Carbon-Coated Graphite Fibers. *Acs Appl Mater Inter* **2018,** *10* (40), 34302.

(13) Liu, Q.; Chen, J.; Li, Y. R.; Shi, G. Q. High-Performance Strain Sensors with Fish-Scale-Like Graphene-Sensing Layers for Full-Range Detection of Human Motions. *Acs Nano* **2016,** *10* (8), 7901.

(14) Dunn, J.; Runge, R.; Snyder, M. Wearables and the medical revolution. *Pers Med* **2018,** *15* (5), 429.

(15) Kim, J.; Kim, M.; Lee, M. S.; Kim, K.; Ji, S.; Kim, Y. T.; Park, J.; Na, K.; Bae, K. H.; Kim, H. K.et al. Wearable smart sensor systems integrated on soft contact lenses for wireless ocular diagnostics. *Nature Communications* **2017,** *8*.

(16) Gao, W.; Emaminejad, S.; Nyein, H. Y. Y.; Challa, S.; Chen, K. V.; Peck, A.; Fahad, H. M.; Ota, H.; Shiraki, H.; Kiriya, D.et al. Fully integrated wearable sensor arrays for multiplexed in situ perspiration analysis. *Nature* **2016,** *529* (7587), 509.

(17) Hensley, A. L.; Colley, A. R.; Ross, A. E. Real-Time Detection of Melatonin Using Fast-Scan Cyclic Voltammetry. *Anal Chem* **2018,** *90* (14), 8642.

(18) Patel, N.; Fagan-Murphy, A.; Covill, D.; Patel, B. A. 3D Printed Molds Encompassing Carbon Composite Electrodes to Conduct Multisite Monitoring in the Entire Colon (vol 89, pg 11690, 2017). *Analytical Chemistry* **2018,** *90* (7), 4934.

(19) MacEachern, S. J.; Keenan, C. M.; Papakonstantinou, E.; Sharkey, K. A.; Patel, B. A. Alterations in melatonin and 5-HT signalling in the colonic mucosa of mice with dextran-sodium sulfate-induced colitis. *Br J Pharmacol* **2018,** *175* (9), 1535.

(20) Roy, R. K.; Lee, K. R. Biomedical applications of diamond-like carbon coatings: A review. *J Biomed Mater Res B* **2007,** *83b* (1), 72.

(21) Schroeder, V.; Savagatrup, S.; He, M.; Ling, S. B.; Swager, T. M. Carbon Nanotube Chemical Sensors. *Chem Rev* **2019,** *119* (1), 599.

(22) Huffman, M. L.; Venton, B. J. Carbon-fiber microelectrodes for in vivo applications. *Analyst* **2009,** *134* (1), 18.

(23) Roberts, J. G.; Sombers, L. A. Fast-Scan Cyclic Voltammetry: Chemical Sensing in the Brain and Beyond. *Analytical Chemistry* **2018,** *90* (1), 490.

(24) Hersey, M.; Berger, S. N.; Holmes, J.; West, A.; Hashemi, P. Recent Developments in Carbon Sensors for At-Source Electroanalysis. *Anal Chem* **2019,** *91* (1), 27.

(25) Brock, T. K.; Mecozzi, D. M.; Sumner, S.; Kost, G. J. Evidence-based point-of-care tests and device designs for disaster preparedness. *Am J Disaster Med* **2010,** *5* (5), 285.

(26) Drain, P. K.; Hyle, E. P.; Noubary, F.; Freedberg, K. A.; Wilson, D.; Bishai, W. R.; Rodriguez, W.; Bassett, I. V. Diagnostic point-of-care tests in resource-limited settings. *Lancet Infect Dis* **2014,** *14* (3), 239.

(27) Daws, L. C. Unfaithful neurotransmitter transporters: focus on serotonin uptake and implications for antidepressant efficacy. *Pharmacol Ther* **2009,** *121* (1), 89.

(28) Schwartz, J. W.; Blakely, R. D.; DeFelice, L. J. Binding and transport in norepinephrine transporters. Real-time, spatially resolved analysis in single cells using a fluorescent substrate. *J Biol Chem* **2003,** *278* (11), 9768.

(29) Mason, J. N.; Farmer, H.; Tomlinson, I. D.; Schwartz, J. W.; Savchenko, V.; DeFelice, L. J.; Rosenthal, S. J.; Blakely, R. D. Novel fluorescence-based approaches for the study of biogenic amine transporter localization, activity, and regulation. *J Neurosci Methods* **2005,** *143* (1), 3.

(30) Horton, R. E.; Apple, D. M.; Owens, W. A.; Baganz, N. L.; Cano, S.; Mitchell, N. C.; Vitela, M.; Gould, G. G.; Koek, W.; Daws, L. C. Decynium-22 enhances SSRI-induced antidepressant-like effects in mice: uncovering novel targets to treat depression. *J Neurosci* **2013,** *33* (25), 10534.

(31) Amphoux, A.; Vialou, V.; Drescher, E.; Bruss, M.; Mannoury La Cour, C.; Rochat, C.; Millan, M. J.; Giros, B.; Bonisch, H.; Gautron, S. Differential pharmacological in vitro properties of organic cation transporters and regional distribution in rat brain. *Neuropharmacology* **2006,** *50* (8), 941.

(32) Baganz, N. L.; Horton, R. E.; Calderon, A. S.; Owens, W. A.; Munn, J. L.; Watts, L. T.; Koldzic-Zivanovic, N.; Jeske, N. A.; Koek, W.; Toney, G. M.et al. Organic cation transporter 3: Keeping the brake on extracellular serotonin in serotonin-transporter-deficient mice. *Proc Natl Acad Sci U S A* **2008,** *105* (48), 18976.

(33) Daws, L. C.; Koek, W.; Mitchell, N. C. Revisiting serotonin reuptake inhibitors and the therapeutic potential of "uptake-2" in psychiatric disorders. *ACS Chem Neurosci* **2013,** *4* (1), 16.

(34) Wood, K. M.; Zeqja, A.; Nijhout, H. F.; Reed, M. C.; Best, J.; Hashemi, P. Voltammetric and mathematical evidence for dual transport mediation of serotonin clearance in vivo. *J Neurochem* **2014,** *130* (3), 351.

(35) West, A.; Best, J.; Abdalla, A.; Nijhout, H. F.; Reed, M.; Hashemi, P. Voltammetric evidence for discrete serotonin circuits, linked to specific reuptake domains, in the mouse medial prefrontal cortex. *Neurochem Int* **2019,** *123*, 50.

(36) Vizi, E. S.; Fekete, A.; Karoly, R.; Mike, A. Non-synaptic receptors and transporters involved in brain functions and targets of drug treatment. *Brit J Pharmacol* **2010,** *160* (4), 785.

(37) Trueta, C.; De-Miguel, F. F. Extrasynaptic exocytosis and its mechanisms: a source of molecules mediating volume transmission in the nervous system. *Frontiers in Physiology* **2012,** *3*.

(38) Ying, Y. L.; Ding, Z. F.; Zhan, D. P.; Long, Y. T. Advanced electroanalytical chemistry at nanoelectrodes. *Chem Sci* **2017,** *8* (5), 3338.

(39) Kurbanoglu, S.; Ozkan, S. A. Electrochemical carbon based nanosensors: A promising tool in pharmaceutical and biomedical analysis. *J Pharmaceut Biomed* **2018,** *147*, 439.

(40) Noked, M.; Soffer, A.; Aurbach, D. The electrochemistry of activated carbonaceous materials: past, present, and future. *J Solid State Electr* **2011,** *15* (7-8), 1563.

(41) Hiremath, N.; Mays, J.; Bhat, G. Recent Developments in Carbon Fibers and Carbon Nanotube-Based Fibers: A Review. *Polym Rev* **2017,** *57* (2), 339.

(42) Yang, C.; Denno, M. E.; Pyakurel, P.; Venton, B. J. Recent trends in carbon nanomaterial-based electrochemical sensors for biomolecules: A review. *Anal Chim Acta* **2015,** *887*, 17.

(43) Henstridge, M. C.; Compton, R. G. Mass Transport to micro- and nanoelectrodes and their arrays: a review. *Chem Rec* **2012,** *12* (1), 63.

(44) Kita, J. M.; Wightman, R. M. Microelectrodes for studying neurobiology. *Curr Opin Chem Biol* **2008,** *12* (5), 491.

(45) Clark, J. J.; Sandberg, S. G.; Wanat, M. J.; Gan, J. O.; Horne, E. A.; Hart, A. S.; Akers, C. A.; Parker, J. G.; Willuhn, I.; Martinez, V.et al. Chronic microsensors for longitudinal, subsecond dopamine detection in behaving animals. *Nat Methods* **2010,** *7* (2), 126.

(46) Lama, R. D.; Charlson, K.; Anantharam, A.; Hashemi, P. Ultrafast detection and quantification of brain signaling molecules with carbon fiber microelectrodes. *Anal Chem* **2012,** *84* (19), 8096.

(47) Jaquins-Gerstl, A.; Michael, A. C. A review of the effects of FSCV and microdialysis measurements on dopamine release in the surrounding tissue. *Analyst* **2015,** *140* (11), 3696.

(48) Stamford, J. A.; Kruk, Z. L.; Millar, J. Regional Differences in Extracellular Ascorbic-Acid Levels in the Rat-Brain Determined by High-Speed Cyclic Voltammetry. *Brain Research* **1984,** *299* (2), 289.

(49) Howell, J. O.; Kuhr, W. G.; Ensman, R. E.; Wightman, R. M. Background Subtraction for Rapid Scan Voltammetry. *J Electroanal Chem* **1986,** *209* (1), 77.

(50) Atcherley, C. W.; Laude, N. D.; Parent, K. L.; Heien, M. L. Fast-Scan Controlled-Adsorption Voltammetry for the Quantification of Absolute Concentrations and Adsorption Dynamics. *Langmuir* **2013,** *29* (48), 14885.

(51) Atcherley, C. W.; Wood, K. M.; Parent, K. L.; Hashemi, P.; Heien, M. L. The coaction of tonic and phasic dopamine dynamics. *Chem Commun* **2015,** *51* (12), 2235.

(52) Abdalla, A.; Atcherley, C. W.; Pathirathna, P.; Samaranayake, S.; Qiang, B. D.; Pena, E.; Morgan, S. L.; Heien, M. L.; Hashemi, P. In Vivo Ambient Serotonin Measurements at Carbon-Fiber Microelectrodes. *Analytical Chemistry* **2017,** *89* (18), 9703.

(53) Nandi, P.; Lunte, S. M. Recent trends in microdialysis sampling integrated with conventional and microanalytical systems for monitoring biological events: A review. *Anal Chim Acta* **2009,** *651* (1), 1.

(54) Saylor, R. A.; Lunte, S. M. A review of microdialysis coupled to microchip electrophoresis for monitoring biological events. *J Chromatogr A* **2015,** *1382*, 48.

(55) Rodeberg, N. T.; Sandberg, S. G.; Johnson, J. A.; Phillips, P. E. M.; Wightman, R. M. Hitchhiker's Guide to Voltammetry: Acute and Chronic Electrodes for in Vivo Fast-Scan Cyclic Voltammetry. *Acs Chemical Neuroscience* **2017,** *8* (2), 221.

(56) Zachek, M. K.; Takmakov, P.; Park, J.; Wightman, R. M.; McCarty, G. S. Simultaneous monitoring of dopamine concentration at spatially different brain locations in vivo. *Biosens Bioelectron* **2010,** *25* (5), 1179.

(57) Howard, C. D.; Keefe, K. A.; Garris, P. A.; Daberkow, D. P. Methamphetamine neurotoxicity decreases phasic, but not tonic, dopaminergic signaling in the rat striatum. *J Neurochem* **2011,** *118* (4), 668.

(58) Kaplan, S. V.; Limbocker, R. A.; Levant, B.; Johnson, M. A. Regional differences in dopamine release in the R6/2 mouse caudate putamen. *Electroanal* **2018,** *30* (6), 1066.

(59) Hashemi, P.; Dankoski, E. C.; Petrovic, J.; Keithley, R. B.; Wightman, R. M. Voltammetric detection of 5-hydroxytryptamine release in the rat brain. *Anal Chem* **2009,** *81* (22), 9462.

(60) Samaranayake, S.; Abdalla, A.; Robke, R.; Wood, K. M.; Zeqja, A.; Hashemi, P. In vivo histamine voltammetry in the mouse premammillary nucleus. *Analyst* **2015,** *140* (11), 3759.

(61) Ross, A. E.; Venton, B. J. Nafion-CNT coated carbon-fiber microelectrodes for enhanced detection of adenosine. *Analyst* **2012,** *137* (13), 3045.

(62) Cryan, M. T.; Ross, A. E. Subsecond detection of guanosine using fast-scan cyclic voltammetry. *Analyst* **2018,** *144* (1), 249.

(63) Schmidt, A. C.; Dunaway, L. E.; Roberts, J. G.; McCarty, G. S.; Sombers, L. A. Multiple Scan Rate Voltammetry for Selective Quantification of Real-Time Enkephalin Dynamics. *Analytical Chemistry* **2014,** *86* (15), 7806.

(64) Sanford, A. L.; Morton, S. W.; Whitehouse, K. L.; Oara, H. M.; Lugo-Morales, L. Z.; Roberts, J. G.; Sombers, L. A. Voltammetric Detection of Hydrogen Peroxide at Carbon Fiber Microelectrodes. *Analytical Chemistry* **2010,** *82* (12), 5205.

(65) Saylor, R. A.; Hersey, M.; West, A.; Buchanan, A. M.; Berger, S. N.; Nijhout, H. F.; Reed, M. C.; Best, J.; Hashemi, P. In vivo Hippocampal Serotonin Dynamics in Male and Female Mice: Determining Effects of Acute Escitalopram Using Fast Scan Cyclic Voltammetry. *Front Neurosci* **2019,** *13*, 362.

(66) Wood, K. M.; Hashemi, P. Fast-scan cyclic voltammetry analysis of dynamic serotonin reponses to acute escitalopram. *ACS Chem Neurosci* **2013,** *4* (5), 715.

(67) Abdalla, A.; West, A.; Jin, Y.; Saylor, R.; Qiang, B.; Peña, E.; Linden, D. J.; Nijhout, H. F.; Reed, M. C.; Best, J.et al. Fast Serotonin Voltammetry as a Versatile Tool for Mapping Dynamic Tissue Architecture: I. Responses at Carbon Fibers Describe Local Tissue Physiology. *Journal of Neurochemistry* **2019,** *0* (ja).

(68) Pathirathna, P.; Yang, Y.; Forzley, K.; McElmurry, S. P.; Hashemi, P. Fast-scan deposition-stripping voltammetry at carbon-fiber microelectrodes: real-time, subsecond, mercury free measurements of copper. *Anal Chem* **2012,** *84* (15), 6298.

(69) Pathirathna, P.; Siriwardhane, T.; McElmurry, S. P.; Morgan, S. L.; Hashemi, P. Fast voltammetry of metals at carbon-fiber microelectrodes: towards an online speciation sensor. *Analyst* **2016,** *141* (23), 6432.

(70) Pathirathna, P.; Siriwardhane, T.; Morgan, S. L.; McElmurry, S. P.; Hashemi, P. Fast voltammetry of metals at carbon-fiber microelectrodes: rapid determination of solution formation constants. *Analyst* **2016,** *141* (21), 6025.

(71) Pathirathna, P.; Samaranayake, S.; Atcherley, C. W.; Parent, K. L.; Heien, M. L.; McElmurry, S. P.; Hashemi, P. Fast voltammetry of metals at carbon-fiber

microelectrodes: copper adsorption onto activated carbon aids rapid electrochemical analysis. *Analyst* **2014,** *139* (18), 4673.

(72) Siriwardhane, T.; Sulkanen, A.; Pathirathna, P.; Tremonti, A.; McElmurry, S. P.; Hashemi, P. Voltammetric Characterization of Cu(II) Complexation in Real-Time. *Anal Chem* **2016,** *88* (15), 7603.

(73) Siriwardhane, T.; Ou, Y. G.; Pathirathna, P.; Hashemi, P. Analysis of Electrochemically Elusive Trace Metals with Carbon Fiber Microelectrodes. *Analytical Chemistry* **2018,** *90* (20), 11917.

(74) Yang, Y. Y.; Pathirathna, P.; Siriwardhane, T.; McElmurry, S. P.; Hashemi, P. Real-Time Subsecond Voltammetric Analysis of Pb in Aqueous Environmental Samples. *Analytical Chemistry* **2013,** *85* (15), 7535.

(75) Adenier, A.; Chehimi, M. M.; Gallardo, I.; Pinson, J.; Vila, N. Electrochemical oxidation of aliphatic amines and their attachment to carbon and metal surfaces. *Langmuir* **2004,** *20* (19), 8243.

(76) Alhedabi, T.; Cattey, H.; Roussel, C.; Blondeau-Patissier, V.; Gharbi, T.; Herlem, G. Experimental and theoretical studies on electropolymerization of polar amino acids on platinum electrode. *Mater Chem Phys* **2017,** *185*, 183.

(77) Barbier, B.; Pinson, J.; Desarmot, G.; Sanchez, M. Electrochemical Bonding of Amines to Carbon-Fiber Surfaces toward Improved Carbon-Epoxy Composites. *J Electrochem Soc* **1990,** *137* (6), 1757.

(78) Deinhammer, R. S.; Ho, M.; Anderegg, J. W.; Porter, M. D. Electrochemical Oxidation of Amine-Containing Compounds - a Route to the Surface Modification of Glassy-Carbon Electrodes. *Langmuir* **1994,** *10* (4), 1306.

(79) Mistlberger, G.; Crespo, G. A.; Bakker, E. Ionophore-Based Optical Sensors. *Annu Rev Anal Chem* **2014,** *7*, 483.

(80) Kamenica, M.; Kothur, R. R.; Willows, A.; Patel, B. A.; Cragg, P. J. Lithium Ion Sensors. *Sensors-Basel* **2017,** *17* (10).

(81) Yang, Y.; Ibrahim, A. A.; Hashemi, P.; Stockdill, J. L. Real-Time, Selective Detection of Copper(II) Using Ionophore-Grafted Carbon-Fiber Microelectrodes. *Anal Chem* **2016,** *88* (14), 6962.

(82) Kishida, K. T.; Saez, I.; Lohrenz, T.; Witcher, M. R.; Laxton, A. W.; Tatter, S. B.; White, J. P.; Ellis, T. L.; Phillips, P. E.; Montague, P. R. Subsecond dopamine fluctuations in human striatum encode superposed error signals about actual and counterfactual reward. *Proc Natl Acad Sci U S A* **2016,** *113* (1), 200.

(83) Shi, Y.; Inoue, H.; Wu, J. C.; Yamanaka, S. Induced pluripotent stem cell technology: a decade of progress. *Nat Rev Drug Discov* **2017,** *16* (2), 115.

(84) Lu, J.; Zhong, X.; Liu, H.; Hao, L.; Huang, C. T.; Sherafat, M. A.; Jones, J.; Ayala, M.; Li, L.; Zhang, S. C. Generation of serotonin neurons from human pluripotent stem cells. *Nat Biotechnol* **2016,** *34* (1), 89.

(85) Hughes, G.; Pemberton, R. M.; Fielden, P. R.; Hart, J. P. The design, development and application of electrochemical glutamate biosensors. *Trac-Trend Anal Chem* **2016,** *79*, 106.

(86) Kozai, T. D. Y.; Jaquins-Gerstl, A. S.; Vazquez, A. L.; Michael, A. C.; Cui, X. T. Brain Tissue Responses to Neural Implants Impact Signal Sensitivity and Intervention Strategies. *Acs Chemical Neuroscience* **2015,** *6* (1), 48.

(87) Putzbach, W.; Ronkainen, N. J. Immobilization Techniques in the Fabrication of Nanomaterial-Based Electrochemical Biosensors: A Review. *Sensors-Basel* **2013,** *13* (4), 4811.

(88) Liu, X.; Luo, L. Q.; Ding, Y. P.; Ye, D. X. Poly-glutamic acid modified carbon nanotube-doped carbon paste electrode for sensitive detection of L-tryptophan. *Bioelectrochemistry* **2011,** *82* (1), 38.

(89) Yu, A. M.; Chen, H. Y. Electrocatalytic oxidation of hydrazine at the poly(glutamic acid) chemically modified electrode and its amperometric determination. *Anal Lett* **1997,** *30* (3), 599.

(90) Okubo, Y.; Sekiya, H.; Namiki, S.; Sakamoto, H.; Iinuma, S.; Yamasaki, M.; Watanabe, M.; Hirose, K.; Iino, M. Imaging extrasynaptic glutamate dynamics in the brain. *P Natl Acad Sci USA* **2010,** *107* (14), 6526.

(91) Szapiro, G.; Barbour, B. Multiple climbing fibers signal to molecular layer interneurons exclusively via glutamate spillover. *Nature Neuroscience* **2007,** *10* (6), 735.

(92) Dzubay, J. A.; Jahr, C. E. The concentration of synaptically released glutamate outside of the climbing fiber-Purkinje cell synaptic cleft. *Journal of Neuroscience* **1999,** *19* (13), 5265.

CHAPTER 2

NOVEL FRONTIERS IN VOLTAMMETRIC TRACE METAL ANALYSIS: TOWARDS REAL TIME, ON-SITE, *IN SITU* MEASUREMENTS[1]

[1] **Holmes, J.;** Pathirathna, P.; Hashemi, P.: "Novel frontiers in voltammetric trace metal analysis: Towards real time, on-site, in situ measurements." *Trac-Trend Anal Chem* 2019, *111*, 206-219.

2.1 Abstract

Metal speciation analysis has wide applicability and reveals how and when metals are available to engage in chemical processes. Real systems can be physically hard to reach, chemically dynamic, and sample collection and pretreatment fundamentally alter speciation. Therefore, there is great interest in *in situ* trace metal speciation sensors that can be integrated into on-site, portable analysis devices. Electrochemistry is an attractive method since the sensing component can be fashioned into a submersible probe. In this review, we define a set of criteria that an electrochemical approach must conform to for *in situ* metal analysis and review methods that closely follow these criteria. As an emerging technique, fast-scan cyclic voltammetry is introduced. Next design and material of analysis probes is detailed, followed by a discussion of portable instrumentation. Finally, studies that show promise towards a portable, *in situ* metal analysis device are showcased and ongoing analytical challenges are outlined.

2.2 Introduction

Trace metals play critical roles in environmental processes as well as in manufacturing and other industrial practices. To better understand and control these systems, it is desirable to analytically determine the concentration of 'free' metal, or speciation. Speciation, as defined by the International Union of Pure and Applied Chemistry (IUPAC), is 'the distribution of an element amongst defined chemical species in a system." Isolating analytical measurements to one specific chemical species, in this case, electrolabile or hexa-aqua complexed metals is best because of the likelihood of 'free' metals to engage chemical and biological processes.[1] Furthermore, speciation can

be dynamic,[2-7] thus the most useful measurement would be at high time resolution. For example, storm drainage or runoff can introduce metal ions into natural water systems quickly, where their presence is pervasive and damaging to ecological and human health. Additionally, discharge of industrial effluents that include metals (widely used as catalysts and components) often lead to rapid environmental contamination and pollution.

With reference to analysis, it is important here to define the difference between on-site and *in situ* measurements. On-site indicates that the data acquisition platform is portable, allowing analysis to be performed at the site of interest, whereas *in situ* signifies that the sensor is directly probing the ambient environment of its sample (*i.e.* sample is not collected). Thus, the most useful analytical speciation data would qualify as both on-site and *in situ.* However, methods that can provide on-site, *in situ* speciation data are severely limited.[8] This is because of the difficulty of accessing hard to reach environmental systems, in addition to the complexity of real matrices. Additionally, natural organic matter (NOM), other natural ligands, and interfering metals can lead to fouling, clogged membranes and probes, and masked detection of the target analyte.[9-11]

Spectroscopic techniques coupled with chromatography, have been used on-site in mobile laboratories, for trace metal analysis because of their excellent sensitivity and reproducibility.[12,13] *In situ* analysis here is challenging though because of bulky instrumentation and high energy needs. In addition, sample collection and pretreatment alter speciation.[4,14,15]

Electrochemical techniques are portable, and show more promise for *in situ* analysis because electrodes can be immersed into samples of interest with minimal

perturbation. In this work, we identify a set of critical criteria the sensing probe must conform to for *in situ* analysis, originally coined the 4 S's: sensitivity, selectivity, size, and speed, plus two additional ones we add here, stability and safe materials.[16] Methods that closely follow these criteria are reviewed, with a focus on voltammetric analysis because most voltammetry modes fulfill 5 or more of our criteria. Specifically, fast-scan cyclic voltammetry is highlighted as an emerging technique. The design and material of analysis probes is detailed with respect to probe size, disposable vs. reusable probes, surface functionalization, and material toxicity. Finally, portable electrochemical instrumentation and ongoing challenges associated with on site, *in situ* analysis are discussed. Overall, this review identifies a current technological gap for *in situ*, on site metal detection and provides an in-depth account of recent, promising developments in electrochemical methods towards this type of analysis.

2.3 Criteria for On-site, *In Situ* Analysis - The 6 S's

The electrochemical sensing component of an *in situ* trace metal sensor should ideally conform to 6 conditions; we coin these benchmarks the 6 S's: sensitivity, selectivity, size, stability, safe materials and speed. Many electrolabile metals of interest are present at trace concentrations (<1 parts per million) and are similarly sized and charged, for example Hg(II), Cu(II), Pb(II), and Cd(II) are all divalent cations, thereby high analytical **sensitivity** and **selectivity** are essential. The **size** of the sensing probe is critical when sampling delicate or elusive systems. Due to the inability to control the sensor's environment, limited opportunities to calibrate on-site, and tendency for fouling, a high degree of signal **stability** and reproducibility must be maintained. Historically, the majority of metal analysis employs Hg as the sensing component; the risks associated

with Hg however have necessitated a new generation of Hg-free, **safe electrode materials.**

The most challenging criteria remains **speed**. Under unremarkable circumstances, an analysis temporal resolution of several minutes is acceptable for risk assessment and safety. However, aqueous metal chemistry can change dynamically in response to tides, storms and effluent discharge where minute to minute analysis is advantageous.[15,17-19] Furthermore, sub-minute analysis is needed to observe chemical changes associated with more delicate processes, such as microbial respiration, that would labilize or complex metals in specific systems quickly.[20,21] Speed is a challenging and complex facet of metal detection. For traditional metal electroanalysis, diffusion, equilibration, nucleation/growth and stripping are time consuming processes but are the price of ultra-high (parts per trillion) sensitivity. It has been greatly challenging to reach an analytical compromise that delivers on both speed and sensitivity, in addition to the other criteria. Furthermore, other considerations to address for *in situ* sensing include: minimal sample treatment, insensitivity to pressure changes, dissolved oxygen, unpredictable flow, and biofouling.

2.4 Voltammetric Techniques

2.4.1 Stripping Voltammetry

Stripping Voltammetry (SV) is the most widely used electroanalytical technique for trace metal analysis. It is generally performed using the steps shown in **Figure 2.1**. Two waveform application modes of stripping voltammetry, square wave anodic stripping voltammetry (SWASV) and differential pulse anodic stripping voltammetry

(DPASV), have been extensively employed for trace metal monitoring mainly due to heightened sensitivity, decreased analysis time, and the ability to make measurements in the presence of dissolved oxygen, given acidified or well buffered media.[22,23]

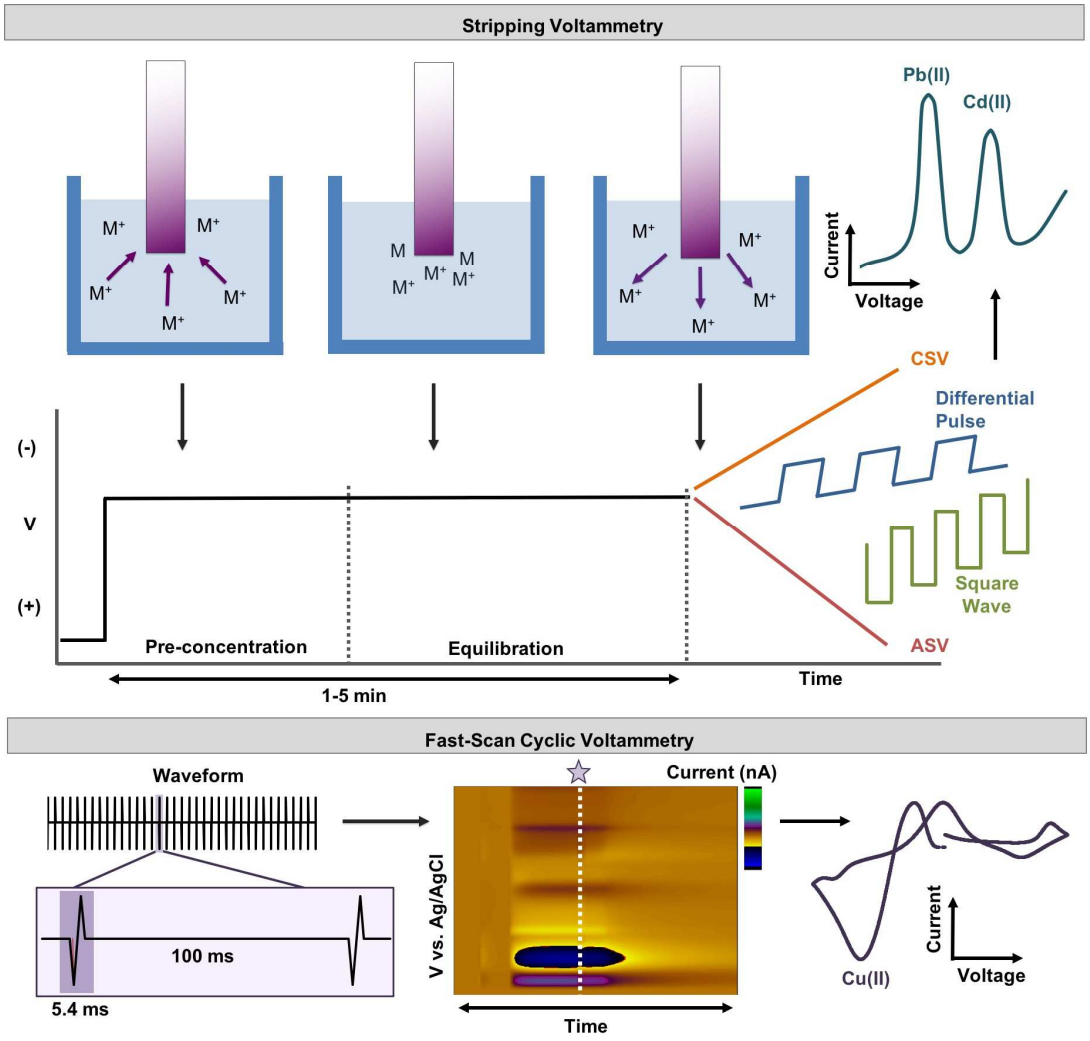

Figure 2.1. Scheme of the main voltammetric techniques and modulations used for metal analysis. In SV, a discrete potential is applied to attract and deposit the analyte of interest onto the electrode surface for up to several minutes. Then the deposited metal is stripped off the surface by ramping the potential in the positive (anodic stripping voltammetry (ASV)) or negative (cathodic stripping voltammetry (CSV)) direction. In FSCV, a unique cyclic waveform, specific to the metal of interest, is applied every 100 ms. The output of both techniques results in a voltammogram with peaks at distinct potentials for each metal ion.

2.4.1.1 SV Sensitivity, Selectivity and Speed

SV is an extremely sensitive electroanalytical method because of the lengthy pre-concentration step, allowing the maximum concentration analyte to deposit onto the electrode surface prior to analysis. Additionally, SV facilitates multi-elemental analysis because different metals can be stripped off the electrode surface at different discrete energies, giving SV a fundamental advantage in selectivity.

The temporal resolution of SV is limited by the lengthy preconcentration step, optimized with respect to holding potential and deposition time for each target analyte, electrode material and matrix for analysis. As speed is often times compromised for sensitivity, a preconcentration time of 1-20 minutes is standard. For this reason, stripping voltammetry is extremely effective for measuring resting metal concentrations; however collecting real-time information in dynamically changing systems is still a difficult task. Limits of detection and temporal resolution for all of the studies discussed in this review are listed in **Table 2.1.**

2.4.2 Fast-Scan Cyclic Voltammetry

Cyclic voltammetry is perhaps the most generally applied voltammetric method throughout various scientific disciplines, though is less prevalent for metal analysis because traditionally there is not sufficient sensitivity[22] and to the best of our knowledge, there have not been any studies in the last decade with the potential for *in situ* measurements. Instead, a unique mode of cyclic voltammetry called fast-scan cyclic voltammetry (FSCV) has emerged as a promising approach for environmental analysis to fulfill the 6 S's.

2.4.2.1 FSCV Sensitivity, Selectivity and Speed

FSCV utilizes scan rates typically from 100 - 2500 V s^{-1} and is most commonly used among neuroscientists to quantify small, cationic biomolecules at low concentrations and high time resolution with carbon fiber microelectrodes (CFMs).[24] In recent years the sensitivity, rapidity and relative simplicity of this method have been exploited to make trace metal measurements. FSCV was first introduced in 2012 and 2013 as an electrochemical tool for real-time quantification of aqueous, laboratory Cu(II) and storm water Pb (II) samples.[25,26]

Selectivity between biological analytes has thus far been achieved via optimization of detection waveforms based on the electron transfer kinetics of different species [27-29]. Unlike SV, FSCV peaks do not provide good selectivity for multielemental analysis because they are broad (due to fast scan rates). For this reason, surface functionalization of the electrode surface with an ion-specific ionophore has been used to boost selectivity of the probe in the presence of interfering metal ions (*vida infra*). Furthermore, with limits of detection (LOD) in the low ppb's for Cu(II) and low ppm's for Pb(II), improvements are in process for environmental monitoring for Pb(II) *via* modification with ionophores.[30]

The temporal resolution of FSCV is the most striking feature of this technique, as typically, CVs are collected every 100 ms. Because metal analysis on metal electrodes can be slow (minutes to 10s of minutes to allow for nucleation/growth preconcentration), the phenomenon of the rapid response on CFMs was underpinned by a thermodynamically favorable adsorption equilibrium of metal (similar to small cationic

biomolecules) to oxygen functionalities on the activated CFM. This adsorption is rapid enough such that 100 ms is sufficient for monolayer adsorption that enabled adequate preconcentration for parts per billion analysis.[31]

FSCV is able to report metal speciation because the original waveforms were optimized to investigate authentic, non-acidified samples. This is a particularly important characteristic of this method since the majority of studies included in this review require significant sample pre-treatment and/or acidification. Furthermore, since authentic systems are usually chemically dynamic, the temporal resolution of this method paves the way for real-time analysis. This was evidenced in **Figure 2.2** by measuring rapid changes in Cu(II) complexation (speciation) in real-time with respect to 5 ligands with differing formation constants of Ligand – Cu(II) binding.[32] In this experiment a near complete complexation reaction was captured in under a minute (**panel B**). To put this into context, the fastest of the other available methods provide readings every minute at best and could not capture these events.

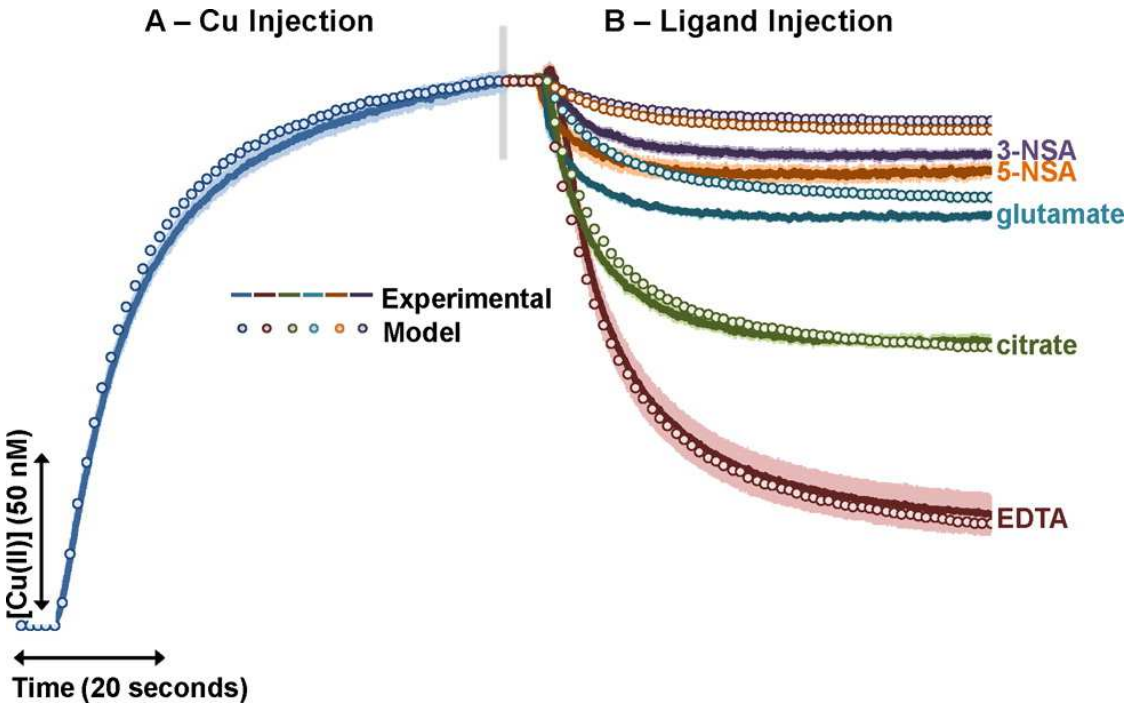

Figure 2.2. Real-time complexation analysis with FSCV. (A) An injection of 1 μM Cu $(NO_3^-)^2$ was allowed to reach a steady state, followed by **(B)** an injection of 5 metal ligands with known formation constants. The complexation of Cu binding can be seen in real-time to each ligand and closely followed a model of this response. Reprinted with permissions from T. Siriwardhane, A. Sulkanen, P. Pathirathna, A. Tremonti, S.P. McElmurry, P. Hashemi, Anal Chem, 88 (2016) 7603-7608. Copyright © 2016 American Chemical Society.

2.4.2.2 FSCV Analysis Modes

The high rates of scanning between potentials creates a large, capacitive current, which must be subtracted out to analyze Faradaic processes during FSCV measurements. This has traditionally meant that FSCV could not provide ambient, or basal, measurements, a major hindrance for trace metal studies. To overcome this limitation, fast-scan controlled adsorption voltammetry (FSCAV) was developed to directly measure absolute analyte concentrations *in vitro* and *in vivo*.[33,34] FSCAV differs from FSCV in that a controlled adsorption period is integrated, in which maximum adsorption of the analyte is achieved. An ambient measurement can be collected every 30 seconds, an improvement on the temporal resolution of SV (1-5 min).

To demonstrate the applicability of fast voltammetry for fast speciation analysis, FSCAV was employed to identify electrolabile Cu(II) in complex matrices and a mathematical relationship (**Figure 2.3**) was constructed to explain the correlation between FSCAV current, free Cu(II), and the formation constants of different Cu(II) binding ligands. By measuring electrolabile Cu(II), this model successfully predicted the formation constant of an unknown ligand in seconds.[35]

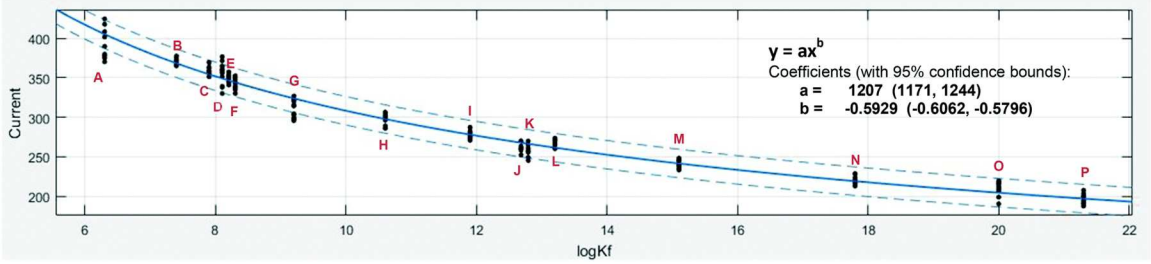

Figure 2.3. The FSCAV response and formation constants for 16 different Cu(II) – ligand complexes fit to an exponential curve. Reprinted with permissions from P. Pathirathna, T. Siriwardhane, S.L. Morgan, S.P. McElmurry, P. Hashemi, Analyst, 141 (2016) 6025-6030. Copyright © 2016 American Chemical Society.

2.5 Electrochemical Probe Design and Material

2.5.1 Size

Electrode configuration and size both the influence the sensitivity and the reproducibility of a given method and greatly play into feasibility for on-site studies. Microelectrodes are generally considered to have dimensions no greater than 25 µm and exhibit enhanced sensitivity for monitoring small molecules. Additionally, small, low-cost disposable sensors have since emerged as an attractive approach for preventing fouling in complex media and replacing the electrode for subsequent measurement. Screen printed electrodes and lab-on-a-chip technology possess innovative and portable sensing platforms that are promising for on-site environmental analysis.

2.5.1.1 Microelectrodes

A cylindrical carbon fiber microelectrode (CFM) is typically used to perform fast voltammetry, ranging from 5-10 µm in diameter and 0-150 µm in length. The advantageous features of CFMs include improved mass transport of analyte to the electrode surface facilitated by hemispherical diffusion, low iR drop, low charging current, and high signal to noise ratio. The hemispherical diffusion of microelectrodes

increases the mass transport to the electrode surface and mimics convection, thus a non-zero steady state current is obtained quickly and stirring becomes negligible, a benefit for *in situ* sensing.[36,37] The low iR drop and high signal to noise ratio permits measurements in high resistance environments such as low-ionic strength media without need for addition of a supporting electrolyte (i.e. no sample pretreatment).[37-39] Furthermore, using SV, microelectrode arrays (MEA) have become a particularly useful tool for multi-elemental analysis.[40-44]

2.5.1.2 Screen Printed Electrodes

The introduction of screen-printed electrodes **(SPEs)** was a major breakthrough for the development of portable tools and devices for rapid trace metals measurements.[45] While screen printing technology is not novel in itself, researchers from different fields have innovated several methods of designing and fabricating low-cost SPE sensors. In general, SPEs are comprised of a 3-electrode system, screen printed on a chemically inert substrate.[46,47] The fabrication process typically involves a surface modification step, serving to change the composition of the working electrode and enhance electrochemical responses.[47,48] SPEs can take the form of a stick, disk, or wafer, and one platform can include up to 300 replaceable sensors.[43,49] One unique substrate, microfluidic paper-based analytical device (μPAD), has emerged as a simple, inexpensive option with potential for commercialization.[50] While most often coupled with colorimetry,[51-57] more voltammetry-based μPADs have been developed (**Figure 2.4**) and show great promise for on-site trace metal monitoring.[58-63]

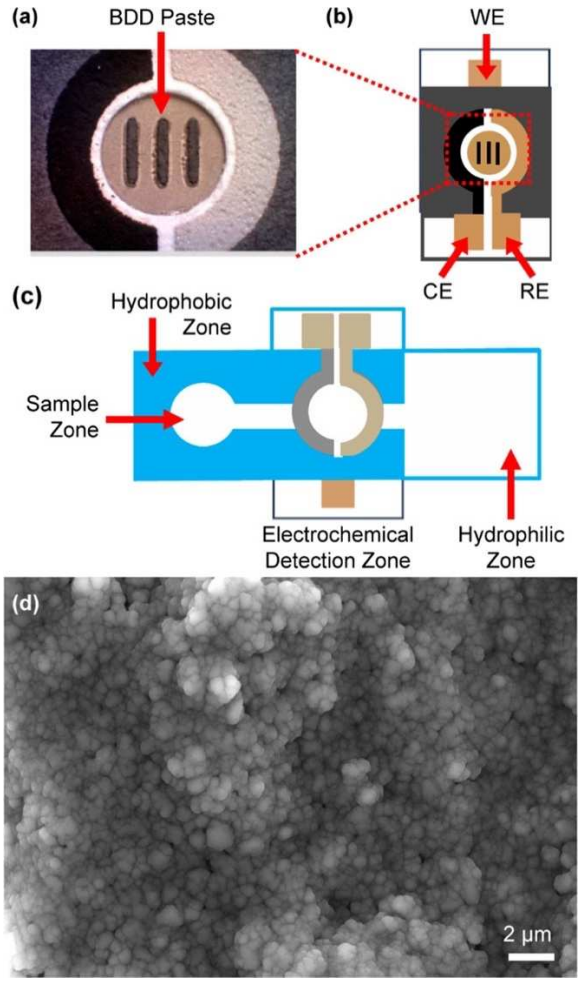

Figure 2.4. Scheme of a Boron Doped Diamond Paste Electrode (BDDPE) on an electrochemical paper based analytical device. (a) photograph of the BDDPE **(b)** 3-electrode system is screen printed onto a paper substrate as the electrochemical sensing component **(c)** design of sampling microfluidic paper device **(d)** SEM image of Boron Doped Diamond Paste surface structure. Reprinted with permission from S. Nantaphol, R.B. Channon, T. Kondo, W. Siangproh, O. Chailapakul, C.S. Henry, Anal Chem, 89 (2017) 4100-4107. Copyright © 2017 American Chemical Society

2.5.1.3 Lab on a Chip

Lab-on-a-chip (LOC) is another attractive approach for on-site analysis because multiple steps, including sampling, separation, and detection, can be combined on a single analysis platform.[64-66] LOCs satisfy the recent trend in miniaturizing electrochemical systems[67] and incorporating microfluidics for environmental analysis, as

seen in **Figure 2.5**. The automated nature of microchips and the small quantity of reagent, sample, and time necessary for multiple measurements show promise for field portable environmental monitoring. A key advantage of LOC technology is versatility, as they can incorporate a suite of analysis modes and electrode materials to enhance sensitivity and allow for multicomponent analysis. Commercially available microchips are generally inexpensive, thus a number of both disposable and renewable working electrochemical sensing platforms have been used including planar Bi, Bi film and Ag rotary disk electrodes.[49,68-72] Such methods are effective for distinguishing between similar divalent ions, Cd(II) and Pb(II), in natural waters.[49,73] One notable study incorporated Bi-MEAs on a disposable LOC device for analyzing Pb(II), Cd(II), and Ni(II) concentrations in lake and tap water.[41,42]

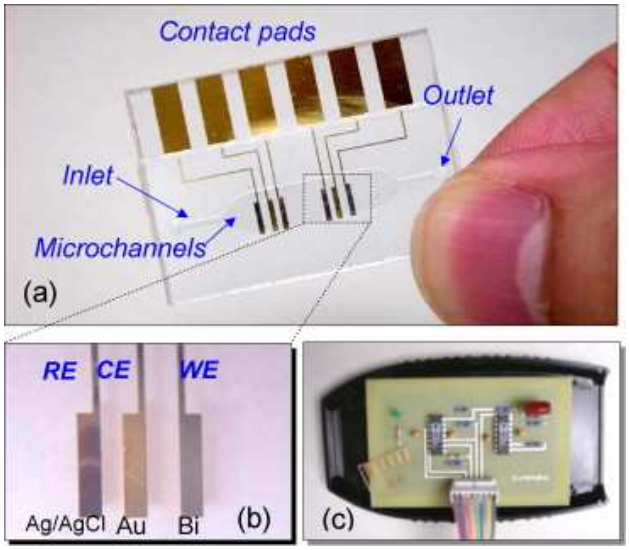

Figure 2.5. Representative assembly of a three-electrode system, microfluidic channels, and customized detection circuits fabricated onto a microchip. Reprinted from Sensors and Actuators, B: Chemical, 134, Z.W. Zou, A. Jang, E. MacKnight, P.M. Wu, J. Do, P.L. Bishop, C.H. Ahn, Environmentally friendly disposable sensors with microfabricated on-chip planar bismuth electrode for *in situ* heavy metal ions measurement, 18-24, Copyright (2008) with permission from Elsevier.

In recent articles reviewing LOCs use for aquatic ecotoxicology, the authors note that LOCs are relatively newer technologies, underutilized for environmental monitoring due to the many logistical challenges that limit their robustness for raw samples, including pressure resistance, air bubbles and clogging within the microfluidic channels, operational complexity, and unsuitability for large or complex samples.[74,75] Additionally, the need for sample preparation is eliminated for some natural water samples such as acid mine drainage that have low pH, however, for samples with higher pH that needs adjustment, speciation is altered,[15] and ultimately compromises the integrity of the sample. Thus, there are ongoing efforts to create sensors that are more robust, easy to use, and do not require sample preparation to make LOCs applicable for on-site analysis.

2.5.2 Stability

There have long been efforts to minimize fouling and improve stability because natural systems are complex and rich in organic material that can poison electrode surfaces. Moreover, metals themselves are prone to build up on and foul the electrode. A highly reproducible electrode response can be garnered using dropping Hg electrodes, which reproducibly preconcentrate analytes of interest as an amalgam.[76-78] However, for toxicity reasons there has been significant impetus to develop alternate strategies. Here we highlight two recent approaches for designing electrodes that afford high reproducibility: one that is based on low-cost disposable sensors and the other that focuses on sensing materials with a renewable surface. Disposable sensors including SPEs and LOCs are popular for simple, portable sensing. Briefly, the sensing component is printed and a stable film of Hg, Bi, or Sb is deposited on top; this significantly curbs toxicity issues since the coating is contained. This approach facilitates reproducibility but

not stability since the majority of amalgam and fused alloy-based sensors do not allow for repeated measurements on one device. While attractive for its simplicity and reproducibility, this strategy can be tedious, especially since often times submersed probes are difficult to frequently access and replace. Additionally, measurements cannot be automated to continuously monitor the site of interest, because it is necessary to replace the sensing component in the probe between each measurement.

For all electrode materials, biofouling from natural organic matter and microorganisms is a major limitation for continuous monitoring.[79] In an effort to extend the probes' stability over time, the design and characterization of electrode materials with a renewable surface and efficient cleaning procedure has been explored. Several groups have introduced 'antifouling steps' into the electrochemical waveform to prevent microbial adsorption.[80,81] Often, this involves the generation of biocide gases such as H_2 or Cl_2, however, it is difficult to use in tandem with surface functionalization methods that prevent such reactions from happening or are destroyed from the process. An alternate approach is the incorporation of non-toxic antifouling reagent into surface functionalization process, including zwitterionic or cation exchange polymers[82-86] and peptides for non-specific protein adsorption.[87-89] Though most studies are not applied for environmental metal monitoring, there is great interest in developing marine antifouling coatings[90] without compromising the method's sensitivity or speed.

Materials such as Ag, Au, and carbon have potential to be renewed; target analytes adsorb to the surface in a monolayer and a cleaning step can be incorporated into the voltammetric sweep to oxidize and renew the surface.[31,68,91-93] Using similar materials for the working, reference, and counter electrodes contributes to enhanced regeneration

of Ag, attributed to the movement of Ag ions between electrodes, redepositing and continuously renewing the working electrode.[68] Van Der Berg *et al.* introduced a unique approach by vibrating a microwire electrode of Au or Ag to increase mass transport to the electrode, due to a decrease in the diffusion layer thickness. This method was robust and effective for improved sensitivity and reproducibility for determining speciation of As, Sb, Cu and others.[94-97]

Measurements on CFMs using FSCV are generally stable and reproducible in complex biological matrices,[98] due to a potential cleaning step included to renew the electrode surface between scans. By ramping the applied potential up to and over +1.3 V, the oxygen moieties on CFMs are regenerated, thus re-primed for further adsorption.[91] Studies of surface functionalized CFMs also show voltammetric responses remain stable over 50 consecutive scans and for up to 16 weeks in open air during storage.[30] Additionally, unfunctionalized carbon fibers have been employed for studying monoamines in brain tissue for up to several months at a time.[98] Thus, the stability and reproducibility of the CFM, along with their use in both complex biological (brain tissue) and environmental (rain water) matrices, demonstrates great promise for use in continuous environmental monitoring.

2.5.3 Surface Functionalization

Voltammetry is an inherently selective technique, because metals oxidize or reduce at discrete peak potentials, however in complex matrices, some analytes greatly out-concentrate others, thus some peaks will mask others present at lower concentrations. In these scenarios a much higher level of selectivity must be conferred towards analytes

of interest present in trace quantities. Modifying analysis methods and electrode surfaces with nanoparticles, complexing agents, polymers, and ionophores has emerged as an attractive approach to improve sensitivity and selectivity. However, it is crucial to consider and curb the toxicity of certain additives for this type of analysis. To avoid contamination, any coating or complexing molecule must have low toxicity and form a stable and irreversible attachment to the electrode surface.

Metal nanoparticles are used as an electrode modification material to enhance the sensitivity and limit of detection, due to the rich and porous surface area formed from the single or multilayer coverage.[99-101] A few notable examples of trace metal detection using nanoparticles include Au nanoparticle modified electrodes used to detect Hg(II) in groundwater[102] and Pt nanoparticle electrodes for differentiating inorganic As(III) and As(V) species.[92]

Certain metals are particularly difficult to analyze using voltammetry; Ni(II) and Co(II) are the prime examples of this because these metals do not easily preconcentrate due to irreversible reduction processes, requiring an extremely negative deposition potential (-1.2 V vs. SCE). Furthermore, Ni tends to form intermetallic compounds that co-deposit and generate unpredictable matrix-dependent stripping patterns. Thus, adsorption stripping voltammetry is employed instead. Here, a complexing agent, dimethylglyoxime (DMG), that complexes Ni(II) and Co(II) with high favorability ($K_{f(Ni)} = 10^{17.4}$, $K_{f(Co)} = 10^{12.85}$) facilitates preconcentration onto the electrode.[43,103-107] The toxicity of DMG however makes it a controversial complexing agent for environmental analysis. Similarly, sensitivity is improved for Pb(II) and Cd(II) by incorporating a macrocyclic chelating solid to enhance analyte deposition,[108] and, while most commonly

used with other detection methods, the popularity of DNA, RNA, and proteins as metal complexing agents has risen for use in electrochemical sensors.[109-114] These apta-sensors are still in the early stages of characterization and optimization.

Conductive polymers have been employed to increase selectivity for metal detection, though few studies are applied in the context of rapid *in situ* metal monitoring. Typically, these polymers function *via* charge exclusion. Conductive polymers including polyaniline-poly(2,2'-dithiodianiline) (PANI-PDTDA) doped with S^{-}[115] and Nafion (NA) coupled with DMG and Bi films[106,107,116] have been employed to facilitate selective and simultaneous detection of Hg(II), Pb(II), Ni(II), Co(II), Cd(II), and Zn(II) ions in aerosols and water analysis. Furthermore, ion-imprinted polymers (IIP) and polymeric nanobeads have also been explored as an option for trace metal detection in real water samples based on size exclusion.[117-123] Ion imprinted materials significantly enhance sensitivity and selectivity, however slowed diffusion through the polymer layer necessitates lengthy extraction or preconcentration times (in many cases >10 minutes) and limits this method's applicability.[123-132]

Due to the broad peaks and poor selectivity of metal ion fast voltammetry, a novel surface functionalization method was introduced to covalently modify CFMs with a Cu(II)-selective ionophore.[30] An ionophore was synthesized and covalently bound to the carbon electrode surface via a reductive coupling of a diazonium salt and click chemistry. The top panel of **Figure 2.6** shows the structure of these ionophore-grafted CFMs and the bottom panel displays the enhanced selectivity of the electrodes for Cu(II) in the presence of 8 interfering divalent metals that were 10-times more concentrated. Furthermore, this

surface functionalization improved the method's LOD in comparison to an unfunctionalized CFM.

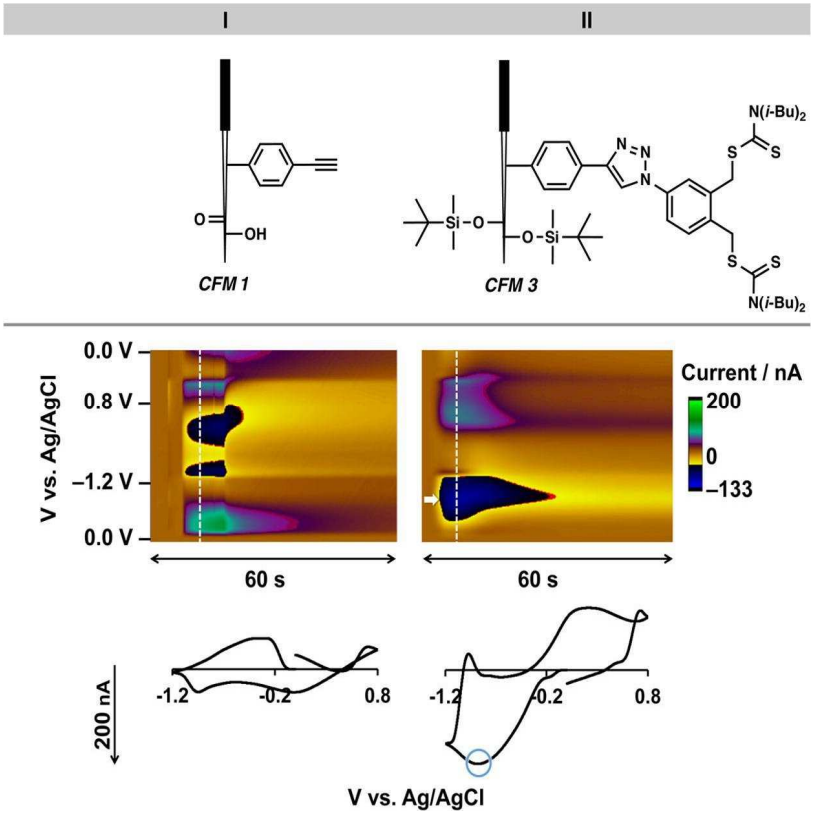

Figure 2.6. Selectivity of ionophore-grafted CFM in the presence of mixed metals. (I) Unfunctionalized CFM show non-faradaic response and **(II)** Ionophore Grafted CFM show clean Cu(II) redox features in a mixed metal solution. Mixed Metal Solution: 1 µM Cu(II) and 10µM each of Zn(II), Cd(II), Ni(II), Co(II), Ca(II), Mg(II), Pb(II), and Mn(II) all with NO_3^- counter ions. Reprinted with permissions from Y. Yang, A.A. Ibrahim, P. Hashemi, J.L. Stockdill, Analytical Chemistry, 88 (2016) 6962-6966. Copyright © 2016 American Chemical Society.

2.5.4 Safe Materials

Hg electrodes have been heavily used among metal analysis groups due to their many attractive features resulting from the stable amalgam formation between Hg and metals. The hanging drop ensures a consistent matrix for nucleation and growth, and provides a new surface for each analysis, hence greatly facilitating reproducibility. This

method is highly sensitive (1 zeptomole with 1 s deposition).[133] The inherent advantageous electrochemical properties of Hg sustains the community's interest in Hg for trace metal monitoring tools. Hg is still used in low concentration as a solid dental amalgam electrode or a thin film as the sensing component for portable trace metal analysis devices.[134-142] Because Hg is toxic to human and aquatic system health, electrochemists have been investigating non-Hg materials as an alternative sensing probe for *in situ* metal analysis.

2.5.4.1 Carbon Electrodes

Because of its excellent electrochemical and mechanical properties, carbon has become one of the most popular solid electrode substrates, often serving as the base sensing component of surface modifications and SPEs.[143,144] The beneficial features of carbon materials include: 1) slow kinetics of carbon oxidation that causes minimal background currents compared to other electrode materials, 2) oxygen functionalities on the carbon surface that ambiently adsorb small cations, 3) ease of chemical modification, 4) a wide potential window, 5) biocompatibility, and 6) the low price and ready-availability of the material.[145-148] For environmental analysis, carbon is an excellent safe material since environmental systems contain large amounts of carbon and are thus not very sensitive to this material. Among different types of carbon materials, glassy carbon, graphite, carbon fibers and new carbon nanomaterials like magneto carbon paste, carbon nanotubes and boron-doped diamond have been employed to develop metal sensors in the last decade.[58,101,116,119,146,149-154] The choice of carbonaceous material depends on the application, the type of analyte and the analysis method. Additionally, as mentioned before, the regeneration and ease of modification of the carbon surface makes this

material much less prone to fouling issues, eliminating the need to replace the sensing component between measurements, and allowing for more continuous environmental monitoring.

2.5.4.2 Bismuth Electrodes

Bi film serves as a greener substitute electrode material for Hg for metal analysis because of the ability to form a multicomponent alloy with metal analytes, analogous to amalgam formation by Hg, that facilitates the nucleation/growth process during the analysis. Insensitivity towards dissolved oxygen eliminates a tedious de-oxygenation step and all-together makes Bi a simple and suitable replacement for Hg.[155]

The efficiency of Bi electrodes is heavily dependent on the design process. Bi electrodes are prepared either by pre-plating Bi on a supporting substrate (*ex situ*) or by adding Bi(III) directly into the sample solution (*in situ* (not to be confused with *in situ* metal analysis as we use frequently in our discussion)) followed by a simultaneous adsorption of Bi and the target metal. Typically, carbonaceous materials are employed as substrates for Bi films including glassy carbon,[156] screen-printed carbon ink,[107,157] graphene,[106,158] and porous carbon composites.[159,160] Additionally, the combination of Bi doped with other materials such as Sb and Ir have been explored for enhancing sensitivity.[156,159,161] Bi has proven useful in a number of environmentally relevant samples including surface,[156,162] and tap waters[160,163] and shows great promise to be used in the field as a reliable material to monitor trace metals.

Although Bi exhibits versatility as a non-toxic electrode material for metal analysis, there are limitations. In particular, the narrow anodic potential window limits

application for multielemental analysis and the insufficient reproducibility of *ex situ* bismuth electrodes necessitates improvement. For these reasons, other electrode materials are also being explored.

2.5.4.3 Antimony Electrodes

The potential window and signals corresponding to model metal ions (Pb(II) and Cd(II)) suggest Sb and Bi alloy formation are similar processes. Consequently, Sb has gained popularity electrode film material for electrochemical stripping analysis of trace metal ions. Sb displays similar or slightly improved sensitivity compared to bismuth, favorable hydrogen evolution, and smaller voltammetric reoxidation than Bi and Hg films, thus lessening interferences near the anodic potential limit. It is easily integrated onto a disposable, commercially available SPE and many groups have coupled Sb film electrode and stripping voltammetry for a variety of applications including, canned foods[164] and water analysis.[165-168] Additionally, many approaches have been explored to determine the best Sb film fabrication method including *in situ,*[167-171] and *ex situ* electrolytic plating,[172,173] Sb nanoparticles,[173] Sb sputtering,[105] fabrication of a macroporous electrode,[174] combination of Sb, Bi, and Sn,[161,170,175-177] and a self-doped co-polymer.[62]

While Sb alloys have yet to be fully characterized, many groups are attempting to understand the mechanism behind Sb's electrochemical properties to improve performance [178,179] and optimize the technique by comparison of carbon substrates as the working electrode base [169,180] and selective measurements in the presence of common interferences.[167,181] At this time, while less toxic than Hg, Sb and its compounds are listed

as priority pollutants,[182] thus the risk associated with using Sb electrodes for *in situ* environmental monitoring still needs to be assessed. Furthermore, Sb is limited to extremely acidic solutions (pH $\leq$ 2), requires nitrogen purging and pretreatment, and preparing *ex situ* Sb film is still challenging thus improvements are necessary for *in situ* analysis.[178] Our discussion is targeted towards portable, *in situ* sensing, however there is an excellent review published in 2018 on emerging "green" metals as electrode materials for trace metal analysis.[183] While *in situ* analysis is not highlighted, these "green" metals would be good candidates for environmental analysis.

2.6 Portable Voltammetric Instrumentation

An *in situ* trace metal speciation sensor should ideally satisfy all 6 S's and thereby be integrated into a portable device for on-site analysis. One commercially available portable system is the voltammetric *in situ* profiling (VIP) system, which incorporates microarrays and submersible sensors to make trace metal concentration measurements with high stability in the field.[22] Bulky instrumentation originally presented challenges, however, this device has been miniaturized and applied to several metal analytes in various applications.[11,184-186] Though, the VIP system is highly sensitive and robust; ongoing challenges include the necessity for an oxygen removal step and safer electrode materials.

Significant progress has also been made towards new portable voltammetric systems by integrating handheld potentiostats, solar panels or batteries, and wireless communication modules as the data acquisition and electrochemical control systems.[49,68,71,137,139,187-190] The integration of injection analysis,[92,108,139,157,175,191] on-chip

automatic sampling and pretreatment, [48,192] and fluid transfer systems controlled by a fluidic motherboard[72] has improved the quality of electrochemical data collected in terms of stability by providing a constant flow of sample and increased mass transfer to the electrode surface. **Figure 2.7** illustrates a representative outline of a total electroanalysis system that is field portable, weighing less than 3 kg.

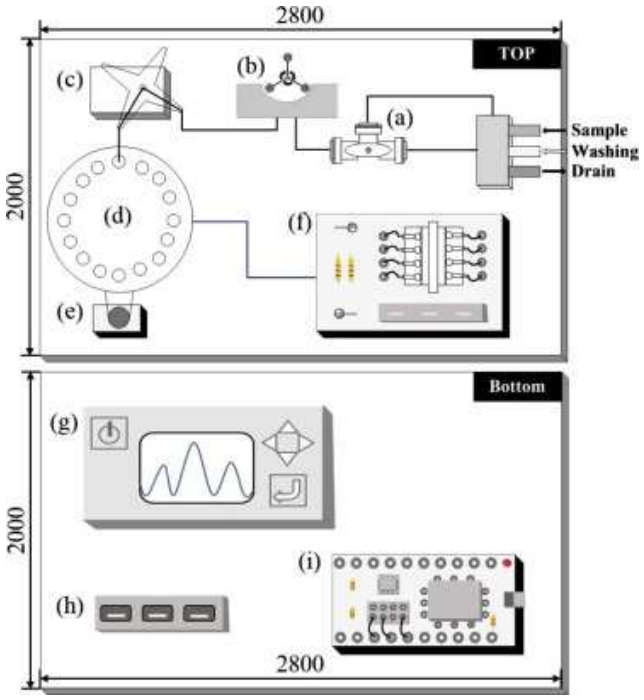

Figure 2.7. Diagram of a total analysis system designed for on-site sensing. Incorporated are microfluidic tubing, a peristaltic pump, a rotary disc voltammetric sensor, portable potentiostat, data acquisition board, electronic controller, and USB and power inputs. Reprinted from Chemosphere, 143, Y.G. Lee, J. Han, S. Kwon, S. Kang, A. Jang, Development of a rotary disc voltammetric sensor system for semi-continuous and on-site measurements of Pb(II), 78-84, Copyright (2016), with permission from Elsevier.

There are just a handful of reports of successful field measurements made on-site with new technology in recent years.[188-190] There is only one recent report of an apparatus capable of performing both on-site and *in situ* analysis, introduced by Van Den Berg et al to study Cu(II) cycling in coastal waters.[193] The group outlined several physical

constraints, including high noise, limited scope, an impractical background subtraction step for oxygen and a 300 second preconcentration period. This method clearly requires a more robust and rapid analysis component to fulfil the 6 S's, which may be met via advanced stripping voltammetry or fast-scan cyclic voltammetry but is a promising start towards determining undisturbed metal speciation *in situ*.

2.7 Towards On-site, *In Situ* Trace Metal Analysis

By means of summarizing the methods described in the discussion above, **Table 2.1** compares fundamental analytical characteristics. An electrochemical sensor capable of rapid *in situ* trace metal monitoring and fulfilling the 6 S's does not yet exist, thus encompassed in this table are the methods that we believe are good candidates from the last 10 years for further development towards a portable *in situ* trace metal sensor. With the 6 S's in mind, excluded from this table are studies reporting LOD's outside of the μg/L range, greater than 5 minutes analysis time, and use of toxic (Hg film) electrode materials. Furthermore, *ex situ* Bi and Sb film electrodes are preferentially featured here, as it is not feasible to form *in situ* Bi or Sb films when directly submersing the electrode into a system of interest. Nearly all studies highlighted require sampling, pretreatment, and often times sample acidification or spiking, limiting electrochemical environmental sensing platforms to *ex situ* methods at this time.

Table 2.1. Electrochemical detection methods for on-site sensing. Electrochemical detection methods that show promise for on-site and *in situ* trace metal monitoring described in this review are compiled here by order of appearance.

Material	Configuration	Analyte	Deposition Time, s	Limit of Detection, µg/L	Methodology	Reference
Carbon Fiber	CFM	Cu(II)	0.1	15.8	FSCV	25
Ionophore Grafted Carbon Fiber	CFM	Cu(II)	0.1	0.32	FSCV	30
Bi-MEA	LOC	Pb(II)	120	0.6	SWASV	41
		Cd(II)	120	0.7		
DMG		Ni(II)	60	0.7	SWAdCSV	
Bi-MEA	LPE	Pb(II)	120	8.2	SWASV	42
		Cd(II)	120	28.2		
DMG		Ni(II)	60	6.9	SWAdCSV	
DMG, Bi-MEA	LOC	Co(II)	30	0.18	SWAdCSV	43
BiFE	LOC	Cd(II)	90	9.3	SWASV	49
Bi-BDDPE	µPAD	Pb(II)	300	1	SWASV	58
		Cd(II)	300	25		
C	Pyrolyzed Paper	Pb(II)	180	0.19	SWASV	59
		Cd(II)		0.16		
BiFE, CNT	µPAD	Pb(II)	240	1	SWASV	61
		Cd(II)		1		
Sb-SPAN-EG	SPCE	Pb(II)	180	0.2	DPASV	62
		Cd(II)		0.41		
Ag	LOC	Pb(II)	300	0.55	SWASV	68
Ag	Rotary Disk	Pb(II)	180	1.28	SWASV	69
BiFE	LPE	Pb(II)	120	0.5	SWASV	70
		Cd(II)		1		
BiFE	LOC	Pb(II)	60	8	SWASV	72
Graphite Foil	LOC	Pb(II)	180	1.8	SWASV	73

		Cd(II)	60	1.2		
AuNP	SPCE	As(III)	120	0.03	SIA-ASV	92
Au	VGME	As(III)	120	0.005	SWASV	94
Au	VGME	Mn(II)	300	0.07	SWASV	97
		Zn(II)		0.02		
AuNP	SPCE	Hg(II)	360	1	SWASV	102
DMG, BiFE	LOC	Ni(II)	90	0.1	SWAdCSV	105
DMG, Nafion	GCE	Ni(II)	120	1.5	SWAdCSV	106
DMG, Nafion, BiFE	CSPE	Ni(II)	240	5	SWAdCSV	107
		Co(II)	240	1		
BiFE, CNT	SPCE	Pb(II)	60	0.01	SIA-SWASV	108
		Cd(II)		0.01		
PANI-PDTDA	SPCE	Pb(II)	120	35	DPASV	115
		Cd(II)		33		
		Hg(II)		26		
		Ni(II)		56		
IIP, MWCNT	CPE	Ag(I)	180	0.013	DPASV	117
IIP	CPE	Pb(II)	80	0.003	DPASV	118
Mag-IIP-NPs	MCPE	Ag(I)	240	0.015	DPASV	119
IIP-PANI, MWCNT	GCE	Pb(II)	60	0.16	DPASV	120
SbNP, MWCNT, Nafion	SPCE	Pb(II)	120	0.65	SWASV	173
		Cd(II)		0.77		
BiFE	LOC	Cd(II)	90	9.3	SWASV	187
Au	SPGE	Pb(II)	240	1.2	SWASV	188
		Cu(II)		1.1		
		Hg(II)		1.1		
DMG, Nafion	SPCE	Ni(II)	120	30	DPASV	190
Au	SPGE	Pb(II)	90	4	SWASV	191

		Cu(II)		2		
		Hg(II)		4		
Ag	VGME	Cu(II)	300	0.003	SWASV	193

Acronyms:

BiFE	Bismuth Film Electrode	MEA	Microelectrode Array
BDDPE	Boron Doped Diamond Paste Electrode	MPCE	Magneto Carbon Paste Electrode
CFM	Carbon Fiber Microelectrode	MWCNT	Multiwalled Carbon Nanotubes
CNT	Carbon Nanotube	µPAD	Microfluidic Paper-Based Analytical Device
CPE	Carbon Paste Electrode	NP	Nanoparticles
CSPE	Carbon Stencil Printed Electrodes	PANI	Polyaniline
DMG	Dimethylglyoxime	PANI-PDTDA	Polyaniline-Poly(2,2'-Dithiodianiline)
EG	Expanded Graphite	SPAN	Sulfonated Polyaniline
IIP	Ion Imprinted polymer	SPE	Screen Printed Electrode
LOC	Lab-on-a-Chip	SPCE	Screen Printed Carbon Electrode
LPE	Lithographically Printed Electrode	SPGE	Screen Printed Gold Electrode
Mag-IIP-NPs	Magnetic Ion Imprinted Polymer Nanoparticles	VGME	Vibrating Gold Microelectrode

There are still many ongoing challenges to consider when designing on on-site analysis device with an *in situ* capable sensing probe. In the laboratory, the optimization of delivery of analyte to the electrode has contributed to enhanced sensitivity[48] via flow injection systems,[92,108,139,157,175,191,192] however this highly controlled convection is still a limitation for making truly *in situ* measurements because it is not possible to control the convection of dynamic environmental systems. Additionally, unpredictable fluctuations in pH, temperature, pressure, and biofouling are also ongoing issues for interpreting signals collected in the field. Finally, the sensitivity of these techniques, while suitable to confirm contamination according to US-EPA drinking water quality standards,[194] for the most part are below the limit of detection for previously reported resting metal concentrations in fresh and seawater.[1,195,196] Altogether, these technological gaps necessitate advancements in the coming years for better trace metal sensing tools. We encourage those highlighted in this review and others to continue their progress towards this common goal: to create a field portable analysis device capable of *in situ* sensing.

2.8 Conclusion

Metals play important chemical roles, acting as nutrients and cofactors in biochemical and environmental processes. They can also exert toxic effects in excess. Electrochemistry has emerged as an attractive analysis strategy due to the inherent portable nature of electrodes. An electrochemical method capable of distinguishing metal speciation is highly desirable, because electrolabile metals are available to engage in chemical processes. The process of sampling and pretreatment alters metal speciation, thus it is necessary make *in situ* measurements. Real environmental systems however are challenging to analyze because real matrices can be chemically harsh, complex and

dynamic. We identified a set of criteria for electroanalysis of trace metals, coined the 6 S's: sensitivity, selectivity, size, speed, stability, and safe materials. Progress towards developing an electrochemical probe for *in situ* metal analysis is discussed in this review, with focus on a promising voltammetric technique (FSCV) that satisfies our 6 criteria.

Novel probe design aspects including electrode materials, configurations, and surface functionalizations are targeted in our discussion. Additionally, we report new developments in portable electrochemical instrumentation for on-site capabilities. In this review, we conclude that there is a clear gap in technology for this specific environmental application, and most techniques are still limited to *ex situ* measurements and analysis. We highlight studies that we believe show potential for on-site, *in situ* measurements, and iterate the importance of actively pursuing technology development to achieve, within the next few years, a truly robust on-site, *in situ* trace metal speciation sensor.

2.9 References

(1) Tercier Waeber, M.-L.; Stoll, S.; Slaveykova, V. Trace metal behavior in surface waters: emphasis on dynamic speciation, sorption processes and bioavailability. *Archives des Sciences* **2012,** *65*, 119.

(2) Thanh, P. M.; Ketheesan, B.; Yan, Z.; Stuckey, D. C. Trace metal speciation and bioavailability in anaerobic digestion: A review. *Biotechnol Adv* **2016,** *34* (2), 122.

(3) Hill, S. J. Speciation of trace metals in the environment. *Chem Soc Rev* **1997,** *26* (4), 291.

(4) Campbell, P. G. C.; Tessier, A. In *Sources and Fates of Aquatic Pollutants*; American Chemical Society, 1987; Vol. 216.

(5) Allen, H. E. The significance of trace metal speciation for water, sediment and soil quality criteria and standards. *Sci Total Environ* **1993,** *134*, 23.

(6) Fytianos, K. Speciation analysis of heavy metals in natural waters: A review. *J Aoac Int* **2001,** *84* (6), 1763.

(7) van Leeuwen, H. P. Metal Speciation Dynamics and Bioavailability: Inert and Labile Complexes. *Environ Sci Technol* **1999,** *33* (21), 3743.

(8) Amde, M.; Yin, Y.; Zhang, D.; Liu, J. Methods and recent advances in speciation analysis of mercury chemical species in environmental samples: a review. *Chemical Speciation & Bioavailability* **2016,** *28* (1-4), 51.

(9) Tercier, M. L.; Buffle, J.; Zirino, A.; Devitre, R. R. *In situ* voltammetric measurement of trace-elements in lakes and oceans. *Anal Chim Acta* **1990,** *237* (2), 429.

(10) Herdan, J.; Feeney, R.; Kounaves, S. P.; Flannery, A. F.; Storment, C. W.; Kovacs, G. T. A.; Darling, R. B. Field evaluation of an electrochemical probe for in situ screening of heavy metals in groundwater. *Environ Sci Technol* **1998,** *32* (1), 131.

(11) Tercier-Waeber, M. L.; Taillefert, M. Remote *in situ* voltammetric techniques to characterize the biogeochemical cycling of trace metals in aquatic systems. *J Environ Monit* **2008,** *10* (1), 30.

(12) Davidson, C. M. In *Heavy Metals in Soils: Trace Metals and Metalloids in Soils and their Bioavailability*; 3rd Edition ed.; Alloway, B. J., Ed.; Springer Netherlands: Dordrecht, 2013, DOI:10.1007/978-94-007-4470-7_4 10.1007/978-94-007-4470-7_4.

(13) Marcovecchio, J. E.; Botté, S. E.; Domini, C. E.; Freije, R. H. In *Handbook of Water Analysis*; 3rd Edition ed.; Gelder, L. S. P. D., Ed.; CRC Press: Boca Raton, FL, 2013, DOI:doi:10.1201/b15314-22

(14) Posacka, A. M.; Semeniuk, D. M.; Whitby, H.; van den Berg, C. M. G.; Cullen, J. T.; Orians, K.; Maldonado, M. T. Dissolved copper (dCu) biogeochemical cycling in the subarctic Northeast Pacific and a call for improving methodologies. *Mar Chem* **2017,** *196*, 47.

(15) Hong, Y. S.; Kinney, K. A.; Reible, D. D. Effects Of Cyclic Changes In Ph And Salinity On Metals Release From Sediments. *Environ Toxicol Chem* **2011,** *30* (8), 1775.

(16) Lama, R. D.; Charlson, K.; Anantharam, A.; Hashemi, P. Ultrafast detection and quantification of brain signaling molecules with carbon fiber microelectrodes. *Analytical Chemistry* **2012,** *84* (19), 8096.

(17) Morrison, M. A.; Benoit, G. Temporal variability in physical speciation of metals during a winter rain-on-snow event. *J Environ Qual* **2005,** *34* (5), 1610.

(18) Feng, C. H.; Guo, X. Y.; Yin, S.; Tian, C. H.; Li, Y. Y.; Shen, Z. Y. Heavy metal partitioning of suspended particulate matter-water and sediment-water in the Yangtze Estuary. *Chemosphere* **2017,** *185*, 717.

(19) Matar, Z.; Pereira, C. S.; Chebbo, G.; Uher, E.; Troupel, M.; Boudahmane, L.; Saad, M.; Gourlay-France, C.; Rocher, V.; Varrault, G. Influence of effluent organic matter on copper speciation and bioavailability in rivers under strong urban pressure. *Environ Sci Pollut R* **2015,** *22* (24), 19461.

(20) Reyes, C.; Schneider, D.; Thurmer, A.; Kulkarni, A.; Lipka, M.; Sztejrenszus, S. Y.; Bottcher, M. E.; Daniel, R.; Friedrich, M. W. Potentially Active Iron, Sulfur, and Sulfate Reducing Bacteria in Skagerrak and Bothnian Bay Sediments. *Geomicrobiol J* **2017,** *34* (10), 840.

(21) Hyun, J. H.; Kim, S. H.; Mok, J. S.; Cho, H.; Lee, T.; Vandieken, V.; Thamdrup, B. Manganese and iron reduction dominate organic carbon oxidation in surface sediments of the deep Ulleung Basin, East Sea. *Biogeosciences* **2017,** *14* (4), 941.

(22) Buffle, J.; Tercier-Waeber, M. L. Voltammetric environmental trace-metal analysis and speciation: from laboratory to in situ measurements. *Trac-Trends in Analytical Chemistry* **2005,** *24* (3), 172.

(23) Tercier-Waeber, M. L.; Buffle, J. Submersible online oxygen removal system coupled to an in situ voltammetric probe for trace element monitoring in freshwater. *Environ Sci Technol* **2000,** *34* (18), 4018.

(24) Rodeberg, N. T.; Sandberg, S. G.; Johnson, J. A.; Phillips, P. E.; Wightman, R. M. Hitchhiker's Guide to Voltammetry: Acute and Chronic Electrodes for in Vivo Fast-Scan Cyclic Voltammetry. *Acs Chem Neurosci* **2017,** *8* (2), 221.

(25) Pathirathna, P.; Yang, Y. Y.; Forzley, K.; McElmurry, S. P.; Hashemi, P. Fast-scan deposition-stripping voltammetry at carbon-fiber microelectrodes: real-time, subsecond, mercury free measurements of copper. *Analytical Chemistry* **2012,** *84* (15), 6298.

(26) Yang, Y.; Pathirathna, P.; Siriwardhane, T.; McElmurry, S. P.; Hashemi, P. Real-time subsecond voltammetric analysis of Pb in aqueous environmental samples. *Anal Chem* **2013,** *85* (15), 7535.

(27) Hashemi, P.; Dankoski, E. C.; Petrovic, J.; Keithley, R. B.; Wightman, R. M. Voltammetric detection of 5-hydroxytryptamine release in the rat brain. *Anal Chem* **2009,** *81* (22), 9462.

(28) Samaranayake, S.; Abdalla, A.; Robke, R.; Wood, K. M.; Zeqja, A.; Hashemi, P. In vivo histamine voltammetry in the mouse premammillary nucleus. *Analyst* **2015,** *140* (11), 3759.

(29) Sanford, A. L.; Morton, S. W.; Whitehouse, K. L.; Oara, H. M.; Lugo-Morales, L. Z.; Roberts, J. G.; Sombers, L. A. Voltammetric Detection of Hydrogen Peroxide at Carbon Fiber Microelectrodes. *Analytical Chemistry* **2010,** *82* (12), 5205.

(30) Yang, Y.; Ibrahim, A. A.; Hashemi, P.; Stockdill, J. L. Real-Time, Selective Detection of Copper(II) Using Ionophore-Grafted Carbon-Fiber Microelectrodes. *Analytical Chemistry* **2016,** *88* (14), 6962.

(31) Pathirathna, P.; Samaranayake, S.; Atcherley, C. W.; Parent, K. L.; Heien, M. L.; McElmurry, S. P.; Hashemi, P. Fast voltammetry of metals at carbon-fiber microelectrodes: copper adsorption onto activated carbon aids rapid electrochemical analysis. *Analyst* **2014,** *139* (18), 4673.

(32) Siriwardhane, T.; Sulkanen, A.; Pathirathna, P.; Tremonti, A.; McElmurry, S. P.; Hashemi, P. Voltammetric Characterization of Cu(II) Complexation in Real-Time. *Anal Chem* **2016,** *88* (15), 7603.

(33) Atcherley, C. W.; Laude, N. D.; Parent, K. L.; Heien, M. L. Fast-Scan Controlled-Adsorption Voltammetry for the Quantification of Absolute Concentrations and Adsorption Dynamics. *Langmuir* **2013,** *29* (48), 14885.

(34) Atcherley, C. W.; Wood, K. M.; Parent, K. L.; Hashemi, P.; Heien, M. L. The coaction of tonic and phasic dopamine dynamics. *Chem Commun* **2015,** *51* (12), 2235.

(35) Pathirathna, P.; Siriwardhane, T.; Morgan, S. L.; McElmurry, S. P.; Hashemi, P. Fast voltammetry of metals at carbon-fiber microelectrodes: rapid determination of solution formation constants. *Analyst* **2016,** *141* (21), 6025.

(36) Henstridge, M. C.; Compton, R. G. Mass Transport to micro- and nanoelectrodes and their arrays: a review. *Chem Rec* **2012,** *12* (1), 63.

(37) Molina, A.; Gonzalez, J. In *Characterization of Materials*, 2012, DOI:doi:10.1002/0471266965.com126 doi:10.1002/0471266965.com126.

(38) Li, M.; Gou, H. L.; Al-Ogaidi, I.; Wu, N. Q. Nanostructured Sensors for Detection of Heavy Metals: A Review. *Acs Sustain Chem Eng* **2013,** *1* (7), 713.

(39) Michael, A. C.; Wightman, R. M. In *Laboratory techniques in electroanalytical chemistry*; 2nd ed.; Heineman, P. T. K. W. R., Ed.; Marcel Dekker, Inc.: New York, 1996.

(40) Baldrianova, L.; Agrafiotou, P.; Svancara, I.; Jannakoudakis, A. D.; Sotiropoulos, S. The effect of acetate concentration, solution pH and conductivity on the anodic stripping voltammetry of lead and cadmium ions at *in situ* bismuth-plated carbon microelectrodes. *J Electroanal Chem* **2011,** *660* (1), 31.

(41) Kokkinos, C.; Economou, A.; Raptis, I. Microfabricated disposable lab-on-a-chip sensors with integrated bismuth microelectrode arrays for voltammetric determination of trace metals. *Anal Chim Acta* **2012,** *710*, 1.

(42) Kokkinos, C.; Economou, A.; Raptis, I.; Speliotis, T. Disposable lithographically fabricated bismuth microelectrode arrays for stripping voltammetric detection of trace metals. *Electrochem Commun* **2011,** *13* (5), 391.

(43) Kokkinos, C.; Economou, A. Microfabricated chip integrating a bismuth microelectrode array for the determination of trace cobalt(II) by adsorptive cathodic stripping voltammetry. *Sensors and Actuators, B: Chemical* **2016,** *229*, 362.

(44) Kokkinos, C.; Economou, A.; Raptis, I.; Speliotis, T. Disposable microfabricated bismuth microelectrode arrays for trace metal analysis by stripping voltammetry. *Procedia Engineering* **2011,** *25*, 880.

(45) Niu, X. H.; Lan, M. B.; Zhao, H. L.; Chen, C.; Li, Y. X.; Zhu, X. Review: Electrochemical Stripping Analysis of Trace Heavy Metals Using Screen-Printed Electrodes. *Anal Lett* **2013,** *46* (16), 2479.

(46) Li, M.; Li, Y.-T.; Li, D.-W.; Long, Y.-T. Recent developments and applications of screen-printed electrodes in environmental assays—A review. *Anal Chim Acta* **2012,** *734*, 31.

(47) Hayat, A.; Marty, J. L. Disposable Screen Printed Electrochemical Sensors: Tools for Environmental Monitoring. *Sensors-Basel* **2014,** *14* (6), 10432.

(48) Zhao, G.; Wang, H.; Liu, G. Recent Advances in Chemically Modified Electrodes, Microfabricated Devices and Injection Systems for the Electrochemical Detection of Heavy Metals: A review. *Int J Electrochem Sc* **2017,** *12* (9), 8622.

(49) Jang, A.; Zou, Z.; Lee, K. K.; Ahn, C. H.; Bishop, P. L. Potentiometric and voltammetric polymer lab chip sensors for determination of nitrate, pH and Cd(II) in water. *Talanta* **2010,** *83* (1), 1.

(50) Akyazi, T.; Basabe-Desmonts, L.; Benito-Lopez, F. Review on microfluidic paper-based analytical devices towards commercialisation. *Anal Chim Acta* **2018,** *1001*, 1.

(51) Mentele, M. M.; Cunningham, J.; Koehler, K.; Volckens, J.; Henry, C. S. Microfluidic paper-based analytical device for particulate metals. *Anal Chem* **2012,** *84* (10), 4474.

(52) Cate, D. M.; Noblitt, S. D.; Volckens, J.; Henry, C. S. Multiplexed paper analytical device for quantification of metals using distance-based detection. *Lab Chip* **2015,** *15* (13), 2808.

(53) Jia, Y.; Dong, H.; Zheng, J.; Sun, H. Portable detection of trace metals in airborne particulates and sediments via muPADs and smartphone. *Biomicrofluidics* **2017,** *11* (6), 064101.

(54) Chen, G. H.; Chen, W. Y.; Yen, Y. C.; Wang, C. W.; Chang, H. T.; Chen, C. F. Detection of Mercury(II) Ions Using Colorimetric Gold Nanoparticles on Paper-Based Analytical Devices. *Analytical Chemistry* **2014,** *86* (14), 6843.

(55) Braga, M. S.; Jaimes, R. F. V. V.; Borysow, W.; Gomes, O. F.; Salcedo, W. J. Portable Multispectral Colorimeter for Metallic Ion Detection and Classification. *Sensors-Basel* **2017,** *17* (8).

(56) Alex, S. A.; Chandrasekaran, N.; Mukherjee, A. State-of-the-art strategies for the colorimetric detection of heavy metals using gold nanorods based on aspect ratio reduction. *Anal Methods-Uk* **2016,** *8* (10), 2131.

(57) Rattanarat, P.; Dungchai, W.; Cate, D. M.; Siangproh, W.; Volckens, J.; Chailapakul, O.; Henry, C. S. A microfluidic paper-based analytical device for rapid quantification of particulate chromium. *Anal Chim Acta* **2013,** *800*, 50.

(58) Nantaphol, S.; Channon, R. B.; Kondo, T.; Siangproh, W.; Chailapakul, O.; Henry, C. S. Boron Doped Diamond Paste Electrodes for Microfluidic Paper-Based Analytical Devices. *Anal Chem* **2017,** *89* (7), 4100.

(59) Silva, L. A. J.; da Silva, W. P.; Giuliani, J. G.; Canobre, S. C.; Garcia, C. D.; Munoz, R. A. A.; Richter, E. M. Use of pyrolyzed paper as disposable substrates for voltammetric determination of trace metals. *Talanta* **2017,** *165*, 33.

(60) Martin-Yerga, D.; Alvarez-Martos, I.; Blanco-Lopez, M. C.; Henry, C. S.; Fernandez-Abedul, M. T. Point-of-need simultaneous electrochemical detection of lead and cadmium using low-cost stencil-printed transparency electrodes. *Anal Chim Acta* **2017,** *981*, 24.

(61) Rattanarat, P.; Dungchai, W.; Cate, D.; Volckens, J.; Chailapakul, O.; Henry, C. S. Multilayer Paper-Based Device for Colorimetric and Electrochemical Quantification of Metals. *Analytical Chemistry* **2014,** *86* (7), 3555.

(62) Liu, R. L.; Cao, H. J.; Nie, Z. B.; Si, S. H.; Zhao, X. L.; Zeng, X. M. A disposable expanded graphite paper electrode with self-doped sulfonated polyaniline/antimony for stripping voltammetric determination of trace Cd and Pb. *Anal Methods-Uk* **2016,** *8* (7), 1618.

(63) Chaiyo, S.; Apiluk, A.; Siangproh, W.; Chailapakul, O. High sensitivity and specificity simultaneous determination of lead, cadmium and copper using mu PAD with dual electrochemical and colorimetric detection. *Sensor Actuat B-Chem* **2016,** *233*, 540.

(64) Rios, A.; Zougagh, M.; Avila, M. Miniaturization through lab-on-a-chip: Utopia or reality for routine laboratories? A review. *Anal Chim Acta* **2012,** *740*, 1.

(65) Culbertson, C. T.; Mickleburgh, T. G.; Stewart-James, S. A.; Sellens, K. A.; Pressnall, M. Micro total analysis systems: fundamental advances and biological applications. *Analytical Chemistry* **2014,** *86* (1), 95.

(66) Guijt, R. M.; Manz, A. Miniaturised total chemical-analysis systems (μTAS) that periodically convert chemical into electronic information. *Sensor Actuat B-Chem* **2018,** *273*, 1334.

(67) Romao, V. C.; Martins, S. A. M.; Germano, J.; Cardoso, F. A.; Cardoso, S.; Freitas, P. P. Lab-on-Chip Devices: Gaining Ground Losing Size. *Acs Nano* **2017,** *11* (11), 10659.

(68) Jung, W.; Jang, A.; Bishop, P. L.; Ahn, C. H. A polymer lab chip sensor with microfabricated planar silver electrode for continuous and on-site heavy metal measurement. *Sensors and Actuators, B: Chemical* **2011,** *155* (1), 145.

(69) Lee, Y. G.; Han, J.; Kwon, S.; Kang, S.; Jang, A. Development of a rotary disc voltammetric sensor system for semi-continuous and on-site measurements of Pb(II). *Chemosphere* **2016,** *143*, 78.

(70) Kokkinos, C.; Economou, A.; Raptis, I.; Efstathiou, C. E. Lithographically fabricated disposable bismuth-film electrodes for the trace determination of Pb(II) and Cd(II) by anodic stripping voltammetry. *Electrochim Acta* **2008,** *53* (16), 5294.

(71) Jang, A.; Zou, Z. W.; Lee, K. K.; Ahn, C. H.; Bishop, P. L. State-of-the-art lab chip sensors for environmental water monitoring. *Meas Sci Technol* **2011,** *22* (3), 032001.

(72) Zou, Z. W.; Jang, A.; MacKnight, E.; Wu, P. M.; Do, J.; Bishop, P. L.; Ahn, C. H. Environmentally friendly disposable sensors with microfabricated on-chip planar bismuth electrode for *in situ* heavy metal ions measurement. *Sensors and Actuators, B: Chemical* **2008,** *134* (1), 18.

(73) Shen, L. L.; Zhang, G. R.; Li, W.; Biesalski, M.; Etzold, B. J. M. Modifier-Free Microfluidic Electrochemical Sensor for Heavy-Metal Detection. *ACS Omega* **2017,** *2* (8), 4593.

(74) Campana, O.; Wlodkowic, D. Ecotoxicology Goes on a Chip: Embracing Miniaturized Bioanalysis in Aquatic Risk Assessment. *Environ Sci Technol* **2018,** *52* (3), 932.

(75) Campana, O.; Wlodkowic, D. The undiscovered country: Ecotoxicology meets microfluidics. *Sensor Actuat B-Chem* **2018,** *257*, 692.

(76) Palecek, E.; Heyrovsky, M. 75 years of J. Heyrovsky's Oscillographic Polarography and Present Constant Current Chronopotentiometry. *Chem Listy* **2017,** *111* (1), 73.

(77) Heyrovsky, M. Ninety Years of Polarography. *Chem Rec* **2012,** *12* (1), 14.

(78) Heyrovsky, M. Polarography-past, present, and future. *Journal of Solid State Electrochemistry* **2011,** *15* (7-8), 1799.

(79) Bixler, G. D.; Bhushan, B. Biofouling: lessons from nature. *Philos Trans A Math Phys Eng Sci* **2012,** *370* (1967), 2381.

(80) McQuillan, J. S.; Morriss, A. K.; Arundell, M.; Pascal, R.; Mowlem, M. C. The anti-bacterial effect of an electrochemical anti-fouling method intended for the protection of miniaturised oceanographic sensors. *J Microbiol Meth* **2017,** *141*, 63.

(81) Gaw, S. L.; Sarkar, S.; Nir, S.; Schnell, Y.; Mandler, D.; Xu, Z. C. J.; Lee, P. S.; Reches, M. Electrochemical Approach for Effective Antifouling and Antimicrobial Surfaces. *Acs Appl Mater Inter* **2017,** *9* (31), 26503.

(82) Goda, T.; Miyahara, Y. Electrodeposition of Zwitterionic PEDOT Films for Conducting and Antifouling Surfaces. *Langmuir* **2018**.

(83) Zhang, Z. G.; Zheng, J. P.; Zhang, Y.; Zhang, W.; Li, L. J.; Cao, Z. Z.; Wang, H.; Li, C. H.; Gao, Y. F.; Liu, J. R. Anti-fouling In situ Deposited Antimony/Nafion Film Electrode for Electrochemical Stripping Analysis. *Int J Electrochem Sc* **2013,** *8* (3), 4183.

(84) Zhang, P.; Fritz, P. A.; Schroën, K.; Duan, H.; Boom, R. M.; Chan-Park, M. B. Zwitterionic Polymer Modified Porous Carbon for High-Performance and Antifouling Capacitive Desalination. *Acs Appl Mater Inter* **2018**, DOI:10.1021/acsami.8b11708 10.1021/acsami.8b11708.

(85) Cao, B.; Tang, Q.; Li, L. L.; Lee, C. J.; Wang, H.; Zhang, Y. Q.; Castaneda, H.; Cheng, G. Integrated zwitterionic conjugated poly(carboxybetaine thiophene) as a new biomaterial platform. *Chem Sci* **2015,** *6* (1), 782.

(86) Leng, C.; Hung, H. C.; Sun, S. W.; Wang, D. Y.; Li, Y. T.; Jiang, S. Y.; Chen, Z. Probing the Surface Hydration of Nonfouling Zwitterionic and PEG Materials in Contact with Proteins. *Acs Appl Mater Inter* **2015,** *7* (30), 16881.

(87) Wang, Y.; Cui, M.; Jiao, M. X.; Luo, X. L. Antifouling and ultrasensitive biosensing interface based on self-assembled peptide and aptamer on macroporous gold for electrochemical detection of immunoglobulin E in serum. *Anal Bioanal Chem* **2018,** *410* (23), 5871.

(88) Wang, G. X.; Su, X. L.; Xu, Q. J.; Xu, G. Y.; Lin, J. H.; Luo, X. L. Antifouling aptasensor for the detection of adenosine triphosphate in biological media based on mixed self-assembled aptamer and zwitterionic peptide. *Biosens Bioelectron* **2018,** *101*, 129.

(89) Wang, G. X.; Han, R.; Su, X. L.; Li, Y. N.; Xu, G. Y.; Luo, X. L. Zwitterionic peptide anchored to conducting polymer PEDOT for the development of antifouling and ultrasensitive electrochemical DNA sensor. *Biosens Bioelectron* **2017,** *92*, 396.

(90) Brisset, H.; Briand, J. F.; Barry-Martinet, R.; Duong, T. H.; Frere, P.; Gohier, F.; Leriche, P.; Bressy, C. 96X Screen-Printed Gold Electrode Platform to Evaluate Electroactive Polymers as Marine Antifouling Coatings. *Analytical Chemistry* **2018,** *90* (8), 4978.

(91) Takmakov, P.; Zachek, M. K.; Keithley, R. B.; Walsh, P. L.; Donley, C.; McCarty, G. S.; Wightman, R. M. Carbon Microelectrodes with a Renewable Surface. *Analytical Chemistry* **2010,** *82* (5), 2020.

(92) Punrat, E.; Chuanuwatanakul, S.; Kaneta, T.; Motomizu, S.; Chailapakul, O. Method development for the determination of arsenic by sequential injection/anodic stripping voltammetry using long-lasting gold-modified screen-printed carbon electrode. *Talanta* **2013,** *116*, 1018.

(93) Fischer, L. M.; Tenje, M.; Heiskanen, A. R.; Masuda, N.; Castillo, J.; Bentien, A.; Emneus, J.; Jakobsen, M. H.; Boisen, A. Gold cleaning methods for electrochemical detection applications. *Microelectron Eng* **2009,** *86* (4-6), 1282.

(94) Salaun, P.; Gibbon-Walsh, K. B.; Alves, G. M.; Soares, H. M.; van den Berg, C. M. Determination of arsenic and antimony in seawater by voltammetric and chronopotentiometric stripping using a vibrated gold microwire electrode. *Anal Chim Acta* **2012,** *746*, 53.

(95) Gibbon-Walsh, K.; Salaun, P.; van den Berg, C. M. Pseudopolarography of copper complexes in seawater using a vibrating gold microwire electrode. *J Phys Chem A* **2012,** *116* (25), 6609.

(96) Salaün, P.; Gibbon-Walsh, K.; Van Den Berg, C. *Speciation of inorganic arsenic in marine waters by stripping analysis at a gold microwire electrode: Proceedings of the 4th International Congress on Arsenic in the Environment, 22-27 July 2012, Cairns, Australia*, 2012.

(97) Gibbon-Walsh, K.; Salaun, P.; van den Berg, C. M. G. Determination of manganese and zinc in coastal waters by anodic stripping voltammetry with a vibrating gold microwire electrode. *Environ Chem* **2011,** *8* (5), 475.

(98) Clark, J. J.; Sandberg, S. G.; Wanat, M. J.; Gan, J. O.; Horne, E. A.; Hart, A. S.; Akers, C. A.; Parker, J. G.; Willuhn, I.; Martinez, V.et al. Chronic microsensors for longitudinal, subsecond dopamine detection in behaving animals. *Nat Methods* **2010,** *7* (2), 126.

(99) Safavi, A.; Farjami, E. Construction of a carbon nanocomposite electrode based on amino acids functionalized gold nanoparticles for trace electrochemical detection of mercury. *Anal Chim Acta* **2011,** *688* (1), 43.

(100) Gumpu, M. B.; Sethuraman, S.; Krishnan, U. M.; Rayappan, J. B. B. A review on detection of heavy metal ions in water – An electrochemical approach. *Sensors and Actuators B: Chemical* **2015,** *213*, 515.

(101) Waheed, A.; Mansha, M.; Ullah, N. Nanomaterials-based electrochemical detection of heavy metals in water: Current status, challenges and future direction. *Trac-Trends in Analytical Chemistry* **2018,** *105*, 37.

(102) Somé, I. T.; Sakira, A. K.; Mertens, D.; Ronkart, S. N.; Kauffmann, J.-M. Determination of groundwater mercury (II) content using a disposable gold modified screen printed carbon electrode. *Talanta* **2016,** *152*, 335.

(103) Kokkinos, C.; Economou, A.; Raptis, I.; Speliotis, T. Disposable mercury-free cell-on-a-chip devices with integrated microfabricated electrodes for the

determination of trace nickel(II) by adsorptive stripping voltammetry. *Anal Chim Acta* **2008,** *622* (1-2), 111.

(104) Zhang, H.; Van Den Berg, C. M. G.; Wollast, R. The Determination of Interactions of Cobalt (Ii) with Organic-Compounds in Seawater Using Cathodic Stripping Voltammetry. *Mar Chem* **1990,** *28* (4), 285.

(105) Kokkinos, C.; Economou, A.; Raptis, I.; Speliotis, T. Novel disposable microfabricated antimony-film electrodes for adsorptive stripping analysis of trace Ni(II). *Electrochem Commun* **2009,** *11* (2), 250.

(106) Pokpas, K.; Jahed, N.; Baker, P. G.; Iwuoha, E. I. Complexation-Based Detection of Nickel(II) at a Graphene-Chelate Probe in the Presence of Cobalt and Zinc by Adsorptive Stripping Voltammetry. *Sensors-Basel* **2017,** *17* (8), 1711.

(107) Mettakoonpitak, J.; Miller-Lionberg, D.; Reilly, T.; Volckens, J.; Henry, C. S. Low-cost reusable sensor for cobalt and nickel detection in aerosols using adsorptive cathodic square-wave stripping voltammetry. *J Electroanal Chem* **2017,** *805*, 75.

(108) Ninwong, B.; Chuanuwatanakul, S.; Chailapakul, O.; Dungchai, W.; Motomizu, S. On-line preconcentration and determination of lead and cadmium by sequential injection/anodic stripping voltammetry. *Talanta* **2012,** *96*, 75.

(109) Chen, Z. B.; Li, L. D.; Mu, X. J.; Zhao, H. T.; Guo, L. Electrochemical aptasensor for detection of copper based on a reagentless signal-on architecture and amplification by gold nanoparticles. *Talanta* **2011,** *85* (1), 730.

(110) Shen, L.; Chen, Z.; Li, Y. H.; He, S. L.; Xie, S. B.; Xu, X. D.; Liang, Z. W.; Meng, X.; Li, Q.; Zhu, Z. W.et al. Electrochemical DNAzyme sensor for lead based on amplification of DNA-Au bio-bar codes. *Analytical Chemistry* **2008,** *80* (16), 6323.

(111) Wu, Y.; Lai, R. Y. Electrochemical Gold(III) Sensor with High Sensitivity and Tunable Dynamic Range. *Anal Chem* **2016,** *88* (4), 2227.

(112) Wu, Y.; Lai, R. Y. A reagentless DNA-based electrochemical silver(I) sensor for real time detection of Ag(I) - the effect of probe sequence and orientation on sensor response. *Biotechnol J* **2016,** *11* (6), 788.

(113) Guerreiro, G. V.; Zaitouna, A. J.; Lai, R. Y. Characterization of an electrochemical mercury sensor using alternating current, cyclic, square wave and differential pulse voltammetry. *Anal Chim Acta* **2014,** *810*, 79.

(114) Wu, Y.; Baker, S. L.; Lai, R. Y. Effects of DNA Probe Length on the Performance of a Dynamics-based Electrochemical Hg(II) Sensor. *Electroanal* **2017,** *29* (10), 2239.

(115) Somerset, V. S.; Hernandez, L. H.; Iwuoha, E. I. Stripping voltammetric measurement of trace metal ions using screen-printed carbon and modified carbon paste electrodes on river water from the Eerste-Kuils River System. *Journal of Environmental Science and Health, Part A* **2011,** *46* (1), 17.

(116) Fu, L.; Li, X.; Yu, J.; Ye, J. Facile and simultaneous stripping determination of zinc, cadmium and lead on disposable multiwalled carbon nanotubes modified screen□printed electrode. *Electroanal* **2013,** *25* (2), 567.

(117) Zhiani, R.; Ghanei-Motlag, M.; Razavipanah, I. Selective voltammetric sensor for nanomolar detection of silver ions using carbon paste electrode modified with novel nanosized Ag(I)-imprinted polymer. *J Mol Liq* **2016,** *219*, 554.

(118) Luo, X.; Huang, W. H.; Shi, Q. Y.; Xu, W. Z.; Luan, Y.; Yang, Y. F.; Wang, H. J.; Yang, W. M. Electrochemical sensor based on lead ionimprinted polymer particles for ultra-trace determination of lead ions in different real samples. *Rsc Adv* **2017,** *7* (26), 16033.

(119) Ghanei-Motlagh, M.; Taher, M. A. Magnetic silver(I) ion-imprinted polymeric nanoparticles on a carbon paste electrode for voltammetric determination of silver(I). *Microchim Acta* **2017,** *184* (6), 1691.

(120) Tarley, C. R. T.; Basaglia, A. M.; Segatelli, M. G.; Prete, M. C.; Suquila, F. A. C.; de Oliveira, L. L. G. Preparation and application of nanocomposite based on imprinted poly (methacrylic acid)-PAN/MWCNT as a new electrochemical selective sensing platform of Pb2+ in water samples. *J Electroanal Chem* **2017,** *801*, 114.

(121) Ashkenani, H.; Taher, M. A. Selective voltammetric determination of Cu(II) based on multiwalled carbon nanotube and nano-porous Cu-ion imprinted polymer. *J Electroanal Chem* **2012,** *683*, 80.

(122) Shamsipur, M.; Hashemi, B.; Dehdashtian, S.; Mohammadi, M.; Gholivand, M. B.; Garau, A.; Lippolis, V. Silver ion imprinted polymer nanobeads based on a aza-thioether crown containing a 1,10-phenanthroline subunit for solid phase extraction and for voltammetric and potentiometric silver sensors. *Anal Chim Acta* **2014,** *852*, 223.

(123) Hu, S. L.; Xiong, X. D.; Huang, S. Y.; Lai, X. Q. Preparation of Pb(II) Ion Imprinted Polymer and Its Application as the Interface of an Electrochemical Sensor for Trace Lead Determination. *Anal Sci* **2016,** *32* (9), 975.

(124) Alizadeh, T.; Hamidi, N.; Ganjali, M. R.; Rafiei, F. An extraordinarily sensitive voltammetric sensor with picomolar detection limit for Pb2+ determination based on carbon paste electrode impregnated with nano-sized imprinted polymer and multi-walled carbon nanotubes. *J Environ Chem Eng* **2017,** *5* (5), 4327.

(125) Bahrami, A.; Besharati-Seidani, A.; Abbaspour, A.; Shamsipur, M. A highly selective voltammetric sensor for nanomolar detection of mercury ions using a carbon ionic liquid paste electrode impregnated with novel ion imprinted polymeric nanobeads. *Mater Sci Eng C Mater Biol Appl* **2015,** *48*, 205.

(126) Ghanei-Motlagh, M.; Taher, M. A.; Heydari, A.; Ghanei-Motlagh, R.; Gupta, V. K. A novel voltammetric sensor for sensitive detection of mercury(II) ions using glassy carbon electrode modified with graphene-based ion imprinted polymer. *Mater Sci Eng C Mater Biol Appl* **2016,** *63*, 367.

(127) Alizadeh, T.; Ganjali, M. R.; Zare, M. Application of an Hg2+ selective imprinted polymer as a new modifying agent for the preparation of a novel highly selective

and sensitive electrochemical sensor for the determination of ultratrace mercury ions. *Anal Chim Acta* **2011,** *689* (1), 52.

(128) Alizadeh, T.; Hamidi, N.; Ganjali, M. R.; Rafiei, F. Determination of subnanomolar levels of mercury (II) by using a graphite paste electrode modified with MWCNTs and Hg(II) -imprinted polymer nanoparticles. *Microchim Acta* **2018,** *185* (1).

(129) Sebastian, M.; Mathew, B. Multiwalled carbon nanotube based ion imprinted polymer as sensor and sorbent for environmental hazardous cobalt ion. *Journal of Macromolecular Science, Part A* **2018**, DOI:10.1080/10601325.2018.1470463 10.1080/10601325.2018.1470463, 1.

(130) Sebastian, M.; Mathew, B. Ion imprinting approach for the fabrication of an electrochemical sensor and sorbent for lead ions in real samples using modified multiwalled carbon nanotubes. *J Mater Sci* **2018,** *53* (5), 3557.

(131) Bojdi, M. K.; Mashhadizadeh, M. H.; Behbahani, M.; Farahani, A.; Davarani, S. S. H.; Bagheri, A. Synthesis, characterization and application of novel lead imprinted polymer nanoparticles as a high selective electrochemical sensor for ultra-trace determination of lead ions in complex matrixes. *Electrochim Acta* **2014,** *136*, 59.

(132) Alizadeh, T.; Amjadi, S. Preparation of nano-sized Pb2+ imprinted polymer and its application as the chemical interface of an electrochemical sensor for toxic lead determination in different real samples. *J Hazard Mater* **2011,** *190* (1-3), 451.

(133) Munteanu, G.; Munteanu, S.; Wipf, D. O. Rapid determination of zeptomole quantities of Pb2+ with the mercury monolayer carbon fiber electrode. *J Electroanal Chem* **2009,** *632* (1–2), 177.

(134) Bi, Z.; Salaun, P.; van den Berg, C. M. Determination of lead and cadmium in seawater using a vibrating silver amalgam microwire electrode. *Anal Chim Acta* **2013,** *769*, 56.

(135) Krystofova, O.; Trnkova, L.; Adam, V.; Zehnalek, J.; Hubalek, J.; Babula, P.; Kizek, R. Electrochemical microsensors for the detection of cadmium (II) and lead (II) ions in plants. *Sensors-Basel* **2010,** *10* (6), 5308.

(136) Zaouak, O.; Authier, L.; Cugnet, C.; Normandin, E.; Champier, D.; Rivaletto, M.; Potin□Gautier, M. Electroanalytical device for cadmium speciation in waters. Part 2: automated system development and cadmium semicontinuous monitoring. *Electroanal* **2010,** *22* (11), 1159.

(137) Zaouak, O.; Authier, L.; Cugnet, C.; Castetbon, A.; Potin□Gautier, M. Electroanalytical device for cadmium speciation in waters. part 1: development and characterization of a reliable screen□printed sensor. *Electroanal* **2010,** *22* (11), 1151.

(138) Superville, P.-J.; Louis, Y.; Billon, G.; Prygiel, J.; Omanović, D.; Pižeta, I. An adaptable automatic trace metal monitoring system for on line measuring in natural waters. *Talanta* **2011,** *87*, 85.

(139) Ribeiro, L. F.; Masini, J. C. Automated determination of Cu (II), Pb (II), Cd (II) and Zn (II) in environmental samples by square wave voltammetry exploiting sequential injection analysis and screen printed electrodes. *Electroanal* **2014,** *26* (12), 2754.

(140) Bi, Z.; Salaün, P.; van den Berg Constant, M. G. Study of Bare and Mercury□ Coated Vibrated Carbon, Gold and Silver Microwire Electrodes for the Determination of Lead and Cadmium in Seawater by Anodic Stripping Voltammetry. *Electroanal* **2013,** *25* (2), 357.

(141) Espada-Bellido, E.; Bi, Z.; van den Berg, C. M. Determination of chromium in estuarine waters by catalytic cathodic stripping voltammetry using a vibrating silver amalgam microwire electrode. *Talanta* **2013,** *105*, 287.

(142) Bi, Z.; Salaün, P.; van den Berg, C. M. G. Speciation of Pb in seawater by pseudopolarography using a vibrating silver amalgam microwire electrode. *Mar Chem* **2013,** *151*, 1.

(143) Stozhko, N. Y.; Malakhova, N. A.; Fyodorov, M. V.; Brainina, K. Z. Modified carbon-containing electrodes in stripping voltammetry of metals - Part I. Glassy carbon and carbon paste electrodes. *Journal of Solid State Electrochemistry* **2008,** *12* (10), 1185.

(144) Stozhko, N. Y.; Malakhova, N. A.; Fyodorov, M. V.; Brainina, K. Z. Modified carbon-containing electrodes in stripping voltammetry of metals. Part II. Composite and microelectrodes. *Journal of Solid State Electrochemistry* **2008,** *12* (10), 1219.

(145) Kurbanoglu, S.; Ozkan, S. A. Electrochemical carbon based nanosensors: A promising tool in pharmaceutical and biomedical analysis. *J Pharm Biomed Anal* **2018,** *147*, 439.

(146) Wang, T.; Yue, W. Carbon Nanotubes Heavy Metal Detection with Stripping Voltammetry: A Review Paper. *Electroanal* **2017,** *29* (10), 2178.

(147) Noked, M.; Soffer, A.; Aurbach, D. The electrochemistry of activated carbonaceous materials: past, present, and future. *Journal of Solid State Electrochemistry* **2011,** *15* (7), 1563.

(148) Shao, Y.; Wang, J.; Wu, H.; Liu, J.; Aksay Ilhan , A.; Lin, Y. Graphene Based Electrochemical Sensors and Biosensors: A Review. *Electroanal* **2010,** *22* (10), 1027.

(149) Yang, W.; Ratinac, K. R.; Ringer, S. P.; Thordarson, P.; Gooding, J. J.; Braet, F. Carbon nanomaterials in biosensors: should you use nanotubes or graphene? *Angewandte Chemie International Edition* **2010,** *49* (12), 2114.

(150) Aragay, G.; Pons, J.; Merkoci, A. Recent trends in macro-, micro-, and nanomaterial-based tools and strategies for heavy-metal detection. *Chem Rev* **2011,** *111* (5), 3433.

(151) Lu, W.; Qin, X.; Liu, S.; Chang, G.; Zhang, Y.; Luo, Y.; Asiri, A. M.; Al-Youbi, A. O.; Sun, X. Economical, green synthesis of fluorescent carbon nanoparticles and their use as probes for sensitive and selective detection of mercury (II) ions. *Analytical Chemistry* **2012,** *84* (12), 5351.

(152) Tiwari, J. N.; Vij, V.; Kemp, K. C.; Kim, K. S. Engineered carbon-nanomaterial-based electrochemical sensors for biomolecules. *ACS Nano* **2016,** *10* (1), 46.

(153) D O'Neil, G.; Newton, M.; Macpherson, J. Direct Identification and Analysis of Heavy Metals in Solution (Hg, Cu, Pb, Zn, Ni) using In-Situ Electrochemical X-Ray Fluorescence. *Anal Chem* **2015,** *87*, 4933.

(154) Le, T. S.; Da Costa, P.; Huguet, P.; Sistat, P.; Pichot, F.; Silva, F.; Renaud, L.; Cretin, M. Upstream microelectrodialysis for heavy metals detection on boron doped diamond. *J Electroanal Chem* **2012,** *670*, 50.

(155) Kokkinos, C.; Economou, A. Stripping analysis at bismuth-based electrodes. *Current Analytical Chemistry* **2008,** *4* (3), 183.

(156) Ouyang, R. Z.; Xu, L. N.; Wen, H. F.; Cao, P. H.; Jia, P. P.; Lei, T.; Zhou, X.; Tie, M.; Fu, X. L.; Zhao, Y. F.et al. A Novel Indium Doped Bismuth Nanofilm for Simultaneous Stripping Determination of Zn(II), Cd(II) and Pb(II) in River Water. *Int J Electrochem Sc* **2018,** *13* (2), 1423.

(157) Chuanuwatanakul, S.; Dungchai, W.; Chailapakul, O.; Motomizu, S. Determination of trace heavy metals by sequential injection-anodic stripping voltammetry using bismuth film screen-printed carbon electrode. *Anal Sci* **2008,** *24* (5), 589.

(158) Liu, G. S.; Chen, J. P.; Hou, X. D.; Huang, W. S. A highly-sensitive electrochemical sensor for the simultaneous detection of Cd2+ and Pb2+ using liquid phase-exfoliated graphene. *Anal Methods-Uk* **2014,** *6* (15), 5760.

(159) Chen, C.; Niu, X.; Chai, Y.; Zhao, H.; Lan, M. Bismuth-based porous screen-printed carbon electrode with enhanced sensitivity for trace heavy metal detection by stripping voltammetry. *Sensors and Actuators. B: Chemical* **2013,** *178*, 339.

(160) Ren, W.; Zhang, Y.; Li, M. J. Sensitive Determination of Zn2+, Cd2+ and Pb2+ at Electrochemically Reduced Nanoporous Graphene Oxide/Bismuth Film Electrode. *Int J Electrochem Sc* **2018,** *13* (2), 1331.

(161) Yi, W. J.; Li, Y.; Ran, G.; Luo, H. Q.; Li, N. B. Determination of cadmium(II) by square wave anodic stripping voltammetry using bismuth-antimony film electrode. *Sensors and Actuators, B: Chemical* **2012,** *166*, 544.

(162) Fang, H.-L.; Zheng, H.-X.; Ou, M.-Y.; Meng, Q.; Fan, D.-H.; Wang, W. One-step sensing lead in surface waters with screen printed electrode. *Sensors and Actuators, B: Chemical* **2011,** *153* (2), 369.

(163) Pan, D.; Zhang, L.; Zhuang, J.; Yin, T.; Lu, W.; Qin, W. On-line determination of lead in tap waters at two-step prepared bismuth electrode. *Int. J. Electrochem. Sci* **2011,** *6*, 2710.

(164) Jiang, X.; Sun, Q.; Zhang, J.; Wang, B.; Du, X. Determination of Sn2+ ion in canned foods using bismuth- and antimony-film electrodes. *Sens. Lett.* **2009,** *7* (1), 91.

(165) Yin, L.; Ling, Y.; Liu, G.; Li, P.; Wu, S. Determination of trace lead and cadmium in water by stripping voltammetry with a copper-based composite antimony film electrode. *Zhongguo Kexue Jishu Daxue Xuebao* **2011,** *41* (6), 550.

(166) Cao, L.; Zhou, G.-y.; Li, Q.-y. Anodic stripping voltammetry of antimony film electrode and research progress in detection of heavy metals in water and food. *Shipin Yu Fajiao Keji* **2015,** *51* (6), 86.

(167) Sosa, V.; Barceló, C.; Serrano, N.; Ariño, C.; Díaz-Cruz, J. M.; Esteban, M. Antimony film screen-printed carbon electrode for stripping analysis of Cd(II), Pb(II), and Cu(II) in natural samples. *Anal Chim Acta* **2015,** *855*, 34.

(168) Slavec, M.; Hocevar, S. B.; Baldrianova, L.; Tesarova, E.; Svancara, I.; Ogorevc, B.; Vytras, K. Antimony film microelectrode for anodic stripping measurement of cadmium(II), lead(II) and copper(II). *Electroanal* **2010,** *22* (14), 1617.

(169) Tesarova, E.; Baldrianova, L.; Hocevar, S. B.; Svancara, I.; Vytras, K.; Ogorevc, B. Anodic stripping voltammetric measurement of trace heavy metals at antimony film carbon paste electrode. *Electrochim Acta* **2009,** *54* (5), 1506.

(170) Ashrafi, A. M.; Vytras, K. Codeposited antimony-bismuth film carbon paste electrodes for electrochemical stripping determination of trace heavy metals. *Int J Electrochem Sc* **2013,** *8* (2), 2095.

(171) Sebez, B.; Ogorevc, B.; Hocevar, S. B.; Veber, M. Functioning of antimony film electrode in acid media under cyclic and anodic stripping voltammetry conditions. *Anal Chim Acta* **2013,** *785*, 43.

(172) Jovanovski, V.; Hocevar, S. B.; Ogorevc, B. *Ex situ* prepared antimony film electrode for electrochemical stripping measurement of heavy metal ions. *Electroanal* **2009,** *21* (21), 2321.

(173) Ashrafi, A. M.; Cerovac, S.; Mudrić, S.; Guzsvány, V.; Husáková, L.; Urbanová, I.; Vytřas, K. Antimony nanoparticle-multiwalled carbon nanotubes composite immobilized at carbon paste electrode for determination of trace heavy metals. *Sensors and Actuators B: Chemical* **2014,** *191*, 320.

(174) Urbanova, V.; Vytras, K.; Kuhn, A. Macroporous antimony film electrodes for stripping analysis of trace heavy metals. *Electrochem Commun* **2010,** *12* (1), 114.

(175) Guzsvany, V.; Nakajima, H.; Soh, N.; Nakano, K.; Svancara, I.; Vytras, K.; Bjelica, L.; Imato, T. Anodic stripping voltammetry combined with sequential injection analysis for measurements of trace metal ions with bismuth- and antimony film electrodes under comparable conditions. *Electroanal* **2011,** *23* (7), 1593.

(176) Chen, C.; Niu, X. H.; Chai, Y.; Zhao, H. L.; Lan, M. B.; Zhu, Y. G.; Wei, G. Determination of lead(II) using screen-printed bismuth-antimony film electrode. *Electroanal* **2013,** *25* (6), 1446.

(177) Maczuga, M.; Economou, A.; Bobrowski, A.; Prodromidis, M. I. Novel screen-printed antimony and tin voltammetric sensors for anodic stripping detection of Pb (II) and Cd (II). *Electrochim Acta* **2013,** *114*, 758.

(178) Perez-Rafols, C.; Serrano, N.; Diaz-Cruz, J. M.; Arino, C.; Esteban, M. New approaches to antimony film screen-printed electrodes using carbon-based nanomaterials substrates. *Anal Chim Acta* **2016,** *916*, 17.

(179) Serrano, N.; Diaz-Cruz, J. M.; Arino, C.; Esteban, M. Antimony- based electrodes for analytical determinations. *Trac-Trends in Analytical Chemistry* **2016,** *77*, 203.

(180) Toghill, K. E.; Xiao, L.; Wildgoose, G. G.; Compton, R. G. Electroanalytical determination of cadmium(II) and lead(II) using an antimony nanoparticle modified boron-doped diamond electrode. *Electroanal* **2009,** *21* (10), 1113.

(181) Dal Borgo, S.; Jovanovski, V.; Hocevar, S. B. Antimony film electrode for stripping voltammetric measurement of Hg(II) in the presence of Cu(II). *Electrochim. Acta* **2013,** *88*, 713.

(182) United States Environmnetal Protection Agency; Vol. 2018.

(183) Economou, A. Screen-Printed Electrodes Modified with "Green" Metals for Electrochemical Stripping Analysis of Toxic Elements. *Sensors (Basel)* **2018,** *18* (4), 1032.

(184) Tercier-Waeber, M. L.; Hezard, T.; Masson, M. In situ monitoring of the diurnal evolution of the dynamic metal species in the Riou-Mort river. *Geochim Cosmochim Ac* **2009,** *73* (13), A1321.

(185) Money, C.; Braungardt, C. B.; Jha, A. N.; Worsfold, P. J.; Achterberg, E. P. Metal speciation and toxicity of Tamar Estuary water to larvae of the Pacific oyster, Crassostrea gigas. *Mar Environ Res* **2011,** *72* (1-2), 3.

(186) Braungardt, C. B.; Achterberg, E. P.; Axelsson, B.; Buffle, J.; Graziottin, F.; Howell, K. A.; Illuminati, S.; Scarponi, G.; Tappin, A. D.; Tercier-Waeber, M. L.et al. Analysis of dissolved metal fractions in coastal waters: An inter-

comparison of five voltammetric in situ profiling (VIP) systems. *Mar Chem* **2009,** *114* (1-2), 47.

(187) Zou, Z. W.; Jang, A.; MacKnight, E. T.; Wu, P. M.; Do, J.; Shim, J. S.; Bishop, P. L.; Ahn, C. H. An on-site heavy metal analyzer with polymer lab-on-a-chips for continuous sampling and monitoring. *Ieee Sens J* **2009,** *9* (5-6), 586.

(188) Almeida, E. S.; Richter, E. M.; Munoz, R. A. A. On-site fuel electroanalysis: Determination of lead, copper and mercury in fuel bioethanol by anodic stripping voltammetry using screen-printed gold electrodes. *Anal Chim Acta* **2014,** *837*, 38.

(189) Zhang, X.; Zhang, Y.; Ding, D.; Zhao, J.; Liu, J.; Yang, W.; Qu, K. On-site determination of Pb2+ and Cd2+ in seawater by double stripping voltammetry with bismuth-modified working electrodes. *Microchem J* **2016,** *126*, 280.

(190) Ferancova, A.; Hattuniemi, M. K.; Sesay, A. M.; Raty, J. P.; Virtanen, V. T. Rapid and direct electrochemical determination of Ni(II) in industrial discharge water. *J Hazard Mater* **2016,** *306*, 50.

(191) Tormin, T. F.; Cunha, R. R.; da Silva, R. A. B.; Munoz, R. A. A.; Richter, E. M. Combination of screen-printed electrodes and batch injection analysis: A simple, robust, high-throughput, and portable electrochemical system. *Sensor Actuat B-Chem* **2014,** *202*, 93.

(192) Henríquez, C.; Laglera, L.; Alpizar, M.; Calvo, J.; Arduini, F.; Cerdà, V. Cadmium determination in natural water samples with an automatic multisyringe

flow injection system coupled to a flow-through screen printed electrode. *Talanta* **2012,** *96*, 140.

(193) Chapman, C. S.; Cooke, R. D.; Salaun, P.; van den Berg, C. M. G. Apparatus for in situ monitoring of copper in coastal waters. *J Environ Monitor* **2012,** *14* (10), 2793.

(194) ; United States Environmental Protection Agency; Vol. 2018.

(195) Sohrin, Y.; Urushihara, S.; Nakatsuka, S.; Kono, T.; Higo, E.; Minami, T.; Norisuye, K.; Umetani, S. Multielemental determination of GEOTRACES key trace metals in seawater by ICPMS after preconcentration using an ethylenediaminetriacetic acid chelating resin. *Analytical Chemistry* **2008,** *80* (16), 6267.

(196) ; GEOTRACES, 2013; Vol. 2018.

CHAPTER 3

IONOPHORE GRAFTED CARBON FIBER MICROELECTRODES AS A TRACE METAL SPECIATION SENSOR[2]

[2] **Holmes, J.;** Ou, Y.; Hashemi, P.: "Ionophore-grafted carbon fiber microelectrodes as a trace metal speciation sensor." – *In preparation* – Environmental Science and Technology.

3.1 ABSTRACT

Metal ions are important nutrients in the environment, however excessive accumulation, originating from natural or anthropogenic sources, is detrimental. This is because metal ions tend to bioaccumulate up the food chain, posing risks to human health. Free, unbound metals are more likely to engage in biological processes. Speciation, however, is highly dependent on environmental factors (i.e. pH and temperature) and is altered by sampling methods, thereby making on-site and *in situ* analysis techniques essential for measuring actual metal concentrations. Electrochemistry is a useful technique for trace metal analysis because electrodes are small, portable, and selective for detection of labile metal ions, though many electrochemical methods are limited by stability, selectivity, and low temporal resolution. Previously, we utilized a voltammetric method called fast-scan cyclic voltammetry that offers sub-second temporal resolution and excellent stability to selectively measure labile Cu(II) on ionophore-grafted carbon fiber microelectrodes (CFM). In this work, we characterize the detection interface of Cu(II) ions at ionophore-grafted CFMs with respect to ionic strength of the matrix, adsorption efficiency, and potential limits during analysis. Additionally, the electrode response in the presence of other divalent metal ions is qualitatively and quantitatively analyzed, and we find that decreases in sensitivity on electrodes that have undergonesurface fouling from interferences can be reversed. This study sheds light on the functionality of ionophore-grafted CFMs as a trace metal speciation sensor.

3.2 INTRODUCTION

Metal ions such as Cu, Zn, and Ni exist naturally in the environment and act as essential nutrients for many biological processes. However, buildup of excess amounts of such metals can be harmful. An index of metal mobility, toxicity, and pollution is speciation.[1,2] Metal ions in the labile state are more likely to participate in chemical processes.[3,4] While the majority of metal ions are in the bound state at equilibrium, when environmental systems are disrupted by anthropogenic or natural events, such as storms, metal ions can be mobilized into natural waters.[5] Because metals bioaccumulate,[6-8] it is critically important to determine speciation in dynamic and rapidly changing environmental systems and to assess how events such as storms affect the ecosystem.

Analysis of environmental systems undergoing rapid speciation changes requires a technique that fulfills a set of analytical criteria including sensitivity, selectivity, speed, and stability.[9] Additionally, on-site and *in situ* monitoring is essential because under environmental conditions, removing a sample from the source inherently changes the sample and alters specification.[10,11] Currently available methods offer sensitive and selective measurements but suffer from bulky instrumentation and are unable to distinguish between free and bound metals.[12-15] Electrochemistry is an attractive approach because electrodes are portable and can selectively measure labile metal ions.[16,17] Ion selective electrodes are the gold standard for electrochemical selectivity, but they suffer from poor stability.[18] Stripping voltammetry is also useful for metal detection because metals oxidize or reduce at discrete potentials that allows them to be identified, though stripping voltammetry requires several minutes to collect each data point.[9]

In light of the limitations associated with other electrochemical techniques, fast-scan cyclic voltammetry (FSCV) performed at carbon fiber microelectrodes (CFMs) has emerged as a breakthrough method for trace metal analysis. Traditionally used for neurochemical analysis due to its sub-second temporal resolution, selectivity, and sensitivity, FSCV is also powerful for detecting metal ions. Our group has previously optimized a Cu(II) specific waveform,[19] performed fundamental studies of the CFM-Cu(II) interface,[20,21] and defined a mathematical relationship between electrode response and Cu(II) complexation.[22,23] One limitation, however, is that the bare CFM surface gives signals from other divalent metals interferences that overlap with the Cu(II) signal. To address this issue, we published a method to functionalize the CFM surface with a Cu(II) specific ionophore in efforts to improve selectivity towards Cu(II) in matrices that include interfering metals and other ligands.[24]

In this work, we optimize this functionalization process and characterize the Cu(II) response on ionophore-grafted CFMs. We first streamline the fabrication, creating multiple ionophore-grafted CFMs simultaneously with high yield. Then we evaluate the sensitivity of ionophore-grafted CFMs to Cu(II) under varying ionic strengths and identify the optimal ionic strength for analysis. The detection mechanism occurring at the analyte-electrode interface is found to be governed by adsorption, evidenced by the goodness of fit between the Langmuir adsorption isotherm and the data set. The adsorption coefficient is determined (K_{ads} = 2.68×10^9). Additionally, we analyze the interference effects of divalent metals and define a waveform suitable for CFMs that have undergone surface modifications. We find that divalent metals decrease the surface concentration of Cu(II) on ionophore-grafted CFMs, but do not obstruct the Cu(II)

voltammetric signature. Furthermore, we find that interference fouling of ionophore-grafted CFMs can be reversed by driving other divalent ions out from the ionophore binding zone, allowing the electrodes to be recovered and reused. With this work, we complete a fundamental characterization study of the ionophore-grafted CFM interaction with Cu(II) ions as a sensing strategy. The results reported in this chapter lay the groundwork for the development of a field portable metal speciation sensor capable of *in situ* analysis.

3.3 MATERIALS AND METHODS

3.3.1 Solutions

All chemicals were purchased from Sigma Aldrich (St. Louis, MO) unless otherwise specified. Imidazole was purchased from Oakwood Chemicals. All experiments were performed at standard temperature and pressure and pH = 5.40. NaCl was used as the background electrolyte, ranging in concentration from 0.0005 M to 0.1 M. Cu(II) concentration was varied between 0.1 μM to 10 μM. Modified electrodes were tested for interferences in a mixed metal solution containing 6 other divalent metals: Cu(II), Zn(II), Cd(II), Ni(II), Ca(II), Pb(II), Co(II) all with NO^{3-} counter ions.

3.3.2 Microelectrodes

CFMs were prepared in-house by vacuum aspirating a 5 μm radius single carbon fiber (T-650, Cytec Industries, NJ) into a glass capillary (0.6 mm external diameter, 0.4 mm internal diameter, A-M systems, Inc., Sequim, WA), which is then pulled with a vertical micropipette puller (Narishige, Tokyo, Japan) to form a carbon-glass seal. The exposed length of the carbon fiber is then cut to a specific length, in this case, either 300 μm or 25 - 50 μm, depending on the ionic strength.

3.3.3 Electrochemistry

3.3.3.1 FSCV

The FSCV instrumentation is comprised of a potentiostat (Dagan Corporation, Minneapolis, MN, USA), a custom-built analog-to-digital converter box and national instruments data acquisition cards. After the data was collected, background subtraction, signal averaging, and digital filtration were performed with custom built software in LabView (Knowmad Technologies LLC, Tucson, AZ). A Cu(II) waveform (−1.2 V to +0.8 V at 10 Hz, resting potential of 0 V, at 600 V s−1) was applied and the resulting current was measured; together the data is presented as current vs. potential plots, called cyclic voltammograms (CVs).

3.3.3.2 FSCAV

A CFM was placed into a $Cu(NO_3)^2$ solution and a waveform (-1.2 V to +0.8 V at 100 Hz, resting potential of 0 V, at 600 V/s) was applied. An electronic relay (ADG-419, Analog Devices) was used to switch between the applied waveform and a constant potential of 0 V for 10 seconds to allow copper adsorption at the electrode surface to reach equilibrium. After 10 seconds, the waveform was reapplied, and the first background subtracted CV that displayed the signature Cu(II) peaks was analyzed. The area of the reduction Cu(II) peak was integrated and converted to adsorbed Cu(II) using a calibration curve. The resulting charge was used to calculate the surface concentration of adsorbed analyte using Faraday's law, where Γ is surface coverage (pmol/cm^2), Q is charge, n is the charge of the molecule (+2 for Cu(II)), F is Faraday's constant, and A is the surface area of the exposed fiber.

(1) $\Gamma_{\text{metal}} = \frac{Q}{nFA}$

Additionally, an advantage of using FSCAV is that the electrodes do not have to be cut to the exact same length because the equation above normalizes the signal based on electrode length.

3.3.4 Modification procedure for ionophore-grafted CFMs

3.3.4.1 Step 1: Reductive coupling of diazonium salt to the CFM surface

A CFM was submerged in a solution of 0.01 M 4-((trimethylsilyl)ethynyl)benzenediazonium tetrafluoroborate (TMS) and 0.1 M tetrabutylammonium hexafluorophosphate (NBu4PF6) in acetonitrile. The potential of the CFM was scanned twice from 0.8 V to -0.6 V and back to 0.8 V vs. Ag/AgCl at a scan rate of 0.05 V/s. The electrode was then rinsed with acetonitrile and acetone. Deprotection of the diazonium salt was achieved by suspending the electrode in a solution of 0.1 M tetra-n-butylammonium fluoride (TBAF) in tetrahydrofuran (THF) for 30 minutes. The resulting electrode was rinsed with THF and acetone.

3.3.4.2 Step 2: Inhibition of surface oxygenated groups of CFM

The CFM was then fixed into an Ar purged air-tight vial containing a solution of 0.10 M tert-Butyldimethylsilyl (TBSCl), 0.11 M imidazole, 0.01 M 4-methylaminopyridine (DMAP), in CH_2Cl_2. A potential of -1.9 V was applied for 2-6 hours.

3.3.4.3 Step 3: Azide-alkyne cycloaddition of ionophore

The CFM was submerged into a stirring solution of 0.01 M azido-ionophore, 0.05 M CuSO4•H2O, and 0.1 M ascorbic acid in dimethylformamide (DMF) for 4-5 hours. The resulting electrode was rinsed with acetone, submerged in a stirred solution of saturated ethylenediaminetetraacetic acid (EDTA) for 10 minutes, and then in a stirred solution of deionized water for 10 minutes.

3.3.5 Langmuir Adsorption Isotherm

A linearized Langmuir adsorption isotherm was fit to the data, where [Cu(II)] is the concentration of Cu(II) in bulk solution, and Γ_{max} is the maximum monolayer adsorption coverage at the carbon surface. K represents the adsorption coefficient (K_{ads}) between Cu(II) in bulk solution and Cu(II) adsorbed to ionophore-grafted carbon, reported in **Figure 3.2**.

$$(2)\ \frac{[\mathrm{Cu(II)}]}{\Gamma_{\mathrm{Cu(II)}}} = \frac{1}{\Gamma_{max}}[\mathrm{Cu(II)}] + \frac{1}{\Gamma_{max}\mathrm{K}}$$

3.4 RESULTS AND DISCUSSION

3.4.1 Optimization of experimental parameters

The ability to detect Cu(II) ions with high specificity is essential for trace metal detection in water systems because other divalent metals interfere with the Cu(II) signal. Ionophore-grafted CFMs are a selective and sensitive tool for Cu(II) detection, and when coupled with fast voltammetric techniques, offer sub-second temporal resolution. Our group previously published a protocol for covalently binding a Cu(II)-specific ionophore to CFMs, reporting enhanced selectivity towards Cu(II) over interfering divalent metals,

16 week shelf life, and a limit of detection = $5x10^{-9}$.[24] Here, we aim to further characterize the interface between ionophore-grafted CFMs and Cu(II) ions to further understand the detection mechanism.

We first made efforts to streamline the modification protocol, modifying many electrodes with high yield. To improve reproducibility, several modifications were required to the protocol (see methods) including: (1) performing the first step as quickly as possible because exposure to oxygen will deactivate the diazonium salt and prevent binding; (2) increasing the time from 2 to 6 hours in the "blocking" step resulted in highly reproducible blocked electrodes, and (3) constructing a parallel circuit to apply the same potential to multiple electrodes simultaneously. There were no changes made to the third ionophore attachment step. During FSCAV analysis, we found that the previously reported electrode size led to overloading (a software limitation that maxes out the observed current) and required a low ionic strength (0.5 mM) to prevent overloading. Cu(II) detection at this length and ionic strength combo did not result in a reproducible Cu(II) signal, as shown in the representative color plot and CV in **Figure 3.1Ai**. This is likely due to the low ionic strength and inability to facilitate mass transport of analyte towards the electrode. For this reason, we reoptimized the electrode size, chosen with respect to both the waveform and the ionic strength in order to maximize the current response while preventing overloading. Our long-term goal is to use ionophore-grafted CFMs as portable, on-site sensors for real water samples. Thus, we chose an electrode length of 25-50 μm because electrodes trimmed to this length did not overload with the Cu(II) waveform in a sample of seawater (I = 0.7 M). By using a higher ionic strength (I

= 25 mM) and electrodes trimmed to 25-50 µm, we obtained a signature Cu(II) reduction peak (**Figure 3.1Aii**).

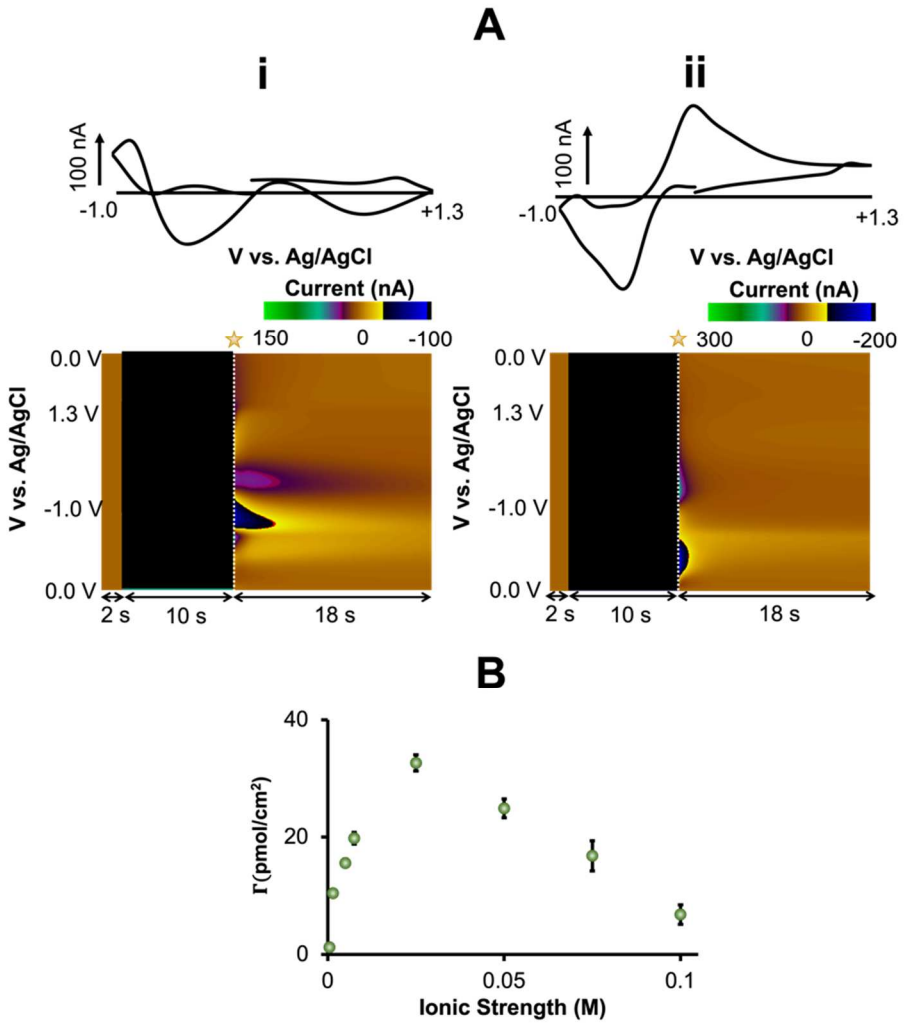

Figure 3.1. Ionic strength characterization. (A) Representative color plots and CVs of 1µM Cu(II) on CFMs cut to (i) 300 µm in 0.5 mM NaCl buffer, and (ii) 25 µm in 25 mM NaCl buffer. **(B)** Surface concentration (Γ) of 1 µM Cu(II) plotted against ionic strength of the background buffer (NaCl). Error bars: SEM.

To assess the utility of this sensor in samples of varying ionic strength, a characterization of sensor response with regards to ionic strength was performed on 3 electrodes (**Figure 3.1B**). We found that at lower ionic strengths (0.5 - 25 mM), the current response increases logarithmically, reaching a plateau at 25 mM. At higher ionic

strengths (25 mM - 100 mM) the surface coverage decays linearly. This result is not surprising, as Bayramoglu *et al.* described the same ionic strength relationship to adsorbed species.[25] Here, we can conclude that at low ionic strengths, the presence of electrolytes facilitates migration of analyte through the bulk solution towards the electrode, as expected. However, at high ionic strengths, electrolyte begins to sterically hinder the space around the electrode, blocking the path of Cu(II) ions towards the electrode. Additionally, at high concentrations, Na^+ ions in solution may compete with Cu(II) ions, lowering the availability of vacant ionophores for Cu(II). When analyzing the corresponding CVs, the signature Cu(II) reduction peak is still present, meaning the competing ions in solution do not perform redox chemistry with the ionophore. Rather, electrolyte most likely statically blocks the interaction of Cu(II) with the ionophore, but does not electrochemically interact with the ionophore itself.

3.4.2 Adsorption properties of Ionophore grafted CFMs

One unique property of electrodes fashioned from carbon materials is the tendency for some analytes to adsorb to the electrode surface. We have previously shown that migration of metals towards carbon electrodes is a process governed by adsorption, and reported the thermodynamic equilibrium constant of Cu(II) adsorption on bare CFM ($K_{ads} = 4.05\times10^9$).[20] This equilibrium constant describes the relationship between the concentration of Cu(II) in solution and the surface concentration adsorbed to the CFM (Γ) and represents the thermodynamic favorability of Cu(II) to adsorb to the bare or ionophore-grafted CFM vs being dissolved in bulk solution. Similar to the adsorption profile of Cu(II) to bare carbon, the plot of Cu(II) surface concentration to Cu(II) in bulk solution on Ionophore-grafted CFM in **Figure 3.2** can be fitted with a Langmuir

adsorption isotherm. This indicates that Cu(II) follows a monolayer adsorption process. **Equation 1** was used to calculate the K_{ads} = 2.68 x10^9. The K_{ads} reported for Cu(II) on a bare CFM and an ionophore-grafted CFM are on the same order of magnitude. This finding is significant because FSCV is heavily governed by adsorption and similar adsorption processes on carbon and ionophore-grafted carbon are likely the reason Cu(II) measurements are possible.

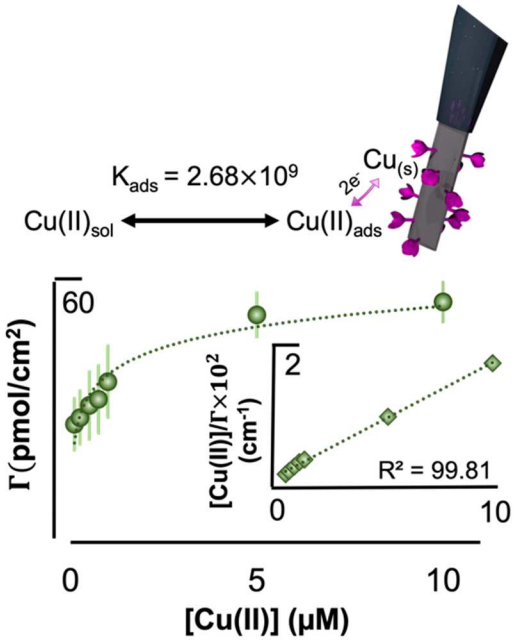

Figure 3.2. Adsorption Profile of Cu(II) on Ionophore-grafted CFMs. Schematic representation of adsorption equilibria of glutamate adsorbed to the ionophore-grafted CFM or in bulk solution**.** Langmuir adsorption isotherm (dotted line) fit with raw data (points) and the linearized isotherm is inset.

3.4.3 Selectivity and waveform optimization

The hallmark feature of ionophore-grafted CFMs is enhanced selectivity towards Cu(II) in the presence of divalent metals and the potential limits of the waveform plays an important role in selectivity over interferences. At high potential limits (1.3 V) the carbon electrode overoxidizes, stripping the outer layer of the carbon to reveal a new

surface.[26] Waveforms scanning to 1.3V are useful for activating and renewing the electrode surface between scans. We hypothesized, however, that scanning to 1.3 V may negatively impact the ionophore modification on the carbon. To test this, we performed FSCAV with two different waveforms on bare and ionophore-grafted CFMs in solutions containing a 5:1 ratio of interferences to Cu(II). **Figure 3.3** shows the color plots and CVs of a Bare CFM (**Figure 3.3A**) and an ionophore-grafted CFM applying a positive potential limit of 0.8 V (**Figure 3.3B**). The selectivity of ionophore-grafted CFMs is displayed here, where a well resolved Cu(II) reduction peak is observed at -0.7 V while the bare CFM generates no distinguishable peaks in the presence of interferences. When a positive potential limit of 1.3 V is applied to an ionophore-grafted CFM (**Figure 3.3C**), there are several non-faradaic switching peaks recorded on the CV, making the Cu(II) signal less distinguishable. Additionally, the waveform scanning up to 0.8 V results in a higher current response. In a matrix were divalent metal interferences are present, the waveform with a positive potential of 0.8 V provides a more reliable signal and higher current response.

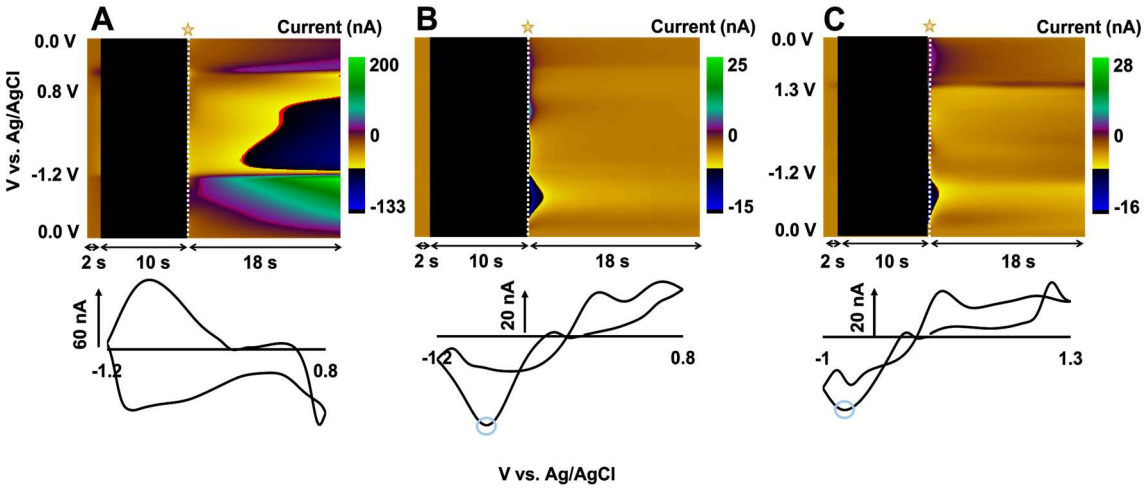

Figure 3.3. Waveform optimization in media containing interferences. A comparison of representative color plots obtained for a mixture of metals including 1 μM Cu(II) and 5 μM of Zn(II), Cd(II), Ni(II), Co(II), Ca(II), Pb(II) in NaCl. All anions are NO3-. The vertical white dashed line indicates where the CV was regenerated from. **(A)** A bare CFM with a modified waveform (-1.2 V to +0.8 V, resting potential of 0 V, at 600 V/s) results in no Cu(II) peak. Both an ionophore-grafted CFM with **(B)** a modified waveform and **(C)** an overoxidizing waveform for Cu(II) (-1.0 V to +1.3 V, resting potential of 0 V, at 600 V/s) result in Cu(II) signature peaks at -0.7 V.

3.4.4 Interference and Stability Characteristics of the Cu(II) signal

The selectivity of a method is based both on resistance to qualitative and quantitative interferences to a signal. In **Figure 3.3** we demonstrated that the ionophore-grafting modification process prevents the electrode from qualitative interference in the presence of divalent metals, indicated by the Cu(II) signal. Here, we test the quantitative interference of divalent metals. In **Figure 3.4A**, the ratio of mixed metal: Cu(II) is systematically increased and the resultant surface concentration is quantified. As the relative amount of mixed metal is increased, the surface concentration of Cu(II) exponentially decays. At a ratio of 2.5 mixed metal: 1 Cu(II), the change in surface concentration reaches significance ($p < 0.5$) and remains significantly different at higher ratios. Although the presence of interfering metals impacts the Cu(II) surface concentration, the Cu(II) peak (denoted with a star) persists throughout various ratios of interference (Inset on the plot are 3 CVs (0:1, 0.5:1, and 5:1)). This indicates that although interfering metals have some affinity for the ionophore and influence the Cu(II)-ionophore interface, the only redox processes occurring at ionophore-grafted CFMs are from Cu(II) metal ions. Thus the ionophore-grafted CFM is qualitatively resistant to interferences but the Cu(II) signal is quantitatively sensitive to the presence of other divalent metal ions.

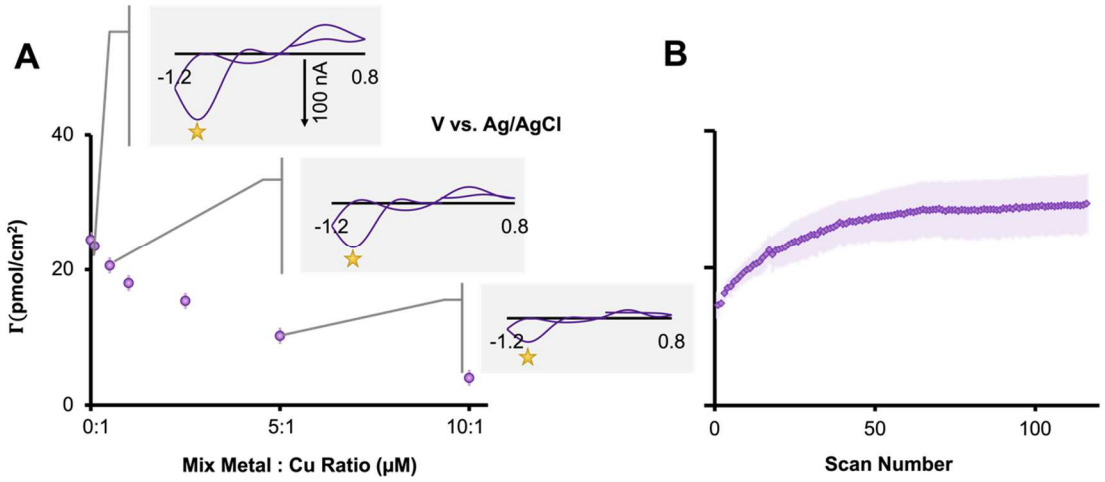

Figure 3.4. Interference fouling and recovery. (A) The ratio of mixed metal: Cu(II) is plotted against the surface concentration. Inset: CVs from 0:1, 0.5:1, and 5:1 ratios. **(B)** CFMs exposed to a 10:1 ratio are placed in a 1 μM Cu(II) solution and the surface concentration is recorded over 120 scans. Inset: Histogram of surface concentration at 3 ratios and after recovery. Error bars: SEM.

After the mixed metal experimental paradigm shown in **Figure 3.4A**, the signal response decreases by 84% at 10:1 ratio ($p < 0.5$). We postulate that this is because the interfering ions inhabit the binding zone of the ionophore, preventing Cu(II) from interacting with active zones. In the interest of recovering an ionophore-grafted CFM that has been fouled by exposure to a 10:1 ratio of mixed metal: Cu(II), the electrode was placed into a solution of 1μM Cu(II), 120 successive files were collected with FSCAV and the surface concentration recorded slowly increased with each file. **Figure 3.4B** shows the recovery of the Cu(II) signal over time, reaching a plateau in signal around file 60 at 28.79 pmol/cm^2. Importantly, the average surface concentration before fouling (**Figure 3.4A**, 0 mixed metal: 1 Cu(II)) is not statistically different from the average surface concentration after a plateau is reached in 1 μM Cu(II) solution (**Figure 3.4B**). This data provides evidence that ionophore-grafted CFMs can be recovered and reused after exposure to a matrix containing divalent interfering metals. We believe this reversal

process is driven by competition effects of Cu(II) over other metals combined with the ionophores high selectivity coefficient towards Cu(II) binding, occurring slowly over time. In the future, we plan to explore a more time efficient recovery protocol, exposing the electrode to a chemical chelating agent (EDTA) in order to free the ionophore sites of bound species.

3.5 CONCLUSION AND FUTURE DIRECTIONS

Metal ions, such as Cu(II), Pb(II), and Hg(II) act as essential nutrients for many biological processes, however excess amounts of such metals can be harmful. Speciation analysis can provide important information on mobility, toxicity and pollution, as metal ions in the free state are more likely to participate in biological processes and bioaccumulate up the food chain. Analysis of environmental systems undergoing rapid speciation changes requires a technique capable of on-site and *in situ* monitoring because removing a sample from the source inherently changes the sample and alters speciation. Electrochemistry is an attractive approach because electrodes are small, portable, and selectively measure free metals. In particular, FSCV performed on CFMs offers sub-second temporal resolution and sensitivity towards Cu(II) detection. FSCV however is limited by signal masking from other divalent metals interferences. To account for this, a surface modification protocol was published by Yang *et al.* in 2016 utilizing a Cu(II) specific ionophore covalently grafted to a CFM.[24]

The incorporation of a binding agent inherently alters the analyte-electrode interface. In this work, we characterize this interface. We first streamline the functionalization process, creating multiple ionophore-grafted CFMs simultaneously with

high yield. We find that the electrode response is highly dependent on the size of the electrode and ionic strength of the solution. By significantly decreasing the electrode length and measuring the surface concentration in response to varying ionic strengths, we identify the optimal ionic strength for analysis. We then identify the mechanism of detection as an adsorption driven process evidenced by fitting experimental data to a Langmuir adsorption isotherm and calculate the adsorption coefficient ($K_{ads} = 2.68x10^9$). Finally we define a waveform best suited for Cu(II) detection on ionophore-grafted CFMs to assess the influence of divalent metal interferences. We find that the presence of other divalent metals influences sensitivity to Cu(II), but does not obstruct the Cu(II) voltammetric signature. Furthermore, we find that interference fouling can be reversed, allowing the electrodes to be recovered and reused. With this work, we complete a fundamental characterization study of the ionophore-grafted CFM interaction with Cu(II) ions as a sensing strategy.

3.6 References

(1) Reeder, R. J.; Schoonen, M. A. A.; Lanzirotti, A. Metal speciation and its role in bioaccessibility and bioavailability. *Rev Mineral Geochem* **2006,** *64*, 59.

(2) Fytianos, K. Speciation analysis of heavy metals in natural waters: A review. *J Aoac Int* **2001,** *84* (6), 1763.

(3) Fernando, Q. Metal Speciation in Environmental and Biological-Systems. *Environ Health Persp* **1995,** *103*, 13.

(4) Templeton, D. M. Speciation in Metal Toxicity and Metal-Based Therapeutics. *Toxics* **2015,** *3* (2), 170.

(5) Mancinelli, E.; Baltrenaite, E.; Baltrenas, P.; Paliulis, D.; Passerini, G.; Almas, A. R. Trace metal concentration and speciation in storm water runoff on impervious surfaces. *J Environ Eng Landsc* **2015,** *23* (1), 15.

(6) Zeng, X.; Xu, X. J.; Boezen, H. M.; Huo, X. Children with health impairments by heavy metals in an e-waste recycling area. *Chemosphere* **2016,** *148*, 408.

(7) Croteau, M. N.; Luoma, S. N.; Stewart, A. R. Trophic transfer of metals along freshwater food webs: Evidence of cadmium biomagnification in nature. *Limnol Oceanogr* **2005,** *50* (5), 1511.

(8) Que, E. L.; Domaille, D. W.; Chang, C. J. Metals in neurobiology: Probing their chemistry and biology with molecular imaging. *Chem Rev* **2008,** *108* (5), 1517.

(9) Holmes, J.; Pathirathna, P.; Hashemi, P. Novel frontiers in voltammetric trace metal analysis: Towards real time, on-site, in situ measurements. *Trac-Trend Anal Chem* **2019,** *111*, 206.

(10) Hong, Y. S.; Kinney, K. A.; Reible, D. D. Effects Of Cyclic Changes In Ph And Salinity On Metals Release From Sediments. *Environ Toxicol Chem* **2011,** *30* (8), 1775.

(11) Posacka, A. M.; Semeniuk, D. M.; Whitby, H.; van den Berg, C. M. G.; Cullen, J. T.; Orians, K.; Maldonado, M. T. Dissolved copper (dCu) biogeochemical cycling in the subarctic Northeast Pacific and a call for improving methodologies. *Mar Chem* **2017,** *196*, 47.

(12) Perez-Fernandez, V.; Rocca, L. M.; Tomai, P.; Fanali, S.; Gentili, A. Recent advancements and future trends in environmental analysis: Sample preparation, liquid chromatography and mass spectrometry. *Anal Chim Acta* **2017,** *983*, 9.

(13) Pesavento, M.; Alberti, G.; Biesuz, R. Analytical methods for determination of free metal ion concentration, labile species fraction and metal complexation capacity of environmental waters: A review. *Anal Chim Acta* **2009,** *631* (2), 129.

(14) Filella, M. Food for Thought: A Critical Overview of Current Practical and Conceptual Challenges in Trace Element Analysis in Natural Waters. *Water-Sui* **2013,** *5* (3), 1152.

(15) Feldmann, J.; Salaun, P.; Lombi, E. Critical review perspective: elemental speciation analysis methods in environmental chemistry - moving towards methodological integration. *Environ Chem* **2009,** *6* (4), 275.

(16) Bansod, B.; Kumar, T.; Thakur, R.; Rana, S.; Singh, I. A review on various electrochemical techniques for heavy metal ions detection with different sensing platforms. *Biosens Bioelectron* **2017,** *94*, 443.

(17) Mota, A. M.; Pinheiro, J. P.; Goncalves, M. L. S. Electrochemical Methods for Speciation of Trace Elements in Marine Waters. Dynamic Aspects. *J Phys Chem A* **2012,** *116* (25), 6433.

(18) Crespo, G. A. Recent Advances in Ion-selective membrane electrodes for in situ environmental water analysis. *Electrochim Acta* **2017,** *245*, 1023.

(19) Pathirathna, P.; Yang, Y.; Forzley, K.; McElmurry, S. P.; Hashemi, P. Fast-scan deposition-stripping voltammetry at carbon-fiber microelectrodes: real-time, subsecond, mercury free measurements of copper. *Anal Chem* **2012,** *84* (15), 6298.

(20) Pathirathna, P.; Samaranayake, S.; Atcherley, C. W.; Parent, K. L.; Heien, M. L.; McElmurry, S. P.; Hashemi, P. Fast voltammetry of metals at carbon-fiber

microelectrodes: copper adsorption onto activated carbon aids rapid electrochemical analysis. *Analyst* **2014,** *139* (18), 4673.

(21) Siriwardhane, T.; Sulkanen, A.; Pathirathna, P.; Tremonti, A.; McElmurry, S. P.; Hashemi, P. Voltammetric Characterization of Cu(II) Complexation in Real-Time. *Anal Chem* **2016,** *88* (15), 7603.

(22) Pathirathna, P.; Siriwardhane, T.; McElmurry, S. P.; Morgan, S. L.; Hashemi, P. Fast voltammetry of metals at carbon-fiber microelectrodes: towards an online speciation sensor. *Analyst* **2016,** *141* (23), 6432.

(23) Pathirathna, P.; Siriwardhane, T.; Morgan, S. L.; McElmurry, S. P.; Hashemi, P. Fast voltammetry of metals at carbon-fiber microelectrodes: rapid determination of solution formation constants. *Analyst* **2016,** *141* (21), 6025.

(24) Yang, Y.; Ibrahim, A. A.; Hashemi, P.; Stockdill, J. L. Real-Time, Selective Detection of Copper(II) Using Ionophore-Grafted Carbon-Fiber Microelectrodes. *Anal Chem* **2016,** *88* (14), 6962.

(25) Bayramoglu, G.; Akbulut, A.; Arica, M. Y. Aminopyridine modified Spirulina platensis biomass for chromium(VI) adsorption in aqueous solution. *Water Sci Technol* **2016,** *74* (4), 914.

(26) Takmakov, P.; Zachek, M. K.; Keithley, R. B.; Walsh, P. L.; Donley, C.; McCarty, G. S.; Wightman, R. M. Carbon Microelectrodes with a Renewable Surface. *Analytical Chemistry* **2010,** *82* (5), 2020.

CHAPTER 4

HUMAN STEM CELL-DERIVED SEROTONIN NEURONS WITH IN VIVO BIOPHYSICAL AND NEUROCHEMICAL CHARACTERISTICS[3]

[3] **Holmes, J.;** Lau, T.; Saylor, R.A.; Hersey, M.; Keen, D.; Fernández-Novel, N.; Hampel, L.; Nijhout, H. F.; Reed, M. C.; Best, J.; Koch, P.; Hashemi, P.: "Human stem cell-derived serotonin neurons with *in vivo* biophysical and neurochemical characteristics" – *In preparation* – Proceedings of the National Academy of Sciences of the United States of America.

4.1 Significance

Chemical studies of the human brain are limited, thus it is very challenging to diagnose brain pathologies in the same way that bodily illness are routinely determined. In this work, we introduce human derived serotonin neurons from induced pluripotent stem-cells as a novel and translational model for studying brain serotonin. Our findings indicate that that these cells, derived from human skin biopsies, can be differentiated into serotonin neurons that create ambient and complete networks and enable serotonin transmission with the same characteristics as observed *in vivo*. Thus, we present a candidate brain model, capable of replicating the *in vivo* environment and providing a personalized platform for studying human brain chemistry.

4.2 Abstract

Diseases of the brain are a profound and growing world health problem. These illnesses are difficult to study, and hence difficult to diagnose and treat. It is not generally not possible to chemically probe the human brain for investigative or diagnostic purposes and biological samples from the periphery, such as blood or urine, do not mirror the brain's chemical environment. In this work, we introduce a novel model system to investigate chemicals, specifically serotonin, in the brain. We utilize human induced pluripotent stem cells (hiPSCs), derived into serotonin neurons (5-HTNs) and apply a host of methods to investigate the biophysical and neurochemical characteristics of the differentiated cells. We present a) morphological, functional and chemical evidence of volume transmission of serotonin release from 5-HTNs, b) evidence that serotonin released from these cells is taken up by multiple monoamine transporters and c) data

showing that serotonin transporters on 5-HTNs respond to acute escitalopram exposure by rapidly internalizing. These three findings represent mechanisms that are conserved between 5-HTNs and *in vivo*. Our findings strongly suggest that 5-HTNs, sourced from the periphery, may provide a translational approach for probing the human brain and studying and diagnosing brain disorders.

4.3 Introduction

What is the difference between diseases of the body and disorders of the mind, that drives the stigma of psychiatric disease? One difference arises because we understand the chemistry of diseases of the body much better than those of the brain. It is generally facile to measure chemical biomarkers of peripheral disease in the blood for diagnosis and treatment. Unfortunately, chemical concentrations in the blood do not reflect those in the brain because the blood-brain barrier regulates chemical traffic in and out of the brain. Additionally, it is not generally possible to biopsy or sample the human brain for diagnosis of psychiatric disease. Therefore, accurate chemical diagnostics for mental illnesses have presented a formidable challenge.

Were we able to provide a model system to probe the chemistry of mental illness, which marker should be targeted? Our group has a long-standing interest in the chemistry of depression as defined by serotonin, or 5-hydroxytryptamine (5-HT). Alterations in serotonin signaling are widely hypothesized to underlie the behavioral phenotypes of depression[1-4] and as such the most popular antidepressants inhibit serotonin reuptake.[5-9] We are deciphering the roles that serotonin plays in depression and antidepressant activity *in vivo* in mice using a variety of analytical methods. This work in animals is

highly informative and we now seek to apply our knowledge of *in vivo* brain serotonin in mice to the human periphery as a means to translate between the two. There are many aspects of the periphery worth exploring; an interesting avenue are induced pluripotent stem cells derived from human tissue skin biopsies (hiPSCs). These stem cells have the ability to differentiate into many different types of cells, including hiPSC-derived neurons with an innate drive to build and maintain functional networks. This drive to create ambient networks ultimately facilitates the formation of brain organelles containing brain region-specific sub-structures.[10,11] Somatic cells obtained from skin biopsies as well as hiPSCs can be differentiated into serotonergic neurons.[12-14] In this article we ask if these neurons function in a similar way to the serotonin neurons in the brain? The answer could open a translational window into brain function.

Here, for the first time, we hypothesize that the biophysicality and neurochemistry of human stem cell-derived serotonin neurons mimic those of *in vivo* serotonin neurons. We confirm that the majority of the differentiated cells develop into serotonergic neurons via expression of phenotype-specific proteins and uptake and release of serotonin and monoamine-specific fluorescent dyes. We verify that these neurons are chemically functional utilizing a combination of optical and electrochemical tools. We show that the evoked voltammetric signals respond to stimulation intensity and tryptophan loading. Importantly, the signals resemble *in vivo* signals found in mice, verified by fitting the data with an *in vivo* computational model that incorporates multiple reuptake mechanisms and autoreceptor control. Finally, following administration of escitalopram (ESCIT), a selective serotonin reuptake inhibitor (SSRI) we chemically and microscopically show dose dependent serotonin transporter (SERT) internalization (a key feature of the *in vivo*

response to SSRIs). Our data point towards stem cell technology as a potential diagnostic tool in neuroscience research.

4.4 Results

4.4.1 Characterization of Human Stem Cell - Derived Serotonin Neurons

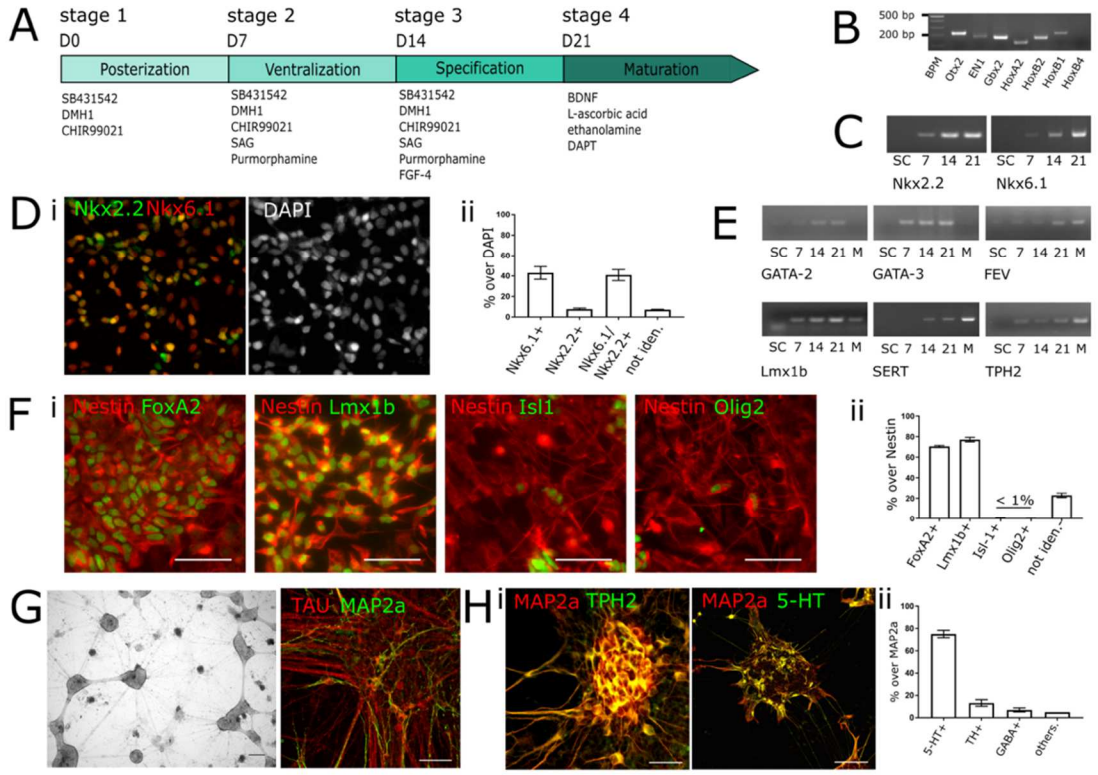

Figure 4.1. Generation of hiPSC-derived serotonin neurons. (A) Schematic overview of differentiation protocol, showing starting days of individual stages and supplements for culture media. **(B)** PCR profile for brain region-specific transcription factors expressed by differentiating cells after posterization. **(C)** PCR profile for Nkx2.2 and Mkx6.1 during the stem cell (SC) and first three stages of serotonergic differentiation. **(D)** Immunofluorescence analysis for both transcription factors show that prior 5-HT specification, 40% of the progenitors are either Nkx6.1- or Nkx6.1/Nkx2.2-positive **(ii)**. Exemplary staining is shown in **(I)**, scale bar: 50 µm. **(E)** The PCR analysis of 5-HT phenotype-specific proteins during differentiation stages; SC: hiPSC, 7: end of posterization; 14: end of ventralization; 21: end of specification; M: 28 days after start of neuronal maturation. **(I): (B)** Microscope image of 5-HTNs on day 28 after induction of neuronal maturation. **(F) (I)** The majority of Nestin-positive progenitors were positively stained for FoxA2 and 5-HT lineage transcription factor Lmx1b. Isl1 and Olig1 immunostaining was only observed in a small number of cells. Scale bar: 25 µm. **(ii)**

graph shows the respective partitions found. **(H)** The PCR analysis of 5-HT phenotype-specific proteins during differentiation stages; SC: hiPSC, 7: end of posterization; 14: end of ventralization; 21: end of specification; M: 28 days after start of neuronal maturation. **(I): (B)** Microscope image of 5-HTNs on day 28 after induction of neuronal maturation. **(G,H)** Microscopy-based analysis of 5-HTN 28 days after the start of neuronal maturation. **(G)** On left: exemplary image of 5-HTN culture, scale bar: 100 µm; on right: immunostainings for the somatodendritic marker protein Map2a and the axonal marker protein Tau indicate neuronal maturity. **(H) (i)** TPH2-positive and 5-HT-positive neurons can be found in clusters of Map2a-positive neurons; scale bars: 25 µm. **(ii)** Quantification of neuronal phenotypes found inside clusters built by Map2a-positive neurons.

We generated serotonin neurons based on a protocol established by Lu and colleagues, that we modified here, for hiPSC-derived serotonin neurons (5-HTNs). [12] This *in vitro* differentiation protocol, based on small molecule signaling, comprises four stages: posterization, ventralization, specification and maturation (**Figure 4.1A** illustrating the different stages and accompanying cell culture supplements). We first generated neuronal precursor cells, progenitors, which express hindbrain markers (**Figure 4.1B**) (***Stage 1***). By activation of sonic hedgehog signaling, these neuronal progenitors were turned into serotonergic progenitors (***Stage 2***). At the end of ventralization, serotonergic progenitors were found to express NKX2.2 and NKX6.1 (**Figure 4.1C-D**), essential transcription factors that initiate early differentiation towards serotonergic fate (***Stage 3***). By giving specificity for serotonin neurons via FGF-4 (a growth factor) signaling activation, we found high serotonergic differentiation efficacy. Specifically, 77 ± 6% of Nestin-positive progenitors expressed the serotonin lineage-specific transcription factors LMX1B and 67 ± 6% FOXA2 (**Figure 4.1F**), while motoneuron-specific transcription factors ISL1 and OLIG2 were only found in a small number of cells (less than 1%).

We found that during differentiation, prior neuronal maturation expression for serotonin lineage-specific transcription factors *FEV*, *GATA2*, *GATA3* and *LMX1B* were

upregulated, in addition to transcripts for tryptophan hydroxylase-2 (TPH2) and the SERT (**Figure 4.1E**). 28 days following ***Stage 3***, hiPSC-derived neurons were found to have established extensive TAU-positive axonal networks, while the cell bodies and neurites inside the clusters were predominantly MAP2a-positive, indicating neuronal polarity (**Figure 4.1G**). During this ***Stage 4***, immunofluorescence analysis for serotonin phenotype markers revealed that the majority of cells inside the neuronal clusters expressed TPH2 and were also positively stained for serotonin (**Figure 4.1H**). Indeed, our quantification revealed that 75 ± 9% of the neurons inside clusters displayed a serotonin phenotype, 13 ± 9% neurons were tyrosine hydroxylase (TH)-positive, the remaining neurons were found to be either of GABAergic or others, such as glutamatergic or motoneuron phenotype (**Figure 4.1H**).

4.4.2 Serotonin Release from 5-HTNs

To test the chemical functionality of the mature 5-HTNs we found presynaptic active zone scaffolding proteins, required to establish and maintain the presynapse,[15-17] localized in the cell bodies and neurites of the 5-HTNs (**Figure 4.2A**). Electrical stimulation caused uptake of the synaptic vesicle marker FM1-43 into vesicles (counterstained for Bassoon, a primary scaffold presynaptic protein) (**Figure 4.2B**). To demonstrate that electrically evoked serotonin release is vesicular, 5-HTNs were loaded with fluorescent false neurotransmitter (FFN) 511 (**Figure 4.2C**). Electrical stimulation causes significant loss of FFN511 fluorescence due to vesicular release: intensity levels dropped from 26 ± 9 to 7.7 ± 1.3 ($p = 0.0399$; $n = 3$ independent experiments (**Figure 4.2D**)).

Figure 4.2E (top) shows an experimental fast scan cyclic voltammetry (FSCV) set up *via* a bird's eye photographic image of the positions of the stimulating and carbon fiber microelectrodes (CFMs) in a cluster of 5-HTNs. The surface of a CFM was imaged with scanning electron microscopy and atomic force microscopy in the bottom panel of **Figure 4.2E**. A significant level of optimization was required to make FSCV measurements in the cell media. The conventional cell culture medium was found to significantly poison the CFM surface thus modifications to the medium were necessary to enable FSCV. The results of the optimization can be found in **Appendix A**. **Figure 4.2F** compares *in vivo* (red), in beaker (grey) and *in vitro* (purple) measurements side by side. i) shows representative color plots, with serotonin oxidation event (pink/green) and reduction events (blue). The corresponding representative CVs are shown in (ii), with the addition of an in-beaker CV superimposed over the cell CV for comparison. Signature electrochemical serotonin responses appear following the stimulation at 0.7 V; oxidation events are denoted *via* a star and the reduction peaks (around 0 V) are highlighted with a cross. Concentration vs. time traces, averaged from four stimulations in one cell preparation or one animal (*in vivo*) are in (iii), extrapolated from the horizontal lines in the color plots in (i).

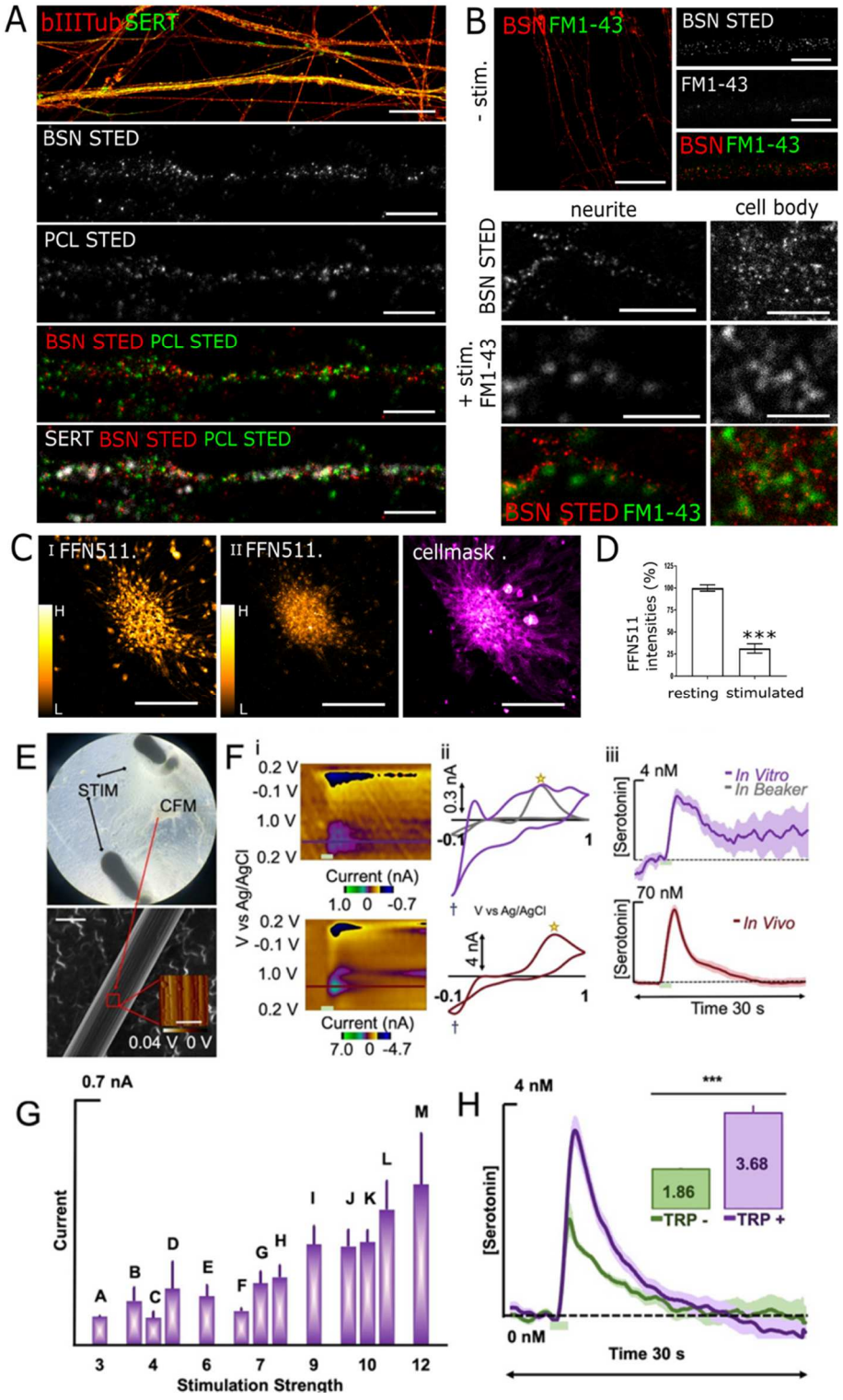

Figure 4.2. Visualization of synaptic and extrasynaptic 5-HT release. (A) Localization of the presynaptic scaffold protein Bassoon (BSN) was detected on neurites of 5-HTN. Top: exemplary image of 5-HTN network identified by betaIII-Tubulin (bIIITub) and SERT immunostaining; scale bar 25 µm. STED microscopy revealed that

BSN-positive neurites (BSN-STED) also contain Piccolo-positive structure (PCL-STED). Scale bars: 2. **(B)** Uptake of the synaptic vesicle dye FM1-43 is triggered by electrical stimulation of 5-HTN. Without stimulation (-stim) no FM1-43 uptake into BSN positive structures is observed. Electrical stimulation of 5-HTN (+stim) induced FM1-43 uptake at BSN-positive actives zones on neurites and cell bodies. Scale bar: 25 μm, STED images: 2 μm. **(C)** Evoked 5-HT release was visualized using FFN511. Images show an exemplary 5-HT cluster **(i)** before and **(ii)** after stimulation. Cellmask staining was applied to determine ROI for quantification of FFN511 release. The Orange Hot LUT bar (NIH ImageJ) indicates pixel intensities. Scale bars: 100 μm. **(D)** Electrical stimulation significantly reduced the amount of detectable FFN511 in 5-HTN (***, $p<0.01$) (E) (top) Experimental set-up: the CFM is lowered onto the cell cluster and two stimulation pins electrically evoke serotonin release. **(Bottom)** A scanning electron microscopy image of the carbon electrode surface (scale bar: 10 μm). An atomic force microscopy image is inset (scale bar: 1 μm), and the color bar is beneath (0 V to 0.04 V). **(F)** *In vivo* (red), *in vitro* (purple) and in beaker (grey) FSCV **(i)** color plots **(ii)** cyclic voltammograms and **(iii)** concentration vs. time traces. **(G)** FSCV current response with respect to stimulation intensity, a function of i) stimulation amplitude ii) frequency, and iii) number of pulses. **(H)** FSCV concentration vs. time traces collected following the addition (n = 10) or omission (n = 3) of TRP to the cellular media 24 hours before analysis. Release averages (nM) are inset showing significant increase in release (***, $p<0.001$) following addition of TRP.

FSCV experiments illustrate that serotonin release is dependent on stimulation parameters as shown in **Figure 4.2G**. A stimulation paradigm was tested on three different cell lines whereby the stimulation parameters, frequency, amplitude and pulse number were randomly applied in different combinations. Each simulation scenario is labeled (**A-M** on **Figure 4.2G**). We arbitrarily assigned a numerical value of 1- 4 to each variable (frequency, amplitude and pulse number) and added these values together to reach a sum (3-12) representing the overall strength of the stimulation (**Table A.1** in **Appendix A** shows breakdown of parameters). It was found that the amplitude of serotonin release depends on overall stimulation strength. Serotonin release is also dependent on tryptophan (TRP) loading. In 10 cell preparations TRP was added to the culture medium 24 hours before analysis, resulting in a maximum release of 3.7 ± 0.3 from the purple concentration vs. time curve (TRP+) in **Figure 4.2H**. When compared to

the green trace (maximum release = 1.9 ± 0.3) from 3 cell preparations where TRP was omitted (TRP-), the addition of TRP increases the release event amplitude by 97.8%. The maximum current response between the two groups was compared (inset histogram), and a two-tailed student's t-test was used to confirm significance ($p = 0.00069$). This result was confirmed by the mathematical model (simulations shown in **Figure A.2 in Appendix A**), where when external tryptophan was increased from 40 μM to 140 μM (as in the cell experiments) vesicular serotonin doubled.

4.4.3 5-HTN Serotonin Reuptake

The fluorescent monoamine transporter substrate, ASP+, enabled us to visualize the uptake capacity of functional plasma membrane monoamine transporters and to also determined SERT's contribution to transporter mediated ASP+ uptake (**Figure 4.3A-C**). After uptake, ASP+ localized to mitochondria thus ASP+ fluorescence was found in cell bodies and neurites (**Figure 4.3A**). Quantitative confocal laser scanning microscopy determined how SERTs participate in ASP+ uptake (**Figure 4.3B**). To this end, cell preparations were treated with 1 and 10 μM ESCIT to inhibit SERT-specific uptake. Our analysis shows that both doses of ESCIT significantly decreased ASP+ uptake to 59.6 ± 1.6 % and 62.2 ± 1.1 %, respectively of control values (**Figure 4.3C**).

We previously modeled evoked serotonin *in vivo* in mice in the context of 2 reuptake mechanisms, Uptake 1 (SERTs) and Uptake 2 (DATs, NETs and OCTs) and prolonged autoreceptor control (seen as a dip below baseline after stimulation). Here we modeled the curves from the 5-HTNs in a similar manner; the model is shown by the dotted trace in **Figure 4.3D,** superimposed over the experimental data. Like we previously found *in vivo*, serotonin release from 5-HTNs followed a two reuptake and

prolonged autoreceptor profile. To investigate which Uptake 1 and 2 transporters are responsible for the dual reuptake profile from 5-HTNs, we performed RNA analysis, which revealed transcripts for NETs and SERTs in all differentiated cells, and DATs in some trials. OCT3, but not OCT1 and OCT2, were detected in terminally differentiated 5-HTN (**Figure 4.3E**).

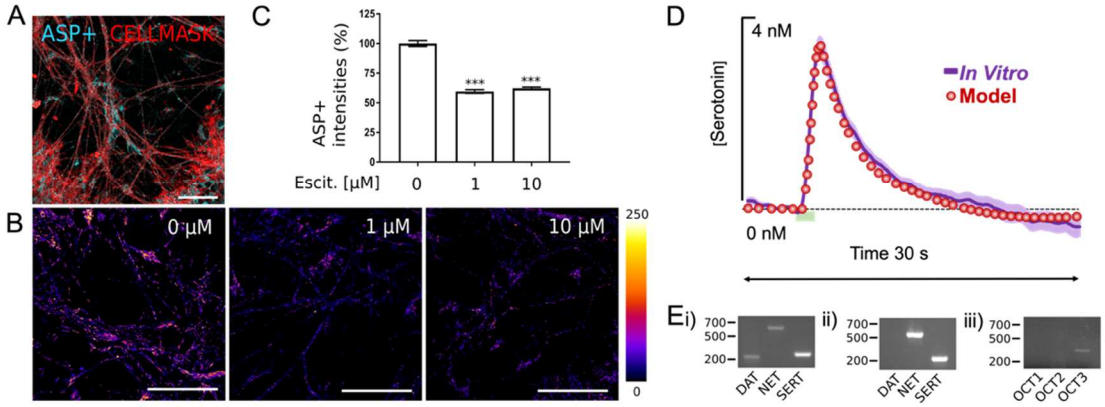

Figure 4.3. Transporter Mediated Serotonin Uptake. (A) Representative projection of a confocal z-stack, scale bar: 50 µm. Cellmask staining was applied to select ROI for quantification of ASP+ uptake. **(B)** Randomly picked z-projections of control and escitalopram-treated 5-HTN. Fire LUT bar (Image J) displays pixel intensities; scale bars: 50 µm. **(C)** Compared to control fluorescence intensities, both escitalopram concentrations significantly diminished uptake of ASP+ by 5-HTN (n = 3 independent experiments; ***, $p<0.001$). **(D)** Representative FSCV current vs time trace collected from control 5-HTNs (purple) (n = 10 independent experiments) and the dotted curve predicted by the mathematical model (red). **(E)** PCR profile of 5-HTN cultures for monoamine transporters shown to contribute to ASP+ uptake: examples for a **(i)** differentiation in which DAT and NET mRNA, and **(ii)** only NET mRNA was detected. **(iii)** In all differentiations made, OCT3 mRNA was detected, but not the transcripts for OCT1 and OCT2. 5-HTN take up the monoamine transporter substrate ASP+.

4.4.4 Real-time Chemical Verification of SSRI Induced SERT Internalization

Immunostainings in **Figure 4.4A** revealed cell surface-located SERTs along neurites and soma of 5-HTNs after 4 weeks of terminal differentiation. We previously observed ESCIT-induced SERT internalization in murine stem cell-derived serotonin neurons [18] and sought to establish whether this phenomenon holds for hiPSCs. We

restricted the SERT internalization experiments here to traceable neurites because these 5-HTNs are localized in dense clusters, and this limits the spatial resolution of antibody-complex emitted fluorescence.[18] Three concentrations of ESCIT (0.1, 0.5, and 1 μM) were administered to three independent terminally differentiated cell preparations. After two hours, fluorescence intensity was evaluated (**Figure 4.4B**). Treatment with 0.1 μM ESCIT caused reduced fluorescence intensity (82 ± 8%, $p = 0.0221$ of control 5-HTNs) indicating significant SERT internalization. This internalization was dose dependent (50 ± 4% and 52 ± 4% respectively for 0.5 and 1 μM ESCIT, compared to control 5-HTNs, $p < 0.0001$ for both treatment conditions).

FSCV was used to determine the chemical consequence of this internalization in **Figure 4.4C**. Three ESCIT concentrations, 0.1, 0.5, and 1 μM, were each added to three separate groups of cell preparations. The control (before drug) concentration vs. time traces (purple) are displayed with traces 2 hours after ESCIT (black). Reuptake rate of extracellular serotonin is decreased after 5-HTNs were treated for 2 hours at all doses administered, and serotonin did not return to baseline. We mathematically modeled the experimental data in **Figure 4.4C** (indicated by dotted trace). To fit the post - ESCIT curves, we first chose parameters so that the computed extracellular serotonin curve matched the control. In the three cases, the parameters were almost identical. Then V_{max} of SERT fit was 80% of normal for 0.1 μM, 50% of normal for 0.5 μM, and 50% of normal for 1 μM, representing 20, 50 and 50% SERT internalization respectively. Serotonin concentrations reached a new steady state after the stimulation. To fit this data, the model hypothesized that the stimulation must cause further, rapid internalization of

the SERTs, specifically 55, 55 and 91% internalization respectively for the three increasing doses.

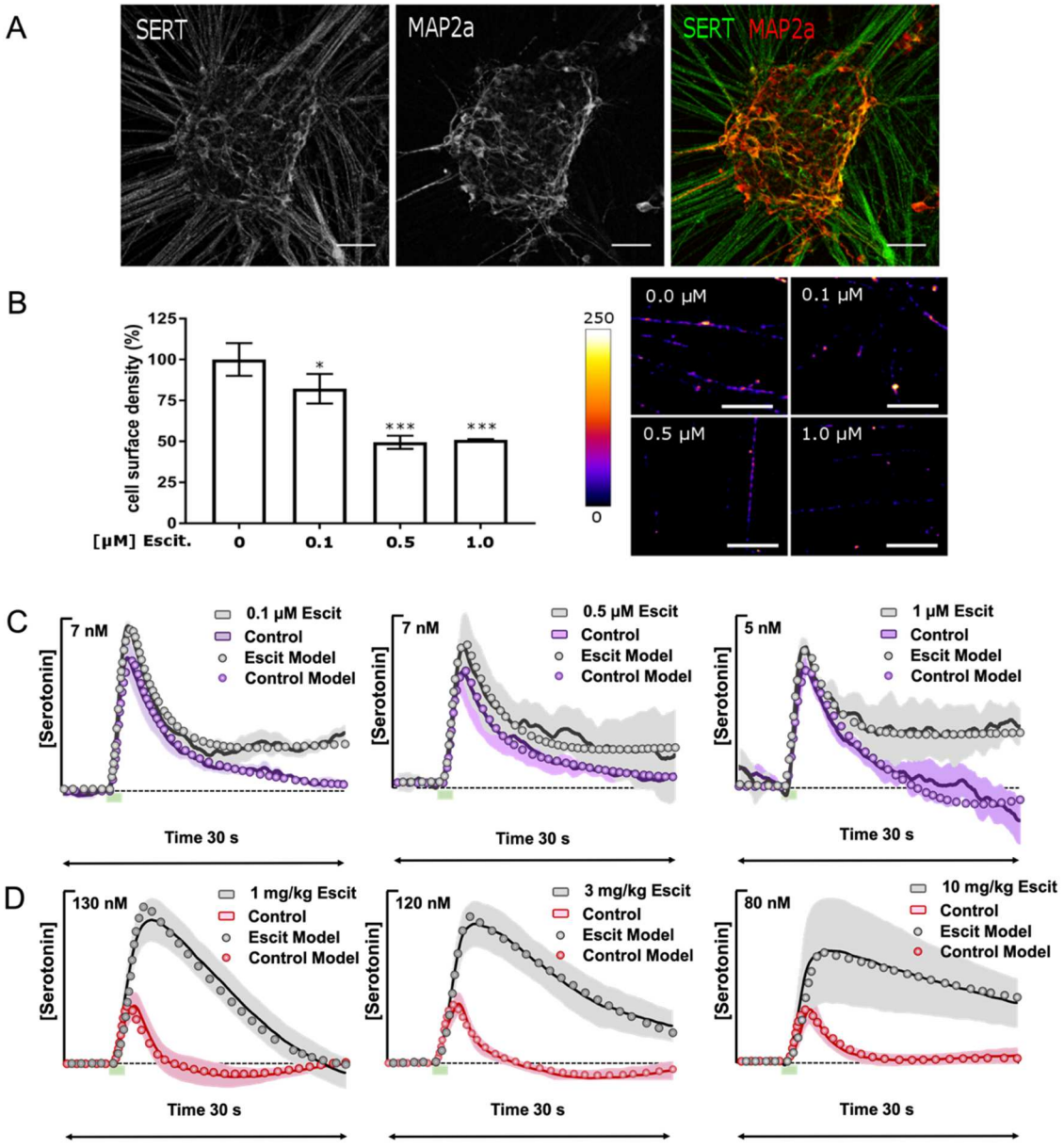

Figure 4.4 ESCIT-mediated SERT internalization. (A) Immunofluorescence analysis of 5-HTN for SERT distribution. SERT signals can be found on Map2a-positive cell bodies and neurites as well as on Map2a-negative axons extending from the cluster. Scale bars: 50 µm. **(B)** Exemplary sum projections made from confocal stacks of ROIs acquired for SERT cell surface measurements. The Fire LUT bar (NIH ImageJ) indicates pixel intensities recorded on SERT-positive neurites, ranging from 0 (black, no emission) to 255 (white, overexposed). Scale bars: 10 µm. After acute ESCIT exposure, SERT cell

surface density significantly decreased for all concentrations tested (*p < 0.05 and *** p < 0.001 compared to control neurons (0 μM escitalopram); 803 ROIs on neurites were quantified in 3 independent experiments). FSCV concentration vs. time traces of serotonin reuptake **(C)** *in vivo* and **(D)** in 5-HTNs. Control curves for *in vivo* (red) and in 5-HTNs (purple) vs. acute escitalopram (black) at 3 doses, 1 mg/kg, 3 mg/kg, and 10 mg/kg, and 0.1 μM, 0.5 μM and 1 μM, respectively. In each of the 6 panels in C and D there are two curves predicted by our mathematical model labelled by small circles. The parameter choices and the information therein are discussed in the text. All calculations were done with the model described in Methods.

Data collected *in vivo* in the CA2 region of the hippocampus in different cohorts of male mice that received 1, 3 and 10 mg/kg (n = 4 per dose), respectively is shown in **Figure 4.4D**. The ESCIT caused dose dependent increases in the $t_{1/2}$ of the serotonin clearance (8.7 s control, 15.7 s 1 mg/kg, 18.2 s 3 mg/kg, and 10 mg/kg did not reach half amplitude within the 30 s file). These data were also modeled (indicated by the dotted trace). As in the case of the cell culture experiments, for each ESCIT experiment, we first chose parameters so that the computed extracellular serotonin curve matched the control. In the three cases, the parameters were almost identical. To fit the ESCIT curves, the V_{max} of SERT fit was 80% of normal for 0.1 μM, 60% of normal for 0.3 μM, and 40% of normal for 1 μM, representing 20, 40 and 60% SERT internalization respectively.

4.5 Discussion

There is great importance for measuring chemicals in the intact human brain, however there are no established routines to probe a human brain for investigative purposes unless a patient is already undergoing surgery. For example, FSCV has been performed in the brains of human Parkinson's disease patients undergoing surgery for deep brain stimulation, measuring dopamine while patients participate in decision making tasks.[19] There are several challenges with this type of measurement however, including little control over the positioning of the electrode, ambient and electrode noise, and

limited opportunity to chemically verify the identity of substrates necessitating post hoc analysis algorithms. Additionally, because these patients are suffering from a severe neurological condition, and are at different stages of disease progression, it is very difficult to compare data between patients. Taken together, these issues (that are commonplace for clinical measurements) make it very attractive to seek an alternative and well controlled model that mimics the human brain, while maintaining the patient specific aspect of clinical measurements. Our interests in a substitute model are in the context of understanding and ultimately establishing biomarkers of psychiatric disease, such as depression. Our work is highlighting strong correlations between serotonin and depression and this is not surprising since this messenger has long been known to play a central role in neuromodulation of mood circuits.[20-23] Thus, we sought to establish a model system to investigate serotonergic transmission.

In this work, we ask can hiPSCs (a readily available, well controlled, patient-specific source for generating human serotonin neurons *ex vivo*) provide a neurochemically functional model for assessing serotonin dynamics *ex vivo*? To answer this question, we ask the following sub-questions:

1. Can hiPSCs be differentiated into serotonin neurons that mirror the biophysicality and neurochemistry of *in vivo* serotonin neurons?
2. Does serotonin release dependent on factors known to enable serotonin volume transmission *in vivo*, for example establishing extrasynaptic and presynaptic release sites?
3. Is serotonin cleared from the synapse via multiple reuptake mechanisms as found *in vivo*?

4. Are adaptive mechanisms, specific to the *in vivo* environment, conserved in stem cell-derived serotonin neurons?

5.5.1. Differentiated 5-HTNs have *In Vivo* Biophysical Features

Previously we generated and characterized mouse embryonic stem cell-derived serotonin neurons expressing human SERTs.[18] Here we sought to do the same with human biopsy-derived stem cells. We modified a previously established protocol to generate hiPSC-derived 5-HTNs,[12] which correspond to dorsal and median raphe nuclei serotonergic neurons.[24-27] The key novelty in our modified protocol are additional cell passages during the differentiation ***Stages 1-3*** and replacement of original recombinant protein with small signaling molecules, while being able to maintain WNT signaling with CHIR concentration shown to provide the optimal yield of 5-HTN. This modification is more cost effective because it does not involve recombinant proteins yet yields mature cells with at the least the same efficiency as the previously established protocol. For example, the values representing % neuronal phenotypes resulting from our modified protocol (**Figure 4.1H**) are comparable to those reported in the original protocol.[12] 5-HTNs may also be obtained from somatic cells *via* direct conversion into induced neurons.[13,14] Compared to small molecule-based differentiation protocols, direct conversion of somatic cells into serotonin neurons is similarly efficient.

A critical new finding here is that the differentiated cells contain key biophysical features of *in vivo* DRN cells. First, 5-HTNs display neuronal maturity (**Figure 1G**) 28 days into ***Stage 4***. Specifically, we observe defined somatodendritic and axonal compartments, constituting a general *in vitro* neuroarchitecture as a prerequisite for the neuronal functionality and connectivity. Furthermore these 5-HTNs express key serotonin

selective proteins; TPH2 and SERT, localized on cell bodies, dendrites and axons emerging from cell clusters, as found *in vivo*.[28,29] The axons and somatodendritic compartments house serotonin-containing vesicles (**Figure 1G**), again as would be expected *in vivo*.[24,25,29]

4.5.2. 5-HTNS are Neurochemically Functional

In vivo serotonin release is thought to occur predominantly at axonal and somatodendritic varicosities with no requirement for opposing postsynaptic structures (*i.e.* volume transmission).[30,31] In **Figure 4.2** we present five pieces of evidence for serotonin volume transmission in 5-HTNs.

I. **Morphological Evidence.** We observe *in vivo*–like localization patterns of presynaptic scaffolding Bassoon and Piccolo proteins and SERTs in 5-HTNs (**Figure 4.2A**). This localization is similar to that previously observed for extrasynaptic active zone-like release sites in dopaminergic neurons, required for volume transmission.[32] Thus, our localization studies indicate that 5-HTNs have the molecular prerequisites to enable volume transmission.

II. **Functional Evidence for Neurotransmitter Release**. In **Figure 4.2B,** we verify the ability of these sites to release neurotransmitter by uptake of the synaptic vesicle dye FM1-43FX. FM dyes are well established fluorescent markers to identify active synaptic vesicle pools and have previously been employed to quantify serotonin release from the soma of leech neurons.[33,34] These studies show that FM dyes are taken up at extrasynaptic sites during electrically evoked, calcium-dependent serotonin release. As in these previous studies, FM dye is perfused over the 5-HTNs before electrical stimulation of the cells. Subsequent confocal microscopy

visualizes this fluorescent dye on cell bodies and neurites of 5-HTNs, verifying stimulation-dependent uptake of this dye by 5-HTNs. To test whether FM uptake occurred at presynaptic structures, we counterstained for Bassoon proteins and found that FM dye-containing vesicles are distributed in accordance with Bassoon localization. This specific distribution indicates extrasynaptic release sites without opposing postsynaptic neurons.

III. **Functional Evidence for Monoaminergic Release.** We monitor monoamine release from our 5-HTNs using fluorescent false neurotransmitters (FFNs; **Figure 4.2C**). FFNs are fluorescent monoamine analogues, which we perfused over the 5-HTNs. These compounds have previously been shown to be selectively taken up by vesicular monoamine transporter 2 (VMAT2), exclusively expressed in monoamine neurons.[35,36] Henke and colleagues first utilized 2-photon microscopy to visualize FFN-labelled serotonin-containing vesicles in slice preparations of rodent DRN serotonin neurons.[37] Recently, we adapted this method for a confocal microscope set up and visualized FFN release from serotonin neuron-like cells *in vitro*.[38] Here, we repeated this experiment and found, using confocal microscopy, FFN signals on the cell bodies and neurites, providing evidence for VMAT2 facilitated monoamine uptake into neurotransmitter-releasing vesicles in 5-HTNs. Furthermore, we found that electrical stimulation results in FFN release from cell bodies and neurites of our 5-HTNs.

IV. **Chemical Evidence for Serotonin Release.** FM dyes and FFNs are an indirect, optical tools to assess neurotransmission. However, one cannot directly translate the behavior of these dyes with specific neurochemistry. To chemically verify the

functionality of these cells, we utilized FSCV. FSCV is an extremely robust and sensitive tool for chemical verification of neurotransmitters in dynamic systems.[39] This method is routinely performed in cell and slice preparations including measurements of catecholamines in chromaffin cells,[40] 2,8-dihydroxyadenine in endothelial cells,[41] dissolved oxygen in pheochromocytoma cells,[42,43] and other analytes in rodent organotypic slice culture preparations.[44-50] Serotonin release has been measured from cells[51,52] and caudate-putamen, DNR and substantia nigra reticulata (SNr) tissue slice preparations.[53-56] All these FSCV models involved evoking transmitter release *via* electrical stimulation. Thus we adopted a similar approach by positioning a stimulating electrode around a cluster of mature cells. For the first time we verify that 5-HTNs do indeed release serotonin in response to stimulation (**Figure 4.2F**). This verification is evidenced by the characteristic position of oxidation and reduction peaks from FSCV color plots and CVs, that we have previously found *in vivo*[9,57-59] and add here for comparison (**Figure 4.2F i and ii**) The concentration of serotonin release from the 5-HTNs (3.7 ± 0.3 nM, n=13) was much lower than serotonin release found *in vivo* in mice (35 ± 3 nM in males, n = 17 and 32 ± 4 nM in females, n = 18 respectively)[59] (**Figure 4.2F iii**). This finding explains the (seemingly) lower signal-to-noise ratio of the cell signals compared to the *in vivo* signals (bigger error bars on cell data). The lower serotonin response in these cells is not surprising since we expect release sites in 5-HTN cultures to be less numerous compared to release sites *in vivo*.

V. **Functional Evidence for Serotonin Release.** It is well-established in the FSCV literature that stimulation strength significantly influences the dynamics of

neurotransmitter release. For example, stimulation dependent alterations in neurotransmitter release are routinely found *in vivo*.[17,60,61]. This phenomenon extends to adrenal[46] and neuronal tissue slice preparations.[53,55,62] Here we investigated the consequences of increasing stimulation strength on serotonin release from 5-HTNs. Stimulation strength was altered *via* random combinations of stimulation frequency, amplitude, and pulse number generating a ranking system to determine stimulation strength (**Figure 4.2C**). 5-HTNs respond to stronger electrical stimulations by releasing more serotonin, showing that stimulation sensitive excitatory mechanisms (found *in vivo*) for release are conserved in 5-HTNs.[60] Another important aspect for validating functionality is the impact of precursor availability. For example, mast cells pre-loaded with TRP release more serotonin when stimulated than those not pre-loaded with TRP.[51] *In vivo*, Stamford and Wightman were able to induce serotonin release from dopaminergic neurons by first depleting dopamine with α-methyl-p-tyrosine, and then preloading with 5-HTP.[63] In accord with these studies, here in 5-HTNs serotonin release amplitude increased almost two-fold (97.8%) by TRP pre-loading (**Figure 4.2D**). This indicates that the 5-HTNs possess 5-HTP sensitive metabolic pathways (including tryptophan hydroxylase and 5-hydroxytryptophan decarboxylase). The presence of this pathway is not unexpected of course since the fluorescence staining in **Figure 4.1H** also verifies the presence of TPH2 within 5-HTNs.

4.5.3. 5-HTNs Mimic In Vivo Reuptake Mechanisms

To investigate reuptake processes in the 5-HTNs, we first utilized the fluorescent monoamine transporter substrate ASP+ (4-(4-(dimethylamino)-styryl)-N-

methylpyridinium). ASP+ can be employed to monitor and quantify monoamine transporter function in live cell imaging experiments. Previously, ASP+ was shown to be taken up by DATs, NETs,[64,65] SERTs[38,66] and OCTs.[67,68] Here, we performed live cell imaging experiments to verify that effective reuptake mechanisms exist in the 5-HTNs. (**Figure 4.3C**). In line with previous observations,[38,66] ASP+ uptake into 5-HTNs is dose dependently reduced in the presence of ESCIT, a selective SERT inhibitor (**Figure 4.3D and E**). Even at the highest dose of ESCIT, there is still active ASP+ reuptake. This may be due to incomplete SERT inhibition via ESCIT or due to multiple reuptake mechanisms for serotonin, that are seen *in vivo*.

Multiple mechanisms for serotonin reuptake were first discussed by Shaskan and Snyder in 1970.[69] Since, two classes of transporters have been identified that govern each uptake mechanism. Uptake 1 is classified as high affinity, low efficiency clearance and is mediated by SERTs, and Uptake 2 is classified as low affinity, high efficiency clearance, controlled by a combination of other monoamine transporters including NETs, DATs[64,65] and OCTs.[70-74]

Previously we provided *in vivo* FSCV evidence for these two reuptake mechanisms in different brain regions. Specifically, most FSCV serotonin clearance curves comprise two distinct slopes, which can be fitted with two discrete Michaelis-Menten kinetic parameters that match the kinetics of Uptake 1 and 2. By computationally modeling the FSCV data using these kinetic parameters, we were able to ascertain the contribution of Uptake 1 and 2 to the clearance of serotonin around the implanted electrode.[75] In this paper, we use a similar approach to verify the presence of these two reuptake mechanisms in 5-HTNs.

In **Figure 4.1** we found evidence of SERTs on 5-HTNs, thus is not surprising that our model captured Uptake 1 processes. To investigate whether the same proteins that regulate Uptake 2 *in vivo* are responsible for the second uptake slope in 5-HTNs (DATs, NETs and OCTs), we utilize RNA analysis. This analysis indeed verifies transcripts for DAT, NET, and OCTs. Thus, in addition to *in vivo* serotonin release mechanisms being conserved in 5-HTNs, we now confirm that reuptake mechanisms are also conserved.

4.5.4. SSRI Induced SERT Internalization: A Response Conserved Between *In Vivo* and 5-HTNs

Previously we differentiated mouse embryonic stem cells into mature, functional serotonin neurons mimicking *in vivo* mouse DRN serotonin neurons.[18] A novel finding with these cells was their dose-dependent response to SSRI treatment, which resulted in rapid (approx. 4 hrs) SERT internalization. Our hypothesis for this observation was that SERT internalization marks the onset of clinical SSRI efficacy *in vivo*. Indeed, a PET study using equimolar doses of citalopram isomers or ESCIT showed less SERT availability in various human brain regions.[76] However, the rapid internalization response *in vitro* is not compatible with the slower (up to several weeks) response in the clinic.[77,78] The reason for this discrepancy is likely based on the difference in dosing between our *in vitro* experiment and clinical regimens. For example, *in vitro*, the drug is present during the entire exposure and is unlikely to be metabolized. *In vivo* in clinical practice, the drug is released slowly and consistently; with only a small fraction going across the blood-brain barrier where it is prone to metabolism.

Here, under control conditions, SERTs are localized ubiquitously in 5-HTNs (**Figure 4.4A**). As in our mouse model, acute ESCIT treatment induced internalization of

SERTs in a dose-dependent (0.1, 0.5 and 1.0 μM) manner (**Figure 4.4B**). SERT internalization is also apparent in these 5-HTNs via FSCV (**Figure 4.4C**). Here the same 3 doses of ESCIT were perfused onto cell cultures and serotonin release was evoked electrically. With all three doses, the serotonin released does not return to baseline. We applied the computational model to these data and found that the model necessitates modification to fit the data. Specifically, the model requires incorporation of an internalization component. We extended this idea to data collected *in vivo* in the mouse hippocampus after the mice were exposed to 3 doses of ESCIT *i.p.* and indeed found that the larger doses given *in vivo* necessitate incorporation of SERTs internalization in the model. A novel finding here, importantly, is that it appears that SERTs in 5-HTNs are sensitive to the large electrical stimulation, and, as the model hypothesizes, also internalize *during* the stimulation; this is evidenced by the signal not returning to baseline after stimulation, showing that a new steady state in ambient serotonin is reached. This effect is apparent to a lesser extent in the *in vivo* curves, likely because of the difference in the nature of how the 5-HTNs are exposed to the ESCIT. When the ESCIT is added to the culture, it is done so as a rapid and consistent bolus. This cell exposure is fundamentally different than a *i.p.* injection *in vivo*, where only a small fraction of ESCIT goes across the blood-brain barrier in a more diffuse concentration profile and is metabolized rapidly once in the brain.[79,80]

This rapid internalization phenomenon is very interesting to us for several reasons. It implies that the mechanisms responsible for SERT internalization can act quickly. Indeed, there is recent evidence for rapid SERT shuttling between cell surface and intracellular compartments [81,82]. Thus, we speculate here that acute ESCIT interferes

with the constitutive shuttling of SERT molecules and enhances retrograde trafficking *via* this rapid process. SERT internalization has not previously been observed with FSCV in tissue slice preparations[53,54,83,84] where serotonin clearance is much more rapid than *in vivo* or in 5-HTNs, even under large SSRI doses. We hypothesize that a high level of connectivity is lost in tissue slice preparations. This hypothesis insinuates that SERT internalization mechanisms necessitate functional networks, and that 5-HTNs possess independent and complete neuronal organizations that are paramount for *in vivo* compensatory mechanisms. Indeed, hiPSC-derived 5-HTNs obtained by small molecule-based differentiation established axonal projections to the cerebellum, hindbrain and spinal cord after being transplanted into the brain of mouse's offspring.[85]

We therefore provide evidence in this study that human stem cell-derived 5-HTNs comprise key morphological and biochemical features of intact *in vivo* serotonin neurons. Our findings may provide a suitable representation of *in vivo* serotonin dynamics from a peripheral source, helping to bridge the translation between basic research in rodent models and the clinical human phenotype.

4.6 Methods

4.6.1 Solutions

All chemicals were used as received and solutions were at room temperature. For FSCV characterizations, cell media (Neurobasal, ThermoFischer Scientific, USA) was used without any additional components. HEPES buffer was prepared by dissolving 20 mM HEPES (Sigma Aldrich, USA), 130 mM NaCl (Fisher Chemical, USA), 5 mM $CaCl_2$ (Sigma Aldrich, USA) in DI water and pH adjusted to 7.4. D-glucose monohydrate

(Millipore, USA) was dissolved into this HEPES buffer to a final concentration of 2.5 mM. Escitalopram oxalate (Sigma Aldrich, USA) was also dissolved into the HEPES buffer to final concentrations of 0.1, 0.5 or 1 μM. Serotonin HCl (Sigma Aldrich) and l-tryptophan (Sigma Aldrich) were dissolved into HEPES buffer.

4.6.2 Generation of hiPSC-derived serotonergic neurons

The differentiation protocol is adopted from the recently published generation of 5-HTN by Lu and colleagues.[12] We have introduced additional mechanical cell passages to promote cluster formation of 5-HTN for fast scan-cyclic voltammetry recordings. The differentiation of hiPSC cells into 5-HTN started from a nearly confluent culture, which was split using trypsin in a ratio of 1:4 before starting the differentiation protocol. First, stem cell culture medium was replaced with neuronal induction medium containing 2 μM SB431542 (Miltenyi Biotech, Bergisch Gladbach, Germany), 2 μM DMH1 (Seleckchem, Houston, United States), and 1.4 μM CHIR 99021 (Cell Guidance Systems, Cambridge, United Kingdom) to generate hindbrain neural stem cells (NSC). At day 3, NSC were mechanically splitted 1:3 and replated on poly-L-lysin/laminin-coated dishes (Sigma Aldrich, St. Louis, United States). On day 7 culture medium was additionally supplemented with 1 μM SAG dihydrochloride (Selleckchem, Houston, United States) and 0.5 μM purmorphamie (Cell Guidance Systems, Cambridge, United Kingdom) to trigger ventralization and promote the differentiation of NSC into rostral hindbrain NSC. Again, cells were split 1:3 at day 10 of differentiation. To prime rostral hindbrain NSC into 5-HT progenitors, 10 ng/mL FGF-4 (Miltenyi Biotech, Bergisch Gladbach, Germany) were added to culture medium starting day 14. At day 17, cells were split 1:3 on poly-L-lysin/laminin-coated 15mm glass coverslips for fast scan-cyclic voltammetry

and immunofluorence analysis, or in 3.5cm Ibidi imaging chambers (Ibidi, Munich, Germany) for live cell imaging experiments. Terminal neuronal maturation was induced by withdrawal of growth factors. To promote neuronal maturation and survival, the culture medium was supplemented with 5 ng/mL BDNF, 5 µM DAPT (both Cell Guidance Systems, Cambridge, United Kingdoms), 30 nM ethanolamine and 100 µM L-ascorbic acid (both Sigma Aldrich, Houston, United States).

4.6.3 RNA profiling of 5-HTN:

For RNA isolation, cells were harvested at hiPSC stage and the end of each differentiation stage (day 7, 14, and 21) and at day 28 after induction of terminal differentiation. After washing 3 times with 1x PBS, cells were resuspended in 1 mL TriFast (PeqLab, Erlangen, Germany). Cell lysates were processed as recommended by the manufacturer to isolate RNA using single step liquid phase separation. After RNA isolation, pellets were dried at room temperature and resuspended with 20 µL H2O-DEPC. Prior cDNA synthesis samples were treated with DNaseI (protocol according to manufacturer, Sigma Aldrich, Houston, United States) and 500 ng RNA were applied for reverse transcription using the iScript cDNA synthesis kit (protocol according to manufacturer, Bio-Rad, Hercules, United States). The remaining RNA was stored at -80°C, the cDNA was stored at -20°C. Primers applied for PCR and PCR conditions are listed in the supplement data.

4.6.4 Immunofluorescence analysis and SERT cell surface density measurements:

If not otherwise stated, all chemicals were obtained from Sigma-Aldrich. Prior immunostainings, cells were fixed in 1% paraformaldehyde at room temperature for 10 min and washed 3 times in 1x PBS. Permeabilization was performed according to

antibodies applied (see supplementary data), using either 0.1% triton-X in 0.1% sodium citrate or 0.1% saponin in 1xPBS containing 10% horse serum (Life Technologies, Germany). Blocking solution (BS) contained 0.01% saponin and 10% horse serum. After 1 h of blocking, primary antibodies were incubated at 37°C for 45 min. Then cells were washed 3 times with BS before secondary antibodies were incubated at room temperature for 60 min. Finally, cells were washed 3 times with 1x PBS and once with ddH2O before being embedded in fluorescent mounting medium (DakoCytomation, Glostrup, Denmark).

Immunostainings for SERT cell surface density measurements were performed as described previously.[18] Briefly, cells were incubated in detergent-free BS for 1 hour at room temperature after fixation in 1% paraformaldehyde. Primary antibodies targeted against an epitope on the second extracellular loop were applied at 37°C for 1 hour. After washing 3 times in BS, cells were permeabilized using 0.1% saponin in BS before TuJ1-antibodies were applied. After washing steps, cells were incubated with Alexa Fluor-conjugated secondary antibodies at 37°C for 45 minutes. Finally, cells were washed 3 times with 1x PBS and once with ddH2O before being embedded in fluorescent mounting medium. Before immunostaining, samples were blinded during the application of ESCIT and assigned random codes (000-500). Samples were decoded after image processing.

4.6.5 Fluorescence, bright field microscopy, and image processing:

Confocal laser scanning microscopy images were acquired on a Leica TCS SP5 (Leica Microsystems, Mannheim, Germany) attached to a DM IRE2 microscope equipped with an acusto-optic beam splitter and a HCX PL APO 63× oil planchromat lens. Excitation lasers were either an argon ion laser (488 nm), a DPSS laser (561 nm) or

a helium neon laser (633 nm). Conventional fluorescence images were acquired using a Leica (new microscope features), equipped with objectives ranging from 5x to 40x and suitable dichroic mirrors for excitation and emission of applied secondary antibody conjugates. Phase contrast and brightfield images were acquired using a Cell Discoverer 7 imaging system (Zeiss, Jena, Germany).

For SERT cell surface measurements, image frames were exclusively selected based on TuJ1-Alexa568 immunostainings without exciting SERT-Alex488 fluorescence. Control SERT-Alexa488 samples were used to adjust laser settings for acquisition of unsatured pixel values. SERT-TuJ1-stacks were acquired with sections taken every 0.5µm. All images were exported to TIFF format, imported to NIH image (version 1.45s; National Institutes of Health, USA) and background corrected. Z-stacks of the TuJ1 immunostainings were used to determine the region of interests (ROIs) on neurites (see supplementary data). Then, the ROIS were imported into the SERT-Alexa488 channels and the integrated fluorescence intensity recorded for SERT-Alexa488-antibody complexes were quantified using the plugin Multi Measure.

Live cell imaging experiments using the fluorescent monoamine transporter substrate ASP+ (Sigma Aldrich) and fluorescent false neurotransmitter (FFN511; Abcam, Cambridge, United Kingdom) were performed using a Leica TCS SP5 equipped with an Ibidi heating system for imaging chambers (Ibidi, Munich, Germany) to keep cells at 37°C. Images were acquired using a 20x or 63x objective; z-sections were acquired every 0.5 µm. For ASP+ live cell image, cells were loaded with 50 µM ASP+ in FSCV buffer for 1 min and subsequently washed with dye-free buffer 3 times. For visualization of FFN511 release, cells were loaded with 10 µM FFN511 in FSCV buffer for 10 min and

subsequently washed with dye-free buffer 3 times. Then, neurons were stained using a 1x working solution of Cellmask Deep Red plasma membrane stain (Life Technologies, Carlsbad, United States). In case of FFN511 live cell imaging, 5-HTN were stimulated to release 5-HT using the electrical parameters applied for FSCV. Image raw data was imported into NIH ImageJ to generate z-projections and quantify fluorescence intensities before and after electrical stimulation using the Multi Measure plugin. ROIs for quantifications were defined in the channel acquired for Cellmask staining.

4.6.6 Statistical analysis

Fluorescence intensities measured using ImageJ were imported into GraphPadPrism software (GraphPad Software Inc., USA) to generate graphs and perform statistical analysis (variance analysis and post hoc-comparison or Student's t-test) of the raw data. P values < 0.05 were considered significantly different to control values. The results on the graphs are displayed as means ± SEMs. For SERT cell surface density, a total of 803 ROI were measured in 3 independent experiments. Regarding live cell imaging experiments, for each fluorescent substrate at least 50 ROIs were measured. Raw values were normalized to control values after statistical analysis. FSCV results are averaged as error bars are depicted as SEMs.

4.6.7 Carbon fiber microelectrodes

Carbon fibers of 7-10 µm in diameter (T-650, Goodfellow, Coraopolis, PA, USA) were aspirated into glass capillaries (4 mm internal diameter, 0.6 mm outer diameter, A-M Systems, Sequim, WA, USA). A vertical pipette puller (Narishige Group, Tokyo, Japan) was employed to create a carbon-glass seal, and the resulting exposed carbon fiber was cut under a microscope to 100 (±5) (5-HTNs) or 150 (±5) (*in vivo*) µm in length.

These electrodes were electroplated with Nafion (Liquion Solution, LQ-1105, 5% by weight Nafion, Ion Power, New Castle, DE, USA) as described previously. [57]

4.6.8 FSCV data acquisition and analysis

FSCV data collection and analysis were performed using WCCV 3.06 software (Knowmad Technologies, LLC, Tucson, AZ, USA), a Dagan potentiostat (Dagan Corporation, Minneapolis, MN, USA), and a Pine Research headstage (Pine Research Instrumentation, Durham NC, USA). The serotonin waveform was applied (0.2 V to 1.0 V to -0.1 V to 0.2 V, with a scan rate of 1000 V/s and 10 Hz frequency, as described previously [57,59]. A Cl^-electroplated silver wire (0.01 in diameter, A-M Systems, Sequim, WA, USA) was as a reference electrode. Electrically-evoked stimulation was performed using an insulated stainless-steel electrode (0.2 mm diameter, untwisted, Plastics One, Roanoke, VA, USA). A biphasic stimulation was applied through a linear constant current stimulus isolator (NL800A Neurolog, Medical Systems Corp, Great Neck, NY) at 60 biphasic pulses at 60 Hz, 250 μA each, 4 ms in width. Stimulation polarity was switched between each file.

4.6.9 FSCV cell measurements

Coverslips containing TRP+ human serotonergic neuronal cell clusters were removed from media were placed into a 35 mm low wall imaging dish (ibidi GmbH, Martinsried, Germany) and covered with a room-temperature solution containing 2.5 mM glucose in HEPES buffer. This dish was placed into a plastic holder covered with aluminum foil and connected to ground to act as a Faraday cage. The cell-containing Faraday cage was placed onto a Leica DM IL inverted microscope to enable visualization of cells and as electrodes were placed. Carbon-fiber electrodes of 100 μm were

employed in all cell studies. Micromanipulators (QUAD, Sutter Instruments, Novato, CA, USA) were employed to position the working carbon-fiber and stimulation electrodes.

4.6.10 Animals

In vivo animal experiments were performed using methods described previously [59] in which a stimulating electrode was placed, in reference to bregma, in the medial forebrain bundle (MFB, AP: -1.58 mm, ML: +1.00 mm, DV: -4.8 mm), a working electrode was placed in the CA2 region of the hippocampus (AP: -2.91 mm, ML: +3.35 mm, DV: -2.5 to -3.0 mm) [86], and a pseudo Ag/AgCl reference electrode was placed in the contralateral hemisphere. Animal use followed NIH guidelines and complied with the University of South Carolina Institutional Animal Care and Use Committee (IACUC) under an approved protocol.

4.6.11 Mathematical modeling

In 2010, we created a mathematical model for 5-HT synthesis, storage in vesicles, release, reuptake by SERTs, and control by autoreceptors, which has been used by us and others to test hypotheses and explain experimental data.[87] Our 2014 collaboration revealed that: (1) there are two reuptake mechanisms, the SERTs and uptake into glial cells by other transporters; (2) autoreceptor effects on release are not instantaneous and persist for many seconds after the extracellular concentration of 5-HT returns to normal [75]. We have therefore created an improved mathematical model for 5-HT release, reuptake, and control, that contains both uptake mechanisms and a detailed model of the mechanisms of autoreceptor function including the auroreceptors, coupled G-proteins, and regulators of G-protein signaling. This new model, based on a previous model,[87] is

used for the simulations in this paper. A publication describing the new model is in preparation. The autoreceptor dynamics is the really new part of the improved model, so we describe it here.

When stimulated in the Hashemi Lab, the 5-HT neurons release 5-HT into the extracellular space. The increase in extracellular 5-HT (eht) causes the concentration of autoreceptors bound to eht (bht) to go up. The increased binding stimulates the conversion of inactive G-protein (G) to its active form, G*. Then G* stimulates the conversion of the regulatory protein, T, to its active form, T*, which deactivates G*. This verbal description is instantiated in the following differential equations for bht, G*, and T*.

$$\frac{d(G^*)}{dt} = a_1(bht)^2(g_0 - G^*) - a_2T^*G^* \quad (1)$$

$$\frac{d(T^*)}{dt} = a_3(G^*)^2(t_0 - T^*) - a_4T^* \quad (2)$$

$$\frac{d(bht)}{dt} = a_5(eht)(b_0 - bht) - a_6(bht) \quad (3)$$

Here b_0, g_0, and t_0 represent the total concentrations of autoreceptors, G-proteins, and T-proteins, respectively. It is the activated G-protein, G*, that inhibits synthesis of 5-HT and inhibits release from the vesicles into the extracellular space. The rate of release, R(t), is given by

$$R(t) = a_7 \,\mathrm{inhib}(G^*)\,\mathrm{fire}(t)\,vht.$$

where fire(t) is the firing rate of the neuron and vht is the vesicular concentration of 5-HT. The function inhib(G*) depends on G* and has the following form:

$$\text{inhib}(G^*) = tonic - a_8 (G^* - G^*_{eq}).$$

At equilibrium there is a tonic amount of inhibition of release. But, when G* rises above its equilibrium level the multiplicative factor inhib(G*) is lower so release goes down. The constants $a_1,\ldots,a_8$ will likely vary somewhat between individuals. This kind of model for autoreceptor dynamics was first presented for histamine H_3 autoreceptor dynamics previously.[88]

4.7 REFERENCES

(1) Holmes, A.; Murphy, D. L.; Crawley, J. N. Abnormal behavioral phenotypes of serotonin transporter knockout mice: parallels with human anxiety and depression. *Biol Psychiatry* **2003,** *54* (10), 953.

(2) Caspi, A.; Sugden, K.; Moffitt, T. E.; Taylor, A.; Craig, I. W.; Harrington, H.; McClay, J.; Mill, J.; Martin, J.; Braithwaite, A.et al. Influence of life stress on depression: moderation by a polymorphism in the 5-HTT gene. *Science* **2003,** *301* (5631), 386.

(3) Daubert, E. A.; Condron, B. G. Serotonin: a regulator of neuronal morphology and circuitry. *Trends Neurosci* **2010,** *33* (9), 424.

(4) Weiss, J. M.; Goodman, P. A.; Losito, B. G.; Corrigan, S.; Charry, J. M.; Bailey, W. H. Behavioral depression produced by an uncontrollable stressor: Relationship to norepinephrine, dopamine, and serotonin levels in various regions of rat brain. *Brain Research Reviews* **1981,** *3* (2), 167.

(5) Meyer, J. H. Imaging the serotonin transporter during major depressive disorder and antidepressant treatment. *J Psychiatry Neurosci* **2007,** *32* (2), 86.

(6) O'Donnell, J. M.; Shelton, R. C. In *Goodman & Gilman's: The Pharmacological Basis of Therapeutics, 12e*; Brunton, L. L.;Chabner, B. A.;Knollmann, B. C., Eds.; McGraw-Hill Education: New York, NY, 2015.

(7) Fakhoury, M. Revisiting the Serotonin Hypothesis: Implications for Major Depressive Disorders. *Mol Neurobiol* **2016,** *53* (5), 2778.

(8) Kohler, S.; Cierpinsky, K.; Kronenberg, G.; Adli, M. The serotonergic system in the neurobiology of depression: Relevance for novel antidepressants. *J Psychopharmacol* **2016,** *30* (1), 13.

(9) Wood, K. M.; Hashemi, P. Fast-scan cyclic voltammetry analysis of dynamic serotonin reponses to acute escitalopram. *ACS Chem Neurosci* **2013,** *4* (5), 715.

(10) Koch, P.; Ladewig, J. A Little Bit of Guidance: Mini Brains on Their Route to Adolescence. *Cell Stem Cell* **2017,** *21* (2), 157.

(11) Renner, M.; Lancaster, M. A.; Bian, S.; Choi, H.; Ku, T.; Peer, A.; Chung, K.; Knoblich, J. A. Self-organized developmental patterning and differentiation in cerebral organoids. *EMBO J* **2017,** *36* (10), 1316.

(12) Lu, J.; Zhong, X.; Liu, H.; Hao, L.; Huang, C. T.; Sherafat, M. A.; Jones, J.; Ayala, M.; Li, L.; Zhang, S. C. Generation of serotonin neurons from human pluripotent stem cells. *Nat Biotechnol* **2016,** *34* (1), 89.

(13) Vadodaria, K. C.; Mertens, J.; Paquola, A.; Bardy, C.; Li, X.; Jappelli, R.; Fung, L.; Marchetto, M. C.; Hamm, M.; Gorris, M.et al. Generation of functional human serotonergic neurons from fibroblasts. *Mol Psychiatry* **2016,** *21* (1), 49.

(14) Xu, Z.; Jiang, H.; Zhong, P.; Yan, Z.; Chen, S.; Feng, J. Direct conversion of human fibroblasts to induced serotonergic neurons. *Mol Psychiatry* **2016,** *21* (1), 62.

(15) Gundelfinger, E. D.; Fejtova, A. Molecular organization and plasticity of the cytomatrix at the active zone. *Curr Opin Neurobiol* **2012,** *22* (3), 423.

(16) Mukherjee, K.; Yang, X.; Gerber, S. H.; Kwon, H. B.; Ho, A.; Castillo, P. E.; Liu, X.; Sudhof, T. C. Piccolo and bassoon maintain synaptic vesicle clustering without directly participating in vesicle exocytosis. *Proc Natl Acad Sci U S A* **2010,** *107* (14), 6504.

(17) Waites, C. L.; Leal-Ortiz, S. A.; Okerlund, N.; Dalke, H.; Fejtova, A.; Altrock, W. D.; Gundelfinger, E. D.; Garner, C. C. Bassoon and Piccolo maintain synapse integrity by regulating protein ubiquitination and degradation. *EMBO J* **2013,** *32* (7), 954.

(18) Matthaus, F.; Haddjeri, N.; Sanchez, C.; Marti, Y.; Bahri, S.; Rovera, R.; Schloss, P.; Lau, T. The allosteric citalopram binding site differentially interferes with neuronal firing rate and SERT trafficking in serotonergic neurons. *Eur Neuropsychopharmacol* **2016,** *26* (11), 1806.

(19) Kishida, K. T.; Saez, I.; Lohrenz, T.; Witcher, M. R.; Laxton, A. W.; Tatter, S. B.; White, J. P.; Ellis, T. L.; Phillips, P. E.; Montague, P. R. Subsecond dopamine fluctuations in human striatum encode superposed error signals about actual and counterfactual reward. *Proc Natl Acad Sci U S A* **2016,** *113* (1), 200.

(20) Ciranna, L. Serotonin as a modulator of glutamate- and GABA-mediated neurotransmission: implications in physiological functions and in pathology. *Curr Neuropharmacol* **2006,** *4* (2), 101.

(21) Vasudeva, R. K.; Kirby, L.; Waterhouse, B. D. *Cellular physiology of the DRN: Implications for anxiety and depression*, 2013.

(22) Challis, C.; Berton, O. Top-Down Control of Serotonin Systems by the Prefrontal Cortex: A Path toward Restored Socioemotional Function in Depression. *ACS Chem Neurosci* **2015,** *6* (7), 1040.

(23) Rial, D.; Lemos, C.; Pinheiro, H.; Duarte, J. M.; Goncalves, F. Q.; Real, J. I.; Prediger, R. D.; Goncalves, N.; Gomes, C. A.; Canas, P. M.et al. Depression as a Glial-Based Synaptic Dysfunction. *Front Cell Neurosci* **2015,** *9*, 521.

(24) Lidov, H. G.; Molliver, M. E. Immunohistochemical study of the development of serotonergic neurons in the rat CNS. *Brain Res Bull* **1982,** *9* (1-6), 559.

(25) Alonso, A.; Merchan, P.; Sandoval, J. E.; Sanchez-Arrones, L.; Garcia-Cazorla, A.; Artuch, R.; Ferran, J. L.; Martinez-de-la-Torre, M.; Puelles, L. Development of the serotonergic cells in murine raphe nuclei and their relations with rhombomeric domains. *Brain Struct Funct* **2013,** *218* (5), 1229.

(26) Kiyasova, V.; Gaspar, P. Development of raphe serotonin neurons from specification to guidance. *Eur J Neurosci* **2011,** *34* (10), 1553.

(27) Bang, S. J.; Jensen, P.; Dymecki, S. M.; Commons, K. G. Projections and interconnections of genetically defined serotonin neurons in mice. *Eur J Neurosci* **2012,** *35* (1), 85.

(28) Gutknecht, L.; Waider, J.; Kraft, S.; Kriegebaum, C.; Holtmann, B.; Reif, A.; Schmitt, A.; Lesch, K. P. Deficiency of brain 5-HT synthesis but serotonergic neuron formation in Tph2 knockout mice. *J Neural Transm (Vienna)* **2008,** *115* (8), 1127.

(29) Sur, C.; Betz, H.; Schloss, P. Immunocytochemical detection of the serotonin transporter in rat brain. *Neuroscience* **1996,** *73* (1), 217.

(30) Quentin, E.; Belmer, A.; Maroteaux, L. Somato-Dendritic Regulation of Raphe Serotonin Neurons; A Key to Antidepressant Action. *Front Neurosci* **2018,** *12*, 982.

(31) Trueta, C.; De-Miguel, F. F. Extrasynaptic exocytosis and its mechanisms: a source of molecules mediating volume transmission in the nervous system. *Front Physiol* **2012,** *3*, 319.

(32) Liu, C.; Kershberg, L.; Wang, J.; Schneeberger, S.; Kaeser, P. S. Dopamine Secretion Is Mediated by Sparse Active Zone-like Release Sites. *Cell* **2018,** *172* (4), 706.

(33) Leon-Pinzon, C.; Cercos, M. G.; Noguez, P.; Trueta, C.; De-Miguel, F. F. Exocytosis of serotonin from the neuronal soma is sustained by a serotonin and calcium-dependent feedback loop. *Front Cell Neurosci* **2014,** *8*, 169.

(34) Cercos, M. G.; De-Miguel, F. F.; Trueta, C. Real-time measurements of synaptic autoinhibition produced by serotonin release in cultured leech neurons. *J Neurophysiol* **2009,** *102* (2), 1075.

(35) Zhang, H.; Gubernator, N. G.; Yue, M.; Staal, R. G.; Mosharov, E. V.; Pereira, D.; Balsanek, V.; Vadola, P. A.; Mukherjee, B.; Edwards, R. H.et al. Dopamine

release at individual presynaptic terminals visualized with FFNs. *J Vis Exp* **2009**, DOI:10.3791/1562 10.3791/1562(30).

(36) Gubernator, N. G.; Zhang, H.; Staal, R. G.; Mosharov, E. V.; Pereira, D. B.; Yue, M.; Balsanek, V.; Vadola, P. A.; Mukherjee, B.; Edwards, R. H.et al. Fluorescent false neurotransmitters visualize dopamine release from individual presynaptic terminals. *Science* **2009,** *324* (5933), 1441.

(37) Henke, A.; Kovalyova, Y.; Dunn, M.; Dreier, D.; Gubernator, N. G.; Dincheva, I.; Hwu, C.; Sebej, P.; Ansorge, M. S.; Sulzer, D.et al. Toward Serotonin Fluorescent False Neurotransmitters: Development of Fluorescent Dual Serotonin and Vesicular Monoamine Transporter Substrates for Visualizing Serotonin Neurons. *ACS Chem Neurosci* **2018,** *9* (5), 925.

(38) Lau, T.; Proissl, V.; Ziegler, J.; Schloss, P. Visualization of neurotransmitter uptake and release in serotonergic neurons. *J Neurosci Methods* **2015,** *241*, 10.

(39) Ou, Y.; Buchanan, A. M.; Witt, C. E.; Hashemi, P. Frontiers in electrochemical sensors for neurotransmitter detection: towards measuring neurotransmitters as chemical diagnostics for brain disorders. *Analytical Methods* **2019,** *11* (21), 2738.

(40) Berberian, K.; Kisler, K.; Fang, Q.; Lindau, M. Improved surface-patterned platinum microelectrodes for the study of exocytotic events. *Anal Chem* **2009,** *81* (21), 8734.

(41) Kathiwala, M.; Abou El-Nour, K. M.; Cohen-Shohet, R.; Brajter-Toth, A. Rapid measurements of 2,8-dihydroxyadenine (2,8-DHA) with a nanostructured electrochemical sensor in 5-fold diluted supernatants of endothelial cells exposed to oxidative stress. *Analyst* **2010,** *135* (2), 296.

(42) Schrock, D. S.; Baur, J. E. Chemical imaging with combined fast-scan cyclic voltammetry-scanning electrochemical microscopy. *Anal Chem* **2007,** *79* (18), 7053.

(43) Koch, J. A.; Baur, M. B.; Woodall, E. L.; Baur, J. E. Alternating current scanning electrochemical microscopy with simultaneous fast-scan cyclic voltammetry. *Anal Chem* **2012,** *84* (21), 9537.

(44) Heien, M. L.; Johnson, M. A.; Wightman, R. M. Resolving neurotransmitters detected by fast-scan cyclic voltammetry. *Anal Chem* **2004,** *76* (19), 5697.

(45) Petrovic, J.; Walsh, P. L.; Thornley, K. T.; Miller, C. E.; Wightman, R. M. Real-time monitoring of chemical transmission in slices of the murine adrenal gland. *Endocrinology* **2010,** *151* (4), 1773.

(46) Walsh, P. L.; Petrovic, J.; Wightman, R. M. Distinguishing splanchnic nerve and chromaffin cell stimulation in mouse adrenal slices with fast-scan cyclic voltammetry. *Am J Physiol Cell Physiol* **2011,** *300* (1), C49.

(47) Cryan, M. T.; Ross, A. E. Subsecond detection of guanosine using fast-scan cyclic voltammetry. *Analyst* **2018,** *144* (1), 249.

(48) Sun, M.; Kaplan, S. V.; Gehringer, R. C.; Limbocker, R. A.; Johnson, M. A. Localized drug application and sub-second voltammetric dopamine release measurements in a brain slice perfusion device. *Anal Chem* **2014,** *86* (9), 4151.

(49) Phillips, P. E.; Johns, J. M.; Lubin, D. A.; Budygin, E. A.; Gainetdinov, R. R.; Lieberman, J. A.; Wightman, R. M. Presynaptic dopaminergic function is largely unaltered in mesolimbic and mesostriatal terminals of adult rats that were prenatally exposed to cocaine. *Brain Res* **2003,** *961* (1), 63.

(50) Jones, S. R.; Joseph, J. D.; Barak, L. S.; Caron, M. G.; Wightman, R. M. Dopamine neuronal transport kinetics and effects of amphetamine. *J Neurochem* **1999,** *73* (6), 2406.

(51) Pihel, K.; Hsieh, S.; Jorgenson, J. W.; Wightman, R. M. Quantal corelease of histamine and 5-hydroxytryptamine from mast cells and the effects of prior incubation. *Biochemistry* **1998,** *37* (4), 1046.

(52) Pihel, K.; Hsieh, S.; Jorgenson, J. W.; Wightman, R. M. Electrochemical detection of histamine and 5-hydroxytryptamine at isolated mast cells. *Anal Chem* **1995,** *67* (24), 4514.

(53) Bunin, M. A.; Wightman, R. M. Quantitative evaluation of 5-hydroxytryptamine (serotonin) neuronal release and uptake: an investigation of extrasynaptic transmission. *J Neurosci* **1998,** *18* (13), 4854.

(54) Bunin, M. A.; Prioleau, C.; Mailman, R. B.; Wightman, R. M. Release and uptake rates of 5-hydroxytryptamine in the dorsal raphe and substantia nigra reticulata of the rat brain. *J Neurochem* **1998,** *70* (3), 1077.

(55) Threlfell, S.; Cragg, S. J.; Kallo, I.; Turi, G. F.; Coen, C. W.; Greenfield, S. A. Histamine H3 receptors inhibit serotonin release in substantia nigra pars reticulata. *J Neurosci* **2004,** *24* (40), 8704.

(56) John, C. E.; Jones, S. R. Voltammetric characterization of the effect of monoamine uptake inhibitors and releasers on dopamine and serotonin uptake in mouse caudate-putamen and substantia nigra slices. *Neuropharmacology* **2007,** *52* (8), 1596.

(57) Hashemi, P.; Dankoski, E. C.; Petrovic, J.; Keithley, R. B.; Wightman, R. M. Voltammetric detection of 5-hydroxytryptamine release in the rat brain. *Anal Chem* **2009,** *81* (22), 9462.

(58) West, A.; Best, J.; Abdalla, A.; Nijhout, H. F.; Reed, M.; Hashemi, P. Voltammetric evidence for discrete serotonin circuits, linked to specific reuptake domains, in the mouse medial prefrontal cortex. *Neurochem Int* **2019,** *123*, 50.

(59) Saylor, R. A.; Hersey, M.; West, A.; Buchanan, A. M.; Berger, S. N.; Nijhout, H. F.; Reed, M. C.; Best, J.; Hashemi, P. In vivo Hippocampal Serotonin Dynamics in Male and Female Mice: Determining Effects of Acute Escitalopram Using Fast Scan Cyclic Voltammetry. *Front Neurosci* **2019,** *13*, 362.

(60) Hashemi, P.; Dankoski, E. C.; Lama, R.; Wood, K. M.; Takmakov, P.; Wightman, R. M. Brain dopamine and serotonin differ in regulation and its consequences. *Proc Natl Acad Sci U S A* **2012,** *109* (29), 11510.

(61) Wiedemann, D. J.; Garris, P. A.; Near, J. A.; Wightman, R. M. Effect of chronic haloperidol treatment on stimulated synaptic overflow of dopamine in the rat striatum. *J Pharmacol Exp Ther* **1992,** *261* (2), 574.

(62) Rice, M. E.; Cragg, S. J.; Greenfield, S. A. Characteristics of electrically evoked somatodendritic dopamine release in substantia nigra and ventral tegmental area in vitro. *J Neurophysiol* **1997,** *77* (2), 853.

(63) Stamford, J. A.; Kruk, Z. L.; Millar, J. Striatal dopamine terminals release serotonin after 5-HTP pretreatment: in vivo voltammetric data. *Brain Res* **1990,** *515* (1-2), 173.

(64) Schwartz, J. W.; Blakely, R. D.; DeFelice, L. J. Binding and transport in norepinephrine transporters. Real-time, spatially resolved analysis in single cells using a fluorescent substrate. *J Biol Chem* **2003,** *278* (11), 9768.

(65) Mason, J. N.; Farmer, H.; Tomlinson, I. D.; Schwartz, J. W.; Savchenko, V.; DeFelice, L. J.; Rosenthal, S. J.; Blakely, R. D. Novel fluorescence-based approaches for the study of biogenic amine transporter localization, activity, and regulation. *J Neurosci Methods* **2005,** *143* (1), 3.

(66) Oz, M.; Libby, T.; Kivell, B.; Jaligam, V.; Ramamoorthy, S.; Shippenberg, T. S. Real-time, spatially resolved analysis of serotonin transporter activity and regulation using the fluorescent substrate, ASP+. *J Neurochem* **2010,** *114* (4), 1019.

(67) Ayala-Lopez, N.; Jackson, W. F.; Burnett, R.; Wilson, J. N.; Thompson, J. M.; Watts, S. W. Organic cation transporter 3 contributes to norepinephrine uptake into perivascular adipose tissue. *Am J Physiol Heart Circ Physiol* **2015,** *309* (11), H1904.

(68) Rytting, E.; Bryan, J.; Southard, M.; Audus, K. L. Low-affinity uptake of the fluorescent organic cation 4-(4-(dimethylamino)styryl)-N-methylpyridinium iodide (4-Di-1-ASP) in BeWo cells. *Biochem Pharmacol* **2007,** *73* (6), 891.

(69) Shaskan, E. G.; Snyder, S. H. Kinetics of serotonin accumulation into slices from rat brain: relationship to catecholamine uptake. *J Pharmacol Exp Ther* **1970,** *175* (2), 404.

(70) Horton, R. E.; Apple, D. M.; Owens, W. A.; Baganz, N. L.; Cano, S.; Mitchell, N. C.; Vitela, M.; Gould, G. G.; Koek, W.; Daws, L. C. Decynium-22 enhances

SSRI-induced antidepressant-like effects in mice: uncovering novel targets to treat depression. *J Neurosci* **2013,** *33* (25), 10534.

(71) Amphoux, A.; Vialou, V.; Drescher, E.; Bruss, M.; Mannoury La Cour, C.; Rochat, C.; Millan, M. J.; Giros, B.; Bonisch, H.; Gautron, S. Differential pharmacological in vitro properties of organic cation transporters and regional distribution in rat brain. *Neuropharmacology* **2006,** *50* (8), 941.

(72) Daws, L. C. Unfaithful neurotransmitter transporters: focus on serotonin uptake and implications for antidepressant efficacy. *Pharmacol Ther* **2009,** *121* (1), 89.

(73) Baganz, N. L.; Horton, R. E.; Calderon, A. S.; Owens, W. A.; Munn, J. L.; Watts, L. T.; Koldzic-Zivanovic, N.; Jeske, N. A.; Koek, W.; Toney, G. M.et al. Organic cation transporter 3: Keeping the brake on extracellular serotonin in serotonin-transporter-deficient mice. *Proc Natl Acad Sci U S A* **2008,** *105* (48), 18976.

(74) Daws, L. C.; Koek, W.; Mitchell, N. C. Revisiting serotonin reuptake inhibitors and the therapeutic potential of "uptake-2" in psychiatric disorders. *ACS Chem Neurosci* **2013,** *4* (1), 16.

(75) Wood, K. M.; Zeqja, A.; Nijhout, H. F.; Reed, M. C.; Best, J.; Hashemi, P. Voltammetric and mathematical evidence for dual transport mediation of serotonin clearance in vivo. *J Neurochem* **2014,** *130* (3), 351.

(76) Lundberg, J.; Christophersen, J. S.; Petersen, K. B.; Loft, H.; Halldin, C.; Farde, L. PET measurement of serotonin transporter occupancy: a comparison of escitalopram and citalopram. *Int J Neuropsychopharmacol* **2007,** *10* (6), 777.

(77) Machado-Vieira, R.; Baumann, J.; Wheeler-Castillo, C.; Latov, D.; Henter, I. D.; Salvadore, G.; Zarate, C. A. The Timing of Antidepressant Effects: A Comparison

of Diverse Pharmacological and Somatic Treatments. *Pharmaceuticals (Basel)* **2010,** *3* (1), 19.

(78) Harmer, C. J.; Duman, R. S.; Cowen, P. J. How do antidepressants work? New perspectives for refining future treatment approaches. *Lancet Psychiatry* **2017,** *4* (5), 409.

(79) Sanchez, C.; Reines, E. H.; Montgomery, S. A. A comparative review of escitalopram, paroxetine, and sertraline: Are they all alike? *Int Clin Psychopharmacol* **2014,** *29* (4), 185.

(80) Bundgaard, C.; Eneberg, E.; Sanchez, C. P-glycoprotein differentially affects escitalopram, levomilnacipran, vilazodone and vortioxetine transport at the mouse blood-brain barrier in vivo. *Neuropharmacology* **2016,** *103*, 104.

(81) Steiner, J. A.; Carneiro, A. M.; Blakely, R. D. Going with the flow: trafficking-dependent and -independent regulation of serotonin transport. *Traffic* **2008,** *9* (9), 1393.

(82) Bermingham, D. P.; Blakely, R. D. Kinase-dependent Regulation of Monoamine Neurotransmitter Transporters. *Pharmacol Rev* **2016,** *68* (4), 888.

(83) John, C. E.; Budygin, E. A.; Mateo, Y.; Jones, S. R. Neurochemical characterization of the release and uptake of dopamine in ventral tegmental area and serotonin in substantia nigra of the mouse. *J Neurochem* **2006,** *96* (1), 267.

(84) Dankoski, E. C.; Wightman, R. M. Monitoring serotonin signaling on a subsecond time scale. *Front Integr Neurosci* **2013,** *7*, 44.

(85) Cao, L.; Hu, R.; Xu, T.; Zhang, Z. N.; Li, W.; Lu, J. Characterization of Induced Pluripotent Stem Cell-derived Human Serotonergic Neurons. *Front Cell Neurosci* **2017,** *11*, 131.

(86) Franklin, K. B. J.; Paxinos, G. *Paxinos and Franklin's The mouse brain in stereotaxic coordinates*, 2013.

(87) Best, J.; Nijhout, H. F.; Reed, M. Serotonin synthesis, release and reuptake in terminals: a mathematical model. *Theor Biol Med Model* **2010,** *7*, 34.

(88) Best, J.; Nijhout, H. F.; Samaranayake, S.; Hashemi, P.; Reed, M. A mathematical model for histamine synthesis, release, and control in varicosities. *Theor Biol Med Model* **2017,** *14* (1), 24.

CHAPTER 5

RADICAL-INITATED ELECTROPOLYMERIZATION OF POLY-GLUTAMIC ACID ON CARBON: IMPLICATIONS FOR BIOLOGICAL ANALYSIS[4]

[4] **Holmes, J.;** Batey, L.; Hashemi, P.: "Radical-initiated electropolymerization of poly-glutamic acid on carbon: Implications for biological analysis" – *Under review* – Journal of the American Chemical Society.

5.1 ABSTRACT

Carbon materials are paramount for analysis of biological molecules of broad relevance. Biocompatibility makes carbon extremely beneficial for electroanalysis in biological systems; however, carbon surfaces are prone to electropolymerization by biological molecules, an effect that has been presumed to poison the electrode, deteriorating sensitivity. In this work, we find that exposure to *in vivo* brain tissue improves the sensitivity of carbon electrodes to dopamine with fast voltammetry. We hypothesize that glutamate, a ubiquitous neurotransmitter highly concentrated in the extracellular space, plays a key role because glutamate is known to electropolymerize on carbon electrodes with slow scan voltammetry. The polymerization mechanism is initiated electrochemically via formation of a radical and propagates to form poly-glutamic acid (PGA), a polymer with an overall negative charge, that may serve to enhance sensitivity towards biological cations like dopamine *via* preconcentration. Here, we provide electrochemical, microscopic, and spectroscopic evidence of PGA growth on carbon microelectrodes. Film formation is visually verified via scanning electron microscopy and energy dispersive x-ray spectroscopy reveals similarities in the elemental profiles of PGA electrodes and electrodes implanted in brain tissue. Morphology is further analyzed with atomic force microscopy, indicating a nucleation and growth-like mechanism of PGA on carbon. The implications of PGA on electrochemical performance are assessed and compared to electrodes conditioned *in vivo*, both providing similar enhanced sensitivity and kinetic response time. Given the similarities between electrodes conditioned in PGA and *in vivo*, ambient glutamate is likely responsible for the majority of *in vivo* polymerization, and PGA is critical for enhancing sensitivity *in vivo*.

5.2 INTRODUCTION

Carbon electrodes have been employed for many decades to study biological phenomena.[1] Carbon is an excellent material for biological analysis because it is cheap, has excellent electron transfer properties, is biocompatible and easy to microfashion.[1] Carbon has been broadly applied in biological analysis to measure a multitude of biologically relevant molecules in sweat,[2-4] tears,[5-7] urine,[8-10] breath,[11] blood,[12,13] and in several organs such as the gut,[14,15] lymph nodes,[16] and the brain.[17,18] A facet of biological electroanalysis at carbon is that biological molecules can electropolymerize on the electrode surface. In general, it is thought that this polymerization constitutes fouling or poisoning of the carbon surfaces whereby electrodes become less sensitive to analytes. Biofouling is proposed to be the primary reason why most biosensors fail during *in vivo* measurements.[19,20]

A particularly well characterized example of biological electropolymerization is during *in vivo* brain analysis. Studies have shown that the neurotransmitters dopamine (DA) and serotonin[21-26] create multiple, unstable, intermediate oxidation products that rapidly polymerize on the electrode surface. As such, steps have been taken to 'clean' electrodes *in situ* or prevent this type of fouling. For example, the application of a high positive potential (around 1.3 V) to carbon fiber microelectrodes (CFMs) results in oxidation of the carbon surface, thereby etching the top-most layer and regenerating the electrode.[27,28] An alternative approach is to utilize different types of carbon; several groups have shown that boron doped diamond is less susceptible to biofouling than other types of carbon electrodes.[29-31] A third method to reduce fouling is to modify the electrode with polymer coatings, like the cation or size exchange polymer Nafion

(NA).[24,32-34] There has been some incoherence about a universal modification procedure using polymers to prevent the fouling.

We began this work by analyzing the effects of brain tissue exposure on carbon with the goal of optimizing parameters for polymer modification of carbon. This work was initially performed under the rationale that exposure to brain tissue would decrease carbon's sensitivity. Surprisingly, we found that the *in vivo* environment in the brain significantly increased CFM sensitivity to DA when measured with fast voltammetry. This led us to hypothesize that polymerization during *in vivo* measurements serves to enhance, not degrade, electrode sensitivity. We postulated that glutamate, an excitatory transmitter, is a key player in these polymerization processes because a) this species is ubiquitous and highly concentrated in the brain (*in vivo* studies utilizing various techniques report 1-30 μM[35]) and b) poly-glutamic acid's (PGA) overall electronegative charge is controlled by pH, and may enhance sensitivity to DA and other positively charged analytes at biological pH *via* preconcentration.[36,37] Additionally, glutamate electropolymerizes to form PGA *via* conventional cyclic voltammetry in a mechanism initiated by the generation of a radical cation when a sufficiently positive potential is applied.[38] The amine group on glutamate covalently grafts to carbon[39,40] and propagation is governed by a chain growth reaction.[39,41] As such, PGA has been employed broadly across biomedical and bioanalytical applications, including as a biocompatible encapsulation method for drug delivery,[42,43] a hydrogel for *in vitro* tissue engineering,[44-46] and as a polymer coating for electroanalytical detection.[47-49]

Here, in support of the idea that glutamate polymerizes on the electrode, we showed evidence of in situ PGA formation on CFMs for the first time with fast-scan

cyclic voltammetry (FSCV). The resultant PGA film was imaged via scanning electron microscopy (SEM), and elemental analysis with Energy Dispersive X-Ray Spectroscopy (EDX) identified the film's chemical composition. Atomic force microscopy (AFM) further revealed the morphological character of PGA on the CFM surface, implying a nucleation and growth mechanism. Finally, the analytical performance (sensitivity and response time) of PGA-modified CFMs was compared to electrodes that had been conditioned *in vivo*. Like the *in vivo* electrodes, PGA modified electrodes displayed increased sensitivity compared to electrodes conditioned in PGA-free buffer. Furthermore, the PGA and *in vivo* CFMs exhibited significantly improved response times. Given the analytical and morphological similarities between *in vivo* and PGA electrodes, we conclude that the majority of *in vivo* polymerization is likely due to glutamate and that this polymerization is actually critical for facilitating *in vivo* measurements of amines in brains of mice.

5.3 RESULTS AND DISCUSSION

5.3.1 PGA electropolymerizes onto CFMs with FSCV

Biological environments are rich in proteins, ligands and many other redox active molecules. Carbon is generally hydrophobic and more resistant to the fouling effects of these agents than other common electrode materials.[29,50] Nonetheless, even the carbon surface is altered when implanted into the brain. The interaction of biomolecules with the carbon surface is particularly problematic for low concentration measurements and/or analysis of rapidly fluctuating species, as is the case for *in vivo* analysis of the brain. There is a general notion that the sensitivity and/or response time of electrodes declines *in vivo,* raising issues for data interpretation since it becomes very difficult to deconstruct

physiological events from inherent facets of the analysis. Researchers have taken different approaches to this problem including *in situ* 'cleaning' of the electrode,[28] post analysis corrections whereby the time aberrations of DA diffusion *in vivo* are modeled,[51-53] and modifications to the electrode surface, which is the method of choice in our own laboratory. A universal scheme for modifying CFMs with polymers to best enhance analytical performance, however, has not been agreed on. Researchers have found differing modification procedures or combinations of polymers to be the most successful.[24,32-34]

We began this work by seeking to compare and contrast different CFM modification procedures in a bid to provide a universal modification scheme to the community. As a starting point, we sought to confirm the fouling effects on CFMs of the *in vivo* environment. A four-point calibration was performed on 4 electrodes in TRIS buffer (commonly employed in FSCV analysis because it has components that mimic amines and proteins in the extracellular matrix). these electrodes were then placed into the nucleus accumbens core region of a mouse brain where DA was monitored for roughly 3 hours with fast scan adsorption-controlled voltammetry (FSCAV). The calibration was repeated following the *in vivo* experiment (calibrations are labeled PRECAL and POSTCAL in **Figure 5.1C**). A representative color plot and cyclic voltammograms (CVs) from these experiments are shown in **Figure 5.1A** and **5.1B**, respectively. Contrary to the general view than the *in vivo* environment is detrimental to electrode sensitivity, we found that the electrode sensitivity actually significantly increased post-calibration vs. pre-calibration. At the 500 nM calibration point, the current

response increased by an average of 156.6 % ($p = 0.016$). In our experiments, this effect persisted when FSCV is used (see **Figure 5.4**).

A previous study displays similar results,[54] where the current response to acetaminophen after *in vivo* measurements is larger than before the experiment, and another where the response change to DA is insignificant.[55] However the majority report decreased sensitivity to DA after *in vivo* exposure. [33,56,57] We attribute our results to the differences in our experimental conditions, such as background buffer (HEPES vs tris), electrode type (disk vs cylinder), waveform (1.0 V vs 1.3 V potential limit), pretreatment before post calibration (overnight soaking in IPA vs no pretreatment post calibration), and animal model (rats vs mice). All in all, our results suggest that an unidentified aspect of the *in vivo* environment contributes to a surface alteration of carbon that improves the sensitivity of the electrode towards DA.

When attempting to identify potential biological monomers that might electrochemically interact with carbon, one candidate that captured our interest was glutamate. Glutamate is a neurotransmitter that is ubiquitous across brain regions. While it is generally accepted that glutamate does not offer analytical electroactivity, glutamate electropolymerization is well established in the literature with conventional cyclic voltammetry.[36,38,58] Thus, we asked whether glutamate electropolymerization occurs at fast scan rates. A triangular waveform was optimized and applied to CFMs with a wide potential window (-1.2 V to 1.3 V to -1.2 V at 400 V/s). Using flow injection analysis (FIA), a pulse of glutamate (0.1 μM) was delivered to 4 different electrodes and the response recorded. A representative color plot and CV of this response are displayed in **Figure 5.1Di** where the electropolymerization peak occurs at 1 V (denoted by the purple

circle). The first six injections in **Figure 5.1D** reveal the polymerization peak, with an average current response of 36.7 ± 2.9 nA. Successive injections of glutamate using FSCV show that this peak diminishes the over time (**Figure 5.1Dii**), decreasing to an average of 11.1 ± 1.0 nA, 30.2% ($p = 0.0002$) of the original amplitude. When the glutamate concentration was increased to 1, 20, and 100 μM, there was no significant change in amplitude. A representative color plot and CV from a 20 μM injection in **Figure 5.1Diii** show that the polymerization peak previously observed is greatly diminished and is indistinguishable from the switching peak (an artifact of the technique near the switching potentials). We believe the disappearance of this peak over several injections is due to fewer available sites for PGA attachment and chain length saturation. The formation of PGA on CFMs with a waveform that scans to 1.3 V is an interesting finding since application of 1.3 V is known to etch and renew the carbon surface thereby increasing sensitivity to DA.[28] This effect has been attributed to overoxidation of the carbon surface, providing a clean surface for the next analysis and for creating oxygen moieties on the surface that pre-concentrate the DA cation prior to analysis.[27,28] Here we suggest that, *in vivo* in mice, 1.3 V also facilitates the signal *via* PGA polymer formation (the polymerization peak at 1 V suggests that this process is actually dependent on the application of a positive potential at or above 1 V). In the following sections, we characterize this surface film.

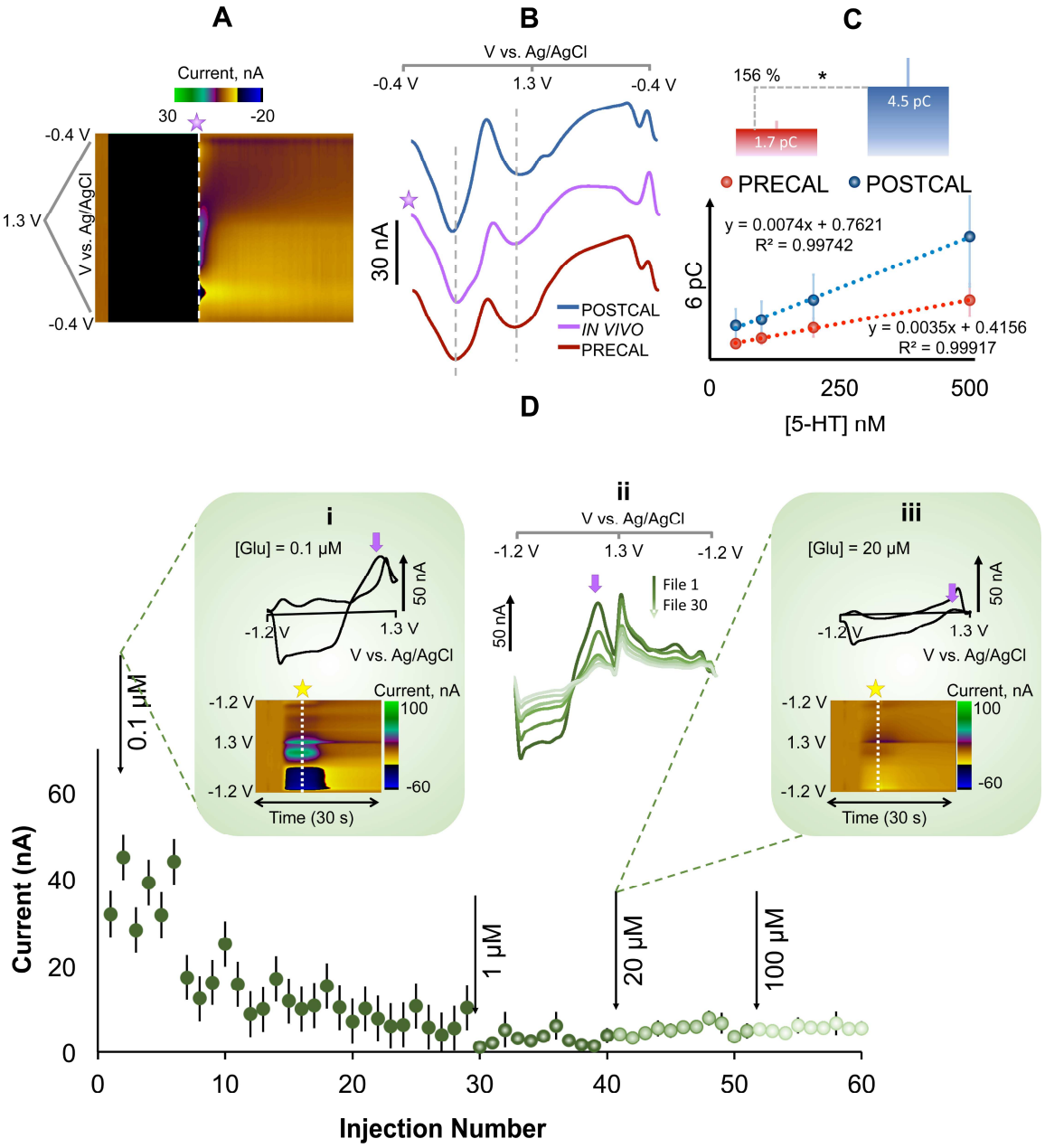

Figure 5.1. PGA Electropolymerization on CFMs. (A) Representative *in vivo* FSCAV color plot and **(B)** cyclic voltammograms in DA (500 mM), before (red), after (blue), and during (purple) *in vivo* measurements. **(C)** Pre and post calibration data from an *in vivo* experiment measuring DA in the mouse nucleus accumbens. Inset histogram depicts a 156 % increase in current response to 500 nM ($p < 0.05$). **(D)** Varying concentrations (0.1, 1, 20, and 100 µM) of glutamate, are measured by 60 successive injections *via* FIA. Color plots and CVs from (i) 0.1 µM and (iii) 20 µM glutamate injections are inset. (ii) Every 4th CV of 0.1 µM glutamate is displayed. Error bars: Standard error of the mean.

5.3.2 PGA can be visualized on CFMs

Given voltammetric evidence of PGA film formation in the previous section, film deposition was verified and characterized via micro- and nano-imaging and elemental analysis. SEM has previously been used to image PGA on different carbon surfaces including glassy carbon,[38,59-61] carbon paste electrodes,[62] carbon nanotubes,[47,49,63,64] graphite,[65] and reduced graphene oxide,[48,63] and other substrates such as Au nanoparticles,[66] however there have been no reports of PGA deposition on CFMs. Here we imaged CFM surfaces with SEM and performed EDX to analyze the elemental profile of the carbon surface. In particular, we were interested in observing the effects of waveform application and modification (testing the importance of 1.3 V) on the CFM surface in the presence of glutamate.

CFMs were treated using the triangular DA waveform for 10 minutes at 60 Hz and 10 minutes at 10 Hz with four different pre-treatment paradigms. SEM and EDX were performed on these electrodes within 24 hrs.

A - PBS, 1.3 V. In **Figure 5.2A**, the CFM was treated in PBS with the triangular waveform with the 1.3 V positive potential limit. The carbon surface appears relatively smooth (**Figure 5.2Ai**) and the elemental analysis, primarily, shows carbon (**Figure 5.2Aii**).

B - Glutamate in PBS, 1.0 V. In **Figure 5.2B** the positive potential limit of the triangular waveform was 1.0 V; this waveform is not considered to overoxidized the carbon surface.[27,28] When treated in 1 μM glutamate, CFMs did not show visible deposits on the CFM. This is because SEM does not have the resolving power to visualize the fine

deposits that occur with low glutamate concentrations (we visualize these with AFM in **Figure 5.3** below). With 10 mM glutamate, significant deposits were visualized (**Figure 5.2Bi**). EDX analysis revealed oxygen (**Figure 5.2Bii**). We believe that this oxygen on PGA-CFMs originates from glutamate molecule (since there is no oxygen peak in the absence of glutamate (**Figure 5.2A**). From glutamate, we also expect a nitrogen peak between the carbon and oxygen (0.4 keV), however the large carbon (0.3 keV) and oxygen (0.5 keV) peaks likely mask this nitrogen peak so that it cannot be resolved. Other elements detected *via* EDX include artifacts of the PBS buffer (Na, P, and Cl). Because a vacuum seal is required to perform SEM/EDX, we attribute this to salt ions becoming trapped in the pores of the PGA coating. This is not unexpected, as other groups have observed the presence of unexpected elements due to the fabrication process. For example, Ding *et al*. and Wang *et al.* observed Fe and Cl peaks on poly(2,5-bis(3,4-ethylenedioxythienyl)pyridine) due to the addition of Ferric chloride as an oxidant during fabrication.[67,68]

C - Glutamate in PBS, 1.3 V. In **Figure 5.2C** the positive potential limit of the waveform was increased to 1.3 V. The CFM has fewer deposits than the 1.0 V waveform (**Figure 5.2Ci**) but the EDX in **Figure 5.2Cii** is nearly identical to that in **Figure 5.2Bii**, detecting carbon, oxygen and PBS buffer artifacts. The lesser visual extent of deposition corresponds to a higher sensitivity to DA FIA (**Figure 5.2Ciii** where responses to 1μM DA are compared before and after CFM treatment in glutamate with 1.0 or 1.3V). From experiments in **Figure 5.1D**, we found that glutamate deposits at 1.0 V. The SEM result here implies that having a positive limit of 1.0 V encourages too thick of a PGA layer that creates a diffusion barrier, problematic for the rapid acquisition rate of FSCV. Previous

reports show that ramping the potential to 1.3 V etches and regenerates the CFM surface. We postulate here that PGA is formed simultaneously as the carbon is etched, thus providing an optimal balance that maintains the PGA film thin enough not to act as a diffusional barrier, but rather a pre-concentration matrix.

D - *In Vivo*, 1.3 V. In **Figure 5.2D**, the electrode was cycled *in vivo* for approximately 15 minutes. When imaged with SEM in **Figure 5.2Di**, there is a visible film on the electrode surface. Such deposits have been previously been seen after *in vivo* implantation, attributed to 'debris and biomaterials'.[33,69] Significantly, the elemental profile is similar to that of the CFMs exposed to glutamate (**Figure 5.2Dii**).

Some conclusions we draw from **Figure 5.2** are: (1) PGA formation can be visualized on CFMs (2) PGA coatings seem thinner with the 1.3V limit waveform (3) similar elemental surface profiles are associated with PGA-CFMs and *in vivo*-CFMs. Deciphering the mechanisms of PGA deposition on CFMs is critical for understanding the electrochemical underpinnings of the *in vivo* signals. One approach to investigating deposition mechanisms is to study the morphology of PGA coatings using AFM.

5.3.3 PGA formation is governed by nucleation and growth

AFM is a useful tool for studying the morphology of conductive coatings on electrodes. This technique could provide insights into how PGA is formed on electrodes *in vivo*. Using this rationale, we compared different PGA deposition paradigms to NA electropolymerization. NA is a perfluorinated and highly sulfonated conductive polymer often deposited onto carbon for biological analysis.[24,32-34] We performed the following experiments to visualize the CFM surface following various modification protocols

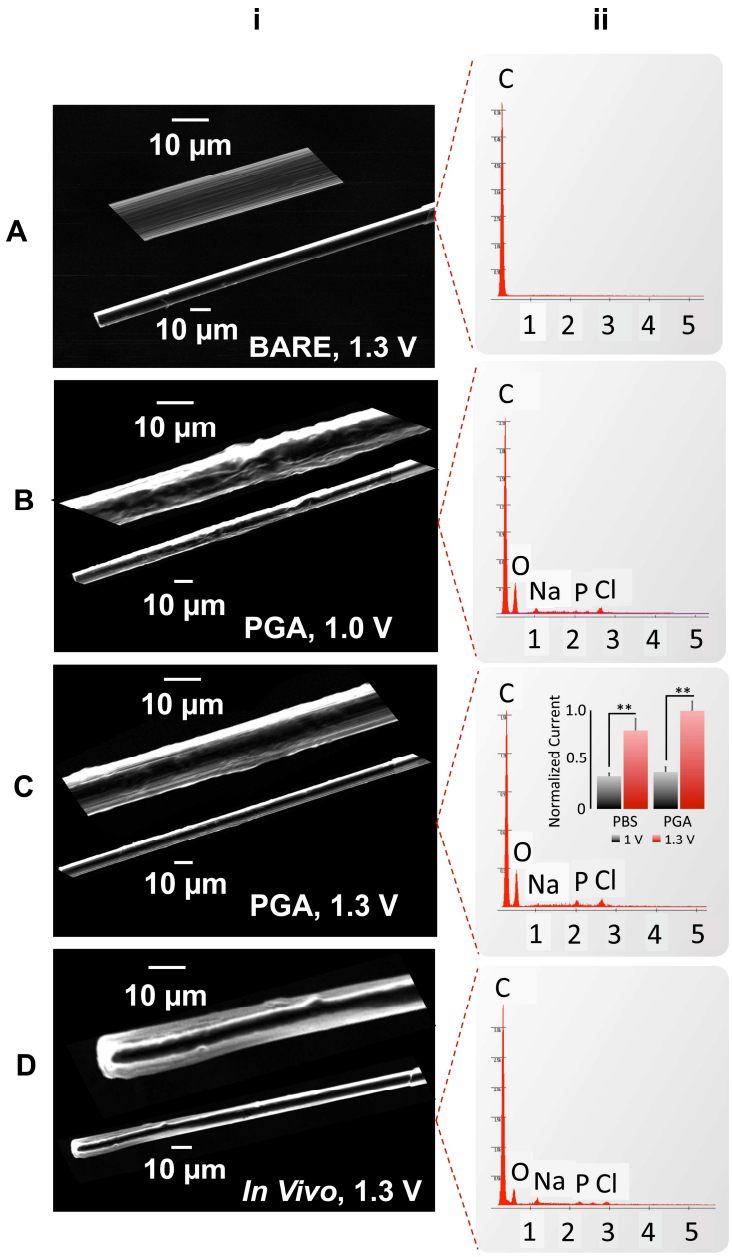

Figure 5.2. PGA coating on CFMs. SEM **(i)** images (Inset: magnified in image of CFM surface) and EDX(ii) spectra of CFMs **(A)** bare, **(B)** treated for 20 minutes (10 min 60 Hz, 10 min 10 Hz) in [10 mM] Glutamate using the triangular DA waveform (to 1.0 V) and **(C)** using the extended DA waveform (to 1.3 V), **(D)** treated in brain tissue. A histogram is inset in **(Cii)** comparing the normalized current response of CFMs to 1 µM DA, cycled at 1.0 V and 1.3 V in PBS and 1 µM Glutamate.

designed to mimic an *in vivo* experiment (background matrix and time frame of *in vivo* experiment).

A - 3 electrodes were imaged:

i) bare

ii) NA electroplated *via* holding a potential of 1.0 V for 30 s

ii) PGA deposited by applying a triangular waveform.

As previously observed with AFM, distinct striations are apparent on bare CFMs (**Figure 5.3Ai**).[70] After deposition of NA (**Figure 5.3Aii**) or PGA (**Figure 5.3Aiii**) on the CFM (glutamate at low concentrations (1uM) in contrast to EDX experiment), a) the striations are shallower and b) the surface is significantly roughened, as seen previously.[36,48,71,72] When comparing the NA coating to the PGA coating, differences in morphology are clear. NA is more uniformly deposited while PGA is deposited more sparsely with large patches of the surface devoid of polymer. Of particular interest is the feature denoted by the arrow in **Figure 5.3Aiii**. Here there appears to be heavy deposition along the vector of a single striation. This behavior implies that the deeper sections of the striations are a more favorable surface for PGA deposition. This could be because there are more ridges or imperfection sites where the polymer can nucleate and grow. Nucleation and growth, dependent on surface imperfections, are described in great detail for metals.[73-75] This finding is not surprising since radical initiated polymers are formed *via* a chain-growth type mechanism.[41,76-78]

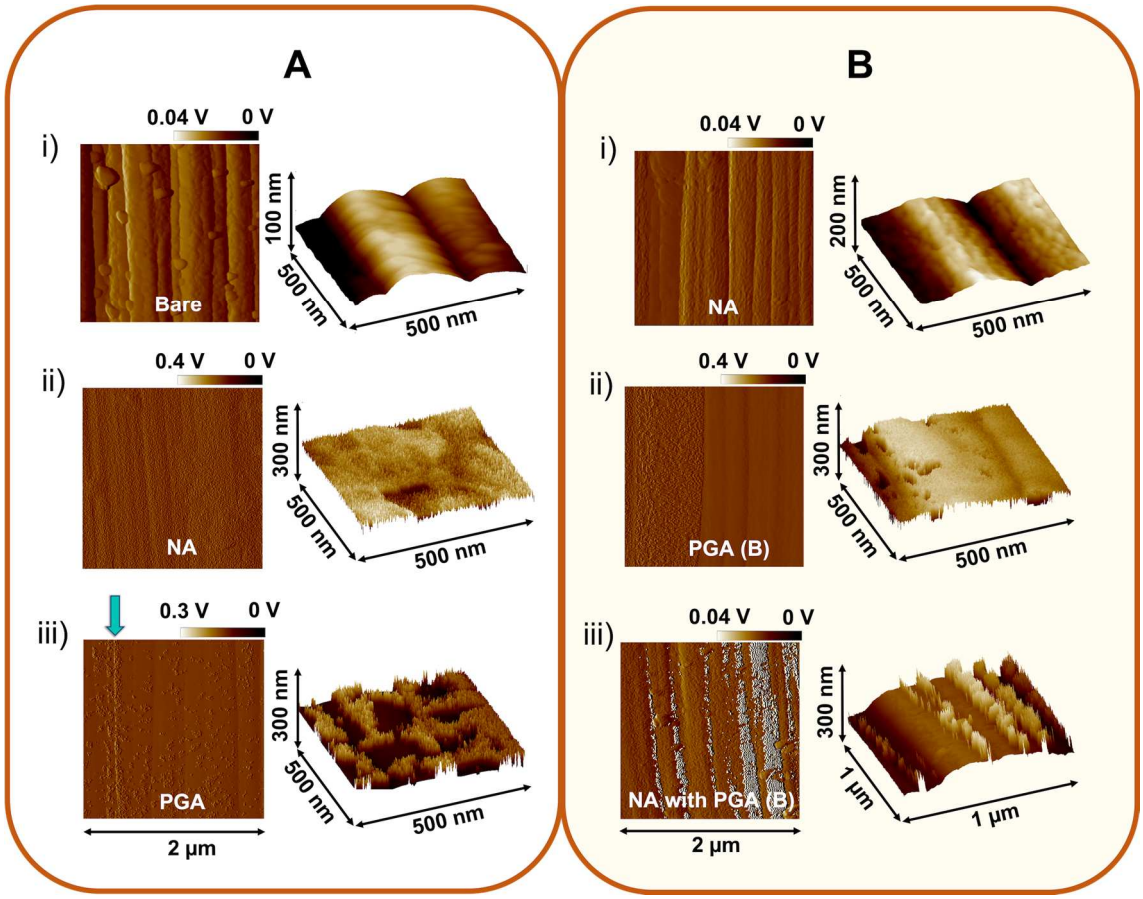

Figure 5.3. PGA Film Morphology. AFM images of CFMs modified **(A) (i)** by surface activation with extended DA waveform (cycled for 20 minutes (10 min 60 Hz, 10 min 10 Hz) in PBS), **(ii)** electroplated NA, and **(iii)** PGA coated with expanded DA waveform (cycled for 20 minutes (10 min 60 Hz, 10 min 10 Hz) in 1 µM glutamate). AFM images of CFM collected following a stability experiment (**Figure 5.1**) lasting around 2.5 hours **(B)**. CFMs are modified with **(i)** Electroplated NA, **(ii)** PGA deposited over the course of the experiment *via* 1 µM glutamate added to the background buffer, and **(iii)** NA with 1 µM glutamate added the background buffer.

B - 4 electrodes were imaged after 2.5 hr analysis time (a time period mimicking an *in vivo* experiment).;

i) NA

ii) NA and PGA co-deposited with glutamate added to the background buffer

iii) PGA with glutamate in the background buffer

NA coated electrodes are commonly employed for *in vivo* analysis, and it has been thought that the NA coating enhances the signal and the stability of the CFM over the time period of an *in vivo* experiment. While this may be the case when lower potential limits are applied (for example, 1.0V positive potential limit of the 'Jackson' waveform utilized for serotonin analysis), it does not hold for 1.3 V. It is seen that in **Figure 5.3Bi**, the rich surface roughness of the NA coating is substantially diminished in comparison to the freshly electroplated NA/CFM in **Figure 5.3Aii**. This shows that the NA coating is not stable after 2.5 hrs of analysis, likely because at 1.3 V the underlying carbon is etched away and *via* this process, a large portion of NA is removed. Given this information, it is interesting that NA-CFMs are still effective for *in vivo* experiments over several hours. This phenomenon suggests that another factor is facilitating *in vivo* stability. To test this, a bare CFM was treated for 2.5 hrs in a buffer with 1 μM glutamic acid (similar concentration to extracellular *in vivo* glutamate levels, **Figure 5.3Bii**) and, a NA coated CFM was treated for 2.5 hrs in the presence of glutamate (**Figure 5.3Biii**). It appears that PGA coated electrodes in **Figure 5.3Aii** and **5.3Bii** both exhibit similar PGA surface features. From this data, we suggest that PGA, and not NA is the more abundant polymer on an electrode performing *in vivo* analysis. We are not able to gather meaningful AFM images of *in vivo* electrodes since the surface is highly contaminated with tissue and salts.

AFM has previously been utilized to image the morphology of PGA on glassy carbon and reduced graphene oxide with similar surface features.[36,48] In these studies deposition *via* conventional cyclic voltammetry produced a homogeneous coating (unlike our non-uniform coatings) with small pores that allowed migration of analytes through the film.[36,48] We believe the different PGA morphology observed in these studies

compared to ours is due to differences in scan rate, with slower scan rates permitting significantly more time for deposition. We conclude from this data that 1) PGA deposition on carbon is initiated by a 'nucleation'-like mechanism and polymerizes *via* a chain-growth reaction, 2) the application of a high potential limit allows PGA to deposit quickly and non-uniformly and 3) the NA surface film is detrimentally affected by the waveform, where the majority of the surface roughness observed in **Figure 5.3Aii** and is lost in **Figure 5.3Biii**.

Electrochemical grafting of amines to carbon surfaces has previously been studied.[40] The reaction mechanism involves the electrooxidation of the amine group, resulting in a radical cation. From this irreversible process, the carbon electrode surface and amine group are covalently bound, and the structure of the starting material is maintained.[39] Additionally, offering a potential not only drives bond formation between aliphatic amine groups and carbon,[40,79] but also facilitates polymerization of small amine-containing molecules such as amino acids.[39] Several aromatic and aliphatic amino acids are capable of electropolymerization, including aniline,[80,81] histidine,[82-86] threonine,[87] arginine,[88] serine,[88] glutamine,[88] lysine,[89] aspartic acid,[90] and glutamic acid. PGA electropolymerization was first reported by Yu and Chen in 1997, where PGA was immobilized onto a glassy carbon electrode to detect hydrazine, a chemical found in fuel with toxic health effects.[38] Yu's method, and other derivative methods, have since been employed to coat PGA for electroanalytical detection of amoxicillin,[59] alpha-synuclein (a protein involved in Parkinson's Disease-related dementia),[66] DA,[47] ascorbic acid,[58,62] norepinephrine,[62] tryptophan,[49] glucose,[60] gallic acid,[48] and uric acid.[58,62] All previous accounts of PGA electropolymerization were accomplished using conventional cyclic

voltammetry, applying a potential range of -0.8 V to 2.0 V at a scan rate of 100 mV/s. The application of a sufficiently positive potential limit results in a signal peak observed around +1.5 V,[38] serving as electrochemical evidence of the formation of a radical cation that initiates free radical polymerization. Though the high potential (+1.5 V) required to initiate this reaction previously is not within the potential window of FSCV waveforms, we hypothesized that adsorption of glutamate to CFMs creates enough thermodynamic favorability to initiate PGA formation with FSCV. On a second scan, a propagation peak is observed at 1.25 V and increases with each subsequent cycle indicative of growth. Taken together the evidence of covalent grafting and polymer growth, we have constructed Scheme 1, depicting the mechanism of C-N bond formation, electropolymerization and structure of PGA.

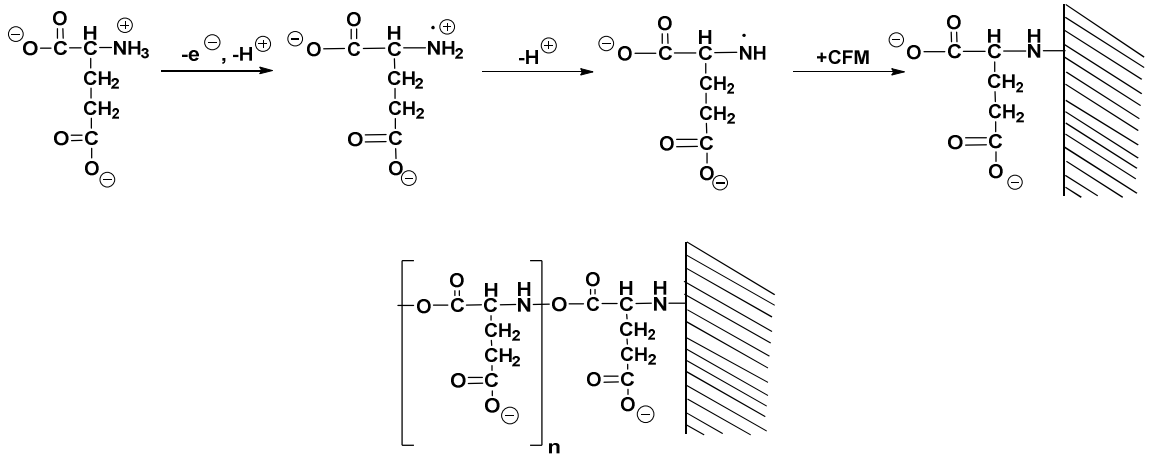

Scheme 1. PGA Electropolymerization Mechanism.

5.3.4 Analytical Response is improved with PGA

In **Figure 5.1** we found that with FSCAV the electrodes were more sensitive after *in vivo* exposure and hypothesized that the PGA film facilitates this increase in

sensitivity. The structure of PGA, with an overall negative charge, provides more support since this negatively charged polymer could enhance preconcentration of cations, such as DA. Here we test whether this phenomenon holds for FSCV analysis by comparing various combinations of CFM modifications towards DA analysis with FIA (representative color plot and CV of 1 μM DA in PBS buffer are shown in **Figure 5.4A**). In **Figure 5.4B**, a histogram evaluates the maximum electrode response by averaging the response of 5 injections of 1 μM DA on 4 electrodes each of:

1) Bare

2) PGA pretreatment with glutamate in background buffer

3) *in vivo* pretreatment

4) *in vivo* pretreatment with glutamate in background buffer.

All modifications facilitate increases in current compared to the bare CFM. A significant increase in sensitivity was observed after *in vivo* exposure (29.2 %, $p = 0.02$), were the CFMs were placed in the cortex of a rodent brain for 20 minutes and DA was immediately measured. Furthermore, when 1 μM glutamic acid is added to the background buffer for an *in vitro* experiment (denoted in **Figure 5.4** with a (B)), an increase in current response to PGA is recorded (16 %, p = ns) with respect to bare. Additionally, a significant increase in *in vivo* CFMs (38 %, $p = 4 \times 10^{-5}$) is observed when 1 μM glutamate is added to the background buffer.

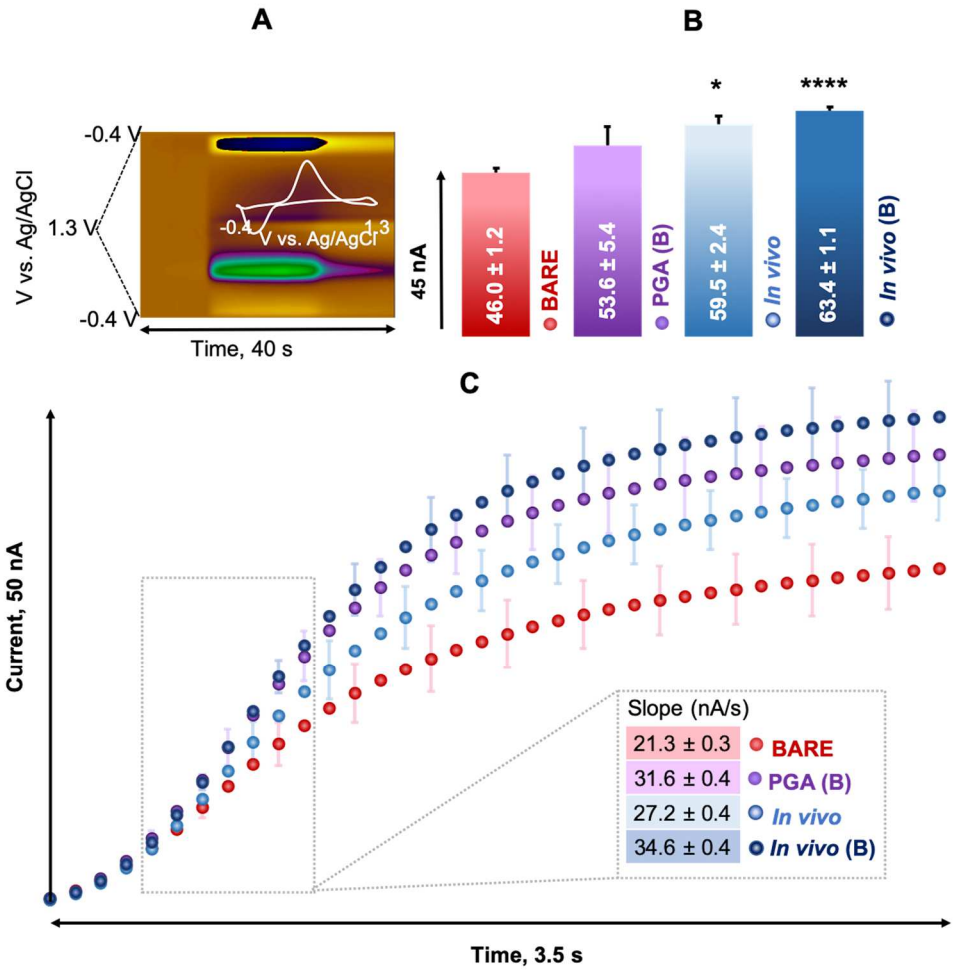

Figure 5.4. Sensitivity and Kinetic Response of modified CFMs. (A) Representative color plot and cyclic voltammogram (inset) of a 1 µM DA injection with FIA. **(B)** Histogram of FIA response to 1 µM DA on 5 different pretreated CFMS: Bare, PGA (glutamate in background buffer at 1 µM), *in vivo* pretreatment, and *in vivo* pretreatment with glutamate in buffer for analysis. (* $p>0.05$, **** $p>0.001$). **(C)** FIA rise curves of the first 3.5 s of a 1 µM DA injection on 4 different CFMs: Bare, PGA (glutamate in background buffer at 1 µM), *in vivo* pretreatment, and *in vivo* pretreatment with glutamate in buffer for analysis. Every third error bar is displayed. The slope of the linear portion of the curve is inset (0.4 - 1 s, $R^2 > 0.99$).

Thus far, we have demonstrated that glutamate polymerizes on CFMs and that the PGA film facilitates responses to DA both *in vitro* and *in vivo*. One concern with FSCV measurements at modified CFMs is whether the films on CFMs create a diffusional barrier that might induce kinetic limitations in the response.[24] We tested whether any of

the modifications slowed down the FSCV response time via FIA in **Figure 5.4C**. The time axis depicts the first 3.5 seconds of the response of the various different modified electrodes. In contrast to the expectation that the presence of polymeric films slow the response time, we found by estimating the slope of the linear portion of the rise curve that all modifications improved the speed of response (*in vivo* - 28.6%, PGA(B) - 49.3%, *in vivo*(B) - 63.4 %) with respect to bare.

PGA is composed of small glutamate units and likely does not sterically hinder DA's adsorption. In fact, the overall negative charge, with partial positive and negative regions throughout the structure seems to be promoting DA's electrostatic access within the PGA coating.

5.4 CONCLUSION

Carbon has served as a vital material for electroanalysis due to its favorable electron transfer properties and ease of fabrication. In particular, carbon probes are extremely beneficial for studying biological systems because they are biocompatible. Like other electrode materials, carbon is subject to surface fouling caused by electropolymerization of biological molecules. It is generally accepted that biofouling leads to decreased sensitivity, however in this work, we found *via* a pre- and post-calibration that exposure to brain tissue in mice increased the electrode response to dopamine. We hypothesized that the ubiquitous neurotransmitter, glutamate, was the cause of this outcome, because glutamate electropolymerization with conventional voltammetry is well documented and results in a cation exchange polymer (polyglutamic acid, PGA) coating on the electrode surface.

Here, we utilized a multifaceted approach to provide voltammetric, microscopic, and spectroscopic evidence of PGA formation on carbon electrodes and analytically compared PGA electrodes to electrodes that have been exposed to the *in vivo* environment. Voltammetry revealed a PGA deposition peak, indicative of growth. SEM visualized the PGA coating and EDX uncovered similar elemental profiles between PGA electrodes and *in vivo* electrodes. Additionally, AFM was used to further characterize PGA morphology, revealing a non-uniform coating indicative of a nucleation and growth type mechanism of polymer deposition. Finally, both PGA electrodes and electrodes that have been exposed to brain tissue demonstrate similar improved kinetic response time with FIA, and improved sensitivity of 1 μM DA with respect to an untreated electrode. From these results, we conclude that ambient glutamate polymerizing on electrodes *in vivo* boosts electroanalytical sensitivity and kinetic response time. Furthermore, the partial positive and negative regions throughout the PGA structure and overall negative charge offers favorable analytical performance for DA measurements.

5.5 REFERENCES

(1) Hersey, M.; Berger, S. N.; Holmes, J.; West, A.; Hashemi, P. Recent Developments in Carbon Sensors for At-Source Electroanalysis. *Anal Chem* **2019,** *91* (1), 27.

(2) Liu, Y. L.; Liu, R.; Qin, Y.; Qiu, Q. F.; Chen, Z.; Cheng, S. B.; Huang, W. H. Flexible Electrochemical Urea Sensor Based on Surface Molecularly Imprinted Nanotubes for Detection of Human Sweat. *Analytical Chemistry* **2018,** *90* (21), 13081.

(3) Gao, W.; Emaminejad, S.; Nyein, H. Y. Y.; Challa, S.; Chen, K. V.; Peck, A.; Fahad, H. M.; Ota, H.; Shiraki, H.; Kiriya, D.et al. Fully integrated wearable sensor arrays for multiplexed in situ perspiration analysis. *Nature* **2016,** *529* (7587), 509.

(4) Wang, L.; Wang, L. Y.; Zhang, Y.; Pan, J.; Li, S. Y.; Sun, X. M.; Zhang, B.; Peng, H. S. Weaving Sensing Fibers into Electrochemical Fabric for Real-Time Health Monitoring. *Adv Funct Mater* **2018,** *28* (42).

(5) Park, J.; Kim, J.; Kim, S. Y.; Cheong, W. H.; Jang, J.; Park, Y. G.; Na, K.; Kim, Y. T.; Heo, J. H.; Lee, C. Y.et al. Soft, smart contact lenses with integrations of wireless circuits, glucose sensors, and displays. *Sci Adv* **2018,** *4* (1), eaap9841.

(6) Kim, J.; Kim, M.; Lee, M. S.; Kim, K.; Ji, S.; Kim, Y. T.; Park, J.; Na, K.; Bae, K. H.; Kyun Kim, H.et al. Wearable smart sensor systems integrated on soft contact lenses for wireless ocular diagnostics. *Nat Commun* **2017,** *8*, 14997.

(7) Reid, R. C.; Jones, S. R.; Hickey, D. P.; Minteer, S. D.; Gale, B. K. Modeling Carbon Nanotube Connectivity and Surface Activity in a Contact Lens Biofuel Cell. *Electrochim Acta* **2016,** *203*, 30.

(8) Levent, A.; Altun, A.; Yardim, Y.; Senturk, Z. Sensitive voltammetric determination of testosterone in pharmaceuticals and human urine using a glassy carbon electrode in the presence of cationic surfactant. *Electrochim Acta* **2014,** *128*, 54.

(9) Degefu, H.; Amare, M.; Tessema, M.; Admassie, S. Lignin modified glassy carbon electrode for the electrochemical determination of histamine in human urine and wine samples. *Electrochim Acta* **2014,** *121*, 307.

(10) Martin, A.; Batalla, P.; Hernandez-Ferrer, J.; Martinez, M. T.; Escarpa, A. Graphene oxide nanoribbon-based sensors for the simultaneous bio-electrochemical enantiomeric resolution and analysis of amino acid biomarkers. *Biosens Bioelectron* **2015,** *68*, 163.

(11) Gholizadeh, A.; Voiry, D.; Weisel, C.; Gow, A.; Laumbach, R.; Kipen, H.; Chhowalla, M.; Javanmard, M. Toward point-of-care management of chronic respiratory conditions: Electrochemical sensing of nitrite content in exhaled breath condensate using reduced graphene oxide. *Microsyst Nanoeng* **2017,** *3*.

(12) Ma, Y.; Shen, X. L.; Zeng, Q.; Wang, H. S.; Wang, L. S. A multi-walled carbon nanotubes based molecularly imprinted polymers electrochemical sensor for the sensitive determination of HIV-p24. *Talanta* **2017,** *164*, 121.

(13) Ferraz, B. R. L.; Guimaraes, T.; Profeti, D.; Profeti, L. P. R. Electrooxidation of sulfanilamide and its voltammetric determination in pharmaceutical formulation, human urine and serum on glassy carbon electrode. *J Pharm Anal* **2018,** *8* (1), 55.

(14) Patel, N.; Fagan-Murphy, A.; Covill, D.; Patel, B. A. 3D Printed Molds Encompassing Carbon Composite Electrodes To Conduct Multisite Monitoring in the Entire Colon. *Anal Chem* **2017,** *89* (21), 11690.

(15) MacEachern, S. J.; Keenan, C. M.; Papakonstantinou, E.; Sharkey, K. A.; Patel, B. A. Alterations in melatonin and 5-HT signalling in the colonic mucosa of mice with dextran-sodium sulfate-induced colitis. *Br J Pharmacol* **2018,** *175* (9), 1535.

(16) Hensley, A. L.; Colley, A. R.; Ross, A. E. Real-Time Detection of Melatonin Using Fast-Scan Cyclic Voltammetry. *Anal Chem* **2018,** *90* (14), 8642.

(17) Lu, Y.; Lyu, H.; Richardson, A. G.; Lucas, T. H.; Kuzum, D. Flexible Neural Electrode Array Based-on Porous Graphene for Cortical Microstimulation and Sensing. *Sci Rep* **2016,** *6*, 33526.

(18) Vitale, F.; Summerson, S. R.; Aazhang, B.; Kemere, C.; Pasquali, M. Neural stimulation and recording with bidirectional, soft carbon nanotube fiber microelectrodes. *ACS Nano* **2015,** *9* (4), 4465.

(19) Wisniewski, N.; Moussy, F.; Reichert, W. M. Characterization of implantable biosensor membrane biofouling. *Fresenius J Anal Chem* **2000,** *366* (6-7), 611.

(20) Wisniewski, N.; Reichert, M. Methods for reducing biosensor membrane biofouling. *Colloids Surf B Biointerfaces* **2000,** *18* (3-4), 197.

(21) Jackson, B. P.; Dietz, S. M.; Wightman, R. M. Fast-scan cyclic voltammetry of 5-hydroxytryptamine. *Anal Chem* **1995,** *67* (6), 1115.

(22) Wrona, M. Z.; Dryhurst, G. Electrochemical Oxidation of 5-Hydroxytryptamine in Aqueous-Solution at Physiological Ph. *Bioorg Chem* **1990,** *18* (3), 291.

(23) Wrona, M. Z.; Dryhurst, G. Oxidation Chemistry of 5-Hydroxytryptamine .1. Mechanism and Products Formed at Micromolar Concentrations. *J Org Chem* **1987,** *52* (13), 2817.

(24) Hashemi, P.; Dankoski, E. C.; Petrovic, J.; Keithley, R. B.; Wightman, R. M. Voltammetric detection of 5-hydroxytryptamine release in the rat brain. *Anal Chem* **2009,** *81* (22), 9462.

(25) Patel, A. N.; McKelvey, K.; Unwin, P. R. Nanoscale Electrochemical Patterning Reveals the Active Sites for Catechol Oxidation at Graphite Surfaces. *J Am Chem Soc* **2012,** *134* (50), 20246.

(26) Berkes, B. B.; Bandarenka, A. S.; Inzelt, G. Electropolymerization: Further Insight into the Formation of Conducting Polyindole Thin Films. *J Phys Chem C* **2015,** *119* (4), 1996.

(27) Takmakov, P.; Zachek, M. K.; Keithley, R. B.; Walsh, P. L.; Donley, C.; McCarty, G. S.; Wightman, R. M. Carbon Microelectrodes with a Renewable Surface. *Analytical Chemistry* **2010,** *82* (5), 2020.

(28) Heien, M. L. A. V.; Phillips, P. E. M.; Stuber, G. D.; Seipel, A. T.; Wightman, R. M. Overoxidation of carbon-fiber microelectrodes enhances dopamine adsorption and increases sensitivity. *Analyst* **2003,** *128* (12), 1413.

(29) Trouillon, R.; O'Hare, D. Comparison of glassy carbon and boron doped diamond electrodes: Resistance to biofouling. *Electrochim Acta* **2010,** *55* (22), 6586.

(30) Einaga, Y. Diamond electrodes for electrochemical analysis. *J Appl Electrochem* **2010,** *40* (10), 1807.

(31) Wang, J.; Chen, G.; Chatrathi, M. P.; Fujishima, A.; Tryk, D. A.; Shin, D. Microchip capillary electrophoresis coupled with a boron-doped diamond electrode-based electrochemical detector. *Analytical Chemistry* **2003,** *75* (4), 935.

(32) Qi, L. J.; Thomas, E.; White, S. H.; Smith, S. K.; Lee, C. A.; Wilson, L. R.; Sombers, L. A. Unmasking the Effects of L-DOPA on Rapid Dopamine Signaling with an Improved Approach for Nafion Coating Carbon-Fiber Microelectrodes. *Analytical Chemistry* **2016,** *88* (16), 8129.

(33) Vreeland, R. F.; Atcherley, C. W.; Russell, W. S.; Xie, J. Y.; Lu, D.; Laude, N. D.; Porreca, F.; Heien, M. L. Biocompatible PEDOT:Nafion composite electrode

coatings for selective detection of neurotransmitters in vivo. *Analytical chemistry* **2015,** *87* (5), 2600.

(34) Ross, A. E.; Venton, B. J. Nafion-CNT coated carbon-fiber microelectrodes for enhanced detection of adenosine. *Analyst* **2012,** *137* (13), 3045.

(35) Moussawi, K.; Riegel, A.; Nair, S.; Kalivas, P. W. Extracellular glutamate: functional compartments operate in different concentration ranges. *Front Syst Neurosci* **2011,** *5*, 94.

(36) Santos, D. P.; Zanoni, M. V. B.; Bergamini, M. F.; Chiorcea-Paquim, A. M.; Diculescu, V. C.; Brett, A. M. O. Poly(glutamic acid) nanofibre modified glassy carbon electrode: Characterization by atomic force microscopy, voltammetry and electrochemical impedance. *Electrochim Acta* **2008,** *53* (11), 3991.

(37) Wang, L. L.; Chen, J. T.; Wang, L. F.; Wu, S.; Zhang, G. Z.; Yu, H. Q.; Ye, X. D.; Shi, Q. S. Conformations and molecular interactions of poly-gamma-glutamic acid as a soluble microbial product in aqueous solutions. *Sci Rep-Uk* **2017,** *7*.

(38) Yu, A. M.; Chen, H. Y. Electrocatalytic oxidation of hydrazine at the poly(glutamic acid) chemically modified electrode and its amperometric determination. *Anal Lett* **1997,** *30* (3), 599.

(39) Adenier, A.; Chehimi, M. M.; Gallardo, I.; Pinson, J.; Vila, N. Electrochemical oxidation of aliphatic amines and their attachment to carbon and metal surfaces. *Langmuir* **2004,** *20* (19), 8243.

(40) Barbier, B.; Pinson, J.; Desarmot, G.; Sanchez, M. Electrochemical Bonding of Amines to Carbon-Fiber Surfaces toward Improved Carbon-Epoxy Composites. *J Electrochem Soc* **1990,** *137* (6), 1757.

(41) Qiu, Y. J.; Reynolds, J. R. Electrochemically Initiated Chain Polymerization of Pyrrole in Aqueous-Media. *J Polym Sci Pol Chem* **1992,** *30* (7), 1315.

(42) Singh, M. N.; Yadav, H. K. S.; Ram, M.; Shivakumar, H. G. Freeze Dried Chitosan/Poly-(Glutamic Acid) Microparticles for Intestinal Delivery of Lansoprazole. *Curr Drug Deliv* **2012,** *9* (1), 95.

(43) Huang, W. J.; Zhang, T. H.; Shi, P. Z.; Yang, D. J.; Luo, S.; Voit, B.; Appelhans, D.; Zan, X. J.; Chen, H. The construction and effect of physical properties on intracellular drug delivery of poly(amino acid) capsules. *Colloid Surface B* **2019,** *177*, 178.

(44) Tsao, C. T.; Chang, C. H.; Lin, Y. Y.; Wu, M. F.; Wang, J. L.; Han, J. L.; Hsieh, K. H. Antibacterial activity and biocompatibility of a chitosan-gamma-poly(glutamic acid) polyelectrolyte complex hydrogel. *Carbohydr Res* **2010,** *345* (12), 1774.

(45) Hsieh, C. Y.; Tsai, S. P.; Wang, D. M.; Chang, Y. N.; Hsieh, H. J. Preparation of gamma-PGA/chitosan composite tissue engineering matrices. *Biomaterials* **2005,** *26* (28), 5617.

(46) Kuo, Y.-C.; Ku, H.-F.; Rajesh, R. Chitosan/γ-poly(glutamic acid) scaffolds with surface-modified albumin, elastin and poly-l-lysine for cartilage tissue engineering. *Materials Science and Engineering: C* **2017,** *78*, 265.

(47) Bui, M. P. N.; Li, C. A.; Seong, G. H. Electrochemical detection of dopamine with poly-glutamic acid patterned carbon nanotube electrodes. *Biochip J* **2012,** *6* (2), 149.

(48) Feminus, J. J.; Manikandan, R.; Narayanan, S. S.; Deepa, P. N. Determination of gallic acid using poly(glutamic acid): graphene modified electrode. *J Chem Sci* **2019,** *131* (2).

(49) Liu, X.; Luo, L. Q.; Ding, Y. P.; Ye, D. X. Poly-glutamic acid modified carbon nanotube-doped carbon paste electrode for sensitive detection of L-tryptophan. *Bioelectrochemistry* **2011,** *82* (1), 38.

(50) Harreither, W.; Trouillon, R.; Poulin, P.; Neri, W.; Ewing, A. G.; Safina, G. Carbon Nanotube Fiber Microelectrodes Show a Higher Resistance to Dopamine Fouling. *Analytical Chemistry* **2013,** *85* (15), 7447.

(51) Venton, B. J.; Troyer, K. P.; Wightman, R. M. Response times of carbon fiber microelectrodes to dynamic changes in catecholamine concentration. *Analytical Chemistry* **2002,** *74* (3), 539.

(52) Engstrom, R. C.; Wightman, R. M.; Kristensen, E. W. Diffusional Distortion in the Monitoring of Dynamic Events. *Analytical Chemistry* **1988,** *60* (7), 652.

(53) Kile, B. M.; Walsh, P. L.; McElligott, Z. A.; Bucher, E. S.; Guillot, T. S.; Salahpour, A.; Caron, M. G.; Wightman, R. M. Optimizing the Temporal Resolution of Fast-Scan Cyclic Voltammetry. *Acs Chemical Neuroscience* **2012,** *3* (4), 285.

(54) Logman, M. J.; Budygin, E. A.; Gainetdinov, R. R.; Wightman, R. M. Quantitation of in vivo measurements with carbon fiber microelectrodes. *J Neurosci Meth* **2000,** *95* (2), 95.

(55) Ewing, A. G.; Wightman, R. M.; Dayton, M. A. In vivo voltammetry with electrodes that discriminate between dopamine and ascorbate. *Brain Res* **1982,** *249* (2), 361.

(56) Roberts, J. G.; Toups, J. V.; Eyualem, E.; McCarty, G. S.; Sombers, L. A. In Situ Electrode Calibration Strategy for Voltammetric Measurements In Vivo. *Analytical Chemistry* **2013,** *85* (23), 11568.

(57) Ewing, A. G.; Dayton, M. A.; Wightman, R. M. Pulse Voltammetry with Microvoltammetric Electrodes. *Analytical Chemistry* **1981,** *53* (12), 1842.

(58) Zhang, L.; Lin, X. Q. Covalent modification of glassy carbon electrode with glutamic acid for simultaneous determination of uric acid and ascorbic acid. *Analyst* **2001,** *126* (3), 367.

(59) Santos, D. P.; Bergamini, M. F.; Zanoni, M. V. B. Voltammetric sensor for amoxicillin determination in human urine using polyglutamic acid/glutaraldehyde film. *Sensor Actuat B-Chem* **2008,** *133* (2), 398.

(60) Zhou, X. C.; Zheng, X. Y.; Lv, R. X.; Kong, D. X.; Li, Q. L. Electrodeposition of platinum on poly(glutamic acid) modified glassy carbon electrode for non-enzymatic amperometric glucose detection. *Electrochim Acta* **2013,** *107*, 164.

(61) Gonzalez-Vargas, C.; Garcia, C.; Celis, F.; Salazar, R. Differential Pulse Voltammetry Determination of Anti-Hypertensive Drug Hydrochlorothiazide in Pharmaceuticals Using Glassy-Carbon Electrode Modified by Electropolymerization with L- and D-Glutamic Acids. *Int J Electrochem Sc* **2018,** *13* (2), 1905.

(62) Ganesh, P. S.; Swamy, B. E. K. Simultaneous electroanalysis of norepinephrine, ascorbic acid and uric acid using poly(glutamic acid) modified carbon paste electrode. *J Electroanal Chem* **2015,** *752*, 17.

(63) Deng, K. Q.; Liu, X. Y.; Li, C. X.; Hou, Z. H.; Huang, H. W. A comparative study of different Fe3O4-functionalized carbon-based nanomaterials for the development of electrochemical sensors for bisphenol A. *Analytical Methods* **2017,** *9* (37), 5509.

(64) Wang, W. S.; Li, S.; Zhang, G. N.; He, J. X.; Ma, Z. Q. Electrochemical Immunoassay for Breast Cancer Markers CA153 Determination Based on Carbon Nanotubes modified Electrode. *Int J Electrochem Sc* **2017,** *12* (11), 10791.

(65) Raj, M.; Goyal, R. N. A poly-(melamine)/poly-(glutamic acid) based electrochemical sensor for sensitive determination of 2-Thioxanthine. *Sensor Actuat B-Chem* **2017,** *250*, 552.

(66) Karaboga, M. N. S.; Sezginturk, M. K. Cerebrospinal fluid levels of alpha-synuclein measured using a poly-glutamic acid-modified gold nanoparticle-doped disposable neuro-biosensor system. *Analyst* **2019,** *144* (2), 611.

(67) Wang, Y. J.; Jamal, R.; Wang, M. C.; Yang, L.; Liu, F. F.; Abdiryim, T. A donor-acceptor-donor-type conjugated polymer-modified TiO2 with enhanced photocatalytic activity under simulated sunlight and natural sunlight. *J Mater Sci* **2017,** *52* (9), 4820.

(68) Ding, S.; Ali, A.; Jamal, R.; Xiang, L.; Zhong, Z. P.; Abdiryim, T. An Electrochemical Sensor of Poly(EDOT-pyridine-EDOT)/Graphitic Carbon Nitride

Composite for Simultaneous Detection of Cd2+ and Pb2+. *Materials* **2018,** *11* (5).

(69) Shepherd, R. K.; Murray, M. T.; Houghton, M. E.; Clark, G. M. Scanning Electron-Microscopy of Chronically Stimulated Platinum Intracochlear Electrodes. *Biomaterials* **1985,** *6* (4), 237.

(70) Pathirathna, P.; Samaranayake, S.; Atcherley, C. W.; Parent, K. L.; Heien, M. L.; McElmurry, S. P.; Hashemi, P. Fast voltammetry of metals at carbon-fiber microelectrodes: copper adsorption onto activated carbon aids rapid electrochemical analysis. *Analyst* **2014,** *139* (18), 4673.

(71) Hiesgen, R.; Aleksandrova, E.; Meichsner, G.; Wehl, I.; Roduner, E.; Friedrich, K. A. High-resolution imaging of ion conductivity of Nafion (R) membranes with electrochemical atomic force microscopy. *Electrochim Acta* **2009,** *55* (2), 423.

(72) Ou, L. B.; Liu, Y. N.; Wang, J. X.; Zhang, L. Enhanced Voltammetric Detection of Epinephrine at a Carbon Nanotube/Nafion Composite Electrode in the Presence of Ascorbic Acid. *J Nanosci Nanotechno* **2009,** *9* (11), 6614.

(73) Simm, A. O.; Ji, X. B.; Banks, C. E.; Hyde, M. E.; Compton, R. G. AFM studies of metal deposition: Instantaneous nucleation and the growth of cobalt nanoparticles on boron-doped diamond electrodes. *Chemphyschem* **2006,** *7* (3), 704.

(74) Hyde, M. E.; Compton, R. G. A review of the analysis of multiple nucleation with diffusion controlled growth. *J Electroanal Chem* **2003,** *549*, 1.

(75) Wildgoose, G. G.; Banks, C. E.; Compton, R. G. Metal nanoparticles and related materials supported on carbon nanotubes: methods and applications. *Small* **2006,** *2* (2), 182.

(76) Hwang, B. J.; Santhanam, R.; Lin, Y. L. Nucleation and growth mechanism of electropolymerization of polypyrrole on gold/highly oriented pyrolytic graphite electrode. *J Electrochem Soc* **2000,** *147* (6), 2252.

(77) Soto, J. P.; Diaz, F. R.; del Valle, M. A.; Velez, J. H.; East, G. A. Nucleation and growth mechanisms during electropolymerization of substituted 3-alkylthiophenes. *Appl Surf Sci* **2008,** *254* (11), 3489.

(78) Koizumi, Y.; Shida, N.; Ohira, M.; Nishiyama, H.; Tomita, I.; Inagi, S. Electropolymerization on wireless electrodes towards conducting polymer microfibre networks. *Nature Communications* **2016,** *7*.

(79) Deinhammer, R. S.; Ho, M.; Anderegg, J. W.; Porter, M. D. Electrochemical Oxidation of Amine-Containing Compounds - a Route to the Surface Modification of Glassy-Carbon Electrodes. *Langmuir* **1994,** *10* (4), 1306.

(80) Baker, C. O.; Huang, X.; Nelson, W.; Kaner, R. B. Polyaniline nanofibers: broadening applications for conducting polymers. *Chem Soc Rev* **2017,** *46* (5), 1510.

(81) Lai, J. H.; Yi, Y. C.; Zhu, P.; Shen, J.; Wu, K. S.; Zhang, L. L.; Liu, J. Polyaniline-based glucose biosensor: A review. *J Electroanal Chem* **2016,** *782*, 138.

(82) Bergamini, M. F.; Santos, D. P.; Zanoni, M. V. B. Screen-Printed Carbon Electrode Modified with Poly-L-histidine Applied to Gold(III) Determination. *J Brazil Chem Soc* **2009,** *20* (1), 100.

(83) Bergamini, M. F.; dos Santos, D. P.; Zanoni, M. V. B. Development of a voltammetric sensor for chromium(VI) determination in wastewater sample. *Sensor Actuat B-Chem* **2007,** *123* (2), 902.

(84) Bergamini, M. F.; Santos, D. P.; Zanoni, M. V. B. Determination of isoniazid in human urine using screen-printed carbon electrode modified with poly-L-histidine. *Bioelectrochemistry* **2010,** *77* (2), 133.

(85) Bergamini, M. F.; Santos, D. P.; Zanoni, M. V. B. Electrochemical behavior and voltammetric determination of pyrazinamide using a poly-histidine modified electrode. *J Electroanal Chem* **2013,** *690*, 47.

(86) Sakthivel, R.; Mutharani, B.; Chen, S. M.; Kubendhiran, S.; Chen, T. W.; Al-Hemaid, F. M. A.; Ali, M. A.; Elshikh, M. S. A Simple and Rapid Electrochemical Determination of L-Tryptophan Based on Functionalized Carbon Black/Poly-L-Histidine Nanocomposite. *J Electrochem Soc* **2018,** *165* (10), B422.

(87) Chitravathi, S.; Swamy, B. E. K.; Mamatha, G. P.; Chandrashekar, B. N. Electrocatalytic oxidation of tyrosine at poly(threonine)-film modified carbon paste electrode and its voltammetric determination in real samples. *J Mol Liq* **2012,** *172*, 130.

(88) Alhedabi, T.; Cattey, H.; Roussel, C.; Blondeau-Patissier, V.; Gharbi, T.; Herlem, G. Experimental and theoretical studies on electropolymerization of polar amino acids on platinum electrode. *Mater Chem Phys* **2017,** *185*, 183.

(89) Zhang, Y. H.; Lei, W.; Xu, Y. J.; Xia, X. F.; Hao, Q. L. Simultaneous Detection of Dopamine and Uric Acid Using a Poly(l-lysine)/Graphene Oxide Modified Electrode. *Nanomaterials-Basel* **2016,** *6* (10).

(90) Shadjou, N.; Alizadeh, S.; Hasanzadeh, M. Sensitive monitoring of taurine biomarker in unprocessed human plasma samples using a novel nanocomposite based on poly(aspartic acid) functionalized by graphene quantum dots. *J Mol Recognit* **2018,** *31* (12).

CHAPTER 6

ENZYME-FREE GLUTAMATE SENSING USING FAST VOLTAMMETRY AT CARBON FIBER MICROELECTRODES[5]

[5] **Holmes, J.;** Buchanan, A. M.; Witt, C. E.; Redden, B.; Wiskur, S.; Hashemi, P.: "Enzyme-free glutamate sensing using fast voltammetry on carbon fiber microelectrodes" – *In preparation* – Analytical Chemistry

6.1 ABSTRACT

Glutamate is the major excitatory neurotransmitter in the central nervous system and plays an important role in healthy brain function. However, dysfunction can result in chronic excitotoxicity and has been linked to several neurological and neurodegenerative disorders. Although glutamate is implicated, the physiological mechanism behind these disorders is still unclear. For this reason, a glutamate sensor for *in vivo* analysis would be highly beneficial for deciphering glutamate neurotransmission in healthy and diseased states. Glutamate measurement strategies are analytically limited because glutamate readily electropolymerizes when a potential is applied to available electrochemical sensors. Additionally, glutamate release events are restricted to the synaptic cleft in most brain regions, making detection challenging with electrodes that are unable to target the synapse due to size restraints. This work details a two-fold approach for direct glutamate detection *in vivo*: 1) electrochemically avert the electropolymerization and 2) target a brain region with extrasynaptic glutamate transmission events. First, we develop a novel electrochemical method using fast-scan cyclic voltammetry on carbon fiber microelectrodes to directly detect glutamate. We evaluate the nature of the voltammetric glutamate signal, identifying adsorption as the detection mechanism and calculating the adsorption coefficient ($K_{ads} = 4.84 \times 10^5$). Additionally, interferences that may mask or disrupt the glutamate signal are then analyzed and a solution towards enhancing specificity with a glutamate specific ionophore is implemented. Finally, we place a CFM into the Purkinje layer of the cerebellum, a region known to participate in volume transmission, and are able to detect a signal resembling the signature glutamate response. This work provides evidence that glutamate can be directly measured with voltammetry

and characterizes the glutamate response. In the future, we plan to covalently attach the proposed ionophore, creating a selective glutamate sensor and to pharmacologically verify the *in vivo* glutamate signal. This innovative sensing platform will be useful for better understanding the neurochemistry of glutamate and the role glutamate plays in psychiatric disorders.

6.2 INTRODUCTION

Glutamate, a major excitatory neurotransmitter, participates in nearly all circuits in the developed central nervous system (CNS). Regulation of this transmitter is essential for normal brain function, and dysfunction can result in chronic excitotoxicity.[1,2] Additionally, the glutamatergic system has been implicated in neurological disorders including Alzheimer's and Parkinson's Disease.[3-5] To better understand glutamate neurotransmission and signaling in health and disease, it is highly desirable to measure glutamate *in vivo*.

Electroanalytical and physiological challenges make glutamate a difficult analyte to directly measure. Within the electrochemical sensing community, it is generally accepted that glutamate is not electroactive.[6,7] Previous generations of glutamate sensors have relied on a chemical recognition agent, like glucose oxidase, however immobilization methods of enzymes to electrode surfaces leads electrodes to suffer from poor shelf life, stability, and catalytic efficiency.[8] We have shown that glutamate, however, does offer measurable electrochemical properties. In **Chapter 5**, we demonstrated that at high positive potentials (1.0 V), glutamate will electropolymerize onto carbon preventing electrochemical detection. To overcome these electrochemical limitations, glutamates electrochemical properties must be further explored.

Physiologically, glutamatergic transmission is contained for the most part to the synaptic cleft. Many probes traditionally employed for *in vivo* analysis are limited by size, unable to penetrate the synaptic cleft and eliciting an immune response from tissue damage.[9] In order to measure glutamate *in vivo*, an area of the brain where glutamate release is more loosely regulated must be targeted with a small probe capable of making sensitive and ultra-selective measurements. One area of promise is the Purkinje layer of the cerebellum where climbing glutaminergic fibers innervate this heavily GABAergic region. It is thought that in this region glutamate participates in volume transmission,[10,11] escaping the synapse where transmission events can be monitored in the extracellular matrix.

Fast-scan cyclic voltammetry (FSCV) has traditionally been employed on carbon fiber microelectrodes (CFMs) to measure dopamine transmission events *in vivo*, however the scope of this technique has expanded significantly in recent years to include a suite of biologically relevant analytes, including serotonin,[12,13] histamine,[14,15] and melatonin,[16] among others.[17-20] Here, we use a similar approach, introducing an enzyme-free voltammetric technique for direct glutamate detection that is suitable for *in vivo* analysis. In this work, we optimize a unique waveform for measuring glutamate while avoiding electropolymerization. Additionally, we explore the nature of the resultant electrochemical response in terms of sensitivity, selectivity, and response mechanism. Glutamate is structurally similar to other amino acids present in biological systems, which presents selectivity limitations. To overcome selectivity issues, we propose modifying the CFM surface with a covalently grafted ionophore demonstrating selective glutamate binding. Finally, we apply this method to glutamate detection *in vivo* in the

Purkinje layer of the cerebellum and find an *in vivo* response that resembles an *in vitro* glutamate signal. With this work, we showcase a novel, enzyme-free method for direct glutamate detection with great potential for assessing the glutaminergic system *in vivo*.

6.3 RESULTS AND DISCUSSION

6.3.1 Novel waveform offers detection platform for glutamate

First, we employed flow injection analysis (FIA), delivering a pulse of 1 mM glutamate to the electrode, to optimize a novel waveform for direct glutamate detection. A resting potential limit of 0.2 V was selected because higher potentials have been shown with conventional and fast voltammetry to polymerize glutamate into poly-glutamic acid (PGA). Additionally, because glutamate possesses an overall negative charge, a positive resting potential aids in electrostatically attracting glutamate towards the electrode surface. The cyclic voltammogram (CV) collected, denoted by a yellow star in **Figure 6.1**, exhibits a broad, reduction peak on the cathodic sweep and oxidation peak on the anodic sweep. The resulting color plot is represented in **Figure 6.1**. Throughout this work, we isolate and monitor the reduction peak, because it appears on the first sweep following the holding potential resulting in a higher current response. The current vs. time trace, marked with a blue star, displays favorable kinetic properties depicted by the sharp rise and decay of FIA curves. A linear calibration curve was generated with an R^2 value of 0.99 and the limit of detection (1.5 μM) was calculated. It is suggested that glutamate in the extracellular space is in the low micromolar range and the concentration estimated from FSCV of basal levels tend to be higher than those reported using other methods so we do believe that the LOD of this will be within the dynamic range.

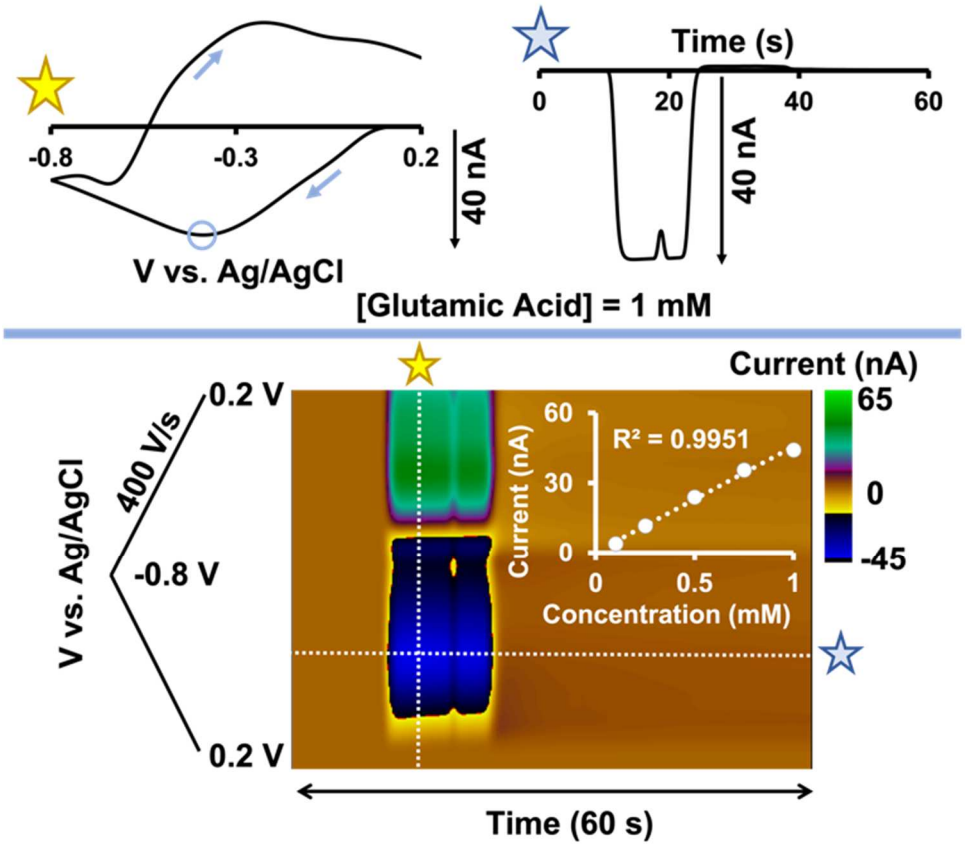

Figure 6.1. Glutamate detection with FSCV. A triangular waveform scanning from 0.2 V to -0.8 V at 400 V/s is optimized for glutamate detection. A representative color plot of 1 mM glutamate is collected *via* FIA, and the calibration curve is inset. The generated CV is denoted with a yellow star and the current vs. time trace with a blue star.

The broad redox peaks of the glutamate CV are unusual for FSCV measurements that typically possess more well defined redox peaks, like those for dopamine, serotonin and Cu(II).[12,21,22] However, histamine when measured with FSCV produces a broad oxidation similar to the types of peaks associated with glutamate.[15] Histamine's oxidation mechanism is not known, however it is postulated that this molecules redox chemistry is governed by a charge transfer process. Due to the similar nature of these peaks, we hypothesize here that glutamate's voltammetric response is also non-faradaic in nature and the result of charge transfer within the molecule. To further decipher the underlying

glutamate redox properties, we first evaluated the detection mechanism at the electrode interface. In **Figure 6.2A**, we systematically increased the scan rate and plotted the log of the scan rate vs. the log of the reduction current. The slope of this plot was found to be close to 1, signifying that the process is adsorption controlled.[23] The resultant cyclic voltammograms are inset. Both peak separation and increasing current response with increasing scan rate is observed, as expected. A plateau following the last point plotted on the log v log plot and increased peak separation at higher scan rates led to the section of 400 V/s as the optimal scan rate.

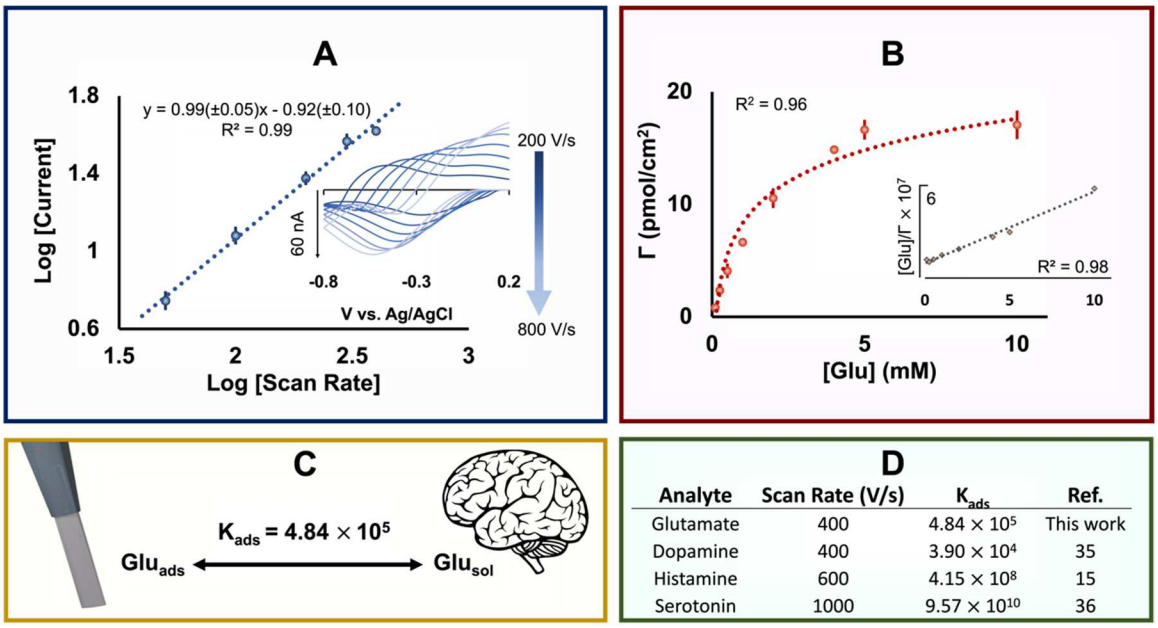

Figure 6.2 Properties of glutamate-CFM interaction. **(A)** The log of scan rate is plotted vs. the log of current, producing a slope = 0.99. Inset are the superimposed CVs of 1mM glutamate at 200 – 800 V/s. **(B)** Langmuir adsorption isotherm (dotted line) fit with raw data (points). The linearized isotherm is inset. **(C)** Schematic representation of adsorption equilibria of glutamate adsorbed to the CFM or in bulk solution. **(D)** Table reporting the K_{ads} and scan rates of several biological molecules detectable with FSCV.

The adsorptive properties of glutamate are further assessed by evaluating the thermodynamic favorability of glutamate adsorption to carbon. We previously reported adsorption isotherm profiles for several metal ions (Zn(II), Ca(II), Al(II), Mg(II), and Cu(II)) and monoamines (serotonin and histamine),[15,24,25] which all agree with a Langmuir adsorption isotherm suggesting monolayer adsorption. To test whether this adsorption mechanism holds true for glutamate, we measured the adsorbed surface concentration (Γ) in response to the glutamate concentrations in bulk solution. We fit the data with a Langmuir adsorption isotherm (**Figure 6.2B**) and found that Langmuir's theory holds true for glutamate adsorption. We used **equation (1)** and plotted the [Glu]/Γ vs. [C] (inset) to calculate the adsorption coefficient (4.84×10^5). Adsorption favorability of glutamate to carbon over bulk solution is depicted in **Figure 6.2C**. We then compared the K_{ads} value to other biologically relevant analytes that have been monitored *in vivo* with FSCV in the table in **Figure 6.2D**. In analyzing these values, a trend presents itself between the optimal scan rate of each analyte and the K_{ads}. Larger K_{ads} values indicate more efficient adsorption processes and kinetic favorability, thus driving faster optimal scan rates.

6.3.2 Glutamate waveform exhibits semi-favorable selectivity

It is important for an analytical method to exhibit selectivity towards an analyte. The large broad peaks showcased in **Figure 6.1** present challenges because other signals could overlap or mask the glutamate peak. Additionally, glutamate is an amino acid and its structure resembles several other amino acids and monoamines present in the body that may interfere with the signal. To test the selectivity of the optimized glutamate waveform, we selected several common biological molecules, neurotransmitters and ions

present in the brain that could interfere with the signal. Each interference was tested at biologically relevant concentrations and the resultant CV's are presented in **Figure 6.3**. At -0.4 V, where the glutamate reduction peak appears, there is virtually no voltammetric response from any of the interferences tested here. Many of the neurotransmitters that are not traditionally considered electroactive, such as GABA, acetylcholine, choline, and histamine offer limited background currents. The electroactive neurotransmitters (dopamine and serotonin) and ions (Mg (II) and Ca (II)) produce significant background currents but do not possess any redox properties within the potential range of the waveform. While this is promising, there were some interferences with reductive properties on the cathodic sweep of this waveform that could prove problematic. The reduction peak of Cu(II) occurs at -0.6 V and overlaps with the broad glutamate reduction peak. Additionally, several precursors and metabolites of glutamate, such as aspartic acid, L-glutathione, and alpha-ketoglutarate, produce similar reduction peaks. This is not unexpected because these molecules are structurally similar. Given just the application of this waveform on a bare CFM, it is difficult to decipher between glutamate and it's precursors or metabolites *in vivo* due to the complexity of the brain's extracellular matrix. However, because FSCV is a background subtracted, only molecules whose concentrations fluctuate over the time scale of file collection (30 seconds) would interfere. Of these, there is no literature to suggest that glutathione and alpha-ketoglutarate are present extracellularly and primarily exist intracellularly to the best of our knowledge.[26,27] There is literature to suggest however that aspartic acid can be found in the extracellularly space, is vesicularly released, and aspartate receptors are present on postsynaptic neurons.[28-30] Furthermore, D'Aniello *et al.* claim that aspartic acid acts as an

excitatory neurotransmitter,[31] while Herring *et al.* report that the concentration of aspartic acid released is too low to be physiologically relevant.[32] At this point, it is difficult to say whether aspartic acid will interfere when electrically evoking glutamate release *in vivo*. For this reason, we believe that a higher degree of specificity is essential for this method to be applied *in vivo*.

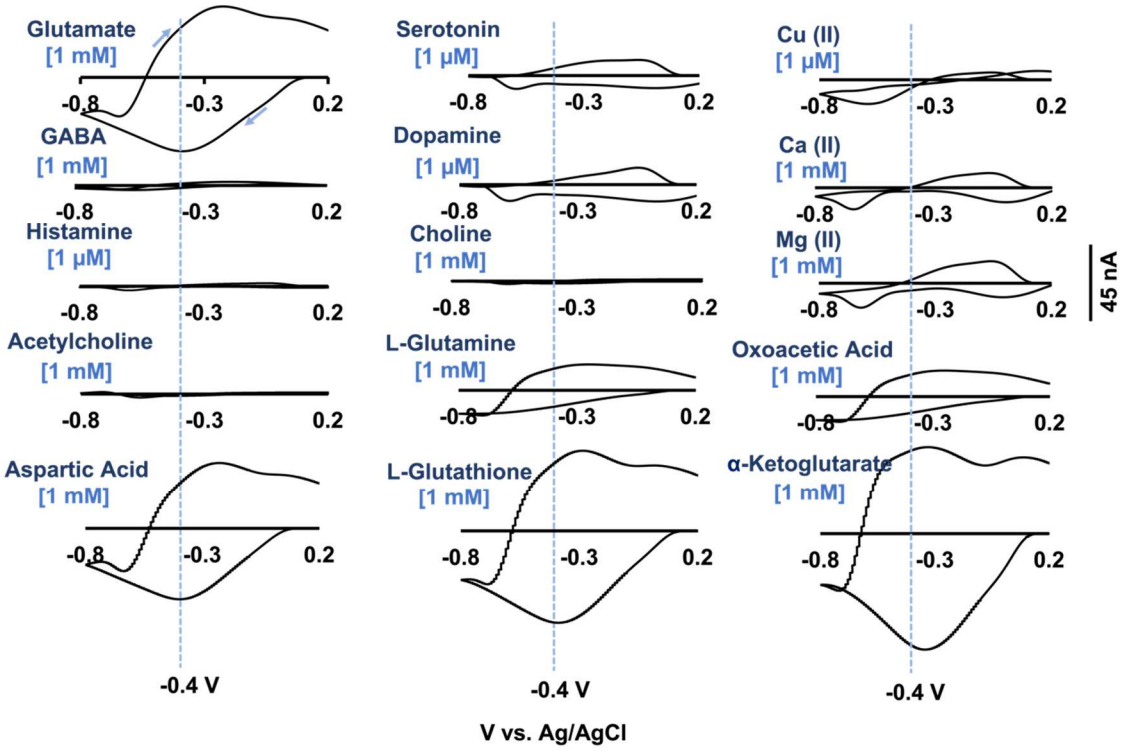

Figure 6.3 Glutamate waveform selectivity. The CVs of glutamate and 14 neurochemically relevant interferences, including neurotransmitters (serotonin, dopamine, GABA, histamine, acetylcholine, choline), ions (Cu(II), Ca(II), Mg(II)) and glutamate precursors or metabolites (L-glutamine, oxoacetic acid, aspartic acid, L-glutathione, α-ketoglutarate). Concentrations of each interference are listed, and the dashed lines denote where glutamate reduction occurs at -0.4 V.

6.3.3 Glutamate specific ionophore improves selectivity

In efforts to improve the selectivity of this method, we are exploring an approach involving surface modifications to the CFM. Previously when faced with insufficient

selectivity, we employed a modification protocol grafting an ionophore to CFMs for selective Cu(II) detection.[33] In collaboration with the Wiskur group at USC, we designed an ionophore with 2 Cu(II) metal centers that trap and bind glutamate (**Figure 4A**). To test the binding capacity of the ionophore to glutamate, we first spiked the ionophore into to a stirring solution of PBS buffer. **Figure 4B** shows 3 CVs collected. We observed a Cu(II) reduction peak at -0.75 V shown, denoted with a yellow star, originating from the Cu(II) ions within the ionophore structure. Systematically, glutamate was added to the spiking solution. Following each glutamate addition, the Cu(II)-ionophore peak decreased in amplitude due to glutamate binding. Upon the addition of 1 μM glutamate, both a glutamate peak at -0.4 V and the Cu(II)-ionophore peak at -0.75 V could be distinguished (blue star). At high glutamate concentrations, the Cu(II)-ionophore peak is indistinguishable and the glutamate peak is prominent, marked by a red star. In **Figure 6.4C**, the concentration of glutamate added was plotted against current from both the Cu(II)-ionophore peak (light blue) and the glutamate peak (dark blue). The yellow, blue, and red stars correspond to the CVs shown in **Figure 6.4B**. Inset, the ratio of the overlapping Cu(II)-ionophore and glutamate peaks are plotted against the concentration of glutamate added. With this method, we might be able to quantify lower concentrations of glutamate by using the Cu(II)-ionophore signal as an off-label. The next step for making this sensor suitable for probing biological systems is to graft this ionophore to the electrode surface. In the future, we plan to employ a similar protocol to the Cu(II) ionophore surface modification procedure described in **Chapter 3** to covalently attach the proposed glutamate ionophore to the CFM.

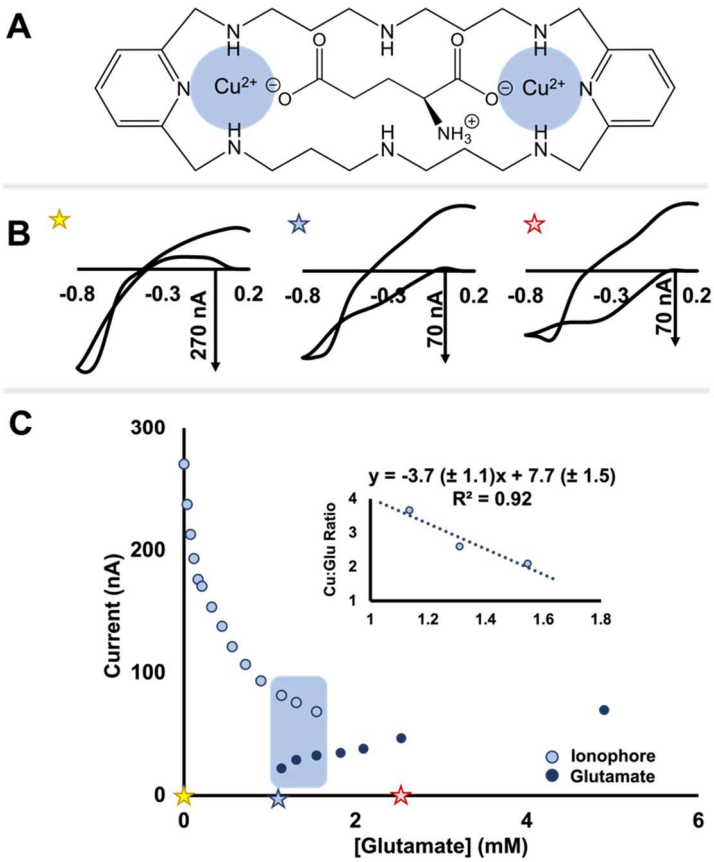

Figure 6.4 Voltammetric characterization of glutamate-ionophore binding. (A) Structure of glutamate and glutamate-specific ionophore containing two Cu(II) metal ion centers. **(B)** CVs containing Cu(II)-ionophore peaks at -0.7 V and glutamate peaks at 0.4 V. The yellow star marks the CV of only Cu(II)-ionophore, the blue star marks the CV after 1mM Glutamate has been added and both peaks are observed, and the red star marks the CV after 2.5 mM Glutamate has been added and only a glutamate peak is observed. (C) Current vs. concentration plot of systematic addition of glutamate to a stirring solution of the synthesized glutamate ionophore. The amplitude of the Cu(II)-ionophore peak is plotted in light blue and the glutamate peak is plotted in dark blue. Inset: plot of Cu: Glutamate peak ratio vs. glutamate concentration.

6.3.4 Glutamate-like signals are collected *in vivo*

In the interest of using this method to measure glutamate transmission *in vivo*, it was imperative to collect preliminary measurements in live tissue. We placed the simulating electrode in the inferior olivary nucleus (ION) and applied a low intensity stimulation for 10 s. Stimulating the ION serves to electrically evoke glutamate release at

the cell bodies of climbing glutamate-mediated fibers that innervate within the GABAergic Purkinje cell layer of the cerebellum.[34]The working electrode is then placed within the Purkinje layer. In most regions of the brain glutamate signaling is restricted to the synapse, however in the cerebellum glutamate is released from the climbing fibers of the Purkinje layer, participating in volume transmission.[10,11] **Figure 6.5** presents preliminary data using the glutamate waveform on a bare CFM collected *in vivo*, with the color plot possessing a broad reduction event.

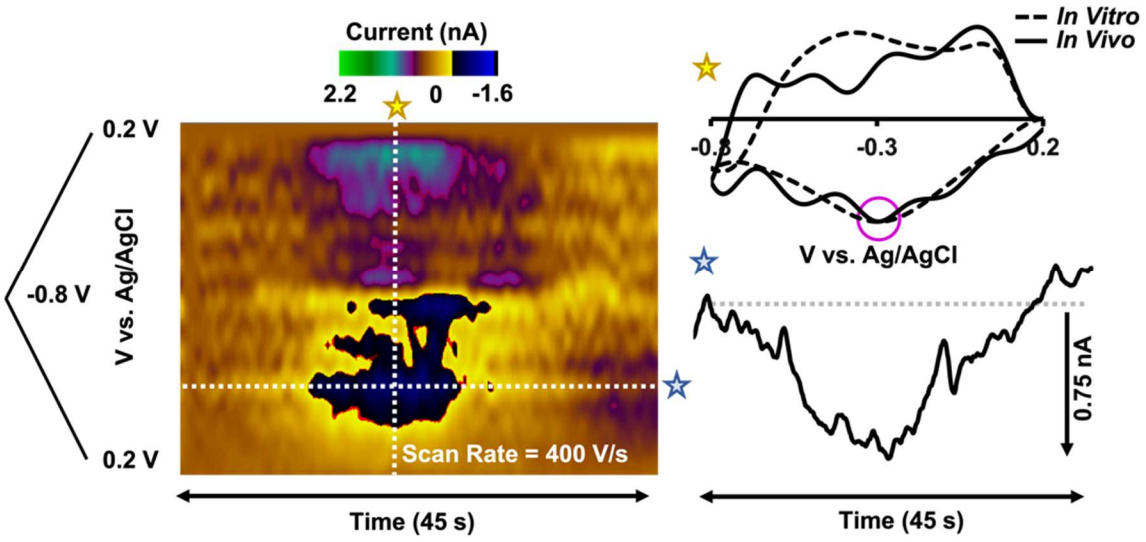

Figure 6.5 *In vivo* glutamate detection. Representative color plot, CV (yellow star), and current vs time trace (blue star) when the glutamate waveform is applied in the Purkinje layer of the cerebellum in mice. A low intensity stimulation is utilized, indicated by the stimulation bar below the color plot. The glutamate CV is superimposed on the FIA collected CV for glutamate, and the reduction peak is highlighted with a pink circle.

The CV collected *in vivo* is overlaid with the CV collected with FIA denoted by the yellow star, revealing similar broad reduction peaks around -0.4 V. The current vs. time trace is denoted by the blue star, with the dashed line representing the baseline. Because of the long, low intensity stimulation, glutamate signals for a longer period unlike the sharp spikes traditionally observed with dopamine and serotonin FSCV. It

should be reiterated here that *in vivo* data was collected on bare CFMs using the glutamate waveform. Though the CV resembles the signature glutamate peak, due to the selectivity issues preciously discussed, we cannot definitively confirm without a doubt that this signal originates from glutamate. There are several strategies we plan to utilize to verify the chemical identity behind this signal, including the incorporation of ionophore-grafted CFMs and administering a pharmaceutical agent targeting the glutamatergic system. The appearance of a glutamate-like signal is extremely promising towards applying FSCV in this new region of the brain.

6.4 CONCLUSION

This chapter summarizes the development and characterization of an enzyme-free direct glutamate measurement platform. First, we introduce an optimized waveform for glutamate detection that prevents PGA formation *via* electropolymerization. With this waveform, glutamate produces a broad reduction peak at -0.4 V, exhibits a favorable kinetic response, and a calculated limit of detection of 1.5 μM. With this method, we further characterized the nature of the detection mechanism by plotting the logarithm of the scan rate vs. the logarithm of the current, and determined the mechanism is governed by adsorption. Data was then fit to a Langmuir adsorption isotherm and the adsorption coefficient was calculated ($K_{ads} = 4.84 \times 10^5$). When compared with other monoamines and biomolecules detectable with FSCV, a trend emerged correlating optimal scan rate with K_{ads}, where larger adsorption coefficients allowed for faster optimal scan rates (i.e. more efficient adsorption). The selectivity of this waveform towards glutamate was assessed by testing several biologically relevant neurotransmitters, ions, precursors and metabolites. While the selectivity results were promising, the broad nature of the

glutamate reduction peak requires a selectivity-boosting strategy for application in a complex matrix like the brain. Here, we introduce a glutamate specific ionophore with two Cu(II) metal centers that serves as a signal-off when binding to glutamate molecules. Voltammetric evidence is provided of glutamate binding via both the reduction of the Cu(II)-ionophore label, and appearance of a glutamate reduction peak. Finally, we present preliminary *in vivo* data collected in the Purkinje layer of the cerebellum where glutamate is volume transmitted. Results reveal a similar voltammetric response *in vivo* as in FIA, a promising step towards the development of an *in vivo* glutamate monitoring protocol. In the future, the next step will be to covalently attach the ionophore to the CFM to allow for *in situ* monitoring, and pharmacologically verify the identity of the in vivo signal as glutamate by administering a drug targeting the glutaminergic system. Altogether, the development of a voltammetric method for direct glutamate detection is the first step towards an *in vivo* glutamate sensing platform. This innovative technology will be useful for studying glutamatergic neurotransmission and the role glutamate signaling plays in prevalent neurological disorders.

6.5 MATERIALS AND METHODS

6.5.1 Chemicals

Experiments were performed at room temperature, standard pressure, and pH = 7.4. Solutions were made by dissolving L-glutamic acid in 1x PBS buffer diluted from a 10x premixed buffer. All chemicals were purchased from Sigma-Aldrich (St. Louis, MO). Glutamate ionophore was synthesized by the Wiskur group at the University of South Carolina and synthesis materials are not included in this chapter.

6.5.2 Electrochemistry, Data Acquisition and Statistics

Electrode fabrication, electrochemistry, data acquisition, and FIA are performed as previously described in **Chapter 4**. The triangular waveform utilized throughout this work scans from -0.2 V to 0.8 V at 400 V/s. All error is calculated using the standard error of the mean.

6.5.3 Adsorption Isotherms

Surface Concentration was calculated using Faradays Law **(Equation 1)**, where Q is the charge obtained from integrating the glutamate reduction peak, n is the number of electrons (n = 2 is assumed), and A is the surface area.

(3) $\Gamma_{\text{metal}} = \frac{Q}{nFA}$

Because glutamate follows monolayer adsorption, the data was fit to a linearized Langmuir adsorption isotherm, where [Glu] is the concentration of glutamate in bulk solution, and Γ_{max} is the maximum monolayer adsorption coverage at the carbon surface. K represents the equilibrium constant (K_{ads}) between glutamate adsorption to carbon and glutamate in bulk solution, reported in **Figure 6.2C**.

(4) $\frac{[\text{Glu}]}{\Gamma_{\text{glu}}} = \frac{1}{\Gamma_{\text{max}}}[\text{Glu}] + \frac{1}{\Gamma_{\text{max}} K_{\text{ads}}}$

6.5.4 Animals

Experiments were completing by performing stereotaxic surgery (David Kopf Instruments, Tujunga, CA) on a C57BL/6J mouse (Jackson Laboratory, Bar Harbor, ME) after administering anesthesia (urethane: 25% wt to volume in 0.9% NaCl solution, Mountainside Medical Equipment, Marcy, NY). Body temperature was sustained at around 37º C with a heating pad (Braintree scientific, Braintree, MA). Stereotactic

coordinates are taken in reference to bregma. A stainless-steel stimulating electrode (diameter: 0.2 mm, Plastics One, Roanoke, VA) was positioned in the ION by implantation though the brainstem. Stimulation Parameters: monophasic, 5 Hz stim frequency, 150 μA amplitude, 75 stim pulses, 0.20 ms pulse width, 15 s event time. Working electrodes placed in the Purkinje layer of the cerebellum (-6.00:AP 0:ML). An Ag/AgCl reference electrode was implanted into the contralateral hemisphere. All handling and surgical procedures were performed in accordance with the IUCAC animal care protocol at the University of South Carolina.

6.6 References

(1) Dong, X. X.; Wang, Y.; Qin, Z. H. Molecular mechanisms of excitotoxicity and their relevance to pathogenesis of neurodegenerative diseases. *Acta Pharmacol Sin* **2009,** *30* (4), 379.

(2) Wang, Y.; Qin, Z. H. Molecular and cellular mechanisms of excitotoxic neuronal death. *Apoptosis* **2010,** *15* (11), 1382.

(3) Wang, R.; Reddy, P. H. Role of Glutamate and NMDA Receptors in Alzheimer's Disease. *J Alzheimers Dis* **2017,** *57* (4), 1041.

(4) Lewerenz, J.; Maher, P. Chronic Glutamate Toxicity in Neurodegenerative Diseases-What is the Evidence? *Front Neurosci-Switz* **2015,** *9*, 469.

(5) Koutsilleri, E.; Riederer, P. Excitotoxicity and new antiglutamatergic strategies in Parkinson's diseaseand Alzheimer's disease. *Parkinsonism Relat D* **2007,** *13*, S329.

(6) Isoaho, N.; Peltola, E.; Sainio, S.; Wester, N.; Protopopova, V.; Wilson, B. P.; Koskinen, J.; Laurila, T. Carbon Nanostructure Based Platform for Enzymatic Glutamate Biosensors. *J Phys Chem C* **2017,** *121* (8), 4618.

(7) Hamdan, S. K.; Mohd Zain, A. In vivo Electrochemical Biosensor for Brain Glutamate Detection: A Mini Review. *Malays J Med Sci* **2014,** *21* (Spec Issue), 12.

(8) Putzbach, W.; Ronkainen, N. J. Immobilization Techniques in the Fabrication of Nanomaterial-Based Electrochemical Biosensors: A Review. *Sensors-Basel* **2013,** *13* (4), 4811.

(9) Kozai, T. D. Y.; Jaquins-Gerstl, A. S.; Vazquez, A. L.; Michael, A. C.; Cui, X. T. Brain Tissue Responses to Neural Implants Impact Signal Sensitivity and Intervention Strategies. *Acs Chemical Neuroscience* **2015,** *6* (1), 48.

(10) Barbour, B.; Keller, B. U.; Llano, I.; Marty, A. Prolonged Presence of Glutamate during Excitatory Synaptic Transmission to Cerebellar Purkinje-Cells. *Neuron* **1994,** *12* (6), 1331.

(11) Szapiro, G.; Barbour, B. Multiple climbing fibers signal to molecular layer interneurons exclusively via glutamate spillover. *Nat Neurosci* **2007,** *10* (6), 735.

(12) Hashemi, P.; Dankoski, E. C.; Petrovic, J.; Keithley, R. B.; Wightman, R. M. Voltammetric detection of 5-hydroxytryptamine release in the rat brain. *Anal Chem* **2009,** *81* (22), 9462.

(13) Saylor, R. A.; Hersey, M.; West, A.; Buchanan, A. M.; Berger, S. N.; Nijhout, H. F.; Reed, M. C.; Best, J.; Hashemi, P. In vivo Hippocampal Serotonin Dynamics in Male and Female Mice: Determining Effects of Acute Escitalopram Using Fast Scan Cyclic Voltammetry. *Front Neurosci* **2019,** *13*, 362.

(14) Samaranayake, S.; Abdalla, A.; Robke, R.; Nijhout, H. F.; Reed, M. C.; Best, J.; Hashemi, P. A voltammetric and mathematical analysis of histaminergic modulation of serotonin in the mouse hypothalamus. *J Neurochem* **2016,** *138* (3), 374.

(15) Samaranayake, S.; Abdalla, A.; Robke, R.; Wood, K. M.; Zeqja, A.; Hashemi, P. In vivo histamine voltammetry in the mouse premammillary nucleus. *Analyst* **2015,** *140* (11), 3759.

(16) Hensley, A. L.; Colley, A. R.; Ross, A. E. Real-Time Detection of Melatonin Using Fast-Scan Cyclic Voltammetry. *Anal Chem* **2018,** *90* (14), 8642.

(17) Cryan, M. T.; Ross, A. E. Subsecond detection of guanosine using fast-scan cyclic voltammetry. *Analyst* **2018,** *144* (1), 249.

(18) Ross, A. E.; Venton, B. J. Nafion-CNT coated carbon-fiber microelectrodes for enhanced detection of adenosine. *Analyst* **2012,** *137* (13), 3045.

(19) Sanford, A. L.; Morton, S. W.; Whitehouse, K. L.; Oara, H. M.; Lugo-Morales, L. Z.; Roberts, J. G.; Sombers, L. A. Voltammetric Detection of Hydrogen Peroxide at Carbon Fiber Microelectrodes. *Analytical Chemistry* **2010,** *82* (12), 5205.

(20) Schmidt, A. C.; Dunaway, L. E.; Roberts, J. G.; McCarty, G. S.; Sombers, L. A. Multiple Scan Rate Voltammetry for Selective Quantification of Real-Time Enkephalin Dynamics. *Analytical Chemistry* **2014,** *86* (15), 7806.

(21) Pathirathna, P.; Yang, Y.; Forzley, K.; McElmurry, S. P.; Hashemi, P. Fast-scan deposition-stripping voltammetry at carbon-fiber microelectrodes: real-time, subsecond, mercury free measurements of copper. *Anal Chem* **2012,** *84* (15), 6298.

(22) Heien, M. L. A. V.; Phillips, P. E. M.; Stuber, G. D.; Seipel, A. T.; Wightman, R. M. Overoxidation of carbon-fiber microelectrodes enhances dopamine adsorption and increases sensitivity. *Analyst* **2003,** *128* (12), 1413.

(23) Bard, A. F., L. Electrochemical methods : fundamentals and applications Wiley: New York, 1980.

(24) Siriwardhane, T.; Ou, Y. G.; Pathirathna, P.; Hashemi, P. Analysis of Electrochemically Elusive Trace Metals with Carbon Fiber Microelectrodes. *Analytical Chemistry* **2018,** *90* (20), 11917.

(25) Pathirathna, P.; Samaranayake, S.; Atcherley, C. W.; Parent, K. L.; Heien, M. L.; McElmurry, S. P.; Hashemi, P. Fast voltammetry of metals at carbon-fiber microelectrodes: copper adsorption onto activated carbon aids rapid electrochemical analysis. *Analyst* **2014,** *139* (18), 4673.

(26) Sedlak, T. W.; Paul, B. D.; Parker, G. M.; Hester, L. D.; Snowman, A. M.; Taniguchi, Y.; Kamiya, A.; Snyder, S. H.; Sawa, A. The glutathione cycle shapes synaptic glutamate activity. *P Natl Acad Sci USA* **2019,** *116* (7), 2701.

(27) Takeda, K.; Ishida, A.; Takahashi, K.; Ueda, T. Synaptic vesicles are capable of synthesizing the VGLUT substrate glutamate from a-ketoglutarate for vesicular loading. *Journal of Neurochemistry* **2012,** *121* (2), 184.

(28) Miyaji, T.; Echigo, N.; Hiasa, M.; Senoh, S.; Omote, H.; Moriyama, Y. Identification of a vesicular aspartate transporter. *P Natl Acad Sci USA* **2008,** *105* (33), 11720.

(29) Morland, C.; Nordengen, K.; Larsson, M.; Prolo, L. M.; Farzampour, Z.; Reimer, R. J.; Gundersen, V. Vesicular uptake and exocytosis of L-aspartate is independent of sialin. *Faseb J* **2013,** *27* (3), 1264.

(30) Yuzaki, M.; Forrest, D.; Curran, T.; Connor, J. A. Selective activation of calcium permeability by aspartate in Purkinje cells. *Science* **1996,** *273* (5278), 1112.

(31) D'Aniello, S.; Somorjai, I.; Garcia-Fernandez, J.; Topo, E.; D'Aniello, A. D-Aspartic acid is a novel endogenous neurotransmitter. *Faseb J* **2011,** *25* (3), 1014.

(32) Herring, B. E.; Silm, K.; Edwards, R. H.; Nicoll, R. A. Is Aspartate an Excitatory Neurotransmitter? *Journal of Neuroscience* **2015,** *35* (28), 10168.

(33) Yang, Y.; Ibrahim, A. A.; Hashemi, P.; Stockdill, J. L. Real-Time, Selective Detection of Copper(II) Using Ionophore-Grafted Carbon-Fiber Microelectrodes. *Anal Chem* **2016,** *88* (14), 6962.

(34) Eccles, J. C.; Llinas, R.; Sasaki, K. The excitatory synaptic action of climbing fibres on the Purkinje cells of the cerebellum. *J Physiol* **1966,** *182* (2), 268.

(35) Yang, C.; Jacobs, C. B.; Nguyen, M. D.; Ganesana, M.; Zestos, A. G.; Ivanov, I. N.; Puretzky, A. A.; Rouleau, C. M.; Geohegan, D. B.; Venton, B. J. Carbon Nanotubes Grown on Metal Microelectrodes for the Detection of Dopamine. *Anal Chem* **2016,** *88* (1), 645.

(36) Abdalla, A.; Atcherley, C. W.; Pathirathna, P.; Samaranayake, S.; Qiang, B. D.; Pena, E.; Morgan, S. L.; Heien, M. L.; Hashemi, P. In Vivo Ambient Serotonin Measurements at Carbon-Fiber Microelectrodes. *Anal Chem* **2017,** *89* (18), 9703.

CHAPTER 7

CONCLUSIONS AND FUTURE PROSPECTS

Electrochemical sensors are an excellent platform for monitoring important analytes in the environment and in biological systems. The advent of microelectrodes has proven significantly beneficial because they can be submerged or implanted causing minimal perturbation of the system being probed, however the complexity of such systems calls for an analysis mode capable of sensitivity, selectivity, and real-time analysis. FSCV is a method that fulfills these criteria and more. Traditionally FSCV has been employed to measure dopamine neurotransmission *in vivo*. In this dissertation work we expand the scope of FSCV in cutting edge model systems that mimic brain chemistry with high integrity and beyond the brain to measure novel analytes.

In **Chapter 2**, we identified a set of criteria necessary for an electrochemical trace metal speciation sensor that we coin the 6 S's: sensitivity, selectivity, size, speed, stability, and safe materials. This chapter reviewed literature from the last 10 years that shows promise towards portable trace metal sensing devices, and highlighted the few available studies that are able to measure trace metals on-site and *in situ*. Finally, we introduced FSCV as an emerging technique capable on satisfying the 6 S's and showing great promise towards on-site sensing.

In **Chapter 3**, we fabricate ionophore-grafted CFMs coupled with FSCV to selectively detect Cu(II) metal ions. The sensitivity of ionophore-grafted CFMs was

evaluated under various electrode lengths and ionic strengths, optimizing the ideal parameters for environmental analysis. Additionally, we defined the detection mechanism of Cu(II) on the ionophore-grafted CFM as monolayer adsorption and analyzed the effects of potential window on the electrode response. Finally, found that divalent metal interferences lower the electrode response in more complex matrices but do not obstruct the Cu(II) qualitatively and the sensitivity effects can be recovered to the original response.

In **Chapter 4**, we measured serotonin in human serotonin neurons derived from iPSCs as a novel analysis model. We employed a suite of optical and electrochemical techniques to evaluate the biophysical and neurochemical characteristics of 5-HTNs. Chemical functionality is verified and electrically evoked serotonin release and reuptake from cells is characterized. Finally, we show that dose dependent alterations in reuptake following the administration of an SSRI resemble the pharmacological changes observed *in vivo* in mice.

In **Chapter 5**, we utilized voltammetric, microscopic, and spectroscopic techniques in a multifaceted study characterizing glutamate electropolymerization on CFMs. First, a waveform is optimized for glutamate deposition and PGA is visualized on the CFM surface with SEM. Then, non-uniform morphology captured with AFM revealed a nucleation and growth like mechanisms of deposition. Finally, the analytical performance of PGA-CFMs and CFMs that have been exposed to brain tissue were evaluated, revealing similarities suggesting that improvements to *in vivo*-CFMs are a result of *in situ* electropolymerization of glutamate in the extracellular matrix.

In **Chapter 6**, we introduced a novel sensing strategy for glutamate detection. For the first time, we were able to directly detect glutamate on an enzyme-free CFM. We first, optimized a waveform that evaded electropolymerization with FSCV, and characterized the voltammetric signal in terms on sensitivity, detection mechanism, and selectivity. Though we do not foresee any interferences when electrically evoking glutamate release, we proposed an ionophore to boost selective detection. Finally, we showed preliminary *in vivo* data of a glutamate signal in the Purkinje layer of the cerebellum.

Our future plans for the continuation of this work are three-fold:

1. Design a trace metal speciation sensor from ionophore-grafted CFMs that is portable and can make *in situ* measurements.
2. Couple serotonin sensing in 5-HTNs as a diagnostic tool for depression and antidepressant screening.
3. Develop a direct glutamate detection platform capable of *in vivo* analysis to assess glutamate's physiological role in neurodegenerative diseases.

Together, this dissertation showcases FSCV as a powerful method towards real-time analysis for many different analytes and applications. These studies provide the groundwork towards sensor design to answer fundamental environmental and biological questions.

APPENDIX A

HUMAN STEM CELL-DERIVED SEROTONIN NEURONS WITH IN VIVO BIOPHYSICAL AND NEUROCHEMICAL CHARACTERISTICS SUPPLEMENTAL INFORMATION[6]

[6] **Holmes, J.;** Lau, T.; Saylor, R.A.; Hersey, M.; Keen, D.; Fernández-Novel, N.; Hampel, L.; Nijhout, H. F.; Reed, M. C.; Best, J.; Koch, P.; Hashemi, P.: "Human stem cell-derived serotonin neurons with *in vivo* biophysical and neurochemical characteristics" – *In preparation* – Proceedings of the National Academy of Sciences of the United States of America.

A.1 STIMULATION PARADIGM

The stimulation series applied to evoke serotonin release in 5-HTNs is shown above. An arbitrary ranking system, shown in the top panel, was utilized to assess stimulation strength with respect to frequency, amplitude and number of pulses, with 1 being the lowest and 4 being the highest intensity stimulation. For each parameter, the rank numbers are added to assign an overall stimulation strength between 3 and 12. The stimulation parameters applied in each trial (A-M) are displayed in the bottom panel, and the assigned stimulation strength for each trial can be found in **Figure 4.2**.

Table A.1 Stimulation Paradigm.

Rank	Frequency	Amplitude	Number of Pulses
1	20	150	20
2	40	200	40
3	60	250	60
4	80	300	80
Trial	**Frequency**	**Amplitude**	**Number of Pulses**
A	20	150	20
B	40	150	20
C	20	200	20
D	20	150	40
E	40	200	40
F	60	200	40
G	40	250	40
H	40	200	60
I	60	250	60
J	80	250	60
K	60	300	60
L	60	250	80
M	80	300	80

A.2 CELL MEDIUM OPTIMIZATION

Cell culture media is comprised of a suite of growth factors, amino acids, vitamins, and nutrients among other components that facilitates cell growth however, often times complex matrices such as these lead to biofouling of the electrode surface. In **Figure A.1A**, the current response of 250 nM serotonin in various buffers are compared, including neurobasal cell culture media, HEPES, glucose (added to provide nutrient for the cells), and ESCIT (the SSRI drug administered). *In vitro* buffer conditions were optimized prior to electrochemical measurements in 5-HTNs on Nafion coated CFMs, trimmed to 150 μm *via* injecting serotonin (250 nM) into a stirred solution. The significant decrease in signal response ($p<0.005$) in the neurobasal media used for culturing cells with respect to each HEPES-based media is evidence of electrode surface fouling. The inset histogram shows the current response to 5 different concentrations of glucose added to the medium, and 2.5 mM glucose was selected. The addition of glucose and ESCIT do not significantly affect the voltammetric signal response at the concentrations used. **Figure A.1B** illustrates a representative color plot and inset cyclic voltammogram of spiked serotonin at 250 nM in the optimized media.

Calibrations were completed in HEPES with 2.5 mM glucose, at Nafion coated CFMs trimmed to 100 μm in length. Serotonin was introduced to the electrode *via* flow injection analysis in a custom-built flow cell described previously, [1,2] delivering in a rectangular 15 s analyte pulse in the indicated buffer. All FSCV data is converted from current to concentration using the calibration factor generated from the calibration curve in **Figure A.1C**.

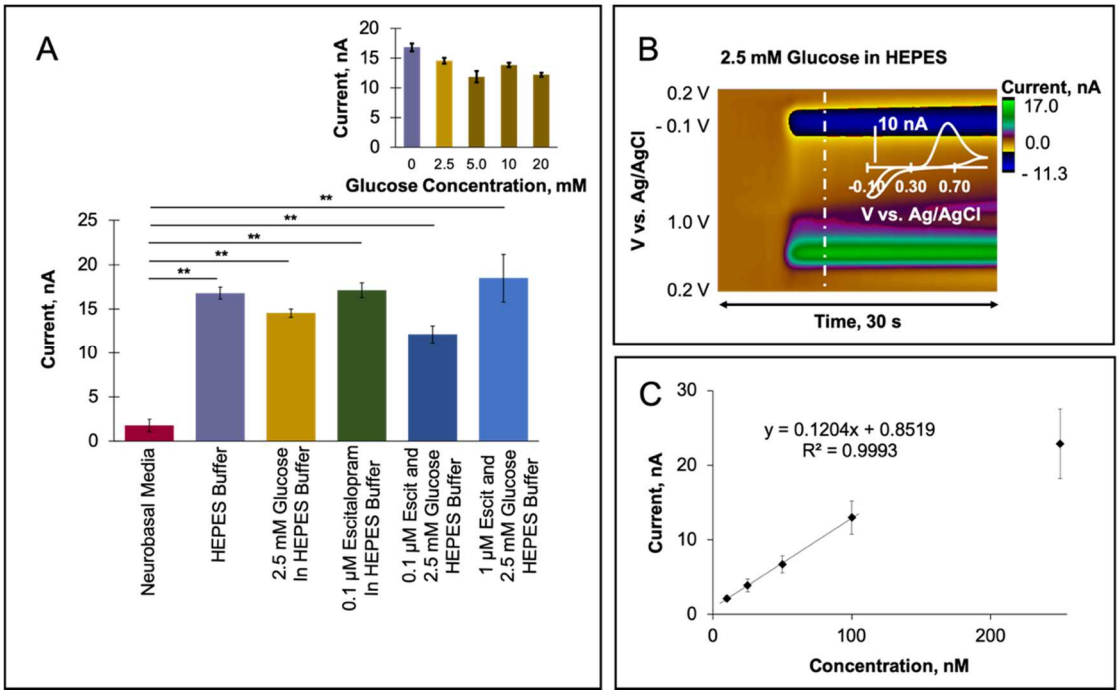

Figure A.1 FSCV Electrolytic Buffer Optimization. (A) Comparisons of electrolytic medium for FSCV analysis including neurobasal media, HEPES, glucose and ESCIT (** P<0.005). Inset is various concentrations of glucose added to the media (ns). **(B)** Representative color plot for selected buffer composition (2.5 mM glucose in HEPES) with cyclic voltammogram inset. 250 nM serotonin was used for all medium optimization experiments. **(C)** Calibration curve, concentration of serotonin in nM vs. current response.

A.3 MODELLING EXTERNAL TRYPTOPHAN

The mathematical model was used to compute how the steady state values of vesicular 5-HT (red curve) and extracellular 5-HT (blue curve) vary with external tryptophan. When external tryptophan varies from 40 µM to 140 µM, vesicular serotonin doubles consistent with the doubling of release as shown in **Figure 4.2H**. Extracellular serotonin varies less than vesicular serotonin because of the homeostatic effect of the autoreceptors.

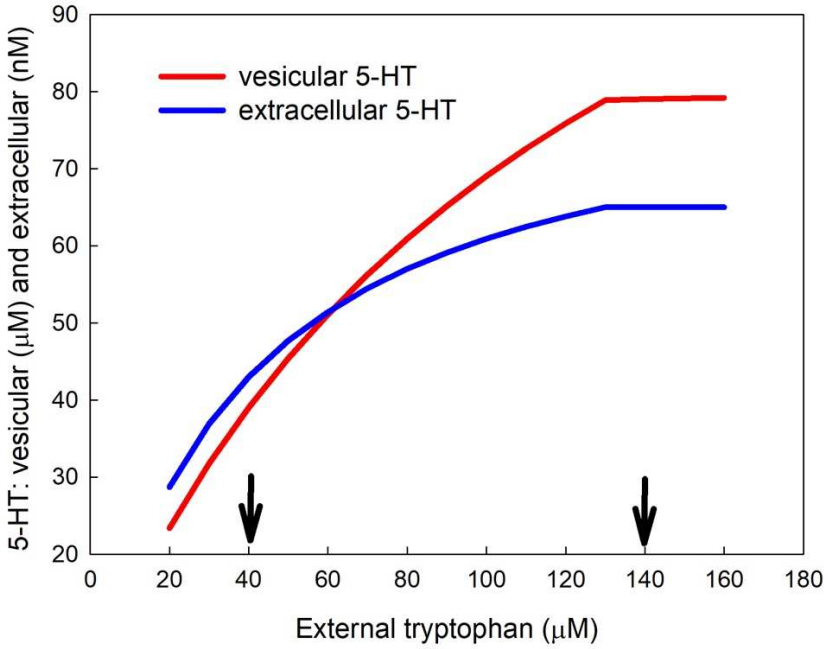

Figure A.2 External tryptophan affects vesicular and extracellular serotonin. Vesicular 5-HT (red curve) and extracellular 5-HT (blue curve) are modelled with respect to extracellular tryptophan.

A.4 REFERENCES

(1) Kristensen, E. W.; Wilson, R. L.; Wightman, R. M. Dispersion in flow injection analysis measured with microvoltammetric electrodes. *Analytical Chemistry* **1986,** *58* (4), 986.

(2) Pathirathna, P.; Yang, Y.; Forzley, K.; McElmurry, S. P.; Hashemi, P. Fast-scan deposition-stripping voltammetry at carbon-fiber microelectrodes: real-time, subsecond, mercury free measurements of copper. *Anal Chem* **2012,** *84* (15), 6298.

APPENDIX B

RADICAL-INITIATED ELECTROPOLYMERIZATION OF POLY-GLUTAMIC ACID ON CARBON: IMPLICATIONS FOR BIOLOGICAL ANALYSIS SUPPLEMENTAL INFORMATION[7]

[7] Holmes, J.; Batey, L.;Hashemi, P.: "Radical-initiated electropolymerization of poly-glutamic acid on carbon: Implications for biological analysis" – *Under review* – Journal of the American Chemical Society.

B.1 EXPERIMENTAL SECTION

B.1.1 Chemicals.

Stock solutions were prepared at room temperature and neutral pH (pH = 7.4) by dissolving glutamic acid and dopamine (DA) hydrochloride (each prepared to a final concentration of 1 μM) into 1x phosphate buffer (PBS) that was diluted from a 10x premixed buffer. All chemicals were purchased from Sigma Aldrich (St. Louis, MO) unless otherwise specified. Liquion (LQ-1105, 5% by weight Nafion^{TM}) was purchased from Ion Power Solutions (New Castle, DE, United States).

B.1.2 Electrochemistry.

Voltammetry was performed on a 2-electrode system. Carbon fiber microelectrodes (CFMs) were hand-made in house as previously described.[1] Briefly, CFMs are fabricated by vacuum-aspirating 7 μm radius carbon-fibers (Goodfellow Corporation, PA, USA) into a glass capillary (1.0 mm external diameter, 0.5 mm internal diameter, A-M Systems, Inc., Sequim, WA). The glass capillary is then pulled with a vertical micropipet puller (Narishige, Tokyo, Japan) to form a carbon-glass seal. The exposed length of the carbon fiber is trimmed to 100 μm under an optical microscope. Ag wire (A-M systems, WA) was electroplated with Cl^- for 30 s in 0.1 M HCl at 5 V to create a pseudo Ag/AgCl reference electrode.

B.1.3 Fast-scan Cyclic Voltammetry (FSCV).

Waveforms were generated using a USB-6431DAC/ADC (National Instruments, TX, USA) device. The working electrode was scanned using a triangular wave form at

400 V/s, from -0.4 V up to 1.0 V or 1.3 V, and then back down to -0.4 V. This waveform was cycled at 60 Hz for 10 minutes and 10 Hz for 10 minutes before analysis.

B.1.4 Fast-scan Controlled Adsorption Voltammetry (FSCAV).

FSCAV was performed as previously described[2] using a CMOS precision analog switch, ADG419 (Analog Devices) to control application of the waveform. The waveform (-0.4 to +1.3, scan rate = 400 V/s) was applied at a frequency of 100 Hz for 2s, then held at a constant potential of -0.4 V for 10 s, followed by reapplication of the wave form for the remainder of the total file collection time of 30s.

B.1.5 Flow Injection Analysis (FIA).

FIA was performed in a system custom built in-house. CFMs were inserted into flangeless short 1/8 nuts (PEEK P-335, IDEX, Middleboro, MA) exposing a small portion of the tip (2 mm) outside of the nut. An HPLC union (Elbow PEEK 3432, IDEX, Middleboro, MA) was modified such that the nut containing the microelectrode was fastened to one end. The out-flowing stream of the FIA buffer was fastened to the other end of the elbow union. Two holes were drilled into the union for the incorporation of the reference electrode and for the ‘waste’ flow stream. A syringe infusion pump (KD Scientific, Model KDS-410, Holliston, MA) was used to maintain the flow. The analyte was introduced into the flow stream for 10 seconds via a six-port HPLC loop injector (Cheminert Valve, VICI, Houston, TX) as a rectangular plug.

B.1.6 Data Acquisition, Analysis, and Statistics.

FSCV was performed using a Dagan Potentiostat, (Dagan Corporation, Minneapolis, NM, United States), National Instruments multifunction device USB-6341 (National Instruments, Austin, TX), WCCV 3.06 software (Knowmad Technologies LLC, Tucson, AZ, United States) and a Pine Research headstage (Pine Research Instrumentation, Durham, NC, United States). Data filtering (zero phase, Butterworth, 2 kHz low-pass) and signal smoothing were done within the WCCV software. Cyclic voltammograms (CV) were used for DA identification. With FSCAV, the first CV after reapplication of the waveform with a signature DA peak (third CV overall) between approximately 0.45 and 0.9 V was integrated to determine charge (pC). Pre-calibrations were performed before *in vivo* experiments and post-calibrations were performed within 24 hours after *in vivo* experiments where charge (pC) was plotted vs. [DA] (nM). All data were averaged over at least 4 electrodes and the standard error of the mean was calculated (represented by error bars). A two-tailed student's t-test was utilized to determine significance between two points ($p < 0.05$).

B.1.7 Animals.

In vivo animal experiments were performed modifying methods described previously by Saylor, Hersey et al.[3] To induce anesthesia, 25% w/v urethane (Sigma–Aldrich Co.) dissolved in 0.9% NaCl solution (Hospira) was injected i.p. (7µl/g of body weight). Body temperature was maintained using a heating pad (Braintree Scientific, Braintree, MA, United States) and stereotaxic surgeries (David Kopf Instruments, Tujunga, CA, United States) were performed with coordinates taken in refence to

bregma. For FSCAV data (**Figure 5.1**), a Nafion™-coated CFM was lowered into the nucleus acumens core region of the brain (AP: +1.10, ML: -1.30, DV: -4.00).[4] For FSCV data (**Figure 5.4**), a CFM was lowered until it was fully immersed in the cortex tissue (AP: -1.1, ML: +0.5)[4] and the triangular DA waveform was cycled for 10 minutes at 60 Hz and 10 minutes at 10 Hz. A pseudo Ag/AgCl reference electrode was placed in the contralateral hemisphere. Animal use followed NIH guidelines and complied with the University of South Carolina Institutional Animal Care and Use Committee under an approved protocol.

B.1.8 Surface modifications.

Nafion™ was electrodeposited by dipping CFMs into solution for 30 s, while applying 1 V, as previously described by Hashemi et al.[5] To deposit PGA, CFMs were dipped in 1 μM glutamate solution (in 1x PBS buffer) and cycled using a triangular waveform for 10 minutes at 60 Hz and 10 minutes at 10 Hz. Different variations of the triangular waveform applied for electropolymerization include: the expanded DA waveform (-0.4 V to 1.3 V),[6] the original DA waveform (-0.4 V to 1.0 V), and a third triangular waveform with a wide potential window (-1.2 V to 1.3 V), all scanned at 400 V/s.

B.1.9 Scanning Electron Microscopy (SEM) / Energy Dispersive X-Ray Spectroscopy (EDX).

Electrodes were prepared for SEM imaging and EDX elemental analysis by depositing PGA, employing both the expanded (1.3 V positive potential limit) and original (1.0 V positive potential limit) triangular DA waveforms, as described

previously. Electrodes were then transported to the SEM in a closed container. The capillary glass was cracked and the tip end of the CFM was secured onto a stage with double sided tape. SEM images were collected using a Zeiss Ultraplus Thermal Field Emission Scanning Electron Microscope with EDX capabilities. Images in **Figure 5.2 Ai, Bi, and Ci** were magnified on the Zeiss software and the image in **Figure 5.2Di** was digitally magnified.

B.1.10 Atomic Force Microscopy (AFM).

Electrodes were prepared for AFM imaging by depositing PGA or NA the day of analysis. Electrodes were transported to the AFM in a closed container, and mounted on a glass slide, with the electrode tip flat to the slide surface. AFM images were collected using a Digital Instruments Dimension 3100 AFM (Veeco Metrology Group) with a NanoScope IIIa Controller and a non-contact tip.

B.2 REFERENCES

(1) Pathirathna, P.; Yang, Y.; Forzley, K.; McElmurry, S. P.; Hashemi, P. Fast-scan deposition-stripping voltammetry at carbon-fiber microelectrodes: real-time, subsecond, mercury free measurements of copper. *Anal Chem* **2012,** *84* (15), 6298.

(2) Atcherley, C. W.; Wood, K. M.; Parent, K. L.; Hashemi, P.; Heien, M. L. The coaction of tonic and phasic dopamine dynamics. *Chem Commun* **2015,** *51* (12), 2235.

(3) Saylor, R. A.; Hersey, M.; West, A.; Buchanan, A. M.; Berger, S. N.; Nijhout, H. F.; Reed, M. C.; Best, J.; Hashemi, P. *In vivo* Hippocampal Serotonin Dynamics

in Male and Female Mice: Determining Effects of Acute Escitalopram Using Fast Scan Cyclic Voltammetry. *Front Neurosci-Switz* **2019,** *13*.

(4) Franklin, K. B. J.; Paxinos, G. *Paxinos and Franklin's The mouse brain in stereotaxic coordinates*, 2013.

(5) Hashemi, P.; Dankoski, E. C.; Petrovic, J.; Keithley, R. B.; Wightman, R. M. Voltammetric detection of 5-hydroxytryptamine release in the rat brain. *Anal Chem* **2009,** *81* (22), 9462.

(6) Heien, M. L. A. V.; Phillips, P. E. M.; Stuber, G. D.; Seipel, A. T.; Wightman, R. M. Overoxidation of carbon-fiber microelectrodes enhances dopamine adsorption and increases sensitivity. *Analyst* **2003,** *128* (12), 1413.

APPENDIX C

PERMISSION TO REPRINT: CHAPTER 2